UNIVERSIDAD
DE GRANADA

Hydrostatic equilibrium in the semiclassical approximation

Julio Arrechea Rodríguez

Thesis submitted for the degree of

DOCTOR OF PHILOSOPHY

Programa de Doctorado en Física y Matemáticas

Supervisors

Carlos Barceló Serón

Departamento de Astronomía Extragaláctica,
Instituto de Astrofísica de Andalucía (IAA-CSIC)

Luis J. Garay Elizondo

Departamento de Física Teórica e IPARCOS,
Universidad Complutense de Madrid

Raúl Carballo Rubio

CP3-Origins, Universidad de Dinamarca del Sur
Florida Space Institute, Universidad Central de Florida

March 2023

Editor: Universidad de Granada. Tesis Doctorales
Autor: Julio Arrechea Rodríguez
ISBN: 978-84-1117-876-1
URI: https://hdl.handle.net/10481/82210

Agradecimientos

Agradezco a mis padres su inagotable apoyo durante estos años. Vosotros me habéis transmitido la fascinación por la ciencia que siento a día de hoy. Gracias a Jacobo, Rocío y Jes por aguantar mis desvaríos de físico, y a Min, por hacerme compañía en tantas tardes de estudio.

A Carlos, Luis y Raúl: no puedo expresar lo afortunado que me siento de haber podido realizar esta tesis bajo vuestra supervisión. Gracias a vosotros he crecido muchísimo en esta etapa, tanto en lo personal como en lo científico. A Gerry y Valen por todo el tiempo y las idioteces que hemos compartido. A Adrià y Alejandro por hacer el confinamiento más soportable. A María por acompañarme en el camino.

To Adrian and Paolo for hosting me in Dublin and Rome. Meeting your groups was an unforgettable life experience. To all the friends I made at UCD and Sapienza, you are wonderful people and amazing scientists. I hope that our paths meet again.

Agradezco a Ana y Xavi, por darme paz, y a todos mis compañeros y compañeras del IAA. Habéis hecho que Granada sea mi hogar y espero regresar algún día a esta hermosa ciudad. Gracias a Víctor y Pasku, con quienes tuve la fortuna de pasar mi último año en Madrid, y al Núcleo, donde sé que siempre podré volver si lo necesito.

Summary

Quantum field theory in curved spacetimes (QFTCS) stands as one of the cornerstones of modern theoretical physics. This theory blends together the gravitational and quantum realms in a unique way: It considers the influence of quantum fields on a classical spacetime, and vice versa. While QFTCS gave birth to the phenomena of cosmological particle creation and Hawking radiation emission in black holes, its impact on the physics of compact relativistic stars has remained, for the most part, undiscussed.

This thesis is an exploratory analysis. Within the framework of QFTCS, we search for new figures of stellar equilibrium supported by the repulsive forces that characterize vacuum energies. To tackle such an ambitious problem, we follow a constructive approach, solving the semiclassical backreaction problem in scenarios of increasing complexity, but always under the assumptions of staticity and spherical symmetry. The renormalized stress-energy tensor (RSET) of quantum matter is modeled through various analytical approximations in order to evaluate its impact on the Schwarzschild and Reissner-Nordström black holes first, to later address (ultra-)compact stars of uniform classical density.

Our explorations lead to the discovery of a novel exotic compact object: the semiclassical relativistic star. These objects are composed of a mixture of classical and quantum matter, sustained thanks to a surprising balance of forces between these two agents. Semiclassical stars can become as compact as black holes but stand out among other proposals since they are i) potentially testable through gravitational-wave observations, and ii) do not rely on any physics beyond QFTCS, which is a solid, well-established framework.

The analyses presented in this thesis venture into *terra incognita*, and unveil a surprisingly rich field of study: hydrostatic equilibrium in semiclassical gravity. The content of this thesis is based on the following publications by the candidate (and collaborators) [1–7]. The content of each Chapter is the following:

- Chapter 1 is a summary of the context in which these investigations are embedded. We provide an overview of the field of semiclassical gravity, with

particular emphasis on approximating renormalized stress-energy tensors. We introduce the Regularized Polyakov RSET (RP-RSET), to be used in Chapters 2 to 5, and review the main physical properties of semiclassical relativistic stars.

- In Chapters 2 and 3 we obtain the semiclassical counterparts to the Schwarzschild and Reissner-Nordström spacetimes, that is, the asymptotically flat, static vacuum (or electrovacuum) geometries incorporating the backreaction of the RP-RSET (regularized with a cutoff). The most remarkable result is the complete absence of event horizons, transformed into curvature singularities by backreaction effects. The semiclassical counterpart to the extremal black hole exhibits a singular, "quasi-extremal" horizon. Consequently, in semiclassical gravity horizons must be evaporative and dynamical. Otherwise, some classical matter fluid must be introduced to obtain regular spacetimes.

- Chapter 4 is the longest Chapter of this thesis as it exhaustively classifies the space of solutions of classical and semiclassical stars of uniform density. We provide a catalogue of all semiclassical stellar solutions, with particular emphasis on a family of objects that can surpass Buchdahl limit while being arbitrarily close to becoming regular. This property suggests exploring other regularization schemes for the RP-RSET that might accomplish strict regularity.

- Chapter 5 contains the central result of the thesis. We find, through minimal assumptions, families of regularization schemes for the RP-RSET that are consistent with stellar spacetimes of arbitrary compactness. The resulting solutions exhibit a series of universal properties: a negative-mass interior with classical pressures that grow inwards, and the absence of curvature singularities and event horizons. We elaborate on the implications of this result.

- Finally, Chapter 6 constitutes a first incursion into one of the future lines of inquiry suggested by this thesis. We rederive the semiclassical Schwarzschild counterpart but through an alternative RSET approximation based on a perturbative reduction of order. We compare these results with those in Chapter 2, allowing to extract robust physical conclusions from semiclassical analyses along the way. Finally, we sketch some preliminary results that apply this method to uniform density stars, showing that semiclassical relativistic stars with akin characteristics also exist under this prescription.

- We conclude with some closing remarks and future prospects in Chapter 7.

I like to think of this thesis as a road map showing the main pathway we followed, but also the various diversions that came along the way. It is a compilation of reflections, ideas, intuitions, and a sort of vessel through which I have attempted to embody my way of experiencing the process of research in theoretical physics. I hope you find joy in reading this thesis, but above all I wish it becomes useful for someone, somewhere (somehow). Do not hesitate contacting me for whatever reason regarding this text. I sincerely appreciate it.

Resumen

La teoría cuántica de campos en espacio-tiempos curvos (QFTCS) es una de las piedras angulares de la física teórica moderna. Esta teoría combina los reinos gravitatorio y cuántico de un modo único, por medio de considerar la influencia de los campos cuánticos sobre un espacio-tiempo clásico, y viceversa. Mientras que la QFTCS originó el estudio de los fenómenos de creación de partículas en cosmología y de emisión de radiación Hawking en agujeros negros, las implicaciones de esta teoría en la física de estrellas relativistas compactas han permanecido, en gran parte, sin ser abordadas.

Esta tesis es una exploración. Dentro del marco de la QFTCS, buscamos nuevas figuras de equilibrio estelar sustentadas por las fuerzas repulsivas características de la energía del vacío. Con el fin de abordar un problema tan amplio, adoptamos un acercamiento progresivo, resolviendo el problema de la *backreaction* semiclásica en situaciones de creciente complejidad, pero siempre bajo los supuestos de estaticidad y simetría esférica. Modelizamos el tensor de energía-impulso renormalizado (RSET) asociado a la materia cuántica por medio de diversas aproximaciones analíticas con el fin de, en primer lugar, analizar su impacto sobre los agujeros negros de Schwarzschild y Reissner-Nordström. Acto seguido, nos centramos en estrellas ultracompactas cuya densidad clásica es constante.

Estas búsquedas nos conducen al descubrimiento de un nuevo objeto compacto exótico: la estrella relativista semiclásica. Dichos objetos están compuestos por una mezcla de materia clásica y cuántica, posibles gracias a un sorprendente equilibrio de fuerzas entre ambos agentes. Las estrellas semiclásicas pueden llegar a ser tan compactas como los agujeros negros, pero destacan frente a otras propuestas similares porque i) es un modelo potencialmente comprobable mediante observaciones de ondas gravitatorias, y ii) no involucran ninguna física más allá de la QFTCS, que se trata de un marco sólido y bien establecido.

Los análisis presentados en esta tesis se adentran en *terra incognita*, y desvelan un campo de estudio sorprendentemente rico: el equilibrio hidrostático en gravedad semiclásica. El contenido de esta tesis está basado en los siguientes artículos del

candidato (y sus colaboradores) [1–7]. El contenido de cada uno de los capítulos es el siguiente:

- El capítulo 1 es un resumen del contexto en el que se enmarcan nuestras investigaciones. Proporcionamos una visión general del campo de la gravedad semiclásica, con especial énfasis en las aproximaciones a los tensores de energía-impulso renormalizados. Introducimos el RSET de Polyakov Regularizado (RP-RSET), del cual hacemos uso en los capítulos 2 a 5, y revisamos las principales propiedades físicas de las estrellas relativistas semiclásicas.

- En los capítulos 2 y 3 obtenemos las contrapartidas semiclásicas de los espacio-tiempos de Schwarzschild y Reissner-Nordström, es decir, las geometrías asintóticamente planas y estáticas del vacío (o electrovacío) que incorporan la *backreaction* del RP-RSET (regularizado con un *cutoff*). El resultado más reseñable es la ausencia completa de horizontes de sucesos, que se transforman en singularidades de curvatura a consecuencia de la *backreaction*. La contrapartida semiclásica del agujero negro extremal exhibe un horizonte singular, "cuasi-extremal". Concluimos que en gravedad semiclásica los horizontes deben ser evaporativos y dinámicos. En caso contrario, es necesario introducir un fluido de materia clásico para obtener espacio-tiempos regulares.

- El capítulo 4 es el más largo de esta tesis ya que contiene una clasificación exhaustiva del espacio de soluciones de estrellas clásicas y semiclásicas de densidad constante. Proporcionamos un catálogo de todas las soluciones estelares semiclásicas, con especial énfasis en una familia de objetos que logran superar el límite de Buchdahl a la vez que están arbitrariamente cerca de convertirse en regulares. Esta propiedad sugiere explorar otros esquemas de regularización para el RP-RSET que consigan lograr una regularidad estricta.

- El capítulo 5 contiene el resultado central de esta tesis. Encontramos, por medio de las mínimas suposiciones, familias de esquemas de regularización para el RP-RSET que son consistentes con la existencia de espacio-tiempos estelares de compacidad arbitraria. Las soluciones resultantes exhiben una serie de propiedades universales: un interior de masa negativa con presiones clásicas que crecen hacia el interior, así como la ausencia de singularidades de curvatura y horizontes de sucesos. Concluimos con una disertación acerca de las implicaciones de este descubrimiento.

- Por último, el capítulo 6 constituye una primera incursión en una de las futuras líneas de investigación surgidas a raíz de esta tesis. Retomamos la contrapartida semiclásica de la geometría de Schwarzschild pero esta vez por medio de una aproximación al RSET alternativa, basada en una reducción de orden perturbativa. Al comparar estos resultados con los del capítulo 2 logramos extraer conclusiones físicas robustas de los análisis semiclásicos. Finalmente, esbozamos algunos resultados preliminares que surgen al aplicar este método a estrellas de densidad constante. Así, probamos la existencia de estrellas relativistas semiclásicas con características afines a las del capítulo 5.
- Concluimos con algunos comentarios finales y perspectivas de futuro en el capítulo 7.

He ideado esta tesis como un mapa de carreteras que muestra el camino principal que seguimos en nuestras investigaciones, pero también los diversos desvíos que se produjeron por el camino. Es una recopilación de reflexiones, ideas, intuiciones y una especie de recipiente a través del cual he intentado plasmar mi forma de experimentar la investigación en física teórica. Espero que la lectura de esta tesis sea de tu agrado, pero sobre todo deseo que sea útil para alguien, en algún lugar (de algún modo). No dudes en ponerse en contacto conmigo por cualquier motivo relacionado con este texto. Te lo agradezco de corazón.

Contents

1 Introduction

> *Telling the truth is impossible; it is either nefarious or ineffable.*
>
> — **María Zambrano**

1.1 Black holes or black stars?

Black holes (BHs) are the ultimate frontier in the human quest for scientific knowledge, as the answers that may dwell in their interiors are only accessible to those who venture beyond a surface of no return: the event horizon. These one-way membranes [8, 9] shield the Universe outside BHs (and the observers residing there) from the unpredictable effects of curvature singularities [10–12]. While, under certain generic assumptions on the properties of collapsing clouds of matter, the formation of event horizons and spacetime singularities (these concepts are inextricably linked [13]) is unavoidable [14], there is a benevolence of sorts in Einstein's theory of general relativity (GR) stemming from the fact that singularities always appear hidden behind event horizons, like those in GR BHs, or inaccessible to physical observers [15, 16], as is the case for the Big Bang singularity [17]. These intriguing properties, together with their extraordinary agreement with recent gravitational-wave [18, 19] and very-long-baseline interferometric [20, 21] observations, has put GR BHs as the most plausible candidates to describe the dark and compact objects that we observe—astrophysical black holes (ABHs) hereafter.

This thesis is born from the increasingly accepted idea that GR BHs could correspond to excessively idealized descriptions of ABHs [13, 22–30], and that the structural properties of ABHs might be far more complex than those of GR BHs, which are essentially vacuum—devoid from any matter—and described only by their mass, charge, and angular momentum [31, 32]. Our modest contribution with this thesis to such an immense field of study is the realization that, already within the framework of quantum field theory in curved spacetimes (QFTCS) [33–36], it is possible to find matter configurations, akin to relativistic stars, supported by

quantum vacuum polarization effects, that can be as compact as BHs, potentially mimicking their observational features while lacking event horizons and spacetime singularities [6].

The motivation, derivation and implications of this result will be detailed throughout this thesis, but to put it in the right context let us have a glimpse on how the notion of BHs has evolved historically [37].

Black holes: the birth of an idea

The existence of gravitationally bound objects so massive that light itself would become unable to escape from their attraction was born in the era of Newtonian gravity and was first postulated by Michell [38] and later (independently) by Laplace [39]. More than a century after, Schwarzschild [40] derived the first vacuum solution within the theory of GR under the assumptions of staticity and spherical symmetry. By vacuum we refer to a solution to the Einstein equations (with cosmological constant $\Lambda = 0$ and $G = c = 1$),

$$G_{\mu\nu} = 8\pi T_{\mu\nu}, \tag{1.1}$$

in absence of any classical stress-energy tensor (SET), so $T_{\mu\nu} = 0$. In (1.1) and expressions therein, Greek indices range from 0 to 3. The line element of spherically symmetric and static spacetimes can be cast, without loss of generality, in the form

$$ds^2 = -e^{2\phi(r)}dt^2 + [1 - C(r)]^{-1}\, dr^2 + r^2 d\Omega^2, \tag{1.2}$$

Here, $d\Omega^2$ is the line element of the unit 2-sphere and $e^{2\phi(r)}$ represents the redshift function of the geometry, related to the redshift suffered by outgoing light rays. These become unable to escape to infinity when $\phi \to -\infty$, so the redshift function encodes how close is the geometry to having a horizon. The other function, $C(r)$, denotes the compactness of the geometry. It is often written as $2m(r)/r$, where $m(r)$ is the Misner-Sharp mass [41–43]. Compactness represents the amount of mass contained within a spherical surface of radius r. The Schwarzschild metric corresponds to

$$e^{2\phi} = 1 - C = 1 - \frac{2M}{r} \tag{1.3}$$

and has a horizon at $r_{\rm H} = 2M$ with M a positive constant, the ADM (Arnowitt-Deser-Misner) mass [44]. Birkhoff's theorem [45, 46] shows that the Schwarzschild metric is the spacetime exterior to any spherically symmetric gravitating body, irrespective of whether it is in equilibrium, like relativistic stars, or collapsing under its own gravity.

The Schwarzschild solution (1.3) was not considered physical at first because the event horizon was thought to be a singular surface. It was Lemaître [47] who first pointed out that the horizon was a perfectly regular place by finding a set of coordinates in which the Schwarzschild metric was manifestly regular. Despite this, it was not until the works of Szekeres [48] and Kruskal [49], who found the maximal extension of Schwarzschild spacetime, that the question of the regularity of the event horizon was completely settled.

The future event horizon in the maximally extended Schwarzschild spacetime conceals a curvature singularity at $r = 0$. This same curvature singularity forms in the gravitational collapse of presureless dust balls [50] (i.e. the Oppenheimer-Snyder model). This model was argued to appropriately capture the defining features of generic stellar collapse, which takes place when the internal pressures of a star become unable to withstand gravitational contraction. Theoretical progress on the generic nature of curvature singularities in GR crystallized in the Penrose singularity theorems [11, 51, 52] proving that their formation in gravitational collapse becomes unavoidable beyond spherical symmetry as long as some energy condition holds [53].

In 1916, Schwarzschild also found the solution describing an incompressible fluid sphere of constant density and isotropic pressures occupying a finite portion of spacetime. Outside the geometry is the Schwarzschild vacuum [54]. The Schwarzschild interior solution provides the simplest model of a hydrostatic equilibrium configuration [55, 56] in GR. It is of the utmost importance to this dissertation, as it exhibits the highest limit to the compactness of any spherical star of isotropic pressure in hydrostatic equilibrium, the so-called Buchdahl limit [57]. Absent in Newtonian gravity, this limit exists due to pressure being a source of gravity itself within GR. When the internal pressures of a fluid sphere become sufficiently large, they contribute towards its own collapse instead of preventing it. This is inevitable unless the matter content violates certain properties that will be reviewed in Subsec. 1.3.1.

Neutron stars are the most compact material bodies known to exist in our universe (excluding ABHs). However, they do not come close to the Buchdahl compactness limit since they are not made up of idealized, incompressible matter and are subject to more stringent mass limits [58–60], beyond which no stable configurations composed of ordinary nuclear matter can exist [61]. These bounds to the stability of compact stars established the following consensus: If a dark object whose compactness is close to that of a BH is identified, it likely corresponds to a BH, a purely vacuum gravitational configuration. Were to be an extremely compact star instead, it has to be composed by matter exhibiting unusual (sometimes identified as “exotic”) properties.

Observations of active galactic nuclei [62], in which a luminosity comparable in magnitude to that of whole galaxies is generated within volumes as small as our solar system, tipped the scales towards acknowledging that supermassive BHs (and not highly dense stellar clusters) where the engines behind such tremendous releases of energy. Numerous detections for supermassive and stellar-mass BH candidates were accumulating [63, 64], with the strongest evidence coming from velocity dispersion measurements of stars oribiting Sgr A* [65]. The recent direct detection of gravitational waves from binary mergers [18] and observations from the Event Horizon Telescope collaboration [20, 21] under the lense of the BH paradigm makes these objects—in particular, their spinning counterparts discovered by Kerr [66]—to be universally accepted.

The confluence of a history of mathematical understanding, together with the development of novel observations, opened a window towards the mysterious entrails of BHs and they eventually took root in the scientific community [67]. Nowadays, it is fairly accepted (although there exists no definite proof [23, 29]) that Kerr BHs are ubiquitous objects in our Universe. This is the idea that we question in this thesis. We propose an alternative to GR BHs that is potentially consistent with current observations while being devoid of the puzzling features (event horizons and curvature singularities) that baffled theorists for decades.

Alternatives to black holes

There is an ongoing effort to find alternatives to the BH paradigm. These alternatives can be postulated within GR and modified theories of gravity, or even be inspired by quantum theories of gravity. Such a surge in interest is motivated by current observations of ABHs being non-conclusive in determining their true nature [22, 23, 29], and by the potential detectability of other proposals through gravitational-wave observations [26, 68–72].

Current efforts to discover and model the properties of exotic compact objects can be divided into two categories: Those models which modify GR BHs inside trapped regions inaccessible to outside observers and which cannot be distinguished from the current paradigm, and proposals that assume drastic deviations from the properties of GR BHs at size-scales comparable to the event horizon itself, confronting the BH paradigm entirely.

The former family of objects is based on the idea that long-lived trapping horizons [73–75] are robust features of ABHs but curvature singularities are dissatisfying and should become regularized by quantum physics. In consequence, deviations from GR BHs are expected deep inside the trapped region, preventing the formation of singularities like quantum-gravitational effects do in Planck stars [76], or

replacing them entirely by the introduction of regular matter cores like in the regular BH proposal [77–80]. Although the metric deformations characteristic of the regular BH model have a minor impact on the region outside the event horizon, the interior is dramatically modified by the appearance of an inner horizon, a surface susceptible to suffering mass-inflation instabilities [30, 81–83].

The latter family encompasses objects of a drastically different nature, in some cases displaying an astrophysically explorable surface which provides distinct observational signatures. These can be split into two sub-types: Those whose compactness values approach (or even surpass slightly) the Buchdahl limit, and those whose compactness values are extremely close (or equal) to that of a BH.

Alternatives with low compactness vary widely in exoticness according to taste. These include boson and Proca stars [84–86], ultracompact anisotropic [87] and vector [88] stars, fermion soliton stars [89], and plenty of other objects within modified theories of gravity [26, 90]. If these objects are compact enough as to display a photon sphere [70], they will produce gravitational-wave echoes. However, they do not contradict the existence of BHs themselves, as they provide no mechanism for avoiding standard gravitational collapse.

Models whose compactness values are extremely close to those of BHs are the so-called BH mimickers: objects whose surface (if any) is located very close above their gravitational radius (up to few Planck lengths). Spacetime below their surface is very different from that of a BH, and may even cease to be well described by a classical theory of gravity. Among them we find gravastars [91] within GR, $2+2$ holes in quadratic gravity [92], and the fuzzball proposal in string theory [93]. They exhibit a photon sphere, but their potential distinguishability from GR BHs through gravitational-wave echoes is model-dependent [71, 94] since their redshifts can be enormous and thus signals could take a very long time to escape from their interiors.

The central result of this thesis is the discovery of a novel type of object that falls within this last category, as it describes a potential equilibrium configuration towards which matter would eventually relax instead of forming a standard BH. As we will advance in Section 1.3, the key ingredient for the existence of these end-states is the combination of highly compactified classical matter and the repulsive effects characteristic of the quantum vacuum.

Quantum physics and gravity

The presence of singularities at the cores of BHs serves as an indication that GR is not a valid effective theory for the gravitational field in regions of large curvatures [95]. Arguably, an adequate description of these regions will be given

by a fully quantum description of the gravitational field [96, 97]. However, while we await the development of such ambitious theoretical framework, there is a more conservative path to explore within the semiclassical approximation to quantum gravity [33, 36]. Semiclassical gravity aims towards capturing the first deviations from GR driven by quantum physics. In particular, those caused by the quantum nature of matter fields propagating on a classical spacetime, which contributes to—and is affected by—their zero-point energies.

The avenue of exploring semiclassical effects has turned out to be extremely successful through the discoveries of a generation of a primordial power spectrum in inflationary models and of Hawking evaporation [98–101]. Consider a quantum field propagating on the spacetime of a collapsing star. Its vacuum state—or state of minimum energy as perceived by certain observers, in this case inertial observers at past null infinity—is defined as the state initially devoid of any particle content. Long after the collapse and formation of a trapped region has occurred, the vacuum is perceived by observers at future null infinity as filled with a thermal bath of quantum particles [102, 103]. The Hawking effect also predicts an influx of negative energy that penetrates the horizon, which slowly evaporates, being an effect of no relevance for ABHs. This process is possible precisely due to the violation of energy conditions [11, 53] induced by quantum fields, necessary to bypass the area law of classical BH dynamics, which states that the area of a BH horizon always grows. The ultimate implications of extrapolating Hawking evaporation process to its limits (which imply the complete disappearance of the trapped region) have crystallized in the BH information paradox, subject of passionate debate in the last four decades [98, 104, 105]. Through evaporation, semiclassical physics aggravates the concerns raised by curvature singularities by putting them in causal contact with external observers.

The Hawking effect shows that the zero-point energies of quantum fields are sensitive to the presence of gravity. This can manifest in two ways [106]: Through spontaneous particle creation which, in the presence of a horizon, is perceived as radiation by distant observers, and through the phenomenon of vacuum polarization (not to mistake with the homonimous observable, i.e. the renormalized two-point function). This phenomenon appears also in quantum electrodynamics when the vacuum of the electromagnetic field generated by a point-like charge becomes polarized by its very presence. In a gravitational context, the role of the point-like charge is played by the mass and the vacuum states of all fields suffer the corresponding polarization [107]. Any distribution of matter, if the gravitational field is sufficiently intense, becomes affected by gravitational vacuum polarization as if it was immersed in a medium that generates an effective energy density and pressure. These contributions are suppressed by Planck's constant, thus negligible

in most situations. In the presence of strong gravitational fields (i.e. large spacetime curvatures) and near event horizons [108–110], however, vacuum polarization effects must be taken into consideration as they can exert a significant backreaction onto the background spacetime [111–114].

Investigations in semiclassical gravity have centered, to a large extent, around slight modifications to the standard BH paradigm (from an astrophysical perspective). The landscape suggested by semiclassical physics motivates, nonetheless, the following question, pivotal to the rest of this thesis: Is the gravitational contribution of vacuum polarization capable of preserving hydrostatic equilibrium beyond the Buchdahl limit? We will prove that the characteristic violations of energy conditions induced by quantum fields are capable of sustaining stellar bodies in situations where they would inevitably collapse if classical matter alone was present. The quantum forces operating in these extremely compact stars permit the existence of regular horizonless objects that can be made as compact as BHs, serving as well-motivated alternatives to the standard paradigm. This novel result could bridge the existing gap between stellar and black-hole physics, evidencing that, when classical and quantum matter are blended together, exciting new possibilities emerge. In this thesis we will not investigate how is the dynamical process to reach these configurations (there are already suggestions of how this could happen [115, 116]). By showing that these configurations can exist we will just assume here that Nature would find the way to generate them. Our results encourage speculating about the possibility that ABHs may not possess event horizons, their structure resembling instead that of an extremely dark and compact "black star" from which information and matter can indeed escape. Despite long-established beliefs, there might exist a path towards revealing the dark secrets within astrophysical black holes.

1.2 Semiclassical gravity and renormalized stress-energy tensors

The QFTCS programme has a long and fruitful history since its inception with Parker's works on cosmological particle creation [117], their later application to BH evaporation [118] and infinite moving mirrors [119], as well as with other groundbreaking discoveries like the Schwinger [120] and Unruh [121, 122] effects. These phenomena all yield an unambiguous answer when estimating the amount of particles produced due to a non-trivial evolution of the background on which the fields propagate. Being particles themselves also a source of gravity,

spontaneous particle creation phenomena must affect the very same background responsible for it. The observable giving account of both particle creation and vacuum polarization contributions mixed together is the renormalized stress-energy tensor (RSET). There exist prescriptions, such as the point-splitting postulated by Christensen [123], to regularize the (otherwise divergent) stress-energy tensor of quantized fields. Nonetheless, when attempting to do this in practice we encounter difficulties in finding closed, analytic expressions for the RSET.

The Anderson-Hiscock-Samuel RSET

Stress-energy tensor regularization and its calculation on different backgrounds is a whole sub-field within QFTCS. Different methods exist for constructing regularized observables in the quantum theory [33, 124–129] and their convenience depends on the problem under consideration. Nonetheless, the underlying logic is common to all of them: Observables that correspond to products of the field operator and its derivatives are ill-defined from a distributional viewpoint. These divergences can be traced back to the fact that fields can be decomposed in sums over an infinite number of modes with arbitrarily large frequencies. As an ultraviolet effect, these divergent terms are all local, depending on the metric and its derivatives, and can be isolated and subtracted through, for example, a point-splitting regularization [119].

While not being the main focus of this thesis, we have included Appendix A with details on the RSET renormalization of a scalar field with arbitrary mass and coupling in the spacetime (1.2) through the Hadamard regularization method [126, 130, 131]. This method relies on Wick rotating the BH spacetime (1.2), where the Euclidean propagator can be expressed as sums of field modes. The point-split RSET corresponds to the action of a differential operator (A.6) onto the point-split Euclidean bi-scalar, from which we have covariantly subtracted all the ultraviolet divergences, enclosed in the Hadamard distribution (A.8), to finally make the points coalesce. This method yields an exact, conserved RSET which naturally decomposes into

$$\langle \hat{T}^{\mu}_{\nu} \rangle_{\text{ren}} = \langle \hat{T}^{\mu}_{\nu} \rangle_{\text{num}} + \langle \hat{T}^{\mu}_{\nu} \rangle_{\text{AHS}}, \tag{1.4}$$

in which $\langle \hat{T}^{\mu}_{\nu} \rangle_{\text{num}}$ is a numerical quantity that depends on infinite (but convergent) sums of the numeric modes that solve the radial wave equation (A.12); and $\langle \hat{T}^{\mu}_{\nu} \rangle_{\text{AHS}}$ is analytic and depends solely on the spacetime metric, its derivatives, and the free parameters of the theory (the field mass m, its coupling ξ, and an arbitrary renormalization scale required to make the logarithmic term in (A.8)

dimensionless). See Appendix C for its components in the notation of Eq. (6.4). Both parts are covariantly conserved independently, i.e., their divergence vanishes

$$\nabla_\mu \langle \hat{T}^\mu_\nu \rangle_{\rm num} = \nabla_\mu \langle \hat{T}^\mu_\nu \rangle_{\rm AHS} = 0. \tag{1.5}$$

Whereas computing the analytic part (or AHS-RSET in what follows) on a fixed background metric is straightforward and can, in fact, be used as an approximation to the full RSET (see more details in Subsection 1.2.1 below), its numerical counterpart requires careful evaluation. An equivalent splitting (1.4) also appears in cosmological scenarios [132] and for the Dirac field RSET [133].

The infinite mode sums present in $\langle \hat{T}^\mu_\nu \rangle_{\rm num}$ (see [127] for the corresponding expressions) converge slowly and an accurate result requires summing over a vast quantity of modes, something computationally inefficient. To bypass this problem, Howard and Candelas [134, 135] developed a method that consisted in splitting the sums in two parts by adding and subtracting a sufficiently high-order WKB expansion, as in Eq. (A.18), which was used to compute the RSET of various fields in the Schwarzschild spacetime [135, 136]. For the conformally invariant field ($m = 0,\ \xi = 1/6$), the numerical contribution $\langle \hat{T}^\mu_\nu \rangle_{\rm num}$ was found to amount to less than ten per cent of the total RSET, revealing that the analytic part was in excellent agreement with the complete, numerical result. Anderson, Hiscock and Samuel [127] later improved the speed of convergence of the mode sums by including higher orders in the WKB expansions and computed $\langle \hat{T}^\mu_\nu \rangle_{\rm ren}$ in the Reissner-Nordström spacetime (3.2) for massless and massive fields. Recent computational advances allowed to obtain, for the first time, the RSET of a minimally coupled, massless scalar field of an evaporating Kerr BH [137]. Current efforts are being dedicated to compute RSETs of fields of different spins in scenarios of great phenomenological relevance.

The semiclassical Einstein equations

Computing the RSET on fixed backgrounds informs about how vacuum energies respond to the curvature of spacetime and can give indication of regions of spacetime where quantum effects become relevant, like inner horizons [138, 139], but the interest of the QFTCS program does not stop there. Once a closed expression for the RSET is available, it is tempting to introduce it in the right-hand side of the Einstein equations as an additional curvature source and analyze its impact on the background spacetime. The resulting expressions are the semiclassical Einstein equations

$$G_{\mu\nu} = 8\pi \left(T_{\mu\nu} + \hbar \langle \hat{T}_{\mu\nu} \rangle_{\rm ren} \right), \tag{1.6}$$

where we explicitly show the dependence on $\hbar$ that accompanies the RSET. The semiclassical equations put on equal footing a classical spacetime geometry with a matter content that can have both classical and quantum contributions. Eqs. (1.6) can be argued to be nothing but an approximation to a quantum theory of gravity in which the gravitational field is treated as classical (see [140] and references therein). Our objective in this thesis is to solve the semiclassical equations in a full, self-consistent manner. That is, we want to determine the background spacetime and the sources that generate it simultaneously, something entirely different from computing the RSET on a fixed background geometry. The numerous difficulties one finds along this path motivate the introduction of approximate RSETs. In the next Subsection, we elaborate on the various subtleties present in semiclassical backreaction analyses.

1.2.1 The trouble with backreaction

Self-consistent solutions to the semiclassical Einstein equations (1.6) describe spacetimes that are consistent with the same vacuum polarization that they generate. The particularities of these configurations will depend on the method followed to estimate quantum contributions, i.e. the physical content included in the RSET. As we will see in what follows, the semiclassical equations are exactly solvable in practice only if the RSET is subjected to additional simplifications.

Perturbative semiclassical gravity

Equations (1.6) result from the truncation to linear order in $\hbar$ of an effective quantum-gravitational action [141, 142]. Such truncation is justified on the basis of a perturbative expansion in $\hbar$ and, in a strict sense, is valid only if terms of superior order are sub-leading with respect to contributions of $\mathcal{O}(\hbar)$. This aspect deems the solutions to the semiclassical equations physically reliable only in the perturbative regime. Nonetheless, the semiclassical equations resulting from the truncated expansion are, in common practice, solved as a closed system [112, 143–145], and their solutions can exhibit corrections non-perturbative in $\hbar$. By non-perturbative we mean that the resulting spacetime does not exhibit a smooth $\hbar \to 0$ limit and/or that the RSET becomes $\mathcal{O}\left(\hbar^{-1}\right)$. Numerous authors have argued that this is plainly inconsistent with the logic behind the semiclassical approximation [36, 140, 141], which only makes sense as a theory governing perturbative corrections over some fixed classical spacetime. Although this interpretation is entirely valid, we will argue that there is still room to gain valuable insight into the way quantum

corrections operate in extreme scenarios by addressing the non-perturbative regime of the semiclassical equations. We elaborate on that in what follows.

Consider the semiclassical equations (1.6) sourced by the RSET (1.4). As detailed before, this RSET is the sum of independently conserved numerical and analytical parts. The numerical portion is not amenable to backreaction analyses in full self-consistency since it is expressed as an infinite mode sum, said modes depending on (and at the same time being the source of) the background spacetime on which they propagate. Thus, without first assuming some "zeroth-order" background we are unable, in practice, to compute the exact RSET. As the full backreaction problem is extraordinarily complex, we are confronted with two options: Limiting ourselves to perturbative backreaction analyses or subjecting the RSET to additional simplifications.

As for the first option, we assume the following expansion of the semiclassical equations holds

$$G^{(0)}_{\mu\nu} + \hbar G^{(1)}_{\mu\nu} + \mathcal{O}\left(\hbar^2\right) = 8\pi T_{\mu\nu} + 8\pi\hbar\langle\hat{T}_{\mu\nu}\rangle_{\text{ren}} + \mathcal{O}\left(\hbar^2\right), \tag{1.7}$$

where the lowest order in $\hbar$ is sourced by the zeroth-order (classical) solution. Then, the corresponding RSET is used to compute $G^{(1)}_{\mu\nu}$, which is subsequently used to obtain the next order, and so on. There exist some applications of this method to compute backreaction with the exact RSET [129] as well as through analytic approximations [146, 147], but they are scarce due to their inherent complexity and the phenomena they give rise to is bound to their perturbative nature.

The second option is the one we adopt in this thesis by proposing well-motivated analytic RSETs for which the semiclassical equations (1.6) can be solved in closed form. The most direct approach would be to neglect the numerical contribution in (1.4) entirely and consider the conserved analytic portion as an approximation to the total RSET. That provides us with analytic semiclassical equations that can be solved in full form. However, this is no easy task as the AHS-RSET has a considerable shortcoming that must be addressed beforehand.

Shortcomings of the AHS-RSET

The most problematic aspect of the AHS-RSET is that it exhibits third and fourth order derivatives of the metric functions. These terms appear in the covariant Taylor expansions of the Hadamard parametrix (A.8) and have many parallels to similar high-derivative terms in the Abraham-Lorenz equation [148]. They are the result of demanding a purely local quantity, the RSET, constructed from an object, the propagator, that is non-local by construction. In addition, there is a local ambiguity

in the RSET, in the form of a free parameter whose value is to be ultimately fixed through experiments. Although this introduces additional uncertainties in the local physics captured by the RSET, non-local contributions associated with vacuum states (whose definition is global) are independent of this free parameter and agree between approximations.

High derivatives in the RSET carry an enlargement of the space of solutions of the theory, as the dimension of the space of initial data required to uniquely determine a solution increases with the differential order of the semiclassical equations. More so, among an enlarged space of solutions there might exist spurious, runaway, or nonphysical solutions that must be disregarded. Simple examples of this are the runaway solutions in the radiation–reaction equation [149, 150] and, within quantum field theory, solutions that trigger instabilities in Minkowski spacetime within Planckian timescales [151].

Given the situation, a programme started by Simon [141] and Parker [144] materialized in a prescription of order reduction, based on imposing a criterion of perturbative consistency onto the semiclassical equations. Simon and Parker regarded every semiclassical solution non-perturbative in $\hbar$ as plain nonphysical, and developed a simple scheme that allowed to obtain a set of semiclassical equations of second order with an initial value problem equivalent to the one from GR. The reduction of order is not exclusive from semiclassical theories and has been extensively used in the radiation reaction problem [149], in theories with quadratic Lagrangians [152] and other effective field theories [153]. Within semiclassical gravity, solutions to order-reduced equations have been mostly obtained in cosmological scenarios [141, 144, 154] and to prove the stability of Minkowski spacetime [155].

In Chapter 6 we detail the first application of the order reduction to semiclassical equations sourced by the AHS-RSET. However, we could not have come to realize the usefulness of this procedure without first appealing to a simpler RSET approximation widely used in the literature: The Polyakov approximation. Contrarily to the AHS-RSET, the Polyakov RSET is only valid for massless and minimally coupled scalar fields. Since modified versions of the Polyakov RSET will be used for most of this thesis (Chapters 2 to 5) we turn to describe its derivation, benefits and drawbacks in the following Subsection.

To summarize, we adopt a self-consistent approach to solving the semiclassical equations (1.6) that is no different from how other modified theories of gravity are treated, where the aim is to classify the complete space of solutions without appealing to these theories being embedded in some superior, unknown framework. Our interest relies in classifying the complete space of solutions of the semiclassical equations without attending to their smoothness in the $\hbar \to 0$ limit, as there is

information in the non-perturbative characteristics that the semiclassical approximation should preserve when higher orders in $\hbar$ are included. These are the characteristics (namely, boundary conditions and singular behavior) associated with the modes in which the field is decomposed, and that eventually percolate onto the defining features of the various vacuum states and, by extension, to the RSET. If these features were not robust, not even Hawking radiation could be trusted as the generic phenomenon that we believe it to be.

1.2.2 The regularized Polyakov approximation

Polyakov RSET

By means of analyzing the propagation of a massless quantum scalar field on a $1+1$ dimensionally-reduced metric [corresponding to the (t,r) sectors of (1.2)], it is possible to obtain an RSET that is simple, analytical, unambiguous, and contains only up to second-order derivatives of the metric functions. The resulting $(1+1)$-dimensional RSET is then taken as the backbone of a $(3+1)$-dimensional RSET. Through this process, we obtain a quantity amenable to self-consistent backreaction analyses at the cost of reducing the physical content of the RSET, which only takes into account the contribution from s-wave modes and neglects their backscattering due to the gravitational potential. This RSET predicts infinite energy and pressure contributions at the radial origin and has vanishing pressures in the angular directions. The missing information about its behavior at $r=0$ has to be supplied by hand by specifying a radial function. This Subsection will be devoted to the derivation of the celebrated Polyakov approximation [156]. Numerous backreaction analyses, both in two-dimensional dilaton gravity and four-dimensional semiclassical gravity, have been done under this approximation [112, 145, 157, 158] that remains indisputably the most prolific RSET approximation on that regard.

The derivation of this RSET in $(1+1)$-dimensional spacetimes requires a point-splitting regularization, which is dramatically simplified by the conformal flatness of the metric. We have moved the details of this regularization to Appendix B. This procedure requires specifying a basis of modes in which the field is expanded. Since the wave equation (B.6) has analytic plane-wave solutions, the Polyakov RSET can be expressed in closed analytic form. We choose the mode decomposition (B.10), which selects the Boulware vacuum as the state in which the RSET is evaluated. The Boulware state reduces to the Minkowski vacuum at the asymptotically flat regions of spacetime, so it is perceived as empty by static asymptotic observers. In exchange, the field modes (B.10) are ill-defined at the event horizon, hence the

Boulware vacuum becomes singular there as well and this singularity shows up in the RSET. Because of this, the Boulware vacuum has been typically regarded as not appropriate to introduce corrections to BHs, only suitable to correct horizonless static stellar structures. This is, however, an important misconception. The main inquiry of this thesis is precisely whether semiclassical gravity contains static stellar solutions beyond those found in the classical theory, and in that search we must impose the Boulware vacuum. When allowed to backreact onto the background spacetime through the semiclassical equations (1.6), the geometry can absorb in some cases the singularity in the RSET through non-perturbative corrections, leading to a perfectly self-consistent solution threaded by the Boulware vacuum, which is also the unique state compatible with the staticity and asymptotic flatness of spacetime. In the remaining of this thesis we will exclusively consider quantum effects in the Boulware vacuum for situations both with and without classical matter.

After regularization, the Polyakov approximation only involves identifying the RSET components in the dimensionally-reduced and the four-dimensional manifolds. First, we write down the RSET components in Schwarzschild coordinates (B.8),

$$\begin{aligned}\langle\hat{T}_{rr}\rangle^{\mathrm{P2}} =& -\frac{l_{\mathrm{P}}^2\psi^2}{2}, \qquad \langle\hat{T}_{tr}\rangle^{\mathrm{P2}} = \langle\hat{T}_{rt}\rangle^{\mathrm{P2}} = 0,\\ \langle\hat{T}_{tt}\rangle^{\mathrm{P2}} =& \frac{l_{\mathrm{P}}^2 e^{2\phi}}{2}\left[2\psi'(1-C)+\psi^2(1-C)-\psi C'\right],\end{aligned} \tag{1.8}$$

where $l_{\mathrm{P}}^2 = \hbar/12\pi$ and $\psi \equiv \phi'$, the prime denoting derivatives with respect to the r coordinate. From the tensor (1.8), conserved in $1+1$ dimensions by construction, we can build a $(3+1)$-tensor which is now conserved in $3+1$ dimensions:

$$\langle\hat{T}_{\mu\nu}\rangle^{\mathrm{P4}} = \frac{1}{4\pi r^2}\delta^a_\mu\delta^b_\nu\langle\hat{T}_{ab}\rangle^{\mathrm{P2}}, \tag{1.9}$$

where Latin indices take only two values: r and t. The multiplicative factor $1/4\pi r^2$ is introduced to ensure conservation of $\langle\hat{T}_{\mu\nu}\rangle^{\mathrm{P4}}$. The appearance of this multiplicative factor is due to the RSET being oblivious to the behavior at $r=0$. This property traces back to the mode decomposition (B.10). Being defined for a field that propagates on a dimensionally-reduced spacetime, these modes are ill-defined at short distances in four-dimensional spacetimes. This property gets transferred to the RSET, making it singular at $r=0$, unless we introduce some regularization mechanism by hand. In the following we elaborate on the singularity of the Polyakov RSET and possible choices of regularization.

Regularity at $r = 0$

The Polyakov RSET (1.9) diverges at $r = 0$ even in entirely regular spacetimes. For the metrics we are analyzing, the Kretschmann scalar $\mathcal{K} = R_{\mu\nu\rho\sigma}R^{\mu\nu\rho\sigma}$ takes the form

$$\mathcal{K} = \frac{4C^2}{r^4} + \frac{2C^{2\prime}}{r^2} + \frac{8\psi^2(1-C)^2}{r^2} + \Big[\psi C' - 2(\psi^2 + \psi')(1-C)\Big]^2 . \tag{1.10}$$

In spherical symmetry a finite Kretschmann scalar ensures that the geometry is devoid of any curvature singularity contained in the Riemann tensor [13, 159]. This criterium excludes non-scalar curvature singularities [160] that manifest upon contracting the Riemann curvature tensor with some tetrad fields associated with physical observers.

From this expression we can obtain the conditions that the metric functions need to satisfy at $r = 0$ in order to guarantee a finite $\mathcal{K}$, hence defining a regular geometry. Written in terms of the redshift and compactness functions ϕ and C, these conditions enforce

$$\phi = \phi_0 + \phi_1 r^2 + \mathcal{O}\big(r^3\big), \qquad C = C_1 r^2 + \mathcal{O}\big(r^3\big), \tag{1.11}$$

where $\phi_0,\ \phi_1$ and C_1 are constants.

Given geometries with the regular local behavior (1.11) at $r = 0$, the proof of the divergence in the $(3+1)$-dimensional Polyakov RSET (1.9) is straightforward. Indeed, by taking the first term in the tt component (1.8) we can see the existence of a $1/r^2$ divergence for the previously described behaviors $\psi \propto r$ and $C \propto r^2$. If we used the Polyakov RSET as a source in the semiclassical equations and tried to look for self-consistent stellar-like configurations, we would not find any compatible with semiclassical effects, even in situations where these should amount to a perturbative correction over the classical solution. Consequently, we explicitly see that the Polyakov RSET is not suitable for the search of regular semiclassical stellar configurations.

Regularized Polyakov RSET

One possibility in order to obtain an appropriate RSET which is at least qualitatively trustworthy through the whole geometry is to regularize the Polyakov RSET. This analysis is addressed in a step-by-step basis, as the first priority is obtaining an RSET that is regular at $r = 0$ and only then we can worry about how accurately this RSET resembles the four-dimensional exact RSET near $r = 0$. That the Polyakov RSET must be regularized in order to deal with practical situations has been noticed

before, for example in the numerical implementation by Parentani and Piran [145] of a semiclassical gravitational collapse. We advance here that our regularization procedure is only valid in static scenarios as it fails to recover a simultaneously regular and covariantly conserved RSET in dynamical spacetimes [145, 161].

Inspired by previous works, we introduce an arbitrary radial function $F(r)$ in the temporal and radial components of the Polyakov RSET as

$$\langle\hat{T}_{\mu\nu}\rangle^{\text{DP}} = \frac{F(r)}{4\pi}\delta^a_\mu\delta^b_\nu\langle\hat{T}_{ab}\rangle^{\text{P2}}, \tag{1.12}$$

the suffix DP standing for Distorted Polyakov. Taking

$$F(r) = 1/r^2 \tag{1.13}$$

returns the usual Polyakov RSET divergent at $r = 0$, but choices of $F(r)$ finite at $r = 0$ return a DP-RSET similarly regular at $r = 0$. The multiplicative factor $F(r)$ constitutes an attempt to regularize the RSET in the most simple and mild way. It is straightforward to check that this regularization of the Polyakov RSET carries along the non-conservation of this object. Thus, finding a proper RSET both regular and conserved requires adding to the Distorted Polyakov RSET an additional Compensatory piece. This Compensatory RSET will be assumed, for simplicity, to have only angular contributions. Its components are obtained by requiring that the divergence of the total tensor vanishes. As a result we obtain the Regularized Polyakov RSET (RP-RSET) which we are going to use for the most part of this thesis.

Leaving the radial function F undetermined, the RP-RSET looks as follows

$$\begin{aligned}
&\langle\hat{T}_{rr}\rangle^{\text{RP}} = -F\,\frac{l_{\text{P}}^2\psi^2}{8\pi}, \quad \langle\hat{T}_{rt}\rangle^{\text{RP}} = \langle\hat{T}_{tr}\rangle^{\text{RP}} = 0,\\
&\langle\hat{T}_{tt}\rangle^{\text{RP}} = F\,\frac{l_{\text{P}}^2 e^{2\phi}}{8\pi}\left[2\psi'\,(1-C) + \psi^2\,(1-C) - \psi C'\right],\\
&\langle\hat{T}_{\theta\theta}\rangle^{\text{RP}} = \frac{\langle\hat{T}_{\varphi\varphi}\rangle}{\sin^2\theta} = -\,(2F + rF')\;\frac{l_{\text{P}}^2 r^2}{16\pi}\,(1-C)\,\psi^2.
\end{aligned} \tag{1.14}$$

Now, the simplest choice of the function F that yields a regular RSET at $r = 0$ is

$$F = \frac{1}{r^2 + \alpha l_{\text{P}}^2}, \tag{1.15}$$

where α is a positive constant parameter that controls the suppression suffered by the RSET at $r = 0$. Whereas $\alpha > 0$ is sufficient for RSET regularity, the semiclassical equations enforce $\alpha > 1$ to have as solutions geometries that are locally regular, i.e. that obey expansions of the form (1.11) (proof can be found in Chapter 2). We

name Cutoff-Regularized Polyakov RSET (CRP-RSET) the expressions that result from applying the regulator choice (1.15) to the RSET (1.14).

Contrarily to the Polyakov RSET, the CRP-RSET is regular at $r = 0$ and contains non-vanishing angular components, both being features that the four-dimensional AHS-RSET (1.4) manifests, but at the same time only exhibiting up to second derivatives of the metric functions. The angular components of the CRP-RSET vanish for $\alpha = 0$ and behave properly in the $r \to 0$ limit when $\alpha \neq 0$, by virtue of the regularity conditions (1.11):

$$\langle \hat{T}_{\theta\theta}(r \to 0) \rangle^{\text{CRP}} = -\frac{\phi_1^2}{2\pi\alpha} r^4 + \mathcal{O}(r^6). \tag{1.16}$$

The regularization scheme that we have adopted is by no means unique, since there exists an infinite number of regularizing functions that ensure that the RP-RSET achieves the desired properties. The choice of a better (i.e. more accurate) regulating function should ideally contain information about characteristics of the spacetime geometry close to the radial origin, and be capable of reproducing the physics predicted by four-dimensional RSET approximations. It will be important to keep this in mind when extracting conclusions from our analysis of the semiclassical equations.

In Chapters 2, 3, and 4 we find the self-consistent semiclassical solutions in absence of classical matter, in presence of an electromagnetic field, and with a perfect isotropic fluid of constant density, respectively. All these analyses consider the CRP-RSET as the source. In the vacuum and electrovacuum cases, since the classical counterparts are already singular (as we will show), the finiteness of the RSET at $r = 0$ only affects solutions where the values of the ADM mass and the charge are Planckian. In the analysis of stellar-like configurations, however, the choice of regularization scheme for the RSET is of key importance, as the sign and magnitude of the RSET in a neighborhood of $r = 0$ have strong implications on the resulting solutions, specially when the configurations are progressively made more compact.

The knowledge gathered from studying constant-density stars in the CRP-RSET approximation leads us to consider other regularization schemes for the RP-RSET that only modify its form within a central core. Under this prescription, we obtain in Chapter 5 semiclassical solutions describing regular stars that surpass the compactness of the stellar objects in general relativity.

1.3 Hydrostatic equilibrium in the semiclassical approximation

We devote this Section to introduce some preliminary notions about stellar equilibrium in general relativity and semiclassical gravity. Then, we highlight the main findings of this thesis relating stellar configurations supported by repulsive quantum effects captured by different RSET approximations.

1.3.1 Surpassing the Buchdahl limit

As we motivated in the first part of this Introduction, if we expect some putative object in hydrostatic equilibrium to supplant ABHs, there is an insurmountable obstacle to be taken into account: The Buchdahl compactness limit.

Buchdahl theorem

The Buchdahl limit is a bound to the maximum compactness that applies to any static and spherically symmetric stellar object in hydrostatic equilibrium satisfying the following properties [57, 70, 162]

1. It smoothly matches the Schwarzschild geometry (1.3) at the surface.
2. Pressure in the angular directions does not surpass pressure in the radial direction.
3. The energy density is a monotonically decreasing function of the radial coordinate from the center of the star to the surface.

Under these assumptions, it is possible to prove that there exists no regular configuration in hydrostatic equilibrium with

$$C_{\mathrm{R}} \equiv C(R) \geq 8/9, \tag{1.17}$$

where C_{R} is the surface compactness (i.e. the value of the C function at the star's surface $r = R$). Surpassing this limit requires that either the matter conforming the star has some degree of exoticness (measured by the violation of properties 2 and 3), or that the exterior geometry differs from Schwarzschild's. There is an immense range of surface compactness values between the Buchdahl limit and the BH limit $C_{\mathrm{R}} = 1$. In fact, if further constraints are put onto the matter fluid that conforms the star (dominant energy condition and causality, mainly), the upper compactness limit decreases [163, 164], making it even more strict. In this thesis,

we limit ourselves to the study of constant-density fluid spheres, as they are the simplest stellar models and, in absence of quantum corrections, they saturate the Buchdahl bound.

We will return to the Buchdahl limit in Chapters 4 and 5, where we will analyze the impact that semiclassical corrections have on it. For now, we will advance that semiclassical effects captured by any adequate RSET approximation are potentially able to overcome all the assumptions behind the Buchdahl limit, making semiclassical gravity a promising theory to look for novel exotic compact objects.

Generic semiclassical effects

In Sec. 1.2 we have introduced two analytic RSET approximations, the AHS-RSET and the RP-RSET. These approximations are distinguished by their trade-off between physical accuracy and mathematical complexity. Despite the aforementioned difficulties in providing a unique, closed expression for the RSET, semiclassical physics exhibits some generic features.

First and foremost, RSETs violate the point-wise energy conditions [108, 165]. Such violations will, of course, depend on the background geometry on which the field propagates and on the characteristics of the field itself. In the vacuum Schwarzschild geometry, the RSET (for massless minimally coupled fields) in the Boulware vacuum violates all point-wise energy conditions [108]. In the interior region of fluid spheres, however, an exact calculation of the RSET is still lacking for non-conformally-invariant fields. Results for conformally invariant fields reveal that the semiclassical energy density can become negative and divergent in the central regions of constant-density stars approaching the Buchdahl limit [166, 167]. Consequently, semiclassical backreaction must be taken into account in stars approaching the Buchdahl limit.

Renormalized tensors are also anisotropic except for some special prescriptions [168], being able to potentially violate the second hypothesis of Buchdahl's theorem. Furthermore, there are scenarios in which violations of energy conditions can become $\mathcal{O}\left(\hbar^0\right)$, e.g. at event horizons or the center of stars in the $C_{\rm R} \to 8/9$ limit. At event horizons, the singular nature of the Boulware vacuum will backreact on the spacetime, dramatically affecting the Schwarzschild solution. In the central regions of stars approaching the Buchdahl limit, the RSET can change the sign of the total energy density (the sum of classical and quantum contributions) making it negative. These generic characteristics of RSETs allow to violate all the hypotheses behind the Buchdahl theorem. Remarkably, this is indeed what we find in semiclassical gravity: The existence of regular stars that surpass Buchdahl limit and that can be made as compact as BHs.

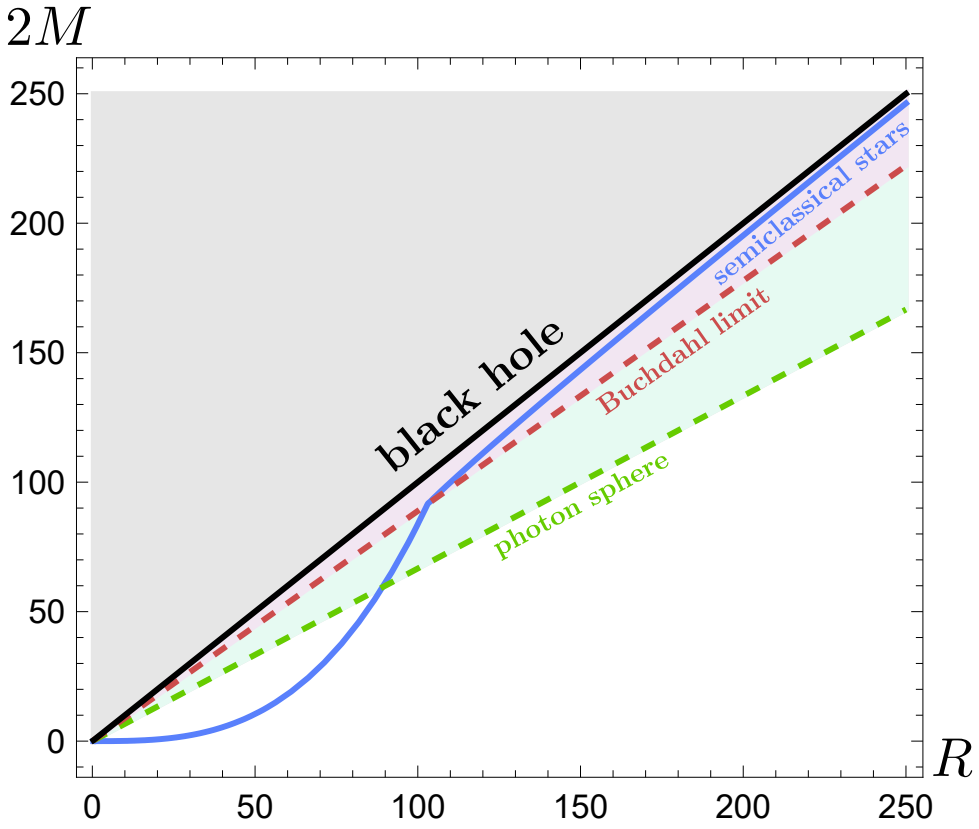

Fig. 1.1.: Mass-radius diagram of semiclassical relativistic stars with $\rho = 10^{-5}$ (in Planck units). The black line represents the compactness parameter of BHs $(C_R = 1)$, the dashed red line denotes the Buchdahl compactness bound $(C_R = 8/9)$, and the dashed green line is the minimum compactness of objects that exhibit a photon sphere $(C_R = 1/3)$. The blue curve represents semiclassical relativistic stars. For stars surpassing the Buchdahl limit, the total mass M grows approximately linearly with the radius R. Each point within the blue curve admits entire families of regulator functions $F(r)$ in the RP-RSET for which the whole geometry is regular. A similar diagram is obtained by applying an order reduction to the AHS-RSET.

1.3.2 Semiclassical relativistic stars

The investigations detailed throughout this thesis materialized in the discovery of a novel family of ultracompact objects supported by semiclassical effects. In short, the contributions from the RSET, when allowed to backreact onto the background spacetime, make the total energy density (the sum of classical and quantum contributions) to violate the third hypothesis of the Buchdahl theorem. The main difficulty we faced in these explorations was to find RSETs that properly capture the most prominent aspects of semiclassical physics while being well defined at the center of stars $(r = 0)$ and of second derivative order in the metric, so that the semiclassical equations (1.6) can be solved in a full self-consistent way. We have derived two RSET approximations that satisfy these requirements: the RP-RSET

(see Subsec. 1.2.2) and the matter-order-reduced AHS-RSET (or MOR-AHS-RSET, see Ch. 6 for details). Both approaches end up giving rise to regular stars with similar qualitative features that surpass the Buchdahl limit. In these situations, the Misner-Sharp mass, which is positive at the surface of the star, decreases towards the interior and becomes negative, to later vanish at $r = 0$. The redshift function decreases monotonically towards the interior and reaches values at $r = 0$ several orders of magnitude smaller than its surface values, indicating that light rays emitted outwards from the center suffer large redshifts.

One of the most remarkable properties of the semiclassical star model that we have found is that it describes whole families of stellar geometries whose surface compactness C_{R} can range from arbitrarily small, thus describing constant-density stars where quantum corrections are perturbative, to arbitrarily large ones, with solutions that approach the black-hole limit $C_{\mathrm{R}} = 1$. In fact, the RP-RSET allows to find perfectly regular stars with $C_{\mathrm{R}} = 1$ while stars sourced by the MOR-AHS-RSET are singular in the $C_{\mathrm{R}} \to 1$ limit. This discrepancy is due to the particularities of the respective exterior vacuum solutions and its implications are left for future study. Instead, here we want to emphasize that the existence of regular semiclassical stars spanning a broad range of compactness values is an extremely appealing feature of this model and can be of great interest to phenomenological studies, such as understanding the mechanisms for the production of gravitational-wave echoes in stars surpassing the Buchdahl limit $C_{\mathrm{R}} = 8/9$ and that approach the black-hole limit $C_{\mathrm{R}} = 1$.

Figure 1.1 shows the mass-radius diagram of the semiclassical stars derived in Chapter 5 (this diagram is identical for the stars derived later in Ch. 6). Straight lines correspond to constant compactness values, and we have represented three relevant compactness values: The compactness of objects that exhibit a photon sphere [26], the Buchdahl limit, and the black-hole limit. The blue curve in Figure 1.1 describes a family of regular semiclassical stars with the same classical density ρ and with different total radius and mass. Typical stellar models present maxima in these diagrams that indicate the presence of unstable branches of solutions. Here, this feature is absent, and we can distinguish three regimes, sub-Buchdahl, Buchdahl, and super-Buchdahl, depending on C_{R}. As mentioned, the sub-Buchdahl regime corresponds to constant-density stars that receive only perturbative quantum corrections. The Buchdahl regime shows a drastic transition in the shape of the blue curve, going from an $M \propto R^3$ behavior below the Buchdahl limit to an $M \propto R$ behavior above it. This indicates an abrupt increase in the magnitude of quantum corrections as the Buchdahl limit is approached. The super-Buchdahl regime displays stars that can become as close to the BH limit as desired. This continuous family of solutions suggests that, in principle, semiclassical stars

could belong to both families, exotic compact objects and BH mimickers. Of course, we are just claiming that these models could serve as qualitative approximations based on effective spacetimes to the surely more complicated structures of ABHs, if they are finally not BHs in the first place.

In summary, our results reveal that two independent modelings of the RSET share a common physics and that semiclassical stars are not just an artifact of one particular RSET approximation. The existence of stars with akin properties within seemingly unrelated approaches allows to derive robust conclusions from semiclassical analyses—and to subject them to tension. Future, more elaborate models of the matter content of semiclassical stars may provide cumulative evidence for the existence of new stages of stellar equilibrium that can be put to the test with forthcoming observational capabilities.

2

Schwarzschild geometry counterpart in semiclassical gravity

2.1 Introduction

This Chapter will be devoted to the derivation and analysis of the semiclassical counterpart to the Schwarzschild spacetime. By semiclassical Schwarzschild counterpart, we mean the spacetime sharing the assumptions of staticity, spherical symmetry, asymptotic flatness and absence of a classical SET (thus vacuum) that characterize the Schwarzschild spacetime, but corrected by the backreaction of an RSET. It corresponds to the self-consistent solution to the semiclassical equations (1.6) in vacuum

$$G^{\mu}_{\nu} = 8\pi\hbar\langle\hat{T}^{\mu}_{\nu}\rangle, \tag{2.1}$$

where the right-hand side is evaluated in the Boulware vacuum state. As explained in the Introduction, this vacuum state guarantees that the RSET is consistent with the aforementioned assumptions of staticity and asymptotic flatness [169]. In exchange, the Boulware state—and, in turn, the RSET—is singular at event horizons, implying that these surfaces cannot exist in the self-consistent solutions to Eqs. (2.1).

As for the approximate scheme followed to derive the RSET, we will work with the Cutoff-Regularized Polyakov RSET (CRP-RSET) derived in Subsec. 1.2.2. This regularization consists in specifying the regulator function F in the components (1.14) to be of the form (1.15), in such a way that the RSET reproduces the correct spherically-symmetric behavior at large distances [145] while ensuring its finiteness at $r = 0$ when evaluated on regular spacetimes. This way, we solve the semiclassical equations (2.1) with an RSET that is well-defined by construction. A similar analysis with the (unregularized) Polyakov RSET was previously pursued in [112, 170]. Our regularization has a minor impact on the qualitative features of most vacuum solutions. Since the classical Schwarzschild spacetime already displays a curvature singularity, we do not expect that the backreaction of the

CRP-RSET manages to regularize it. Nonetheless, the CRP-RSET allows to extend the space of solutions found in [112] to situations in which the ADM mass M is comparable in magnitude to the Planck length $l_{\rm P}$. In this regime (which lies outside the regime of validity of semiclassical gravity), the solutions rely heavily on the particular form of the RP-RSET.

A remarkable characteristic of the semiclassical static solutions is that they cannot posses sub-extremal horizons. By sub-extremal we mean a horizon characterized by a positive surface gravity

$$\kappa = \psi e^{\phi}\sqrt{1-C}|_{r=r_{\rm H}}, \tag{2.2}$$

which corresponds to a behavior of the metric functions of the form

$$e^{2\phi} \propto \frac{r-r_H}{r_{\rm H}}, \qquad 1-C \propto \frac{r-r_H}{r_{\rm H}}. \tag{2.3}$$

The RP-RSET shows a divergence at $r = r_{\rm H}$ when evaluated over such spacetimes. This can be seen directly from Eq. (1.9) by calculating e.g. the energy density and radial pressure

$$\begin{aligned}\rho_{\rm s} =& e^{-2\phi}\langle\hat{T}_{tt}\rangle^{\rm P4} = \frac{l_{\rm P}^2}{8\pi r^2}\left[2\psi'(1-C)+\psi^2(1-C)-\psi C'\right],\\ p_{\rm s}^r =& (1-C)\,\langle\hat{T}_{rr}\rangle^{\rm P4} = -\frac{l_{\rm P}^2\psi^2}{8\pi r^2}(1-C).\end{aligned} \tag{2.4}$$

Assuming the metric behaves as (2.3), we have

$$\rho_{\rm s} = p_{\rm s}^{\rm r} \propto -\frac{l_{\rm P}^2}{r_{\rm H}^3\,(r-r_{\rm H})} + \mathcal{O}\left(\frac{r-r_{\rm H}}{r_{\rm H}}\right)^0. \tag{2.5}$$

Note that, to ensure that these divergence are physical, the RSET must be expressed in a set of coordinates regular at the horizon, such as the Kruskal coordinates [101]. An alternative (though equivalent) proof involves evaluating the RSET components in an orthonormal frame associated to a timelike observer in free fall [171]. In particular, regularity of the RSET at $r = r_{\rm H}$ is not possible if the following quantity [172]

$$\mathcal{E} = \left(\langle\hat{T}_r^r\rangle^{\rm P4} - \langle\hat{T}_t^t\rangle^{\rm P4}\right)e^{-2\phi} \propto -\frac{l_{\rm P}^2}{r_{\rm H}^2\,(r-r_{\rm H})^2} + \mathcal{O}\left(\frac{r-r_{\rm H}}{r_{\rm H}}\right)^0, \tag{2.6}$$

diverges. Since the RP-RSET is clearly singular at sub-extremal horizons, any self-consistent solution to the semiclassical Eqs. 2.1 will be horizonless. A similar

divergence in the RP-RSET (although milder) shows up at extremal horizons, as we will see in Ch. 3.

There is a twofold interest behind studying the semiclassical counterpart to the Schwarzschild spacetime. Firstly, on a technical front, this analysis establishes the bases of the tools and techniques that we will apply from Chapter 3 to 5. Secondly, the situation with positive ADM mass has a clear physical interpretation as the exterior geometry to any fluid sphere coexisting with vacuum polarization effects. In absence of classical matter, we find no regular spacetimes sourced solely by vacuum polarization effects. Since event horizons are also absent in the solutions due to the characteristics of the Boulware vacuum state, this finding suggests the need for introducing classical matter in order to construct static spacetimes free from pathologies, i.e. with singularities not hidden behind event horizons. On top of this, the present analysis constitutes a proof for the nonexistence of regular semiclassical geons [173] originated solely by the effects of quantum vacuum polarization that are captured through the Polyakov model.

This Chapter is organized as follows. First, in Section 2.2 we cast the semiclassical equations into a single, first order ordinary differential equation whose solutions can be found analytically in some special regimes. In Section 2.3 we integrate this equation from an asymptotically flat region inwards, providing analytic arguments that determine the solution uniquely. The main properties of these geometries are highlighted. Finally, in Section 2.5 we elaborate on the implications of these findings and pave the way for their generalization to the electrovacuum scenario.

2.2 Self-consistent vacuum semiclassical equations

In what follows we present and solve the semiclassical Einstein equations (2.1) sourced by the CRP-RSET [i.e. the RSET (1.14) where $F(r)$ obeys (1.15)]. The rr and tt components of the equations (2.1) become

$$C = \frac{2r\psi + l_{\rm P}^2 r^2\psi^2/(r^2+\alpha l_{\rm P}^2)}{1+2r\psi + l_{\rm P}^2 r^2\psi^2/(r^2+\alpha l_{\rm P}^2)}, \tag{2.7}$$

$$C' = \frac{-C/r + r l_{\rm P}^2(1-C)\left(\psi^2+2\psi'\right)/(r^2+\alpha l_{\rm P}^2)}{1+r l_{\rm P}^2\psi/(r^2+\alpha l_{\rm P}^2)}. \tag{2.8}$$

These expressions are reducible to a single, first order differential equation for ψ by replacing (2.7) and its first derivative in (2.8), resulting in

$$\psi' = -\mathcal{A}\left(\psi - \mathcal{R}_1\right)\left(\psi - \mathcal{R}_2\right)\psi, \tag{2.9}$$

with

$$\begin{aligned}
\mathcal{A} =& \frac{l_{\rm P}^2 r\left[\left(r^2+\alpha l_{\rm P}^2\right)^2+\alpha l_{\rm P}^4\right]}{\left(r^2+\alpha l_{\rm P}^2\right)^2\left[r^2+(\alpha-1)l_{\rm P}^2\right]},\\
\mathcal{R}_{1,2} =& -\Bigg[\left(r^2+\alpha l_{\rm P}^2\right)^2+l_{\rm P}^2\left(r^2/2+\alpha l_{\rm P}^2\right)\\
&\pm\Bigg(\left[r^2+\alpha l_{\rm P}^2\right]^4-l_{\rm P}^2\Big\{r^2\left(r^2+\alpha l_{\rm P}^2\right)^2\\
&+l_{\rm P}^2\left[\left(r^2/2+\alpha l_{\rm P}^2\right)^2-r^4/2\right]\Big\}\Bigg)^{1/2}\Bigg]\\
&\times\left[\mathcal{A}\left(r^2+\alpha l_{\rm P}^2\right)\left(r^2+(\alpha-1)l_{\rm P}^2\right)\right]^{-1}.
\end{aligned}$$

This is the central expression of this Chapter, from where the function ψ is obtained by integrating Eq. (2.9). The C function can then be derived from the constraint Eq. (2.7), and so the complete spacetime metric.

Some observations about Eq. (2.9) are relevant at this stage. This expression is singular at $r^2 = (1-\alpha)l_{\rm P}^2$, where the denominator of $\mathcal{A}$ vanishes. The introduction of the positive parameter α as regulator of the RP-RSET is enough to construct a CRP-RSET that is finite for any given regular fixed background spacetime. However, dealing with the self-consistent semiclassical equations requires imposing more stringent conditions to the regulator function $F(r)$. To completely remove divergences caused by an ill-behaved RSET we need to take α greater than 1. Otherwise, we will face a singularity at $r^2 = (1-\alpha)l_{\rm P}^2$ reminiscent of the divergence of the Polyakov RSET at $r = 0$. In previous works, this singularity was regarded as a semiclassical version of the Schwarzschild central singularity [112] or as a numerical instability limiting the resolution of numerical analyses [170]. Our understanding is that the nonphysical divergence at $r = 0$ of the Polyakov RSET (which is rooted to the dimensional reduction adopted to derive it) is transformed by the non-linearity of the semiclassical equations into a singularity at $r = \sqrt{1-\alpha}l_{\rm P}$, which gets removed by taking $\alpha > 1$. By eliminating this divergence, the solutions to Eq. (2.9) can now be explored all the way up to $r = 0$ without any restrictions.

2.2.1 From roots to branches

Let us dissect various peculiarities of the semiclassical equations. We turn our attention to Eq. (2.9), whose right-hand side is a cubic polynomial in ψ. The non-vanishing roots of this polynomial, $\mathcal{R}_1$ and $\mathcal{R}_2$, are negative-definite for any positive r and α. We can deduce several properties of the solutions by inspecting Eq. (2.9), since the sign of ψ' depends on whether ψ takes values on the different intervals defined by $\mathcal{R}_1, \mathcal{R}_2$, and 0, being monotonic within each of these intervals.

In addition to these roots, Eq. (2.9) has two non-trivial, negative-valued exact solutions

$$\psi_\pm = -\frac{r^2+\alpha l_{\rm P}^2}{r l_{\rm P}^2}\left(1 \pm \sqrt{1-\frac{l_{\rm P}^2}{r^2+\alpha l_{\rm P}^2}}\right). \tag{2.10}$$

They correspond to negative infinite values of the compactness when plugged in Eq. (2.7). Consequently, their Kretschmann scalar (1.10) is infinite. Nonetheless, their interest resides in (2.9) being a first-order differential equation satisfying the hypotheses of Picard-Lindelöf's theorem [174], which ensures that no other exact solution will intersect $\psi_\pm$ at any finite radius. See Fig. 2.1 below for a pictorial representation of these exact solutions together with the roots $\mathcal{R}_{1,2}$.

The last remarkable feature of the semiclassical vacuum equations involves Eq. (2.7), which is a quadratic polynomial in ψ. The roots of this polynomial are

$$\psi = -\frac{r^2+\alpha l_{\rm P}^2}{r l_{\rm P}^2}\left(1 \pm \sqrt{1+\frac{l_{\rm P}^2}{r^2+\alpha l_{\rm P}^2}\frac{C}{1-C}}\right). \tag{2.11}$$

This expression has two branches depending on the $\pm$ sign. Interestingly, only the branch with the $-$ sign is analytic and can be deformed into the classical equations in the $l_{\rm P} \to 0$ limit. The $+$ sign branch lacks a well-defined classical limit and is inherently semiclassical. We shall call this branch the concealed branch, and the other one the unconcealed branch, and maintain this assignation during the rest of the thesis. The presence of new branches of solutions is a signature of theories that modify the Einstein field equations by adding terms either of high derivative order and/or of a greater power. In particular, the Polyakov RSET introduces $\mathcal{O}(\psi^2)$ terms in Eq. (2.7) giving rise to this new branch with no well-defined $l_{\rm P} \to 0$ limit. As we will show, the solutions that we will describe exhibit smooth jumps between branches. Consequently, we analyze the semiclassical equations as a whole and do not discard any solution *à priori* based on the smoothness of its classical limit.

2.3 Vacuum solutions

In this Section we will prove that the semiclassical Schwarzschild counterpart is a singular asymmetric wormhole. The proof is detailed in the upcoming Subsections, but let us sketch it here for extra clarity. We start the analysis by imposing conditions at the only asymptotically flat region in the spacetime. Therefore, we first prove in Subsec. 2.3.1 that the semiclassical solutions have the expected Schwarzschild-like behavior at large distances and describe an asymptotically flat region (up to sub-leading corrections). Then, monotonicity arguments are used throughout Subsec. 2.3.2 on the function ψ to show that the geometry displays, instead of an event horizon, a wormhole throat at some value of the radial coordinate $r_{\rm B} > 0$ greater than the Schwarzschild radius $r_{\rm H} = 2M$. Finally, the semiclassical equations are integrated on the interior (concealed) side of the wormhole in Subsec. 2.3.3, which ends in a curvature singularity.

2.3.1 Asymptotically flat regime

We first assume C is positive at a fiducial reference radius $r_{\rm ref}$ and that the solution initially belongs to the unconcealed branch of ψ. Under these two conditions, $\psi(r_{\rm ref})$ is positive via Eq. (2.11), since the unconcealed branch guarantees $\psi > 0$ when $C > 0$. Similarly, $\psi' < 0$ due to the negativity of the roots in the right-hand side of Eq. (2.9).

In an outwards integration, ψ cannot cross $\psi = 0$ at a finite radius because $\psi = 0$ is an exact solution of Eq. (2.9) and so it cannot be intersected by any other solution. In addition, ψ cannot tend to a constant positive value in the limit $r \to \infty$ because in that case ψ' would not vanish asymptotically, producing a contradiction. The only possibility that remains is that ψ tends to 0 asymptotically with r.

To prove this last statement, we assume a polynomial decay for the asymptotic form of ψ

$$\psi \propto r^{-\eta}, \quad \eta > 0, \quad \text{when } r \to \infty. \tag{2.12}$$

This means that ψ' is proportional to $-\eta\, r^{-\eta-1}$. On the other hand, replacing the previous ansatz in (2.9) returns the relation:

$$\psi' \propto -2r^{-\eta-1} + \cdots \tag{2.13}$$

where sub-leading terms in r have been neglected. Therefore, we obtain $\eta = 2$, i.e.,

$$\psi \simeq \frac{\psi_{\rm c}}{r^2}, \tag{2.14}$$

with ψ_c an integration constant. The redshift function ϕ follows from integrating (2.14). The g_{tt} metric component results

$$e^{2\phi} \simeq e^{2\psi_c/r} = 1 - \frac{2\psi_c}{r} + \mathcal{O}\left(r^{-2}\right), \tag{2.15}$$

where we have absorbed an irrelevant re-scaling of the time coordinate.

Knowing the asymptotic behaviour of ψ, the compactness C can be obtained through (2.7). For large r is found to be

$$C \simeq \frac{2\psi_c}{r} \tag{2.16}$$

at leading order. Lastly, taking $\psi_c = M$ we conclude that the semiclassical counterpart to the Schwarzschild vacuum solution has the same asymptotic properties as the Schwarzschild solution.

A distant observer should not be able to distinguish any semiclassical departure from classical general relativity. This happens because the density and pressures of the quantum substance diminish towards infinity at a rate greater than $1/r^2$ and, in fact, proportional to $1/r^5$ and $1/r^6$, respectively. The situation differs if the Hartle-Hawking or Unruh states, perceived as thermal baths by static asymptotic observers [175], are considered. While at large distances semiclassical corrections amount to perturbative contributions, deviations from the Schwarzschild metric start taking a prominent role as we move towards the internal region in our integration. These deviations become extreme as we get close to $r = 2M$, completely removing the horizon.

2.3.2 Integrating inwards

The function ψ is positive and grows monotonically inwards. To determine the qualitative behavior of ψ we work on a case-by-case scenario. Let us first address the possible behaviors of ψ at $r = 0$. We assume ψ obeys the following expansion around $r = 0$

$$\psi = \psi_0 + \psi_1 r + \psi_2 r^2 + \mathcal{O}\left(r^3\right), \tag{2.17}$$

where ψ_0 is a positive constant. Replacing this expansion in (2.9) and keeping terms non-vanishing at $r = 0$ we obtain

$$\psi_1 = -\frac{2\alpha\psi_0}{(\alpha-1)\,r} - \frac{2\left[(\alpha+1)\,\psi_0^2 + \alpha\psi_1)\right]}{\alpha-1} + \mathcal{O}(r), \tag{2.18}$$

from where no solution with $\psi_0 \neq 0$ exists, contradicting our initial hypothesis.

Since no finite ψ at $r=0$ is solution of the semiclassical vacuum equations, only the possibility of a positive divergent ψ at $r=0$ remains. Take the ansatz

$$\psi \simeq \frac{\psi_0}{r^\beta}, \text{ with } \beta > 0 \tag{2.19}$$

and replace it in (2.9) to obtain

$$\frac{\beta\,(\alpha-1)\,\psi_0}{r^{\beta+1}} = \frac{2\alpha\psi_0}{r^{\beta+1}} + \frac{2\,(\alpha+1)\,\psi_0^2}{r^{2\beta}} + \frac{(\alpha+1)\,\psi_0^3}{\alpha r^{3\beta-1}} + \mathcal{O}\Big(r^{1-\beta}\Big). \tag{2.20}$$

In view of this expression, if $0<\beta<1$, terms linear in ψ_0 dominate, but the corresponding solution

$$\beta = \frac{2\alpha}{\alpha-1} > 2, \tag{2.21}$$

is inconsistent with our assumption. If, on the contrary, $\beta>1$, the last term in the right-hand side dominates and there is again no solution with $\psi_0 \neq 0$. Therefore, the only possibility is $\beta=1$, for which all terms in (2.20) contribute at equal order. We obtain the pair of solutions

$$\psi_0^{(\pm)} = -\alpha \pm \sqrt{\alpha\,(\alpha-1)} < 0. \tag{2.22}$$

Given that these two values are negative, we find again a contradiction with the initial hypothesis (i.e. ψ must diverge towards positive infinity). As a consequence, no solutions with positive (finite or divergent) ψ at $r=0$ exist. In conclusion, ψ necessarily diverges at some finite nonzero radius that we shall denote $r_{\rm B}$.

Let us analyze the form of this divergence at $r=r_{\rm B}$. Again, by assuming that $\psi\to+\infty$ when $r\to r_{\rm B}$, we can safely neglect all the powers of ψ less than cubic in Eq. (2.9), reducing it to the form

$$\psi' \simeq -\frac{[(r^2+\alpha l_{\rm P}^2)^2+\alpha l_{\rm P}^4]\,l_{\rm P}^2 r\psi^3}{[r^2+(\alpha-1)l_{\rm P}^2]\,(r^2+\alpha l_{\rm P}^2)^2}, \tag{2.23}$$

whose exact solutions are given by

$$\psi = \pm\, l_{\rm P}^{-1}\left[\frac{\alpha l_{\rm P}^2\,(r^2-r_{\rm B}^2)}{(r^2+\alpha l_{\rm P}^2)\,(r_{\rm B}^2+\alpha l_{\rm P}^2)} - \alpha\ln\frac{r^2+\alpha l_{\rm P}^2}{r_{\rm B}^2+\alpha l_{\rm P}^2} + (1+\alpha)\ln\frac{r^2+(\alpha-1)l_{\rm P}^2}{r_{\rm B}^2+(\alpha-1)l_{\rm P}^2}\right]^{-1/2}, \tag{2.24}$$

from where only the positive sign is consistent with our initial hypothesis of asymptotic flatness. Notice that restricting to positive ψ means the solution belongs to the unconcealed branch of (2.11).

The divergent behavior becomes clear upon expanding the logarithms in powers of $(r - r_{\rm B})$. The solution then acquires the simplified form

$$\psi \simeq \sqrt{\frac{k_0}{4(r - r_{\rm B})}}, \tag{2.25}$$

where the constant

$$k_0 = \frac{2\left[r_{\rm B}^2 + (\alpha - 1)l_{\rm P}^2\right]\left(r_{\rm B}^2 + \alpha l_{\rm P}^2\right)^2}{r_{\rm B} l_{\rm P}^2\left[(r_{\rm B}^2 + \alpha l_{\rm P}^2)^2 + \alpha l_{\rm P}^4\right]} > 0 \tag{2.26}$$

contains all dependence on the regulator parameter α.

The form of the ϕ function follows from integrating Eq. (2.25) in a neighborhood of $r_{\rm B}$,

$$\phi(r) = \phi_{\rm ref} + \int_{r_{\rm ref}}^{r} \psi(r')dr'. \tag{2.27}$$

Owing to the specific divergence of ψ, proportional to $(r - r_{\rm B})^{-1/2}$, it follows that ϕ does not go to $-\infty$ when r goes to $r_{\rm B}$ (which we can always assume to be smaller than $r_{\rm ref}$). Instead, we obtain

$$\phi \simeq \sqrt{k_0(r - r_{\rm B})} + \phi_{\rm B}, \tag{2.28}$$

which is manifestly finite at $r = r_{\rm B}$. This is contrary to what occurs at the event horizon, where ψ diverges as $(r - r_{\rm H})^{-1}$ and so does ϕ.

The compactness function

$$C \simeq 1 - k_1\left(r - r_{\rm B}\right), \tag{2.29}$$

follows from Eq. (2.25), with

$$k_1 = \frac{4\left(r_{\rm B}^2 + \alpha l_{\rm P}^2\right)}{r_{\rm B}^2 l_{\rm P}^2 k_0}.$$

The metric written in Schwarzschild coordinates is singular at $r = r_{\rm B}$. This is a coordinate singularity, evidenced by transforming from the Schwarzschild radial coordinate r to a proper radial coordinate l, defined through the relation

$$\frac{dl}{dr} = \frac{1}{\sqrt{k_1(r - r_{\rm B})}}. \tag{2.30}$$

Integrating this definition yields

$$r - r_{\rm B} = \frac{k_1}{4}\left(l - l_{\rm B}\right)^2. \tag{2.31}$$

In the proper radial coordinate l the resulting metric for $l \gtrsim l_{\rm B}$ becomes

$$ds^2 \simeq -\exp\left[\sqrt{k_0 k_1}(l-l_{\rm B})+2\phi_{\rm B}\right]dt^2+dl^2 + \left[\frac{k_1}{4}\left(l-l_{\rm B}\right)^2+r_{\rm B}\right]^2 d\Omega^2. \tag{2.32}$$

The non-singular metric (2.32) suggests its extension beyond $l = l_{\rm B}$. In terms of the Schwarzschild radial coordinate r, this implies the presence of a second branch in which now r increases as l decreases. The relation between the radial coordinates on this second branch would be

$$\frac{dl}{dr} = -\frac{1}{\sqrt{k_1(r-r_{\rm B})}}. \tag{2.33}$$

Indeed, we can explicitly check that this extension exists: the metric for $l \lesssim l_{\rm B}$ implies the following form for ψ,

$$\psi \simeq -\sqrt{\frac{k_0}{4(r-r_{\rm B})}}, \tag{2.34}$$

and this negatively divergent ψ is a solution of the differential equation (2.9). That is, continuity of the metric at $r_{\rm B}$ requires the function ψ to jump from $+\infty$ to $-\infty$. The redshift function $e^{2\phi}$ crosses this jump in an absolutely smooth fashion, and remains non-zero through it.

Let us summarize our analysis up to this point. We have shown that the semi-classical vacuum solution corresponding to a positive asymptotic mass exhibits a surface of minimum areal radius $r_{\rm B}$, or minimal surface. This surface is therefore identified as a wormhole throat. The redshift function remains positive in passing through the wormhole throat, even if $C \to 1$ as $r \to r_{\rm B}$; hence, no horizon is formed. This wormhole is not mirror-symmetric through the throat, precisely because of the behavior of the redshift function, which decreases towards the interior side of the wormhole. The geometry around the throat could be made symmetric (entailing a discontinuity in the derivative of the redshift function at $l = l_{\rm B}$), by introducing a shell of matter with a SET proportional to $\delta(l - l_{\rm B})$. This constitutes a proof that there are no asymptotically flat symmetric wormholes in vacuum in semiclassical gravity *à la Polyakov*. However, we will stick to the strict vacuum solution as in future chapters it will correspond to the exterior of a material body and we want to avoid the introduction of distributional components in the SET. It is also interesting to notice that, at the throat, we are also passing smoothly from the unconcealed to the concealed branch in Eq. (2.11). In turn, the self-consistent

vacuum semiclassical solution lacks a well-defined classical limit, being more than just a perturbative modification of the Schwarzschild solution. We will encounter a similar wormhole geometry in the under-charged semiclassical Reissner-Nordström geometry from Chapter 3, for which the Schwarzschild geometry is the limit case of vanishing charge.

Before ending this Subsection let us remark that Eq. (2.32) provides a reliable approximation to the near-neck metric in the following regimes. If $r_{\rm B} \gg \sqrt{\alpha} l_{\rm P}$, then

$$0 < r - r_{\rm B} \ll \frac{l_{\rm P}^2}{r_{\rm B}}. \tag{2.35}$$

On the other hand, if the wormhole throat is small ($r_{\rm B} \ll \sqrt{\alpha} l_{\rm P}$) then it must be

$$0 < r - r_{\rm B} \ll r_{\rm B}. \tag{2.36}$$

2.3.3 Through the wormhole

As a consequence of the absence of an event horizon, a new, uncovered region of spacetime emerges. This portion of spacetime, described by a solution that belongs to the concealed branch, has characteristics very different from the unconcealed region. As we will show, the semiclassical vacuum generates a new internal asymptotic region of infinite negative Misner-Sharp mass. A description of the geometry of the other side of the wormhole can be determined from arguments involving Eq. (2.9).

The argument starts as follows: The roots $\mathcal{R}_{1,2}$ and the exact solutions $\psi_\pm$ diverge towards negative infinity in the $r \to 0$ limit. As the boundary conditions at the throat imply $\psi \to -\infty$ as $l \to l_{\rm B}^-$ ($r \to r_{\rm B}$ from the inside), it is guaranteed that ψ will take values below the two roots $\psi_\pm$ close enough to the throat. In Figure 2.1 we have plotted the two roots and exact solutions from Eq. (2.9). We have also plotted the portion that lives in the concealed branch of a numerical solution, showing its divergent behavior at the throat.

Let us describe the features of the solution. The solution ψ must initially increase with r (in the concealed branch, where r decreases with l) up to its unavoidable crossing with $\mathcal{R}_1$. Then, it starts decreasing but it can neither cross back the root $\mathcal{R}_1$ nor cross the exact solution. As both $\mathcal{R}_1$ and ψ_+ have the same leading-order asymptotic behavior for large r, the physical exact solution must acquire this same asymptotic behavior but always staying between these two curves. The unphysical solution ψ_+ acts as an attractor to which solutions converge asymptotically [176].

Assuming that ψ deviates slightly from the non-physical exact solution ψ_+, and measuring this deviation by a function $\chi(r)$, such that $\psi = \psi_+ + \chi(r)$, we can replace

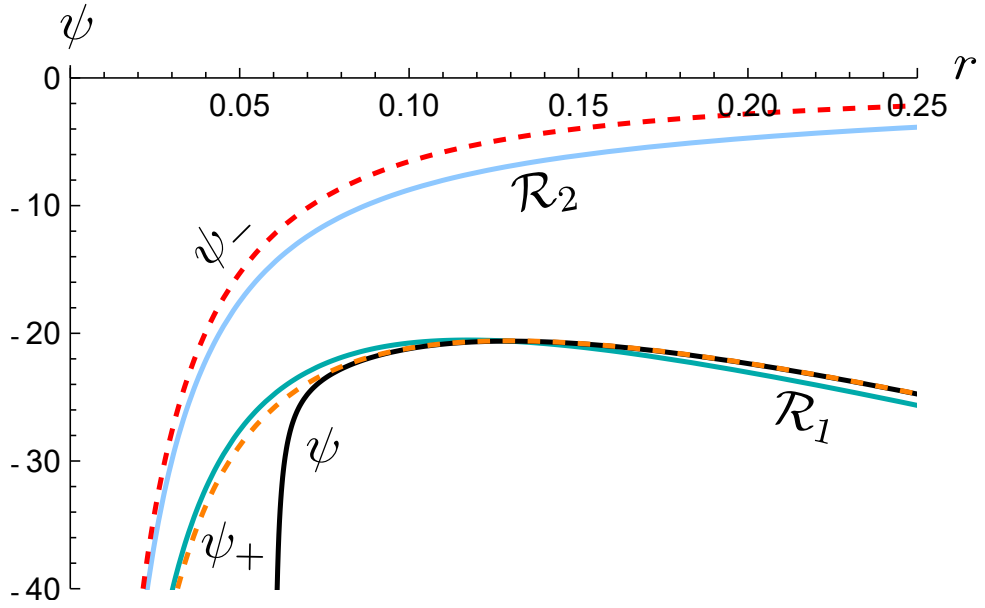

Fig. 2.1.: Plot of $\mathcal{R}_1$, $\mathcal{R}_2$ and the unphysical exact solutions, with $\psi_\pm$ for $\alpha = 1.01$. The black curve corresponds to a numerical solution with $r_{\rm B} = 0.06$. The numerical solution intersects $\mathcal{R}_1$ at $r \approx 0.13$, reaching a maximum, and then decreases, remaining confined between $\mathcal{R}_1$ and ψ_+.

this expression in (2.9), neglect $\mathcal{O}(\chi^2)$ and $\mathcal{O}(\chi^3)$ terms, expand in the $r \to \infty$ limit and solve for χ. Dropping terms decreasing faster than r^{-3} asymptotically, we arrive at the relation

$$\chi' = -\mathcal{D}\chi + \mathcal{O}\left(\chi^2\right), \tag{2.37}$$

where

$$\mathcal{D} = \left[16r^4 + 8l_{\rm P}^2 r^2\left(2\alpha - 1\right) + l_{\rm P}^4\left(32\alpha - 5\right)\right] \times \left(4l_{\rm P}^2 r^3\right). \tag{2.38}$$

Now we solve Eq. (2.37) to obtain the asymptotic deviation from the exact solution

$$\chi \simeq -\frac{\chi_0}{l_{\rm P}}\left(\frac{r}{l_{\rm P}}\right)^{2-4\alpha} e^{-2r^2/l_{\rm P}^2}\left[1 - \frac{\left(5 - 32\alpha\right) l_{\rm P}^2}{8r^2}\right], \tag{2.39}$$

where χ_0 is a dimensionless integration constant. This result is consistent (when taking $\alpha = 0$) with the asymptotic behavior found in [170]. The sign of χ is negative due to the solution ψ approximating ψ_+ from below. The presence of a regulator causes a faster decay of the deviation (2.39) for large r. Compactness diverges exponentially towards negative infinity in this limit,

$$C \simeq -\frac{\left(r/l_{\rm P}\right)^{4\alpha-3}}{2\chi_0} e^{-2r^2/l_{\rm P}^2}\left[1 + \frac{(9 - 32\alpha) l_{\rm P}^2}{8r^2}\right]. \tag{2.40}$$

Finally, the line element can be written as

$$ds^2 \simeq \left(\frac{r}{l_{\rm P}}\right)^{1-4\alpha} e^{-2r^2/l_{\rm P}^2} \left\{ -a_0 \left(1 - \frac{l_{\rm P}^2}{8r^2}\right) dt^2 + \frac{2\beta_0 r^2}{l_{\rm P}} \left[1 - \frac{(9-32\alpha)l_{\rm P}^2}{8r^2}\right] dr^2 \right\} + r^2 d\Omega^2. \tag{2.41}$$

where a_0 is a positive dimensionless constant coming from the integration of ψ. The resulting geometry has a null singularity at radial infinity since the time and radial components of the metric vanish. This asymptotic region is singular and leads to a negatively divergent curvature scalar

$$R \simeq -\frac{e^{-2r^2/l_{\rm P}^2}(2\alpha - 1)}{l_{\rm P}^2 \chi_0} \left(\frac{r}{l_{\rm P}}\right)^{-5+4\alpha}. \tag{2.42}$$

This curvature singularity has an infinite negative Misner-Sharp mass associated to it, the source of this mass being the vacuum energy of the quantized field. The singular region is located at an infinite radial distance in the r coordinate, but at finite proper distance from the throat. This can be seen by integrating the asymptotic form

$$\left(\frac{dl}{dr}\right)^2 = 2\chi_0 \left(r/l_{\rm P}\right)^{3-4\alpha} e^{-2r^2/l_{\rm P}^2} \left[1 - \frac{(9-32\alpha)l_{\rm P}^2}{8r^2}\right]. \tag{2.43}$$

The exponential factor leads to a finite proper distance $l_{\rm I} < l_{\rm B}$ for the location of this internal asymptotic region.

2.3.4 Other asymptotic behaviors

For completeness, we finish this section by describing the solutions to the semiclassical equations with negative and vanishing ADM mass.

Based on our results for the asymptotically flat regime, we first consider the analysis of the geometry when $M < 0$. In this case, the asymptotic form of the functions ψ and C, again for the unconcealed branch, follows from taking a negative value for the integration constant in (2.14) and (2.16)

$$\psi \simeq -\frac{|M|}{r^2}, \quad C \simeq -\frac{2|M|}{r}. \tag{2.44}$$

Given a faraway referential radius $r_{\rm ref}$, the negative function $\psi(r)$ for $r \in (r_{\rm ref}, +\infty)$ is always larger than the nonphysical exact solution ψ_- and both roots, which are always smaller than ψ_- (see Figure 2.1). Integrating the solution inwards, as it

cannot cross ψ_- and neither can the roots, the solution is monotonically decreasing. Following the same argument as in Subsection 2.3.1 we show that ψ diverges as

$$\psi \simeq \frac{-\alpha + \sqrt{\alpha\,(\alpha-1)}}{r} \tag{2.45}$$

in the $r \to 0$ limit. Replacing this solution in Eq. (2.8) and solving for C in the $r \to 0$ limit we find

$$C \simeq -|M| r^{-\frac{2(\alpha+1)}{\alpha-1}\left[1-\alpha+\sqrt{\alpha(\alpha-1)}\right]}. \tag{2.46}$$

This solution has a curvature singularity at $r = 0$ that corresponds to the semiclassical counterpart of the naked singularity of the classical Schwarzschild geometry endowed with a negative asymptotic mass. Note that in the limit $\alpha \to \infty$ we recover the Schwarzschild metric.

Finally, the solution with $M = 0$ corresponds to Minkowski spacetime, where the zero-point energy of the scalar field can be renormalized away, and hence it does not contribute to curvature. This solution, for which the RSET vanishes, marks the boundary between positive and negative mass solutions, that is, between wormholes and naked singularities. Since for wormhole solutions the radius of the throat $r_{\rm B}$ is directly related to the asymptotic mass M, taking $r_{\rm B} \to 0$ corresponds to making the mass vanish, thus recovering Minkowski spacetime in this limit.

2.4 Geometric characteristics of the semiclassical Schwarzschid counterpart

The asymmetric wormhole

The semiclassical counterpart to the positive-mass Schwarzschild solution is an asymmetric wormhole with asymptotically flat and singular internal asymptotic regions at both ends. Figure 2.2 contains a numerical plot of a particular case. In this plot we can appreciate that the compactness function C grows to 1 at the neck of the wormhole, only to start decreasing exponentially as we deepen in the internal asymptotic region. On the other hand, the redshift function is always monotonically decreasing, vanishing only at the internal asymptotic region. The approximate location of the classical horizon is now replaced by a wormhole throat with a nonzero redshift value. In a sense, the horizon has been pushed away towards an internal singular infinity.

The distribution of the Misner-Sharp mass along the radial direction can be interpreted as if an infinite negative energy was concentrated in the internal singular

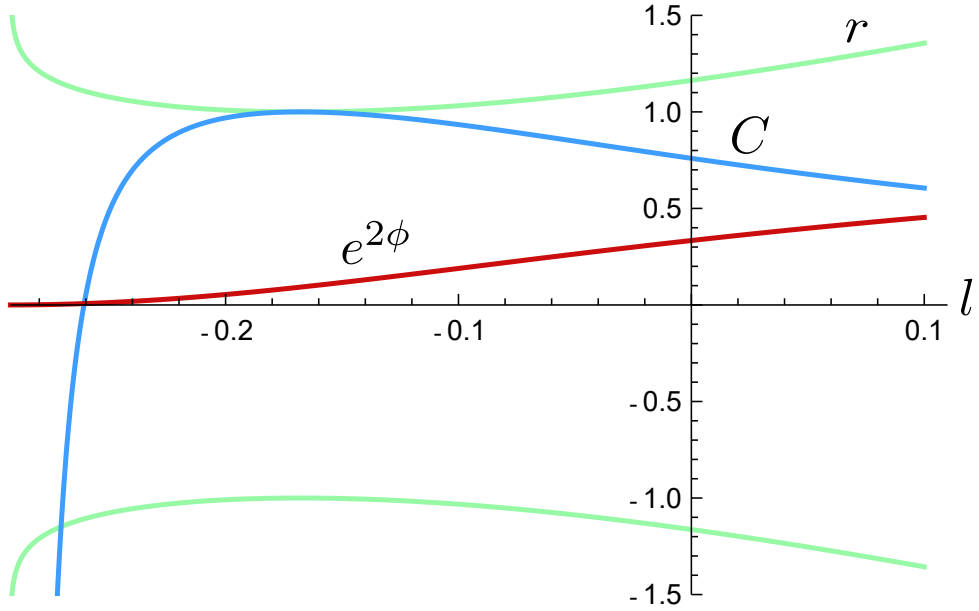

Fig. 2.2.: Numerical plot of the semiclassical counterpart of the Schwarzschild vacuum geometry. The horizontal axis is the proper coordinate l while the above and below curves (green) represent the radial coordinate r (in units of $r_{\rm B}$). The redshift function, and the compactness are plotted in red and blue, respectively. The right side of the wormhole is asymptotically flat whereas the left side is asymptotically singular. Both regions are joined by a minimal surface of radius $r = r_{\rm B}$. We have chosen $M = 0.1$ and $\alpha = 1.01$ to better highlight the properties of the geometry, which are identical for larger ADM masses.

region, generating a cloud of negative vacuum energy distributed throughout the entire spacetime. In going from the internal asymptotic region towards the neck, this negative energy density increases the value of the Misner-Sharp mass. When one reaches the throat itself the Misner-Sharp mass is already positive. Once the throat has been surpassed, the semiclassical negative energy now progressively decreases the value of the Misner-Sharp mass, leading finally to the asymptotic mass M.

Notice that within the vacuum solutions analyzed here there is none which is regular, with the exception of Minkowski spacetime. Moreover, the causality of the wormhole solutions (see the left panel in Fig. 2.3 for a conformal diagram), reveals that the singular region is null as opposed to the spacelike singularity in the Schwarzschild solution. This is caused by the asymptotic vanishing of the time and radial components of the metric (2.32). Moreover, observers following timelike trajectories reach this singularity at finite proper time and null rays reach it at a finite value of the affine parameter. This indicates that there are no “mass without mass" solutions of any sort (using Wheeler’s terminology [173]) in the semiclassical theory: vacuum energy cannot by itself generate regular self-gravitating configura-

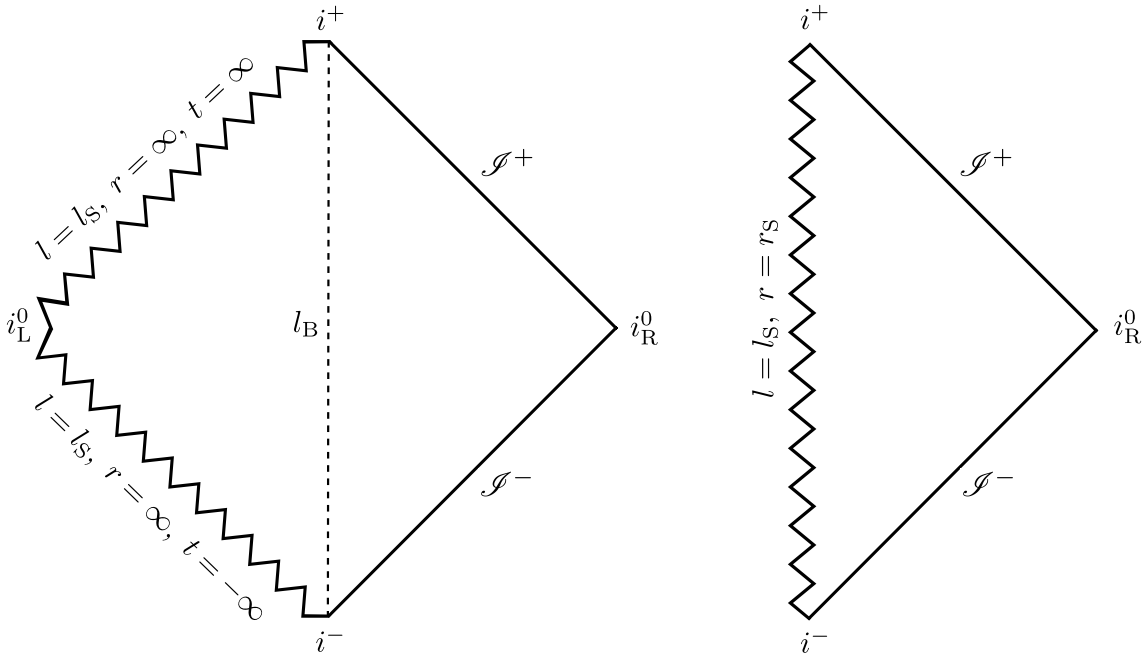

Fig. 2.3.: Left panel: Penrose diagram corresponding to the singular wormhole solution for the CRP-RSET. The dashed lines denote the location of the wormhole neck. To their right, the asymptotically flat portion of spacetime is depicted alongside its asymptotic regions. The left hand side of the diagram shows the internal past and future null singularities, which are located at finite proper distance from the neck $l_{\rm S} - l_{\rm B}$. The point $i^0_{\rm L}$ is singular as well, and is reached in finite proper time by spacelike geodesics. Right panel: Penrose diagram associated with the vacuum solution for the OR-RSET (described in Chapter 6). In this case, the singularity is timelike and constitutes a naked singularity. While differences in the modelization of the semiclassical source result in singularities of different sorts, both models agree on the absence of event horizons.

tions. The introduction of a material content of some sort is therefore a necessary requirement in order to obtain regular and semiclassically consistent geometries.

Studies involving semiclassical backreaction in the Boulware state have been pursued in the literature in the context of BHs in two-dimensional dilaton theories [158, 177], the Russo-Susskind-Thorlacius model [178], and the s-wave RSET approximation in semiclassical gravity [112], where the effect of the potential barrier is simulated through the coupling between the quantized massless scalar and a dilaton [101]. In these studies, a generic phenomenon is the event horizon getting destroyed by the backreaction of the RSET. Peculiarly, null singularities appear as ubiquitous features, even when the RSET is the one associated with a conformally invariant field that satisfies the $(3+1)$-dimensional trace anomaly [168]. On a related front, the vacuum solutions from Einstein-Weyl gravity [179] share many similarities with the wormholes described in this Chapter as well.

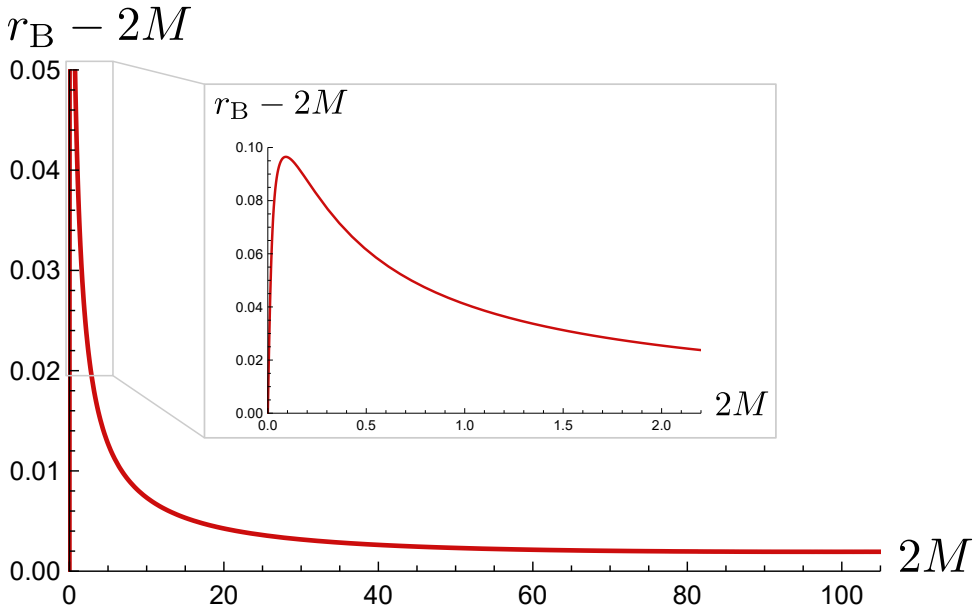

Fig. 2.4.: Numerical plot of the deviation $r_B - 2M$ in terms of twice the ADM mass of the geometry. The difference $r_B - 2M$ reaches a maximum as we approach small values of $2M$, while in the $M \to 0$ limit r_B goes to 0.

Regarding the location of the wormhole throat, in figure 2.4 we show the value of $r_B - 2M$ with respect to the gravitational radius $2M$ (in Planck units). We see that for a range of masses large enough as compared with the Planck mass, the difference is of the order of $10^{-2} l_P$. This difference increases for smaller masses and vanishes in the $M \to 0$ limit.

Reflections on RSET approximations

In order to analyze potentially regular geometries sourced by an internal matter content plus the semiclassical vacuum contributions it is necessary to have control of the effects of the semiclassical energies up to arbitrarily small radii. Initially, we ignored how the regularizing parameter α would affect the solutions found in [101]. The presence of the regulator brings the singular asymptotic region closer to the throat, in terms of proper distance, than when no regulator is present [notice the factor $1/r^{4\alpha}$ in Eq. (2.43)]. On the other hand, within the regularized theory there exist solutions that can come as close as desired to $r = 0$. No matter how small the ADM mass of the system is, the solutions are always asymmetric wormholes. The Minkowski solution is a singular limit of the solutions as $r_B \to 0$.

In Chapters 4 and 5 we will address semiclassical backreaction in stellar spacetimes. The solutions here described are the external spacetime to these material bodies. Furthermore, there are situations in which a similar structure (i.e. a wormhole throat connecting to a null singularity) realizes inside matter. We will

encounter solutions in which these wormhole throats can be arbitrarily small by tuning the parameters that characterize the star (energy density, mass and radius). It is in this regime where the RSET regularization scheme becomes of great importance, as distances close $r = 0$ are explored. Eventually, we will leave aside the CRP-RSET in favor of more elaborate regularization schemes that influence the short-distance behavior of the RSET in other ways. In vacuum, these alternative families of RP-RSETs only affect solutions with small ADM mass (for which $r_{\rm B}$ lies within the region where the RSET depends strongly on its regularization), so all the observations made in this Chapter apply to other regularization schemes that we will consider in the future.

A different possibility is using an RSET approximation that is four-dimensional from the start, namely the analytical AHS-RSET [127] introduced in Sec. 1.2. Despite the aforementioned shortcomings of this approximation, a set of well-posed, second-order vacuum semiclassical equations can be derived by means of further approximations. This is the approach we follow in Chapter 6, where we obtain the complete set of semiclassical vacuum solutions in this prescription. For the massless minimally coupled field, the backreacted geometry has no event horizon nor wormhole neck, displaying a (timelike) naked singularity (see Fig. 6.1). This naked singularity is located above the Schwarzschild radius of the spacetime, as depicted in Fig. 6.2, and at distances similar to where the wormhole neck appears with the CRP-RSET. Finally, the conformal diagram for this spacetime is depicted in the right panel of Fig. 2.3, where it can be clearly compared with the conformal diagram of the asymmetric wormhole.

While the backreaction of the various existing analytical RSETs gives rise to spacetimes with different characteristics as the $r = 2M$ region is approached, the fact that the horizon transforms into a curvature singularity by the vacuum polarization of the Boulware vacuum state is robust and independent of the approximation. We will return to this discussion and provide additional details in Chapter 6.

2.5 Conclusions

In this Chapter we have obtained and analyzed the characteristics of the semiclassical counterpart to the Schwarzschild geometry. As a source of the semiclassical equations, we have considered a Cutoff-Regularized version of the Polyakov RSET. Under this simple choice of regularization, we obtain a set of equations without the pathologies that emerge from the dimensional reduction followed to obtain the Polyakov RSET in the first place. The semiclassical Schwarzschild counterpart with positive ADM mass is an asymmetric wormhole. The neck of the wormhole

(or surface of minimum radius) replaces the classical event horizon and connects the asymptotically flat region with a null singularity located at finite affine distance from the neck.

No regular and static vacuum geometry is compatible with quantum vacuum polarization effects. Eternal horizons are not a feature of vacuum semiclassical solutions. Hence, within the semiclassical paradigm, if an equilibrium (static) state is reached at some point during evolution towards a dark compact object, it should be given by a horizonless configuration. The evaporating BH paradigm circumvents this situation, as trapping horizons should be formed dynamically by a collapse process and then shrink slowly. Hence, it is assumed that the geometry would be never static, except perhaps at the end of a long evaporation process where the horizon itself might disappear. Let us remark that, in principle, there are two semiclassically consistent possibilities. On the one hand, non-equilibrium configurations with non-extremal trapping horizons and, on the other hand, equilibrium configurations with no horizons whatsoever.

3

Reissner-Nordström geometry counterpart in semiclassical gravity

3.1 Introduction

In this Chapter we generalize the semiclassical Schwarzschild counterpart from Chapter 2 to the electrovacuum case by deriving the semiclassical counterpart to the Remissness-Nordström spacetime. In GR, by electrovacuum we mean the case in which the spacetime contains a central electromagnetic charge with its associated Coulomb field. The electromagnetic stress-energy tensor sourcing this spacetime is obtained from solving the Einstein-Maxwell equations in spherically symmetric and static situations, i.e.

$$T_{\mu}^{\nu(\mathrm{em})} = \mathrm{diag}\,(-1,-1,1,1)\,\frac{Q^2}{8\pi r^4}. \tag{3.1}$$

Here, $Q^2 = Q_{\mathrm{e}}^2 + Q_{\mathrm{m}}^2$, where $Q_{\mathrm{e}},\ Q_{\mathrm{m}}$ denote the electric and magnetic charges, respectively. The Reissner-Nordström spacetime [180–183] is characterized by

$$e^{2\phi} = 1 - C = 1 - \frac{2M}{r} + \frac{Q^2}{r^2}. \tag{3.2}$$

This solution shows several unique features due to the presence of charge. The zeroes of the redshift function determine the location of its two horizons

$$r_{\pm} = M \pm \sqrt{M^2 - Q^2}. \tag{3.3}$$

Therefore, depending on the charge-to-mass ratio of the geometry, it can exhibit two, one, or no horizons whatsoever. This splits the Reissner-Nordström family into three categories:

- Sub-extremal ($Q < M$), which shows a timelike singularity covered by outer and inner horizons at r_- and r_+ respectively. The Schwarzschild BH is the particular case where $Q = 0$.

- Super-extremal ($Q > M$), where the value of the charge surpassing that of the mass gives rise to a naked singularity.

- Extremal BHs ($Q = M$), for which outer and inner horizons become coincident, forming an extremal horizon at the end of an spatially infinite neck.

The double horizon structure present in the sub-extremal Reissner-Nordström BH is similar to that exhibited by Kerr BHs, while preserving the benevolence of spherical symmetry. For this reason, the analysis of Reissner–Nordström geometries is also used as a proxy to understanding the more complicated Kerr case. The presence of a second internal horizon adds some special features to these geometries. For example, different analyses show that, as opposed to the outer horizon, the inner horizon is highly unstable under both classical and quantum perturbations [184, 185]. RSETs associated to vacuum states regular at the outer horizon have a generic divergence at the inner horizon [138, 186]. Recently, the flux components of the RSET in the past Unruh state were computed at the Cauchy horizon of the Kerr BH [139], showing the corresponding divergences. Semiclassical backreaction will, presumably, destroy the inner horizon and transform it into a curvature singularity.

The semiclassical equations in electrovacuum take the form

$$G_{\mu\nu} = 8\pi \left(T^{(\mathrm{em})}_{\mu\nu} + \hbar \langle \hat{T}_{\mu\nu} \rangle \right), \tag{3.4}$$

where the semiclassical source in (3.4) is, again, the CRP-RSET (1.14) with $F(r) = 1/(r^2 + \alpha l_{\mathrm{p}}^2)$ and $\alpha > 1$. The electromagnetic SET is trivially conserved and traceless, and it modifies the vacuum semiclassical equations in a way that allows to apply the same techniques used in Chapter 2 to find the semiclassical Reissner-Nordström counterpart. This family of solutions displays three distinct regimes depending on whether the charge is above or below a critical value Q_{crit}. In the under-charged regime $Q < Q_{\mathrm{crit}}$ we find singular asymmetric wormholes, whereas in the over-charged regime $Q > Q_{\mathrm{crit}}$ we obtain naked singularities. Both families of solutions are qualitatively identical to the ones presented in Chapter 2, with the exception that over-charged naked singularities receive contributions from the electromagnetic stress-energy tensor. The separatrix solution $Q = Q_{\mathrm{crit}}$ between both regimes is reminiscent of extremal BHs, in the sense that it preserves an event horizon but it gets transformed into a singularity of the non-scalar type [160]. We will elaborate on these solutions in the rest of this Chapter, but let us emphasize here that our major finding is the non-existence of regular static electrovacuum solutions in semiclassical gravity.

Semiclassical backreaction analyses in charged BHs are scarce in the literature and almost nonexistent for fields in the Boulware state in non-extremal situations. On the contrary, perturbative analyses [in the same spirit as Eq. (1.7)] for fields in the Hartle-Hawking state have flourished in the context of two-dimensional dilatonic theories [187, 188], and for conformally invariant [189, 190] and large-mass fields in four dimensions [191]. Among the Reissner-Nordström family, a solution that grabbed an extraordinary amount of interest is the zero-temperature extremal BH, for which the Boulware and Hartle-Hawking states coincide. The works [192, 193] address the self-consistency of two-dimensional extremal dilatonic BHs under semiclassical corrections in the Polyakov and s-wave approximations. According to [192], the semiclassical counterparts to these BHs develop a mild singularity at the event horizon. The appearance of such singularity is in connection with the divergence of the Polyakov RSET there [see Eq. (3.6) below. This divergence only appears in static situations and disappears when an extremal configuration is reached as the endstate of some dynamical process. We elaborate on this discussion in Subsec. 3.5.3.

Let us explicitly show the divergent behavior of the Polyakov RSET at extremal horizons by considering the following profiles for the metric functions, for which the surface gravity (2.2) vanishes,

$$e^{2\phi} \propto \left(\frac{r-r_{\rm H}}{r_{\rm H}}\right)^2 + \mathcal{O}\left(\frac{r-r_{\rm H}}{r_{\rm H}}\right)^3, \qquad 1-C \propto \left(\frac{r-r_{\rm H}}{r_{\rm H}}\right)^2 + \mathcal{O}\left(\frac{r-r_{\rm H}}{r_{\rm H}}\right)^3, \quad (3.5)$$

which result in finite semiclassical density and pressures at $r = r_{\rm H}$.

$$\rho_{\rm s} = p^{\rm r}_{\rm s} \propto \frac{l_{\rm P}^2}{r_{\rm H}^4} + \mathcal{O}\left(\frac{r-r_{\rm H}}{r_{\rm H}}\right). \quad (3.6)$$

Despite the finiteness of the Polyakov RSET at the extremal horizon, the energy density measured by a freely falling observer [171, 172] at the surface $r = r_{\rm H}$ diverges as

$$\mathcal{E} = \left(\langle \hat{T}^r_r \rangle^{\rm P4} - \langle \hat{T}^t_t \rangle^{\rm P4}\right) e^{-2\phi} \propto -\frac{l_{\rm P}^2}{r_{\rm H}^3\,(r-r_{\rm H})} + \mathcal{O}\left(\frac{r-r_{\rm H}}{r_{\rm H}}\right)^0. \quad (3.7)$$

This divergence is milder than the one appearing in the sub-extremal case, analogous to the Schwarzschild situation [see Eq. (2.6)]. Consequently, the horizon is not replaced by a wormhole neck, but transformed into a singular surface where curvature invariants remain finite.

Let us summarize the content of this Chapter. Section 3.2 presents the electrovacuum semiclassical equations and their characteristics. Sections 3.3, 3.4 and 3.5

contain details about the characteristics of the under-charged, over-charged and quasi-extremal regimes of solutions. We conclude with some final remarks in Sec. 3.6.

3.2 Self-consistent electrovacuum semiclassical equations

We write down the semiclassical Einstein equations (3.4) as a first order differential equation for ψ to then discuss some of their most salient properties. By analyzing these expressions we are able to determine the existence of three types of semiclassical solutions depending on the charge-to-mass ratio of the geometry (as in the Reissner-Nordström family), and reconstruct the shape of the solutions living in each of these three regimes. The tt and rr components of the semiclassical field equations are, respectively,

$$C + rC' = \frac{Q^2}{r^2} + \frac{l_{\rm P}^2 r^2}{r^2+\alpha l_{\rm P}^2}\left\{\left[2\psi' + \psi^2\right](1-C) - \psi C'\right\}, \tag{3.8}$$

$$-2r\psi + C(1+2r\psi) = \frac{Q^2}{r^2} + \frac{l_{\rm P}^2 r^2}{r^2+\alpha l_{\rm P}^2}\psi^2(1-C). \tag{3.9}$$

Solving algebraically for C in the second equation and plugging the obtained expression into the first equation results into the first-order differential equation for the variable ψ:

$$\begin{aligned}
\psi' =& A_0 + A_1\psi + A_2\psi^2 + A_3\psi^3, \quad \text{with} \\
A_0(r) =& Q^2\mathcal{D}(r), \\
A_1(r) =& 2r\left[r^2 - Q^2\left(2 + \frac{l_{\rm P}^2}{2\left[r^2+\alpha l_{\rm P}^2\right]}\right)\right]\mathcal{D}(r), \\
A_2(r) =& r^2\left[2\left(r^2-Q^2\right)\left(1 + \frac{l_{\rm P}^2 r^2}{2\left[r^2+\alpha l_{\rm P}^2\right]^2}\right) + \frac{l_{\rm P}^2(2r^2-5Q^2)}{r^2+\alpha l_{\rm P}^2}\right]\mathcal{D}(r), \\
A_3(r) =& \frac{r^3 l_{\rm P}^2}{r^2+\alpha l_{\rm P}^2}\left[r^2\left(1 + \frac{\alpha l_{\rm P}^4}{\left[r^2+\alpha l_{\rm P}^2\right]^2}\right) - Q^2\left(1 + \frac{l_{\rm P}^2[r^2+2\alpha l_{\rm P}^2]}{[r^2+\alpha l_{\rm P}^2]}\right)\right]\mathcal{D}(r), \\
\mathcal{D}(r) =& -\frac{r^2+\alpha l_{\rm P}^2}{r^2\left(r^2-Q^2\right)\left[r^2+l_{\rm P}^2(\alpha-1)\right]}.
\end{aligned} \tag{3.10}$$

In addition to the non-physical singularity at $r = l_{\rm P}\sqrt{1-\alpha}$, which we remove taking $\alpha > 1$, the quantity $1/\mathcal{D}$ vanishes at $r = Q$ as well. This surface has special properties that we will discuss in Sec. 3.4.

The right-hand side of Eq. (3.10) is a cubic polynomial in ψ and can be factorized in roots that are functions of r. These roots are defined piecewise and can be matched along different intervals of the radial coordinate so that, when plotted, they appear as continuous curves. We have adopted the following definition

$$\mathcal{R}_1 = \begin{cases} \mathcal{S}_1 & r \leq Q \\ \mathcal{S}_2 & Q < r \leq r_{\rm i}^- \\ \mathcal{S}_3 & r_{\rm i}^- < r \leq r_{\rm div} \\ \mathcal{S}_1 & r > r_{\rm div} \end{cases}, \quad \mathcal{R}_2 = \begin{cases} \mathcal{S}_3 & r \leq r_{\rm i}^- \\ \mathcal{S}_2 & r > r_{\rm i}^- \end{cases}, \quad \mathcal{R}_3 = \begin{cases} \mathcal{S}_2 & r \leq Q \\ \mathcal{S}_1 & Q < r \leq r_{\rm div} \\ \mathcal{S}_3 & r > r_{\rm div} \end{cases},$$

where the expressions for $\mathcal{S}_i$ are, in terms of the coefficients in Eq. (3.10),

$$\begin{aligned} \mathcal{S}_1 &= -\frac{A_2}{3A_3}\left[1 + \frac{2^{1/3}\left(3A_1A_3 - A_2^2\right)}{A_2\mathcal{H}} - \frac{\mathcal{H}}{2^{1/3}A_2}\right], \\ \mathcal{S}_{2,3} &= -\frac{3 \pm i\sqrt{3}}{2}\left(1 + \frac{A_2}{3A_3}\right)\mathcal{R}_1, \end{aligned} \tag{3.11}$$

with

$$\begin{aligned} \mathcal{H} = \Big[&-2A_2^3 + 9A_1A_2A_3 - 27A_3A_0 \\ &+\sqrt{\left(2A_2^3 - 9A_1A_2A_3 + 27A_3^2A_0\right)^2 - 4\left(A_2^2 - 3A_1A_3\right)^3}\Big]^{1/3}. \end{aligned} \tag{3.12}$$

The symbols $r_{\rm i}^-$ and $r_{\rm div}$ in (3.11) mark the lower and upper limits of a region where the roots acquire a non-zero complex part. Particularly, $\mathcal{R}_1$ and $\mathcal{R}_2$ become complex conjugate roots within this interval. The occurrence of complex roots has no impact on solutions, since, as we will prove in the following sections, solutions of (3.10) with support in the interval $r \in (Q, r_{\rm div})$ have to intersect certain fixed points.

For the Schwarzschild counterpart, one of the three roots is trivial $(\mathcal{R} = 0)$, while the others always take negative values. The presence of charge introduces a non-vanishing zeroth-order term term in (3.10), $A_0 \neq 0$, modifying the shape of the roots (in particular, these now take positive values) and, in consequence, the domain of the solutions.

In Fig. 3.1 we show a plot of the roots and the two exact solutions (2.10) for a particular value of the charge parameter. The curves $\psi_\pm$ are exact solutions independently of the value of Q. In fact, we can rewrite (3.10) as

$$\psi' = \mathcal{F}_{\rm Sch}(r, \psi) + \mathcal{G}(r, Q, \psi)(\psi - \psi_-)(\psi - \psi_+), \tag{3.13}$$

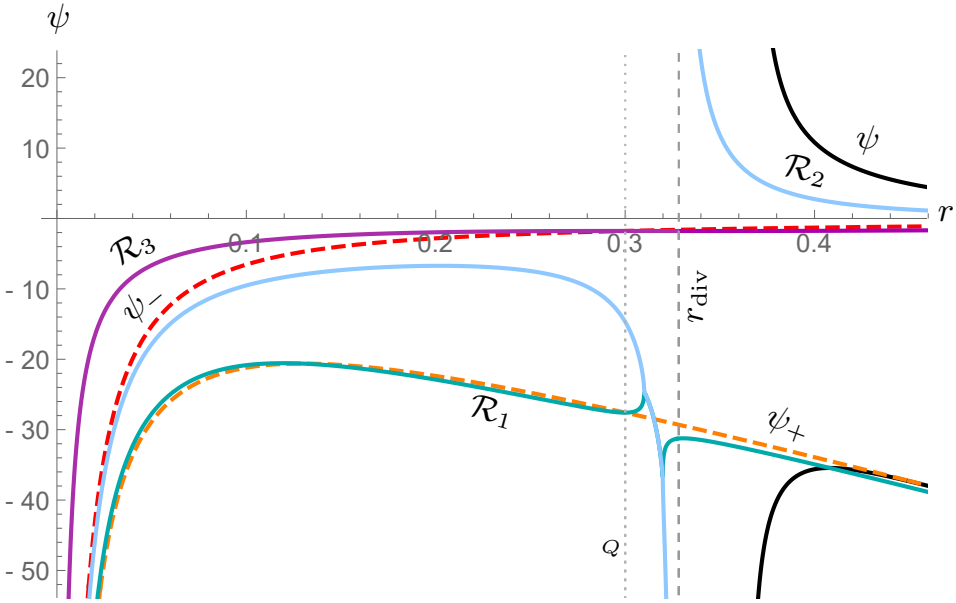

Fig. 3.1.: Plot of the roots $\mathcal{R}_{1,2,3}$ (continuous curves) and the exact solutions $\psi_\pm$ (dashed lines). The roots are defined piecewise, and take negative values except for the positively diverging portion of $\mathcal{R}_2$. Its asymptote at $r = r_{\rm div}$ (vertical, dashed line) marks the separatrix solution between the sub-extremal and super-extremal regimes. The dotted vertical line is $r = Q$. In this figure, we have taken $\alpha = 1.01$ and $Q = 0.3$ for visualization purposes. A numerical solution ψ describing a wormhole of asymptotic mass $M = 0.285$ has been drawn in black. The procedure giving rise to such solution is detailed in later sections.

where $\mathcal{F}_{\rm Sch}$ corresponds to the right hand side of (3.10) evaluated at $Q = 0$, and

$$\mathcal{G} = \frac{l_{\rm P}^2 Q^2 \left(1 + \dfrac{l_{\rm P}^2 r}{r^2 + \alpha l_{\rm P}^2}\psi\right)}{(r^2 - Q^2)\left[r^2 + (\alpha - 1) l_{\rm P}^2\right]}. \tag{3.14}$$

This shows explicitly why $\psi_\pm$ can be exact solutions of (3.10) for arbitrary values of the charge Q even if they do not depend on Q, given that the Q-dependent terms in (3.10) vanish identically for $\psi = \psi_\pm$.

Similarly to what happened for the Schwarzschild counterpart, smooth transitions between both branches take place under certain conditions, resulting in solutions that are more than a mere one-parameter deformation of the classical spacetime. There are two distinct situations that indicate the presence of a transition between branches: either the function ψ jumps from $+\infty$ to $-\infty$, or the quantity $\mathcal{G}$ (3.14) vanishes at some finite radius. These conditions follow from the requirement that the discriminant of Eq. (3.9) (seen as a second-order polynomial for ψ) vanishes.

To end this Section let us stress that, since Eq. (3.10) is a first order differential equation for ψ, we can apply the uniqueness and existence theorem as long as $r \neq Q$; note that for $r \to Q$ the right-hand side of (3.13) diverges as $(r-Q)^{-1}$, which makes the differential equation singular there. This implies that solutions of this equation cannot intersect at finite r but for the surface $r = Q$. In turn, we will show that the exact solutions (2.10) act as boundaries for the remaining solutions. In addition, the roots (3.11) denote the turning points of ψ. These features will allow us to characterize the solutions of (3.10) thoroughly.

3.2.1 Asymptotically flat regime

Let us start analyzing the behavior of (3.10) at large radial distances and imposing asymptotic boundary conditions in order to select the solutions describing asymptotically flat spacetimes. Assuming that the metric (1.2) is asymptotically flat, the leading-order term in the expansion of ψ is identical to (2.13), since Q-dependent contributions decay faster with r.

Now, we allow the next sub-leading terms to enter expression (3.10), informing us about the first Q-dependent corrections,

$$\psi' \simeq -\frac{2\psi}{r}\left(1 + r\psi\right) + \frac{Q^2}{r^4}. \tag{3.15}$$

Integrating this expression twice yields

$$\phi \simeq \psi_{c_1} + \frac{1}{2}\ln\left[\cosh\left(\frac{\sqrt{2}Q}{r} + \psi_{c_2}\right)\right], \tag{3.16}$$

which now displays the leading asymptotic behavior characteristic of the Reissner-Nordström metric, in which

$$e^{2\phi} \simeq 1 - \frac{2M}{r} + \frac{Q^2}{r^2} + \mathcal{O}(r^{-3}). \tag{3.17}$$

To recover the above expression one just needs to choose the integration constants ψ_{c_1} and ψ_{c_2} as

$$\psi_{c_1} = \frac{1}{2}\ln\left[\operatorname{sech}\left(\psi_{c_2}\right)\right], \quad \psi_{c_2} = -\operatorname{arctanh}\left(\frac{\sqrt{2}M}{Q}\right). \tag{3.18}$$

The behavior for C is found by replacing (3.16) inside (3.9) and taking the leading order contribution for large r. We obtain $(1-C) \simeq e^{-2\phi}$ in the asymptotic limit, so the Reissner-Nordström geometry is fully recovered.

After fixing the asymptotic behavior of the different solutions, we proceed by integrating the semiclassical equations towards decreasing r. In doing so, several scenarios arise depending on the balance between the charge Q and the asymptotic mass M. We start our integration from the asymptotic region, with positive ψ (recall this condition is equivalent to assuming $M > 0$), situating the solution above all roots and analytical exact solutions depicted in Fig. 3.1. Eq. (3.10) guarantees that ψ grows monotonically inwards unless it intersects one of the roots. In view of Fig. 3.1, there exist three possibilities: the solution ψ either diverges at some radius $r > r_{\text{div}}$; it grows sufficiently slow as to cross r_{div}, encountering a maximum and extending to $r \simeq 0$; or it stays in between both regimes, diverging at $r = r_{\text{div}}$ at the same exact rate as the root $\mathcal{R}_2$ does. The solution will belong to one of these regimes depending on the relative values of Q, M and α. In turn, as long as $M > 0$ and $\alpha > 1$, there exists a critical value of the charge Q_{crit} that corresponds to the separatrix solution. In the following we analyze these three cases individually.

3.3 Under-charged regime

The first solutions we analyze are deformed continuously to the Schwarzschild counterpart in the limit $Q \to 0$, and are valid up to a critical value of the charge Q_{crit} that depends on the parameters of the integration.

3.3.1 Near-neck expansion

Assuming that the function ψ diverges at some finite radius $r_{\text{B}} > r_{\text{div}}$, the differential equation (3.10) can be approximated, at leading order in ψ, by

$$\psi' \simeq A_{3\text{B}}\psi^3. \tag{3.19}$$

The term $A_{3\text{B}}$ is just the coefficient A_3 in (3.10) evaluated in the $r \to r_{\text{B}}$ limit, where it takes a constant value

$$\begin{aligned} A_{3\text{B}} = &- l_{\text{P}}^2 r_{\text{B}} \left[r_{\text{B}}^2 \left(1 + \frac{\alpha l_{\text{P}}^4}{\left[r_{\text{B}}^2 + \alpha l_{\text{P}}^2 \right]^2} \right) - Q^2 \left(1 + \frac{l_{\text{P}}^2 \left[r_{\text{B}}^2 + 2\alpha l_{\text{P}}^2 \right]}{\left[r_{\text{B}}^2 + \alpha l_{\text{P}}^2 \right]^2} \right) \right] \\ &\times \left\{ \left(r_{\text{B}}^2 - Q^2 \right) \left[r_{\text{B}}^2 + l_{\text{P}}^2 (\alpha - 1) \right] \right\}^{-1}. \end{aligned} \tag{3.20}$$

Note that the sign of this constant depends on Q. Integrating the differential equation (3.19) returns the following pair of solutions

$$\psi \simeq \pm\sqrt{\frac{k_0}{4(r-r_{\rm B})}} + \mathcal{O}\left(r-r_{\rm B}\right)^{1/2}, \tag{3.21}$$

where

$$k_0 = -\frac{2}{A_{3\rm B}}. \tag{3.22}$$

Again, the $\pm$ signs indicate that there are two solutions, one per branch. For the moment, we take the $+$ sign. Later, we will connect it to the $-$ sign solution.

For each of the two solutions (3.21) to be real, the constant k_0 must be positive, which in turn implies that

$$|Q| < r_{\rm B}\sqrt{\frac{\alpha l_{\rm P}^4 + \left(r_{\rm B}^2+\alpha l_{\rm P}^2\right)^2}{l_{\rm P}^2\left(r_{\rm B}^2+2\alpha l_{\rm P}^2\right)+\left(r_{\rm B}^2+\alpha l_{\rm P}^2\right)^2}}. \tag{3.23}$$

This is the semiclassical equivalent of the condition that guarantees the non-extremal nature of the classical Reissner-Nordström BH (i.e. $Q<M$). We will analyze in more detail the content of the constraint (3.23) below; for the moment let us keep describing the elements of the metric.

The redshift function follows from integrating Eq. (3.21) and the compactness from replacing Eq. (3.21) in (3.9). In the $r\to r_{\rm B}$ limit, these quantities become

$$\phi = \sqrt{k_0(r-r_{\rm B})} + \phi_{\rm B} + \mathcal{O}\left(r-r_{\rm B}\right)^{3/2}, \tag{3.24}$$

$$C = 1 - k_1(r-r_{\rm B}) + \mathcal{O}\left(r-r_{\rm B}\right)^{3/2}, \tag{3.25}$$

where

$$k_1 = \frac{4(r_{\rm B}^2-Q^2)(r_{\rm B}^2+\alpha l_{\rm P}^2)}{l_{\rm P}^2 r_{\rm B}^2 k_0} > 0, \tag{3.26}$$

and the integration constant $\phi_{\rm B}$ (to be found numerically) denotes the value of the redshift function at $r=r_{\rm B}$.

We can express the line element in coordinates adapted to wormhole spacetimes through the transformation (2.30) matching signs to obtain a continuous and differentiable metric through $l=l_{\rm B}$, obtaining

$$ds^2 \simeq -e^{\sqrt{k_0 k_1}(l-l_{\rm B})+2\phi_{\rm B}}dt^2 + dl^2 + \left[\frac{k_1}{4}\left(l-l_{\rm B}\right)^2 + r_{\rm B}^2\right]^2 d\Omega^2, \tag{3.27}$$

which is identical in form to Eq. (2.32). The line element (3.27) proves that the charged case exhibits the same type of elimination of the horizon as the uncharged

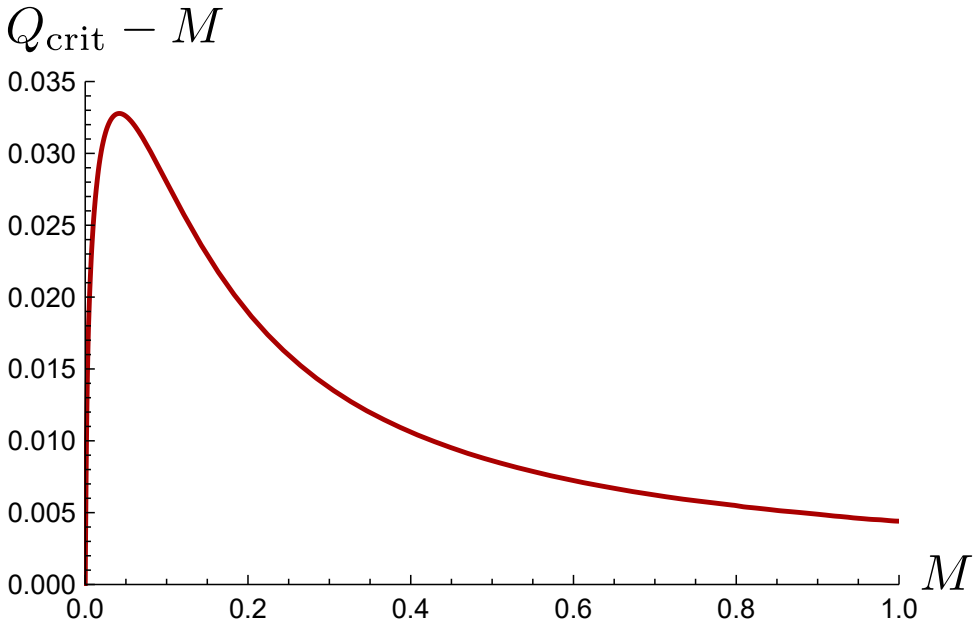

Fig. 3.2.: Plot of the quantity $Q_{\rm crit} - M$ in terms of M. The parameter $Q_{\rm crit}$ denotes the value of the charge that separates under-charged from over-charged spacetimes.

situation: substitution by a wormhole neck. The role of the charge here is, similarly to the classical situation, to produce a repulsive contribution that slows down the growth rate of the Misner-Sharp mass inwards. Thus, the neck radius is dragged towards smaller values of r as Q increases.

In the $Q \to 0$ limit, this family of solutions connects smoothly with the semiclassical Schwarzschild counterpart. On the other hand, the solution (3.21) provides an upper bound for the charge parameter given by (3.23). Since the neck radius $r_{\rm B}$ can only be found numerically, we are unable to provide an exact bound for Q in terms of the asymptotic mass M without numerically integrating the full equations. In Figure 3.2 we have plotted the lowest charge value $Q_{\rm crit}$ that takes the solution out of the wormhole regime for several (although quite small in Planck units) asymptotic masses. We find that the separatrix charge $Q_{\rm crit}$ needs to surpass the asymptotic mass M. This is so because the vacuum polarization of the scalar field, by backreacting on the geometry, modifies ("dresses") the mass of the spacetime, while charge stays constant throughout the geometry. In order to compensate for this increase in mass as smaller radii are approached, $Q_{\rm crit}$ lies above its classical value $Q_{\rm crit} = M$, as the expansion of (3.23) in the $l_{\rm P} \to 0$ limit shows

$$|Q| \lesssim r_{\rm B}\left[1 - \frac{l_{\rm P}^2}{2r_{\rm B}^2} + \mathcal{O}\left(\frac{l_{\rm P}}{r_{\rm B}}\right)^4\right], \tag{3.28}$$

where $r_{\rm B} > r_+$ always. Since for classical sub-extremal BHs $r_+ > M$, we conclude that the smallest value of Q that does not obey (3.23) must be greater than M.

3.3.2 Asymptotic singularity

Below the neck, in virtue of Eq. (3.10) and the roots and exact solutions depicted in Fig. 3.1, ψ grows with r until crossing $\mathcal{R}_1$, and then decreases monotonically confined between the curves $\mathcal{R}_1$ and ψ_+.

Assuming that, asymptotically in r, the ψ function obeys

$$\psi = \psi_+ + \beta(r), \tag{3.29}$$

where $\beta(r)$ measures the deviation from the exact solution. Replacing in (3.10), keeping terms up to linear order in β and taking the limit $r \to \infty$ results in

$$\beta' \simeq -\frac{\{-16r^4 + 8l_{\rm P}^2\left[Q^2 + r^2(1-2\alpha)\right] + l_{\rm P}^4(5-32\alpha)\}}{4l_{\rm P}^2 r^3}\beta, \tag{3.30}$$

which integrated (3.30) gives

$$\beta = \beta_0 \left(\frac{r}{l_{\rm P}}\right)^{1-4\alpha} e^{-\frac{2r^2}{l_{\rm P}^2}} \left[1 - \frac{Q^2}{r^2} - \frac{l_{\rm P}^2(5-32\alpha)}{8r^2} + \mathcal{O}(r^{-4})\right], \tag{3.31}$$

where β_0 an integration constant with dimensions of inverse of length. Inserting this in Eq. (3.29) and integrating to obtain the redshift function and compactness yields the asymptotic metric

$$\begin{aligned} ds^2 \simeq \left(\frac{r}{l_{\rm P}}\right)^{1-4\alpha} e^{-2r^2/l_{\rm P}^2} \Bigg\{ & -a_0 \left(1 - \frac{l_{\rm P}^2}{8r^2}\right) dt^2 \\ & + \frac{2\beta_0 r^2}{l_{\rm P}} \left[1 - \frac{(9-32\alpha)l_{\rm P}^2}{8r^2}\right] dr^2 \Bigg\} + r^2 d\Omega^2. \end{aligned} \tag{3.32}$$

Q-dependent terms enter this expression as subdominant contributions, so they do not alter the asymptotic form of the geometry, which is the same as in the Schwarzschild case (2.41). This becomes evident already at the level of Eq. (3.10), where terms proportional to Q are subleading with respect to the "vacuum", RSET-dependent contributions already present in the Schwarzschild case. From this perspective, there is no qualitative difference with respect to the Schwarzschild case ($Q = 0$) discussed in Ch. 2.

In the following sections, we will turn to other non-wormhole geometries with values of the charge greater than or equal to the separatrix value $Q_{\rm crit}$.

3.4 Over-charged regime

3.4.1 Solution across r_{div}

We now turn to the situation where the resulting geometries have no wormhole neck, extending all the way down to $r = 0$. This behavior manifests in two ways: Either by considering a negative mass ($M < 0$), or by increasing Q beyond its critical value Q_{crit} while $M > 0$. In the latter case, compactness increases inwards, although its growth rate slows down as Q increases. Similarly, the repulsion exerted by the electromagnetic field slows down the growth rate of ψ, displacing the surface r_{B} towards smaller radii. As Q increases, the root $\mathcal{R}_2$, which diverges (while remaining positive) at r_{div}, is eventually intersected by the solution. Indeed, the explicit expression for r_{div} can be derived from solving the polynomial expression $A_3 = 0$ for r. From all the roots that factorize this expression, the one which corresponds to the surface of infinite $\mathcal{R}_2$ turns out to be

$$\begin{aligned} r_{\text{div}} = &\Big\{2^{4/3}Q^4 + 2Q^2\left[Q^2\mathcal{V} + l_{\text{P}}^2\left(3^{3/2}\mathcal{U} + \alpha\mathcal{V}\right)\right]^{1/3} + \left[2Q^2\mathcal{V} + 2l_{\text{P}}^2\left(3^{3/2}\mathcal{U} + \alpha\mathcal{V}\right)\right]^{2/3} \\ &+2l_{\text{P}}^2\left[2^{1/3}Q^2(3+2\alpha) - 2\alpha\left(Q^2\mathcal{V} + l_{\text{P}}^2\left[3^{3/2}\mathcal{U} + \alpha\mathcal{V}\right]\right)^{1/3}\right] + 2^{4/3}l_{\text{P}}^4\alpha(\alpha-3)\Big\} \\ &\times\left[6Q^2\mathcal{V} + 6l_{\text{P}}^2\left(3^{3/2}\mathcal{U} + \alpha\mathcal{V}\right)\right]^{1/6}, \end{aligned} \tag{3.33}$$

with

$$\begin{aligned} \mathcal{U} = &\Big\{Q^8(4\alpha-1) + 2l_{\text{P}}^2Q^6\left[\alpha(9+8\alpha) - 2\right] + \alpha l_{\text{P}}^4Q^4\left[12 + \alpha(47+24\alpha)\right] \\ &+4\alpha^2l_{\text{P}}^6Q^2\left[\alpha(9+8\alpha) - 3\right] + 4\alpha^3l_{\text{P}}^8(1+\alpha)^2\Big\}^{1/2}, \\ \mathcal{V} = &\,2Q^4 + l_{\text{P}}^2Q^2(9+4\alpha) + 2\alpha l_{\text{P}}^4(9+\alpha). \end{aligned} \tag{3.34}$$

In the $l_{\text{P}} \to 0$ limit,

$$r_{\text{div}} \simeq Q + \frac{l_{\text{P}}^2}{2Q} + \cdots, \tag{3.35}$$

which implies that, in the classical limit, this surface lies at $r = Q$. In short, in the classical situation the surface $r = Q$ serves as a separatrix between sub-extremal Reissner-Nordström geometries, for which ψ diverges at $r = r_+ > Q$, and super-extremal Reissner-Nordström geometries, where ψ is bounded from above. The solution where ψ diverges exactly as $(r-Q)^{-1}$ corresponds to the extremal BH. The introduction of the length scale l_{P} associated to quantum corrections displaces the separatrix surface outwards. Figure 3.3 shows a plot of the quantity $r_{\text{div}} - Q$ in terms of the charge Q.

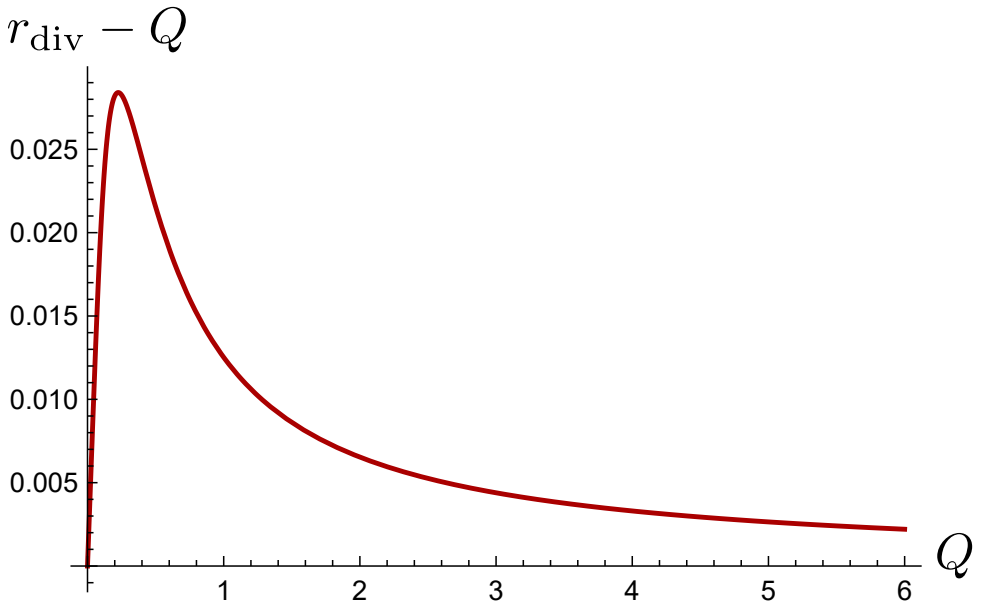

Fig. 3.3.: Plot of the quantity $r_{\rm div} - Q$ for various values of the charge Q. Whereas for large charges this quantity tends to zero, in the regime of small charges comparable, in magnitude, to $l_{\rm P}$, this difference increases appreciably, going to 0 again in the $Q \to 0$ limit.

The crossing with $\mathcal{R}_2$ at $r = r_{div}$ corresponds to a maximum in ψ, preventing the appearance of a wormhole neck. Instead, the coordinate r now extends to $r = 0$. In doing so, ψ has to cross $r = Q$, the surface where the differential equation (3.10) is singular (check Fig. 3.4). We can prove that the solution is regular there taking into account Eq. (3.13). Both $\psi_\pm$ [see Eq. (2.10)] are compatible with a regular behavior of the differential equation at $r = Q$, as for the $\psi_\pm$ solutions, the Q-dependent terms in (3.10) (which contain the possible singularities) vanish identically. Any other solution must intersect ψ_+ or ψ_- at $r = Q$ to avoid a singularity. Since the right-hand side of (3.13) is divergent, the Picard-Lindelöf theorem does not hold at $r = Q$, allowing solutions to intersect at that precise surface. The solution we are describing in this section will intersect first ψ_-.

Let us derive the form of the solution ψ around $r = Q$ by assuming

$$\psi = \psi_- + \xi(r), \tag{3.36}$$

in a neighborhood of $r = Q$, where ξ is the function that measures the deviation between solutions. To guarantee the finiteness of (3.14), ξ must vanish at least linearly as r approaches Q. Replacing (3.36) and its first derivative in (3.13) and dropping terms beyond linear order in ξ, we obtain in the $r \to Q$ limit

$$\xi'(r) \simeq \frac{\xi(r)}{r - Q}, \tag{3.37}$$

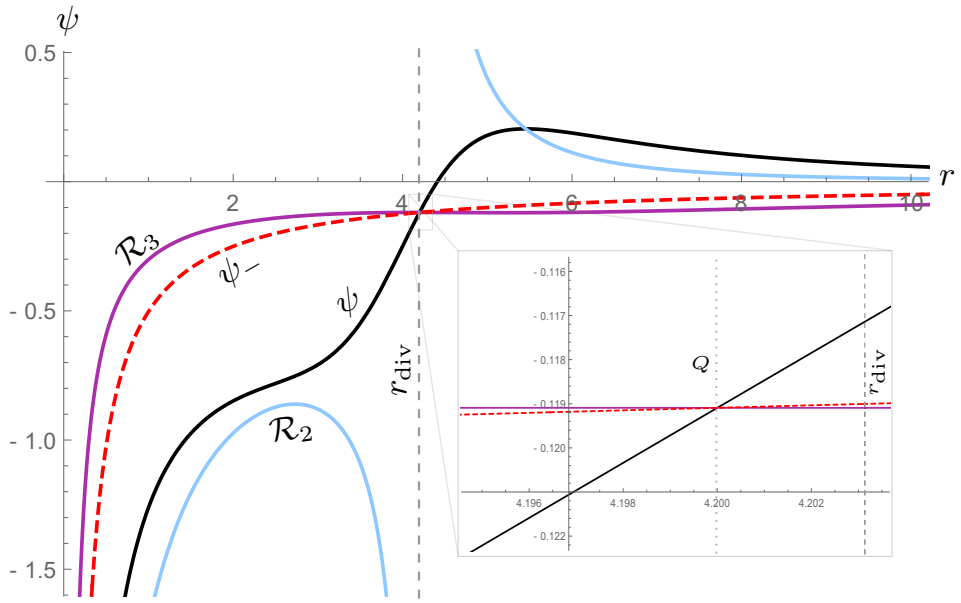

Fig. 3.4.: Numerical plot of an over-charged solution (black curve) alongside the roots $\mathcal{R}_{2,3}$ and the exact solution ψ_-. Once it intersects $\mathcal{R}_2$, the solution must cross ψ_- at $r = Q$ and becomes trapped between $\mathcal{R}_2$ and ψ_- by self-consistency of the differential equation. If the maximum for ψ is reached closer to $r_{\rm div}$, then the solution decreases more abruptly and can intersect $\mathcal{R}_2$ zero, one or two times, but the behavior at $r = 0$ remains unchanged. For this plot we have chosen $M = 4, Q = 1.05M$ and $\alpha = 1.01$. The region around the intersection point $r = Q$ has been depicted in detail.

which upon integration returns

$$\xi \simeq (r - Q)\,\xi_0, \tag{3.38}$$

where γ_0 is an integration constant with dimensions of inverse of length squared. Thus, as ψ crosses $r = Q$, it does so in a manner that ensures that the right-hand side of (3.13) does not diverge.

We can qualitatively describe the behavior of these solutions in an exhaustive way. After the solution crosses $r = Q$ towards smaller radii, it can intersect $\mathcal{R}_3$ zero times, once or twice. In the first case, ψ stays confined between the exact solution ψ_- and the root $\mathcal{R}_3$, its value decreasing until it reaches $-\infty$, as depicted in Fig. 3.4. The situation in which there are two intersections with $\mathcal{R}_3$ occurs whenever ψ decreases sufficiently fast (after crossing $r = Q$) so that it intersects the rightmost part of $\mathcal{R}_3$. After the first intersection, it grows until $\mathcal{R}_3$ is encountered for a second time. In between these two situations there is one in which $\mathcal{R}_3$ is touched once tangentially at the same point in which $\mathcal{R}_3$ reaches its maximum value, which becomes a saddle point of ψ.

The other possibility that we mentioned at the beginning of this section requires a negative asymptotic mass, $M < 0$. In this case, identical to the one described in Subsec. 2.3.4, Ch. 2, ψ takes negative values above ψ_- at infinity. By self-consistency of (3.10), the solution decreases monotonically inwards, goes across r_{div}, and diverges towards $-\infty$ in the $r \to 0$ limit, confined between $\mathcal{R}_3$ and ψ_-. Thus, the $r \simeq 0$ behavior of the over-charged solution and the geometry with negative asymptotic mass is the same. One of the shared features is the existence of a curvature singularity at $r = 0$, as it is analyzed in the next section.

3.4.2 Singularity at $r = 0$

The form of the solution close to the origin in the over-charged regime comes from a combination between the (singular) electromagnetic field and the effects of vacuum polarization. The magnitude of the CRP-RSET describing quantum fluctuations near $r = 0$ is strongly affected by the value assigned to the regulator α. Indeed, if the CRP-RSET is sufficiently suppressed by considering a large α, the dominant source of compactness in the $r \to 0$ limit will come from terms proportional to the charge Q. We obtain the form of the metric close to the radial by solving the semiclassical equations in this limit.

The procedure is as follows: In order to simplify (3.8), we need to obtain the form of solutions of Eq. (3.10) near the origin; The resulting approximate expression and its first derivative ψ' are then inserted in (3.8). Therefore, we start by assuming ψ takes the form

$$\psi = \frac{a}{r}, \tag{3.39}$$

which is the only profile both divergent at $r \to 0$ and compatible with Eq. (3.10). Replacing (3.39) and its first derivative in Eq. (3.10) and expanding in the $r \to 0$ limit, we obtain the following solutions for the constant a:

$$a_0 = -\frac{\alpha}{2+\alpha}, \quad a_\pm = -\left(\alpha \pm \sqrt{\alpha(\alpha-1)}\right). \tag{3.40}$$

The first of these values is a solution that appears as a consequence of the introduction of the electric charge. We have not been able to relate it with any of the situations described in this Chapter, so chances are that this solution does not connect with an asymptotically flat region. The last two values correspond to evaluating the exact solutions $\psi_\pm$ in the $r \to 0$ limit. The complete solution depicted in Fig. 3.4 stays within the branch in which initial conditions have been imposed (in other words, imposing asymptotic flatness implies that the concealed branch is never explored), so we stay with the coefficient a_- in (3.40), which has

a well-defined classical limit. Terms sub-leading with respect to the leading order (3.39) (which would be linear in r) can be derived, but the leading-order form of ψ is sufficient to illustrate our point here.

After replacing (3.39) and its derivative in (3.8), we obtain the following approximate linear differential equation for the compactness

$$C' = \frac{[(2-a_-)a_- - \alpha]\, C}{(\alpha + a_-)\, r}\left[1 + \mathcal{O}(r)\right] + \frac{\alpha Q^2}{(\alpha + a_-) r^3}\left[1 + \mathcal{O}(r^{-1})\right]. \tag{3.41}$$

Integrating Eq. (3.41) is straightforward and yields

$$C = c_1 \left(\frac{r}{l_{\rm P}}\right)^{b_1}\left[1 + \mathcal{O}\left(r^2\right)\right] + c_2 \left(\frac{Q}{r}\right)^2\left[1 + \mathcal{O}\left(r^0\right)\right], \tag{3.42}$$

where c_1 is an arbitrary integration constant and b_1 and c_2 are known parameters whose values are shown in Eqs. (3.43, 3.44) below. The value of c_1 is determined by numerical integration and will have some unknown dependence on M, Q, α and $l_{\rm P}$. Since, in view of Fig. 3.4, ψ approaches ψ_- in the $r \to 0$ limit, this ensures that compactness must diverge towards negative infinity, implying $c_1 < 0$. The exponent of the first term is found to be

$$b_1 = -\frac{2(1+\alpha)\left[1 - \alpha + \sqrt{\alpha(\alpha-1)}\right]}{\alpha - 1}, \tag{3.43}$$

whereas the second coefficient is

$$c_2 = -\frac{\alpha}{2}\left\{2\sqrt{\alpha(\alpha-1)} - \alpha\left[\alpha + 1 - \sqrt{\alpha(\alpha-1)}\right]\right\}^{-1}. \tag{3.44}$$

In the $r \to 0$ limit, compactness has a divergence whose strength (i.e. the power of the term that diverges faster in the $r \to 0$ limit) is modulated by the value of the regulator. For large α we essentially recover the behavior from the classical Reissner-Nordström geometry, as expected for a fully suppressed CRP-RSET, whereas in the $\alpha \to 1$ limit, b_1 diverges. Although for $\alpha = 1$ the CRP-RSET is itself regular, the feedback mechanism provided by the semiclassical equations moves the Polyakov divergence to $r = 0$. An already singular geometry is being coated by a cloud of negative mass coming from vacuum polarization which nourishes from this singularity. Hence, it is expected that the leading divergence in C becomes more than polynomially strong in the $\alpha \to 1$ limit. In consequence, and as long as $\alpha < \frac{1}{2}\left(1 + \sqrt{17}\right)$, the first term in (3.42) dominates over the second one. For large α, however, the electromagnetic charge carries the leading-order divergence.

There exists an intermediate situation where both terms in (3.42) diverge at the same rate as $r \to 0$. This occurs for the exact value $\alpha = \frac{1}{2}\left(1+\sqrt{17}\right)$, for which $b_1 = -2$. Replacing this value of the regulator α in (3.41) and integrating yields

$$C = \frac{\left(1+\sqrt{17}\right)Q^2}{4r^2}\log r + \mathcal{O}\left(r^{-2}\right). \tag{3.45}$$

This solution acts as the separatrix between two distinct behaviors of the compactness function at the curvature singularity. It describes a situation where the divergent accumulation of vacuum polarization becomes comparable to that of the mass contribution coming from the singular electromagnetic source. Then, both contributions intertwine and give rise to a dominant divergence in C that depends on Q times a logarithmic contribution. It is somewhat remarkable that a particular regularization prescription for the RSET in the vicinity of $r = 0$ is capable to enhance the strength of a singularity that depends on the classical SET, given that the sole interaction between the quantum and classical sources is through the spacetime geometry, as both sources are conserved independently.

In summary, this section has illustrated that the over-charged regime, which guarantees the presence of a naked singularity, shows a hierarchy of divergent behaviors depending on how we adjust the regulator. For small α, the dominant contribution to the compactness comes from the backreaction of vacuum polarization on the vicinity of the singularity. However, if the CRP-RSET is sufficiently dampened, the contribution coming from the singular charge-source giving rise to the electromagnetic field is uncovered. In between both regimes there exists a separatrix solution where the dominant divergence becomes a mix of quantum and classical contributions.

3.5 Quasi-extremal regime

In between both of the aforementioned regimes (asymmetric wormholes and naked singularities) there exists a single separatrix solution for which ψ diverges at precisely r_{div}, reminiscent of the classical extremal BH. In the present section we will characterize this separatrix.

3.5.1 Geometry around the quasi-extremal horizon

The separatrix solution corresponds to the case in which the divergence in ψ takes place at the same radius where $\mathcal{R}_2$ diverges, i.e. at $r = r_{\text{div}}$. Furthermore, it can be

checked that this divergence in ψ occurs at the same pace as $\mathcal{R}_2$ blows up, that is, as $(r - r_{\text{div}})^{-1}$. Take a behavior of the form

$$\psi = \frac{1}{\lambda(r - r_{\text{div}})^{\gamma}}, \quad \text{with } \gamma > 0. \tag{3.46}$$

Now, taking the limit $r \to r_{\text{div}}$ in (3.10) reveals that the coefficient A_3 vanishes as $A_3 \propto (r - r_{\text{div}})$. This can be straightforwardly checked by factorizing the numerator of A_3 (3.10), which is a polynomial of sixth degree for the radial coordinate with one root equal to r_{div} (3.33). Assuming the profile (3.46), the following approximate relation is derived from (3.10):

$$-\frac{\gamma}{\lambda}(r-r_{\text{div}})^{-\gamma-1} = \frac{B}{\lambda^3}(r-r_{\text{div}})^{-3\gamma+1} + \frac{A_2(r_{\text{div}})}{\lambda^2}(r-r_{\text{div}})^{-2\gamma} + \mathcal{O}\left[(r - r_{\text{div}})\right]^{-\gamma}, \tag{3.47}$$

where $B = A_3/(r-r_{\text{div}})|_{r=r_{\text{div}}}$ has a finite value at $r = r_{\text{div}}$. Consistency of the above expression enforces $\gamma = 1$. Therefore, both the quadratic and cubic terms in ψ from Eq. (3.10) enter at leading order in the $r \to r_{\text{div}}$ limit. Simplifying terms, the expression reduces to a quadratic equation for λ

$$\lambda^2 + \lambda A_2(r_{\text{div}}) + B = 0, \tag{3.48}$$

Solutions of Eq. (3.48) return two values of λ, which we denote as $\lambda_{\pm}$ (the $\pm$ label here denotes the sign of λ). We have found the explicit analytical expressions of $\lambda_{\pm}$ by using the software Mathematica. They correspond to lengthy expressions that are not illuminating, so we avoid writing them here. The coefficient λ_{-} is negative-valued and hence comes in conflict with our integration condition from the asymptotic region. The profile (3.46) indicates the presence of an outer horizon at $r = r_{\text{div}}$, for which the redshift function vanishes at $r = r_{\text{div}}$ with a positive slope. Hence, only the constant λ_{+} reproduces the required behavior of an outer horizon. Therefore, we restrict to $\lambda = \lambda_{+}$ in order to derive the approximate form of the geometry in what follows.

Given that $\psi = \phi'$ by definition, Eq. (3.46) with $\gamma = 1$ and $\lambda = \lambda_{+}$ is integrated to give to the redshift function

$$e^{2\phi} \simeq f_0 \left| \frac{r - r_{\text{div}}}{r_{\text{div}}} \right|^{2/\lambda_{+}}, \tag{3.49}$$

with f_0 a positive integration constant. The power with which the redshift function vanishes is modulated by λ_{+}, which has an involved dependence on α, l_{P}, and Q. For example, Figure 3.5 shows a plot of the exponent $2/\lambda_{+}$ in terms of the charge Q for various values of the regulator. We observe that, for $Q \gg l_{\text{P}}$, it goes as

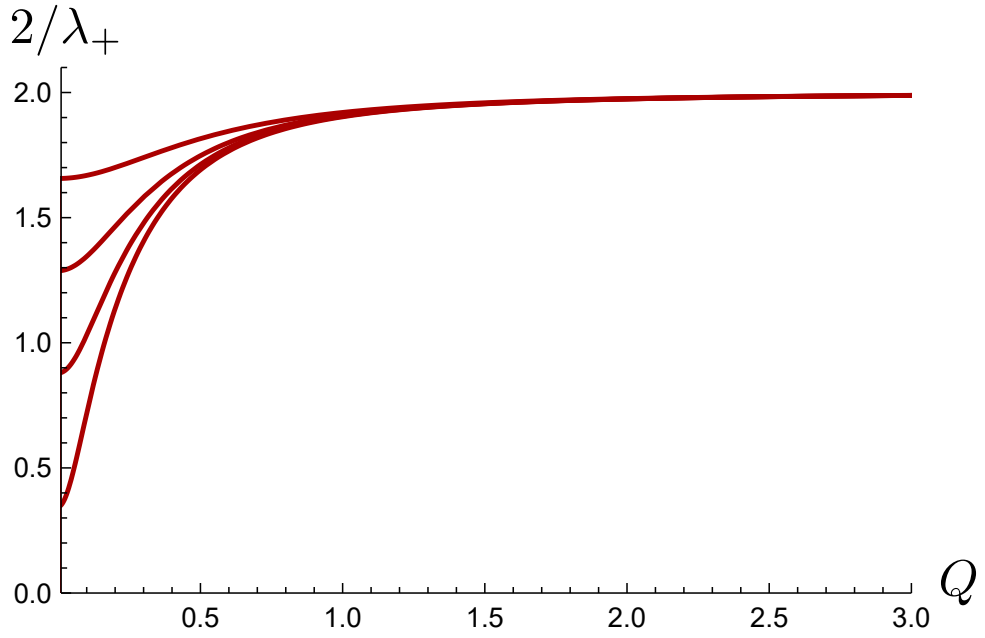

Fig. 3.5.: Plot of the exponent of the redshift function in terms of the charge Q for various values of α (from bottom to top, α takes the values $1.01, 2, 4$ and 10, respectively). In the limit $Q \to 0$ it goes to a constant value depending on α while for large Q it approaches the extremal BH solution from below. The extremal BH is only recovered for $|Q| \to \infty$. For small Q the redshift function can have a Schwarzschild-like horizon.

$$\frac{2}{\lambda_+} = 2 - \frac{4l_{\rm P}^2}{Q^2} + \mathcal{O}\left(\frac{l_{\rm P}^4}{Q^4}\right) \tag{3.50}$$

and the extremal Reissner-Nordström solution (for the $r > M = Q$ geometric patch) is strictly recovered only in the limit of $l_{\rm P} = 0$. On the other hand, the compactness function can be derived from (3.9)

$$C = 1 - \kappa \left(\frac{r - r_{\rm div}}{r_{\rm div}}\right)^2 + \mathcal{O}\left[(r - r_{\rm div})^3\right], \tag{3.51}$$

with

$$k_+ = \frac{\lambda_+^2 (r_{\rm div}^2 - Q^2)(r_{\rm div}^2 + \alpha l_{\rm P}^2)}{l_{\rm P}^2 r_{\rm div}^2} > 0. \tag{3.52}$$

Given the classical limits of the quantities $r_{\rm div}$ in Eq. (3.35) and λ_+ in Eq. (3.50), we obtain $k_+ = 1$ for $Q \gg l_{\rm P}$, thus reproducing the extremal Reissner-Nordström compactness function.

The local form of the metric for $r > r_{\rm div}$ in this solution is

$$ds^2 \simeq -f_0 \left|\frac{r - r_{\rm div}}{r_{\rm div}}\right|^{2/\lambda_+} dt^2 + \left[\sqrt{\kappa}\left(\frac{r - r_{\rm div}}{r_{\rm div}}\right)\right]^{-2} dr^2 + r^2 d\Omega^2. \tag{3.53}$$

This metric has several interesting features that we turn to describe. One remarkable characteristic is that the redshift function of the geometry vanishes with a smaller exponent than in the classical extremal solution. The radial part of the geometry, however, retains the quadratic dependence on $r - r_{\text{div}}$. The affine distance between the horizon r_{div} and any point of the spacetime is infinite, as in ordinary extremal spacetimes. This is why we refer to these solution as "quasi-extremal".

Now we shall continue the solutions beyond r_{div}. We could do that in a completely symmetric fashion. However, this would imply, on the one hand, that the radius would diminish inwards, but moreover, that the solution is no longer a proper vacuum solution as it would correspond to having a null shell localized at the horizon. On the contrary, we can select a solution with a negatively diverging behavior at r_{div}, $\psi = -1/\lambda(r_{\text{div}} - r)$, assuming now $r < r_{\text{div}}$. This selection breaks the symmetry of the construction and is more akin to a quantum version of the extremal Reissner-Nordström solution. Consistency with the idea that now the redshift function slope should be positive makes us to select again the λ_+ value inside the horizon. Thus, the final local form of the metric is (3.53), which is now valid for a sufficiently small open interval containing $r = r_{\text{div}}$.

In crossing the horizon, the solution jumps from the unconcealed branch to the concealed branch of the semiclassical corrections. Recall that the concealed branch has no well-defined classical limit. Therefore, the quasi-extremal solution cannot be found by perturbatively deforming the extremal Reissner-Nordström BH. This will be more clearly seen when analyzing the next order expansion of the metric around $r = r_{\text{div}}$ (see right below). Thus, our self-consistent analyses reveal that the presence of horizons enforces non-perturbative backreaction effects, typically completely removing horizons, or at most maintaining an extremal-like horizon with the special characteristics we are describing.

3.5.2 Singularity at the quasi-extremal horizon

A notable difference with the classical extremal BH resides in the value of the exponent in the redshift function, $1/3 < 2/\lambda_+ < 2$ (in the $\alpha \to 1$ limit). The necessary absolute value in (3.49) spoils the analyticity of the metric at the quasi-extremal horizon r_{div}. Despite this unusual behavior of the metric, curvature scalars calculated from (3.53) that are quadratic in the Ricci and Riemann tensors are finite and analytic at r_{div} (although a different type of singularity is indeed present, as seen in what follows). This somehow unexpected result comes from the fact that any appearance of the function ψ in the Kretschmann scalar (1.10) is accompanied by C factors which complete eliminate potential divergences.

The finiteness and analyticity of curvature invariants at the quasi-extremal horizon from the particular form of (3.53) describing the leading-order contributions in an expansion around $r = r_{\text{div}}$. The next order in the expansion introduces additional terms in ψ which do not coincide with the classical solution in the $l_{\text{P}} \to 0$ limit. As mentioned above, this is another clear indication that the quasi-extremal solution has an inherently quantum nature. Let us illustrate this point by assuming ψ acquires an additional contribution:

$$\psi = \frac{1}{\lambda_+(r - r_{\text{div}})} + \Psi(r), \tag{3.54}$$

where $\Psi(r)$ is some function that either diverges slower than $(r - r_{\text{div}})^{-1}$ or does not diverge at all. Inserting this ansatz in (3.10), expanding in $r - r_{\text{div}}$, and taking into account the cancellation of the leading order contributions, we obtain the expression

$$\Psi' \simeq \left(A_1 + 2A_2\Psi + \frac{3B\Psi}{\lambda_+}\right)\left[\frac{1}{\lambda_+(r - r_{\text{div}})} + \Psi\right] - \Psi^2\left[A_2 - B\left(r - r_{\text{div}}\right)\Psi\right] + A_0, \tag{3.55}$$

where all coefficients are evaluated at $r = r_{\text{div}}$.

Let us assume first that Ψ diverges slower than $1/(r - r_{\text{div}})$. This assumption implies that the leading form of the previous equation is

$$\Psi' = \left(2A_2 + \frac{3B}{\lambda_+}\right)\lambda_+^{-1}\frac{\Psi}{(r - r_{\text{div}})}, \tag{3.56}$$

which after solving implies

$$\Psi \propto \frac{1}{(r - r_{\text{div}})}, \tag{3.57}$$

but this is against our starting assumption. Therefore Ψ must be finite at $r = r_{\text{div}}$.

Hence, the only remaining possibility for the consistency of (3.55) is that Ψ equals a constant that causes the vanishing of all divergent contributions. An extra term linear in $r - r_{\text{div}}$ can be added to (3.54) so that the remaining constant terms vanish as well. The solution ψ takes the form

$$\begin{aligned}
\psi &= \frac{1}{\lambda_+(r - r_{\text{div}})} + \Psi_1 + \Psi_2(r - r_{\text{div}}) + \mathcal{O}\left[(r - r_{\text{div}})^2\right], \\
\Psi_1 &= -\frac{A_1\lambda_+}{3B + 2A_2\lambda_+}, \\
\Psi_2 &= \frac{3B\Psi_1^2 + \lambda_+\left[A_0 + (A_1 + A_2\Psi_1)\,\Psi_1\right]}{-3B + \lambda_+\left(\lambda_+ - 2A_2\right)}\lambda_+.
\end{aligned} \tag{3.58}$$

The coefficients Ψ_1 and Ψ_2 do not reduce to the extremal BH solution in the classical limit. The main reason behind this is linked to how semiclassical modifications extend the space of solutions of the classical theory. Indeed, the quasi-extremal geometry emerges as a consequence of the terms cubic in ψ the RSET introduces in (3.10) and, as a consequence, it does not connect with the extremal BH solution when these cubic terms are suppressed. From a different perspective, as we already mentioned, part of the support of the solution lies within the concealed branch, which is intrinsically quantum and has no classical limit.

Replacing expression (3.58) in Eq. (3.9) we obtain the following approximate expression for the compactness

$$1-C=\kappa\left(\frac{r-r_{\text{div}}}{r_{\text{div}}}\right)^2\left[1+\kappa_1(r-r_{\text{div}})+\mathcal{O}\left(r-r_{\text{div}}\right)^2\right], \tag{3.59}$$

with

$$\kappa_1=\frac{2\lambda_+}{l_{\text{P}}^2 r_{\text{div}}}\left\{\lambda\left[r_{\text{div}}^2+l_{\text{P}}^2\left(\alpha+r_{\text{div}}\Psi_1\right)\right]-\frac{l_{\text{P}}^2Q^2}{r_{\text{div}}^2-Q^2}+\frac{\alpha l_{\text{P}}^4}{r_{\text{div}}^2+\alpha l_{\text{P}}^2}\right\}>0. \tag{3.60}$$

The Kretschmann scalar (1.10) takes the form

$$\begin{aligned}\mathcal{K}=\frac{4\left(\lambda_+^4+\kappa^2\right)}{\left(\lambda_+ r_{\text{div}}\right)^4}\Big\{1+&\frac{\kappa^2 r_{\text{div}}\left(2+\lambda_+\right)\left(\kappa_1+2\lambda\Psi_1\right)-4\lambda_+^4}{r_{\text{div}}\left(\lambda_+^4+\kappa^2\right)}(r-r_{\text{div}})\\&+\mathcal{O}\left[\left(r-r_{\text{div}}\right)^2\right]\Big\}.\end{aligned} \tag{3.61}$$

The constant term corresponds to the "bulk" contribution coming from the leading-order contributions in the line element (3.53). Additional vanishing terms appear in curvature invariants when subdominant contributions are taken into account. The quasi-extremal metric is non-analytic at the horizon but, due to its particular form, this behavior does not reflect on curvature invariants. Similar tendencies were found in [192, 193] in the context of extremal BHs in dilatonic gravity coupled to a quantum scalar field, in the sense that quantum-corrected extremal geometries acquire non-analytic contributions at the corrected horizon.

There exists another notion of curvature singularity that does not rely on curvature invariants. This is the definition given in [160] of non-scalar singularities: those where the components of curvature tensors, when evaluated for a suitable tetrad at the singular region, show divergences. By suitable we mean a particular tetrad field which is parallel transported along a physical curve that approaches

the singular point. For this particular case, we choose an orthonormal tetrad field associated to an ingoing timelike geodesic path on the near-horizon metric (3.53)

$$e^{\mu}_{(0)} = f_0^{-1}\left\{\left|\frac{r_{\rm div}}{r-r_{\rm div}}\right|^{2/\lambda_+}, \sqrt{\kappa f_0}\left|\frac{r-r_{\rm div}}{r_{\rm div}}\right|^{1-1/\lambda_+}, 0, 0\right\}. \tag{3.62}$$

By computing a component of the Riemann curvature tensor contracted with this tetrad, we obtain

$$R_{(0)\theta\theta(0)} = R_{t\theta\theta t}e^t_{(0)}e^t_{(0)} + R_{r\theta\theta r}e^r_{(0)}e^r_{(0)} = \frac{\kappa}{f_0}\left(\frac{\lambda_+ - 1}{\lambda_+}\right)\left|\frac{r-r_{\rm div}}{r_{\rm div}}\right|^{1-2/\lambda_+}. \tag{3.63}$$

Note that, for $1 < 2/\lambda_+ < 2$, this physical component of the curvature is singular. We only recover a well-defined geometry in the classical limit $\lambda_+ \to 1$. For smaller values of the exponent of the redshift function, divergences appear at higher-order derivatives of the Riemann curvature tensor.

The extremal BH is more stable against quantum perturbations than sub-extremal BHs. As we have seen, vacuum polarization eliminates these horizons replacing them with a wormhole neck. The particular case of the extremal BH results in a different kind of modification, in the sense that the horizon itself is preserved and becomes a curvature singularity. An important difference between these two cases can be understood by looking at the geometry beyond the quasi-extremal horizon. The shape of the solution can be again univocally determined by arguments concerning the roots and exact solutions. Figure 3.6 contains a plot of one of these solutions, showing details of the inner part of the geometry. In the inner region $r < r_{\rm div}$, the solution ψ, now living in the concealed branch, approaches $-\infty$ from below the root $\mathcal{R}_2$. Then, it crosses $r = Q$ in a similar fashion as it occurred in the over-charged regime (see Sec. 3.4), with the difference that the exact solution intersected is now ψ_+. After intersecting the exact solution, it meets the condition for a branch jump given by the vanishing of $\mathcal{G}$ (3.14) and the solution switches to the unconcealed branch back again. More explicitly, the branch jump requires that the solution ψ takes the value

$$\psi(r_{\rm jump}) = -\frac{r^2_{\rm jump} + \alpha l^2_{\rm P}}{l^2_{\rm P} r_{\rm jump}}. \tag{3.64}$$

Once the transition to the unconcealed branch has occurred, the solution stays within this branch, growing until it reaches a maximum and remaining trapped between $\mathcal{R}_2$ and ψ_-. The behavior of ψ near $r = 0$ is similar to the over-charged regime. The main difference now is that the singularity is no longer naked, but

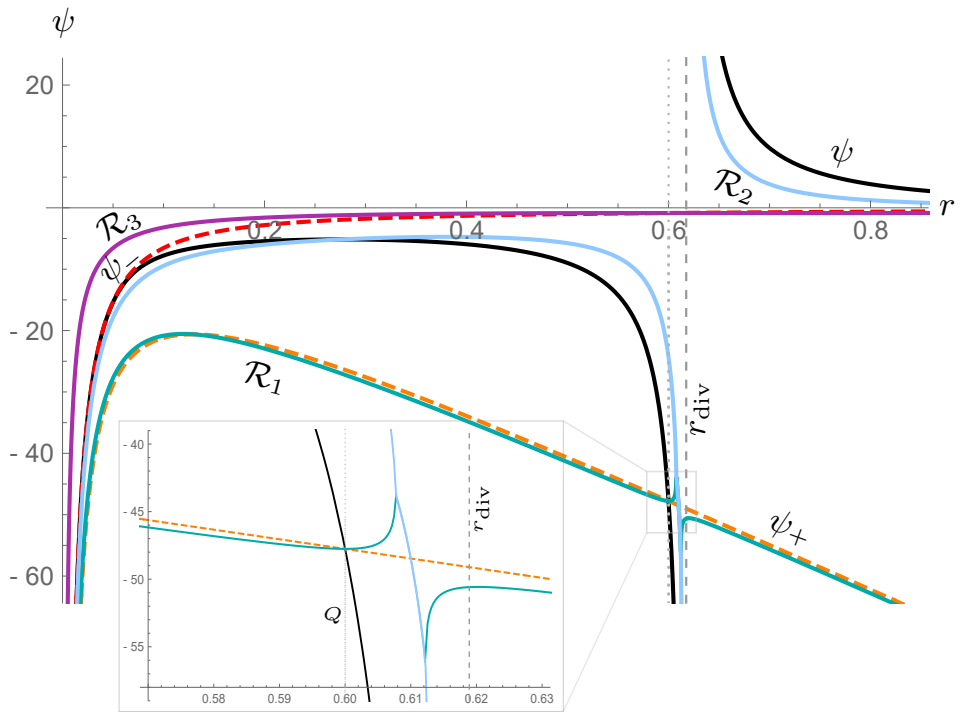

Fig. 3.6.: Numerical plot of a quasi-extremal solution (black curve), with $Q = 0.60$, $M \simeq 0.59$ and $r_{\rm div} \simeq 0.62$. The roots and exact solutions appear represented, together with the vertical dashed and dotted lines denoting $r = r_{\rm div}$ and $r = Q$, respectively. The solution has a branch jump at the quasi-extremal horizon. In the region $r < r_{\rm div}$, ψ intersects the exact solution ψ_+ and the root $\mathcal{R}_1$ exactly at $r = Q$ (zoomed figure). Then, the solution jumps to the unconcealed branch at $r_{\rm jump} \simeq 0.58$ and grows towards smaller r until crossing $\mathcal{R}_2$, reaching a maximum, and starts decreasing confined between $\mathcal{R}_2$ and ψ_-. The asymptotic behaviour near $r \simeq 0$ is the same as for super-charged solutions.

covered by a horizon at the end of an infinite wormhole neck. It is interesting to recall that this is the separatrix between two solutions, both harboring naked singularities, either at radial infinity in the wormhole regime, or at the radial origin for the over-charged family. Beyond its neck, the wormhole geometry stays within the concealed branch, extending towards an asymptotically singular region at radial infinity. However, since the quasi-extremal solution does not have its radial coordinate reverted but just elongated through an infinite spatial tube, it extends towards $r = 0$. Therefore, below the (singular) quasi-extremal horizon there is just a narrow region where the solution is non-perturbative, and the perturbative regime is recovered once we go sufficiently deep beyond the horizon. Nevertheless, this narrow band where quantum corrections become non-perturbative, as well as the non-scalar singularity, persist under changes of the regulator, only disappearing in the limit of infinite charge.

3.5.3 Viability of semiclassical extremal black holes

To end this Section we want to take the opportunity to revisit a long-standing discussion (see Refs. [172, 194–196]) concerning the existence of extremal BHs solutions in semiclassical gravity. Our analysis, in agreement with previous studies on the topic [192, 193], indicates that regular static extremal BHs do not exist when backreaction from the RSET is incorporated.

Despite the singular behavior (3.7) of the Polyakov RSET at extremal horizons, numerical computations for the RSET of massless scalar fields show it is regular at the extremal horizon [146]. Notwithstanding this, when the backreaction of this RSET is incorporated, extremal BHs are not semiclassical solutions at first order in perturbation theory [194] (as long as $r_{\rm H} < |Q|$ [196]), indicating that semiclassical corrections are incompatible with regular extremal horizons.

This striking discrepancy between the Polyakov RSET (which comes from a dimensional reduction) and the exact, numerical RSET (which is four dimensional) at the extremal horizon has turned out to be a puzzling subject. Relevant contributions to these matters were given in [197–199], where the authors proved that the singularity in the Polyakov RSET at extremal horizons is only present in the static case. For extremal BHs formed dynamically, the RSET acquires extra flux terms that, at late times, cancel the singular contributions present in the static situation. The four-dimensional RSET is already regular in the eternal situation, thus we presume its dynamical counterpart will necessarily be regular as well.

There are two possibilities for explaining these discrepancies between RSETs. One is that the singularity appearing in the s-wave sector of the theory captured by dimensionally-reduced approach is compensated by singularities appearing in

higher multipoles. The second possibility, and the more likely, is that the spherically symmetric fluctuations captured through the Polyakov and s-wave approaches do not correspond to the s-wave sector of the four-dimensional theory, thus the discrepancy appears as a natural consequence of the dimensional reduction. At the classical level, due to the separability of the wave equation, a four-dimensional scalar field can be decomposed into an infinite number of $(1+1)$-dimensional fields, one for each multipole value l. At the quantum level, however, this equivalence does not hold when constructing regularized observables, as renormalization counterterms do not obey such decomposition in spherical harmonics. This disagreement between $(1+1)$-dimensional and $(3+1)$-dimensional quantities is called the dimensional reduction anomaly [200, 201], and it is responsible for the discrepancies among the different prescriptions for computing analytical RSET approximations. A proof for this statement would require to examine whether the dimensional-reduction anomaly associated with the s-wave mode compensates the divergence appearing in the Polyakov RSET at the extremal horizon.

All in all, these investigations strongly suggest that extremal BHs are indeed not consistent with semiclassical effects. Our work in particular is the first one to address the self-consistent backreaction of the Polyakov RSET in a four-dimensional extremal BH and it concludes that a non-scalar singularity is present at the quasi-extremal horizon.

3.6 Conclusions

In this Chapter we have obtained the complete set of self-consistent electro-vacuum solutions in the semiclassical approximation taking the CRP-RSET as describing the quantum material content of the spacetime. For the Boulware vacuum state, the only state compatible with staticity and asymptotic flatness, three families of solutions have been obtained depending on the charge-to-mass ratio.

Under-charged solutions ($Q < Q_{\text{crit}}$) are wormhole geometries with essentially the same features as the Schwarzschild geometry counterpart obtained in Chapter 2. Increasing the charge makes the wormhole neck shrink, which nevertheless always sits above the classical gravitational radius $r_+ = M + \sqrt{M^2 - Q^2}$. On the other side of the neck, there is a null naked singularity at finite affine distance from the neck for all geodesics. Similarly to the Schwarzschild counterpart, the effect of the regulator α is to extend the space of solutions to wormholes of arbitrarily small size.

Over-charged solutions ($Q > Q_{\text{crit}}$) connect the asymptotically flat region with a naked curvature singularity at $r = 0$. This geometry can be thought of as composed

by a cloud of infinite negative mass coming from vacuum polarization, originated from the backreaction of vacuum energy caused by the infinite charge density of the electromagnetic field. Depending on the characteristics of the regulator, the contribution of this cloud of vacuum polarization can be suppressed so that the dominant singular contribution at short distances comes from the electromagnetic SET. This geometry exemplifies a situation where slight modifications in the regulator parameter α strongly change the features of the solution near $r = 0$.

Separating both regimes there exists a quasi-extremal geometry ($Q = Q_{\text{crit}}$) reminiscent of the extremal BH. This solution proves that the Polyakov RSET is incompatible with the existence of extremal horizons not formed dynamically. In the quasi-extremal solution, quantum backreaction retains the horizon structure, transforming it into a non-scalar curvature singularity [160]. The backreacted geometry is thus more alike to its classical counterpart than geometries of the wormhole kind, with the caveat that non-perturbative corrections still occur in a narrow band behind the singular horizon.

In view of this, we conclude that semiclassical electro-vacuum static geometries in the Boulware vacuum state are all singular. This singularity is located either at radial infinity or at the radial origin, with the exception of the quasi-extremal solution, which has a singularity at the horizon itself. Furthermore, in situations where the growth of the CRP-RSET near $r = 0$ is not considerably suppressed, the strength of the central singularity, present in both the under-charged and quasi-extremal regimes, increases with respect to the classical case due to the divergent accumulation of mass coming from the vacuum polarization of the scalar field. Semiclassical gravity reveals that introducing a classical matter fluid is therefore a requirement for constructing static geometries free from singularities. This is the line that will be followed in the remaining of this thesis.

4

Semiclassical constant-density spheres

4.1 Introduction

Chapters 2 and 3 of this thesis have addressed the semiclassical counterparts to the Schwarzschild and Reissner-Nordström spacetimes, respectively. When the ADM mass is positive, these counterparts are singular asymmetric wormholes (excluding the quasi-extremal case). Contrarily to classical situations, in which curvature singularities are hidden behind the event horizon (thus, predictability of GR is not jeopardized [118]), in semiclassical gravity event horizons get transformed into curvature singularities themselves. Furthermore, their wormhole shape indicates that they cannot result from the collapse of spherical distributions of matter [202], being thus inappropriate to describe the end-state of gravitational collapse at late times when the system has settled to a (quasi-)static configuration. These characteristics motivate the following approaches: Either we drop the staticity assumption and consider evaporating BHs [145], or we stick to strictly static situations and introduce classical matter into the picture. The second approach is the one we follow in this thesis, motivated by the fact, explained in Subsec. 1.3.1, that the RSET can in principle violate the hypotheses behind Buchdahl's theorem. This occurs, in particular, by the introduction of negative energy densities in the innermost regions of highly compact stars [166, 167], by inducing anisotropies in the pressure, and by significantly modifying the Schwarzschild exterior, motivating the search for horizonless ultracompact objects spheres that can describe the late-time outcome of some collapse process [107].

In this Chapter and in Chapter 5 we address the problem of finding self-consistent stellar solutions in semiclassical gravity with particular emphasis on stars that can violate the Buchdahl limit. Due to the exploratory nature of this analysis, we investigated exhaustively the whole space of stellar solutions to identify the most significant deviations from their classical counterparts. This is the main focus of this Chapter, where, as simplifying assumptions, we model the classical fluid as a perfect fluid of constant density and isotropic pressures and the semiclassical source via the CRP-RSET. We do not find strictly regular stars surpassing Buchdahl limit

sourced by these stress-energy tensors but, remarkably, the space of solutions is modified in a way that suggests that more elaborate regularizations for the RP-RSET can result in entirely regular spacetimes. In Chapter 5 we explore these improved regularization schemes. The reader can find a condensed summary and comparison between the classical and semiclassical figures of equilibrium in Sec. 5.2.

Equipped with the CRP-RSET, our aim is to obtain the complete set of static, spherically symmetric solutions to Einstein equations with a perfect fluid of constant density in the semiclassical theory (the classical counterparts were found by Lemaître [47], with the exception of one solution [203]). Constant-density solutions depict inhomogeneous and isotropic cosmologies. Among all the cosmological spacetimes analyzed, we focus on stellar spacetimes: those which have a surface that connects smoothly with the Schwarzschild vacuum solution. The Schwarzschild stellar interior solution belongs to this latter family. We will obtain self-consistent solutions for sub-Buchdahl (with compactness $C_{\rm R} < 8/9$, where $C_{\rm R} \equiv C(R) = 2M/R$, R is the surface radius of the star and $M \equiv m(R)$ the Misner-Sharp mass at the surface [41–43]) as well as super-Buchdahl configurations ($8/9 < C_{\rm R} < 1$). There will be situations in which the semiclassical solutions here obtained are non-perturbative, in the sense that they do not have a classical counterpart in the $\hbar \to 0$ limit. Notice the slight change in notation with respect to Chapters 2 and 3. In those Chapters, M corresponds to the ADM mass while in the present Chapter and Ch. 5 it will denote the total mass of the star. The symbols $C_{\rm R}$ and $C(R)$ are used equally throughout the rest of the thesis.

This Chapter is organized as follows. We will start in the next Section by presenting a structured summary of the catalog of solutions that we have found. Table 4.2 will allow a clear comparison between the classical and semiclassical situations. We will also show Table 4.1 containing pictorial examples for each of the situations. Before presenting these Tables, we will introduce an important aspect of stellar equilibrium configurations that we have denoted *criticality*. Criticality is related to the existence of constant offsets in the mass at $r = 0$ and will serve as a classifying criterion. After that, the next Sections will provide the technical details associated with each class of solutions, both classical and semiclassical. Section 4.3 contains a review on the classical equations of stellar structure and their constant-density solutions. We describe them here for easier comparison with the semiclassical case. Later, in Section 4.4, we write down the CRP-RSET and write down the self-consistent semiclassical equations. In Section 4.5 we turn to the analysis of the solutions to the self-consistent semiclassical field equations, the core of the Chapter, in which the notion of criticality is more subtle than in the classical case. We have nevertheless been able to characterize completely the space of solutions, obtaining numerical solutions of particular interest as well as

analytical approximate expressions in certain regimes. Section 4.6 will provide some conclusions and pave the road for the main result of this thesis, presented in Chapter 5.

4.2 Classifying stellar spacetimes

This Section contains a summary of all the findings of this Chapter contextualized and compared with the classical theory. We start by introducing the necessary preliminaries to present our classification scheme.

The metric is described by the static and spherically symmetric line element (1.2). For some of the geometries that we will discuss, it will be convenient to use a different (proper) radial coordinate l defined through the relation

$$\frac{dr}{dl} = \pm\sqrt{1-C}. \tag{4.1}$$

The coordinate l can run along the entire real line, being particularly well adapted to study the wormhole spacetimes presented in Chapters 2 and 2. In the coordinates (4.1) the line element (1.2) becomes

$$ds^2 = -e^{2\phi(l)}dt^2 + dl^2 + r(l)^2 d\Omega^2. \tag{4.2}$$

Let us now consider two definitions that will describe part of the solutions discussed in this Chapter:

* *Strict stellar spacetime:* A regular geometry in which matter extends from $r(l_0) = 0$, representing the center of the structure, up to a finite radius $r(l_{\rm S}) = R$. The geometry for $l > l_{\rm S}$ is the asymptotically flat Schwarzschild solution for the classical field equations or its semiclassical counterpart for the semiclassical equations (see Chapter 2). At the center $l = l_0$ (we will set $l_0 = 0$ in the following without loss of generality), the geometry must be regular, in particular having finite curvature scalars (1.10).

* *ϵ-strict stellar spacetime:* This is a possibly irregular spacetime (e.g. with diverging curvature invariants) but such that it does not show any signs of these possible irregularities if analyzed only for radii larger than some $r_\epsilon = r(l_\epsilon) \ll R, r_\epsilon > 0$. By this we specifically mean that the pressure and compactness are finite for $l > l_\epsilon$, and that

$$|C(r_\epsilon)| < 2M_{\rm P}\frac{r_\epsilon^2}{l_{\rm P}^3} = 2\rho_{\rm P} r_\epsilon^2. \tag{4.3}$$

The radius r_ϵ represents an internal close-to-Planckian sphere and this last condition implies that, whatever happens inside this core, its effective mass (either positive or

negative) does not exceed Planckian values ($M_{\rm P}$). By construction, all strict stellar spacetimes are ϵ-strict spacetimes for arbitrary values of ϵ down to $\epsilon = 0$.

4.2.1 Classical equations of stellar equilibrium

The SET of a perfect fluid is given by

$$T_{\mu\nu} = (\rho + p)u_\mu u_\nu + p g_{\mu\nu}, \tag{4.4}$$

where ρ and p are the energy density and the isotropic pressure of the fluid, measured by an observer comoving with the static fluid with 4-velocity u^μ. Possible contributions to the curvature coming from shear stress, fluid viscosity, or heat transfer are not included in this model. The tt and ll components of the resulting classical Einstein equations are

$$-2r''r + 1 - (r')^2 = 8\pi r^2 \rho, \tag{4.5}$$

$$2rr'\phi' - 1 + (r')^2 = 8\pi r^2 p, \tag{4.6}$$

where the $'$ denotes derivatives with respect to the l coordinate. In addition, covariant conservation of the SET provides the conservation equation

$$p' = -(\rho + p)\phi'. \tag{4.7}$$

If we interpret a relativistic star as a finite potential well, the continuity equation (4.7) guarantees that any decrease of the redshift function with decreasing l, or deepening of the potential, is compensated by a corresponding growth in the fluid pressure.

Equations (4.5)-(4.7) form a closed system of differential equations as long as we supply them with an equation of state that relates pressure and density. In the present work we will consider the equation of state

$$\rho = \text{const.} \tag{4.8}$$

This idealized incompressible fluid is insensitive to changes in pressure [53]. This equation of state both allows for a simple treatment and uncovers interesting phenomena. For instance, as the energy density is independent from pressure, it allows for a better understanding of how the fluid arranges itself towards attaining equilibrium. In addition, the density profile (4.8) saturates the hypothesis of Buchdahl's theorem [57, 70] stating that energy density must be non-increasing towards the surface. With this equation of state we can see in a clear form the

appearance of the Buchdahl compactness bound. Any surpassing of this bound in the semiclassical theory will necessarily be produced by the backreaction of the RSET.

We proceed by constructing the differential equation for the pressure known as the TOV (Tolman-Oppenheimer-Volkoff) equation, obtained by replacing Eq. (4.7) in Eq. (4.6),

$$p' = -\frac{(\rho + p)\left[8\pi r^2 p + 1 - (r')^2\right]}{2rr'}. \tag{4.9}$$

According to this relation, pressure decreases monotonically outwards as long as $r'(l) > 0$ and the numerator remains positive. Turning points for pressure can take place only if the numerator vanishes. This can occur either because the Misner-Sharp mass is negative [which implies $r' > 1$ in virtue of (4.1)], or because pressure reaches sufficiently negative values. These situations are realizable in the uniform density case and will be explored in Section 4.3.

4.2.2 Criticality

Now we are going to introduce the notion of criticality in the context of the classical solutions of stellar equilibrium, which will be later transported to the semiclassical solutions. In general terms, the integration of equation (4.5) with the change of variable (4.1) leads to

$$r' = \pm\sqrt{1 - \frac{8\pi r^2 \rho}{3} - \frac{M_0}{r}}. \tag{4.10}$$

In this equation there is an integration constant M_0, first noticed by Tolman and Volkoff [55, 56], that accounts for a constant mass in the spacetime.

By inspection of Eq. (4.10) together with condition (4.52) it becomes evident that having a nonzero M_0 produces a curvature singularity at the radial origin. Let us also highlight that, by replacing Eq. (4.10) inside the TOV equation (4.9), we observe that the latter admits a complete analytical solution only in the $M_0 = 0$ case (progress towards obtaining analytical solutions for nonzero M_0 was made by Wyman [204]), requiring numerical integration otherwise.

Endowing the spacetime with a constant mass $M_0 \neq 0$ generates a singularity at $r = 0$, implying that the solution acquires features of vacuum geometries. These are characterized by the mass being a constant parameter of the solution and not a quantity identified with some well-defined physical source. In that sense, M_0 can be either positive or negative. A positive M_0 indicates the presence of a positive, singular mass, introducing a singularity at some $r(l_{div}) > 0$ where the pressure diverges. The final configuration resembles a BH surrounded by matter forced to maintain hydrostatic equilibrium, causing the horizon to become singular. On the

other hand, a negative M_0 introduces a naked singularity in the spacetime, as in the negative-mass Schwarzschild solution. The repulsion exerted by this negative mass aids the fluid towards attaining equilibrium (pressure no longer diverges) but at the cost of introducing a singularity at $r = 0$.

Analyzing how the total ADM mass relates to the matter content of the spacetime, we can find a correspondence between three notions of mass: the ADM mass, the mass coming from the fluid energy density ρ, and M_0, given by

$$M_{\text{ADM}} = M_{\text{cloud}} + M_0. \tag{4.11}$$

Here, M_{cloud} equals the outcome of the integral

$$M_{\text{cloud}} = \int_0^R dr\, 4\pi r^2 \rho. \tag{4.12}$$

When the ADM mass is equal to M_{cloud} we are in the critical situation. Consider integrating the equations of stellar equilibrium from the surface of a star of radius R and total mass M inwards. Since M_{cloud} is related to the energy density of the sphere of fluid, the value of ρ that enforces $M_0 = 0$ in (4.11) is given by

$$\rho = \rho_{\text{c-clas}} = \frac{3C(R)}{8\pi R^2} \tag{4.13}$$

and we will refer to this particular value as the critical density of the geometry. Any deviation from the critical value $\rho = \rho_{\text{c-clas}}$ results in a non-critical solution with a nonzero M_0 that accounts for the respective excess or defect in mass. Particularly, an under-density (sub-critical case) translates into a positive M_0 to account for the missing mass in the right hand side of (4.12), while an over-density (super-critical case) is balanced by a negative M_0.

Non-critical constant-density solutions have been sparsely noticed in the literature. These were first analyzed by Oppenheimer and Volkoff [56, 58], while further insight was provided by Wyman [204]. Since the equation for the compactness in the classical equations (4.6) is readily integrable, relation (4.13) alone guarantees regularity in the compactness. In the semiclassical theory, however, the equation for the compactness is inextricably linked with that of the redshift function and it is difficult to discern whether negative energies, which have the potential to tame divergences in p, originate from semiclassical zero-point energies or from a super-critical unbalance. When integrating the semiclassical equations from the surface of a star of radius R and mass M inwards, it is not directly clear which density parameter should be used for the integration. One has to (numerically) explore different values of ρ and discern the precise value that separates two types

of behavior. This is the reason behind the need to properly understand both critical and non-critical configurations.

Let us adopt the following definition:

* *Critical stellar spacetime:* As we have discussed, when integrating inwards from a radius R, with compactness $C(R) < 1$ and density ρ, the classical equation for the compactness exhibits a qualitative change of behavior when going from $\rho < \rho_{\rm c}$ to $\rho > \rho_{\rm c}$, where $\rho_{\rm c}$ stands for a critical value of the density. In the classical case, this follows straightforwardly from Eq. (4.10), as the integration constant M_0 in the latter equation changes sign. As we will show, we find equivalent changes in behavior in the semiclassical case. We will call a configuration *critical* when it is precisely the separatrix between two different behaviors of the compactness, which in the classical case corresponds to a configuration with regular compactness and $M_0 = 0$. However, notice that our definition of criticality does not imply regularity. On the one hand, the pressure can be divergent in some critical solution. On the other hand, as we will show in the semiclassical case using the CRP-RSET, some critical solutions lack a strictly regular compactness at the radial origin. All strict stellar spacetimes are critical stellar configurations, but the converse is not true. As we will show, around critical solutions the semiclassical equations uncover new forms of ϵ-strict stellar spacetimes which are absent in classical gravity.

Finally, notice that criticality is a common property of stellar spacetimes and not just an artifact of considering a constant-density equation of state. The observations raised here are expected to apply to a broad class of equations of state even if, for them, a relation such as Eq. (4.10), where M_0 appears explicitly, cannot be derived.

4.2.3 The catalogue of solutions

The purpose of this Subsection is two-fold. First, it is aimed to serve as a distilled guide for the content and main results of the rest of the Chapter; second, it is devised as a map of the classical and semiclassical sets of stellar configurations with constant density.

All the stellar solutions described in this Chapter are listed in the table of Figure 4.1. In addition, Figure 4.2 shows illustrative numerical plots that highlight the overall features of the solutions described in the table in Fig. 4.1. These Figures are organized as follows:

- First of all we distinguish between the classical and the semiclassical theory based on the CRP-RSET. In both cases, we discriminate between sub-Buchdahl and super-Buchdahl stars, depending on whether their surface compactness is below or above the Buchdahl limit (given by the most compact strict stellar

spacetime in each situation). In the classical case and for a star of constant density, this limit corresponds to $C(R) = 8/9$. In the semiclassical theory there is no clear notion of Buchdahl limit due to the introduction of a preferred length scale $l_{\rm P}$. Now, the maximum $C(R)$ allowed by strict stellar spacetimes depends on the values of $R,\ \rho$, and the particular regularization scheme adopted for the RP-RSET. In our semiclassical integrations, we do not impose any additional restriction on how large the values of the classical pressure can become as long as they are finite. We do this to make the discussion as close as possible to the analysis of classical configurations approaching the Buchdahl limit, in which the same logic is followed.

- Taking a stellar radius R and a surface compactness $C(R)$ we can integrate the equations of equilibrium inwards for different values of ρ. By changing the parameter ρ one realizes that there is a gross change in behavior for the compactness function when passing through a critical value $\rho_{\rm c}$. Attending to this value, we separate the different solutions as being sub-critical, critical, or super-critical.

- For the semiclassical case, we distinguish three possibilities depending on where the star surface connects with the vacuum solution. Since the vacuum solution has a wormhole shape, the matter boundary can be located outside, inside, or at the neck itself. The value of $\rho_{\rm c}$ changes strongly depending on the region where the surface is located. Regardless, we find a similar distinction between critical and non-critical geometries.

- For each of the cells in the classification scheme from Fig 4.1 (see Fig. 4.2 for the corresponding numerical solutions) we have added the asymptotic behavior of the pressure $p(l)$ and the compactness $C(l)$ at the smallest value of l reached by each solution. This corresponds to $l = 0$ for stars which extend to $r = 0$, independently of whether the configuration is regular or singular there, or to some $l = l_{\rm div} > 0$ for stars with a singularity at $r(l_{\rm div}) > 0$.

- Finally, the cells corresponding to strict stellar spacetimes have yellow background and those in which we find ϵ-strict stellar configurations have orange background.

We will describe the different regimes shown in Fig. 4.1 in the remaining of the Section.

Let us start this summary from the sub-critical sub-Buchdahl corner of the classical solutions (Subsec. 4.3.3). These configurations are irregular. When the density reaches the critical value $\rho_{\rm c}$ for a given compactness the geometry becomes

			Sub-Critical ($l = l_{\text{div}}$)	Critical ($l = 0$)	Super-Critical ($l = 0$)
Classical	Sub-Buchdahl		$p \to \infty$ $C > 0$	$p = p_c$ $C = 0$	$p = -\rho$ $C \to -\infty$
	Super-Buchdahl		$p \to \infty$ $C > 0$	$p \to \infty$ $C \to -\infty$	$p = -\rho$ $C \to -\infty$
Semiclassical	Outside neck	Sub-Buchdahl	$p \to \infty$ $C \to -\infty$	$p = p_c$ $C = 0$	$p = -\rho$ $C \to -\infty$
		Super-Buchdahl	$p \to \infty$ $C \to -\infty$	$p \to \infty$ $C \to -\infty$	$p = -\rho$ $C \to -\infty$
	At neck	Super-Buchdahl	$p \to \infty$ $C \to -\infty$	$p \to \infty$ $C \to -\infty$	$p = -\rho$ $C \to -\infty$
	Inside neck	Sub-Buchdahl	$p \to \infty$ $C \to -\infty$	$p \to \infty$ $C \to -\infty$	$p = -\rho$ $C \to -\infty$
		Super-Buchdahl	$p \to \infty$ $C \to -\infty$	$p \to \infty$ $C \to -\infty$	$p = -\rho$ $C \to -\infty$

Fig. 4.1.: This table shows the complete set of classical and semiclassical stellar solutions of constant density. We distinguish whether the energy density ρ takes values below, above, or at the critical value ρ_c; if the compactness is below or above the Buchdahl limit; and, for semiclassical stars, if their surface is located outside, inside, or at the neck itself. Each cell shows the behavior of pressure and compactness at the smallest value of l in the domain of definition of the solution. Light-green cells correspond to singular geometries. Yellow cells are strict stellar spacetimes. The orange color percolating into the rightmost part of sub-critical cells and the leftmost part of super-critical cells represents ϵ-strict spacetimes. This family of spacetimes includes the subset of sub-critical solutions with small wormhole necks. See Figure 4.2 for the respective numerical solutions for each cell of the table.

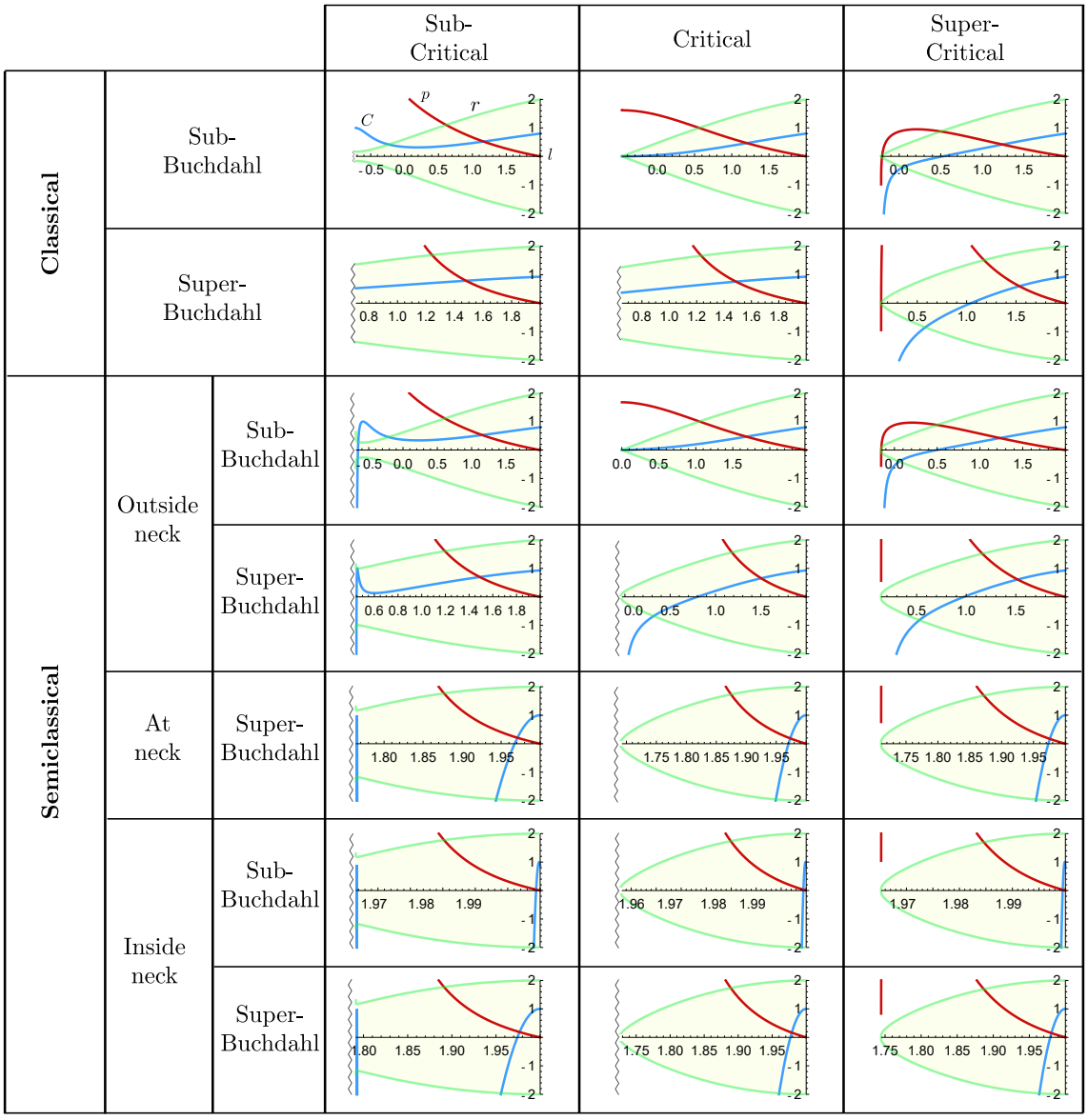

Fig. 4.2.: (Caption next page).

Fig. 4.2.: (Previous page). This table shows numerical integrations for each of the distinct regimes found for classical and semiclassical stellar solutions. The criteria for classifying the solutions is the same followed in Fig. 4.1. The three regimes (sub-critical, critical and super-critical) appear represented for sub-Buchdahl and super-Buchdahl stars in both classical and semiclassical theories. In the semiclassical case, distinction is made on whether the star surface is located outside, inside, or at the neck of the vacuum wormhole geometry. In the semiclassical regime we show ϵ-strict solutions in the cases where no regular critical solutions exist. Each cell shows a numerical integration of a constant-density star. All but critical sub-Buchdahl stars, which are integrated from $l = 0$ outwards, are integrated from the surface $l_{\rm S} = R = 2$ inwards until the center of spherical symmetry or a singularity is reached. We stick to the following color criteria for the represented functions throughout the rest of the Chapter: the shape function $r(l)$ is represented in green, the pressure $p(l)$ in red, and the compactness function $C(l)$ in blue. The region where the classical fluid is present is filled in yellow for pictorial purposes. Spacetime singularities are depicted by a vertical zigzag line and correspond in every case with a divergent pressure. In super-Buchdahl super-critical plots the pressure grows inwards outside the plot window (with no divergences), to just come back inside the plot window when closer to the radial origin. Inside-the-neck sub-Buchdahl stars have $C(R) < 8/9$ and their compactness function grows to 1 inside the structure, generating a local maximum in the shape function $r(l)$ just below the surface. The semiclassical critical profiles from the fourth row downwards are pictorial representations of how the respective exact critical solutions would look like, rather than complete numerical integrations. This is due to the numerical instability of our numerical algorithm at the critical density. See Fig. 4.1 for the asymptotic behaviors of the pressure and the compactness in each situation.

a strict stellar spacetime (Subsec. 4.3.1). Going into the super-critical regime (Subsec. 4.3.4), the compactness $C(r)$ becomes irregular at the origin, diverging to $-\infty$. For a small window of densities just above the critical solution $\rho_{\rm c}$ we find ϵ-strict stellar configurations.

Focusing now on the sub-critical super-Buchdahl cell we have again irregular solutions (Subsec. 4.3.3). The difference with the sub-Buchdahl case is that when reaching the critical density ρ_c, although the compactness function is well-behaved at the radial origin, the pressure diverges before reaching the origin (a divergence at the origin happens precisely in the Buchdahl limit; Subsec. 4.3.2). Going further into the super-critical regime (Subsec. 4.3.4) we find solutions for which the pressure is regular until the origin, but at the cost of making a highly irregular compactness. ϵ-strict configurations are only found very close to criticality at the Buchdahl limit or below it.

Turning now to the semiclassical counterparts, the Schwarzschild vacuum geometry is drastically modified by semiclassical corrections in the Boulware vacuum state, becoming an asymmetric wormhole (see Chapter 2 and Fig. 2.2 for a detailed plot of the region around the neck). This leaves three distinct regions (outside, inside, or at the wormhole neck itself) in which to match the vacuum geometry with the surface of a star.

Let us start the route from the sub-critical, sub-Buchdahl, outside-the-neck configurations. These are irregular configurations that display characteristics from vacuum solutions, i.e. they are singular wormhole-like configurations (Subsec. 4.5.2). For the critical case we find strict stellar spacetimes (Subsec. 4.5.1) that amount to perturbative corrections of the classical regular stars. On the other side, super-critical configurations display naked singularities, with negative divergent compactness and Misner-Sharp mass at $r = 0$ (Subsec. 4.5.3).

Passing to the sub-critical super-Buchdahl case, we again find wormhole-like configurations (Subsec. 4.5.2). In the same manner, the super-critical regime exhibits naked singularities (Subsec. 4.5.3). We find that the critical solution is one with a special profile of divergent pressure and compactness, which appears resilient to quantum corrections (Subsec. 4.5.4). An important difference between the classical and semiclassical super-Buchdahl critical configurations is that, in the latter case, close to criticality we find an ample window of ϵ-strict configurations. In Fig. 4.2, for the cases where no regular critical configuration exists, we have shown an example of these ϵ-strict configurations instead.

Stars matched at the neck, analyzed in Subsec. 4.5.7, show as well three distinct regimes (sub-critical, super-critical and critical) which depict asymptotic behaviors similar to those of the super-Buchdahl outside-the-neck case, depending on whether the density is above or below the critical value $\rho_{\rm c}$. Additionally, we find that the

surface of the star displays different properties depending on the value of ρ. For sufficiently small ρ, the surface of the star corresponds to a minimal surface for the shape function r, or neck. By increasing ρ, this bouncing surface for the shape function gets pushed towards the interior of the star, disappearing eventually for $\rho \geq \rho_c$.

The situation for stars inside the neck (Subsec. 4.5.6) can be summarized saying that there are again three regimes, sub-critical, super-critical, and critical, with the same asymptotic behaviors seen for the super-Buchdahl, outside-the-neck case. The only caveat is that the critical density ρ_c increases as the surface of the star R is moved away from the neck, becoming trans-Planckian not far from it (in proper distance, see Fig. 4.18 below). Therefore, reaching criticality for these configurations requires extremely dense classical fluids that compensate the negative masses generated by vacuum polarization [176].

4.3 Classical solutions

Next we turn to the analysis of the set of solutions to the classical equations of stellar equilibrium for a perfect fluid of constant density. Throughout this Section we will describe the solutions from the first two rows in Figs. 4.1 and 4.2. We have found that it is more convenient to start the analyses by considering how the equations of equilibrium integrate outwards starting from a regular radial origin.

4.3.1 Solutions with a regular center

The first set of solutions we are going to describe can be seen as part of inhomogeneous cosmologies. In this context, they were analyzed by Lemaître [47] and later by Tolman [55]. Here we shall recall these analyses using our notation and perspective. Some of these solutions can be used to build interiors of stellar spacetimes. The suitable interiors retrieved in this first analysis are all critical, by construction, and result in sub-Buchdahl configurations (the only ones that are regular in the classical theory).

First, integrating Eq. (4.10) returns

$$r = \frac{\sin(Al)}{A}, \tag{4.14}$$

with $A = \sqrt{8\pi\rho/3}$. The periodic character of the shape function $r(l)$ is consistent with a cosmological interpretation. The shape function extends between two zeroes which correspond to two poles of the inhomogeneous cosmologies.

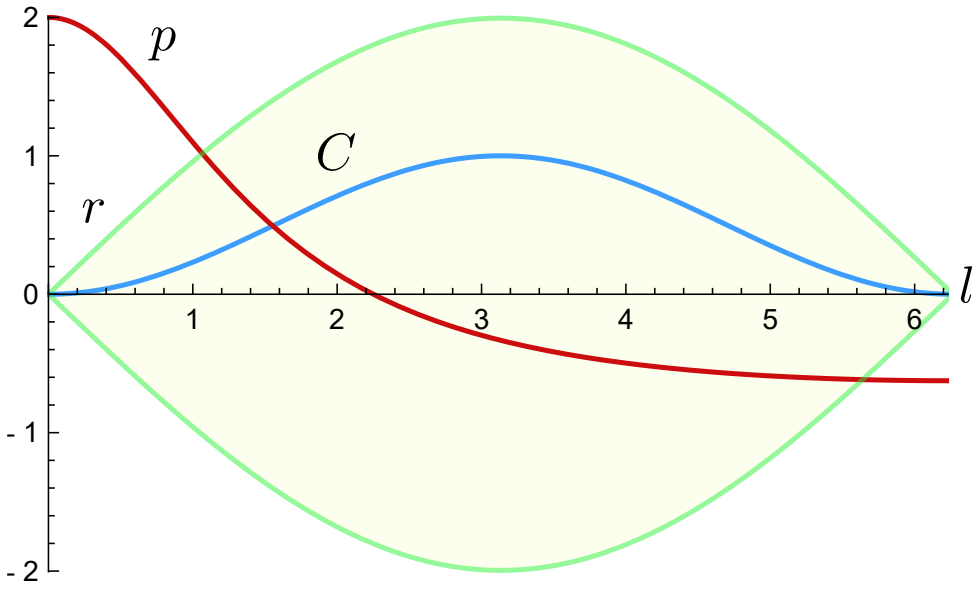

Fig. 4.3.: Plot of a positive pressure solution to the equations of structure. The above and below green lines represent the shape function $r(l)$ and the region in between both curves has been colored for pictorial purposes. The blue line denotes the compactness function of the geometry $C(l)$, which reaches 1 at the radial maximum and vanishes at the poles. The red curve is the pressure of the solution (in units of ρ) for a star with $\rho = 0.03$ and $p(0) = 2\rho$. Notice that the region of positive pressure corresponds to a relativistic star with $C(l_S) \simeq 0.82$. This solution has an enormous density compared to that of astrophysical objects, but the physics of classical critical solutions is scale-invariant.

With both ρ and r known, integration of the TOV equation (4.9) is straightforward and yields

$$p = \rho \left\{ \frac{2}{3} \left[1 - B_0 \cos\left(Al\right) \right]^{-1} - 1 \right\}. \tag{4.15}$$

Let us now extract the physical content of the above expression. The central pressure $p(0)$ is determined by the integration constant B_0. For any $B_0 \neq 1$ pressure is finite at $l = 0$, so these kind of geometries (those with regular center), will be analyzed first. By varying the value of p at the origin, we can divide cosmological solutions in the following three families, with their respective separatrices:

1. $p(0) > -\rho/3$. This guarantees that both the strong energy condition (SEC) and the null energy condition (NEC) hold at $l = 0$. As Fig. 4.3 shows, the resulting cosmologies are regular everywhere and have a pressure that decreases between the two poles. Solutions with $p(0) > 0$ reach a surface of zero pressure at l_S where the geometry can be matched with the Schwarzschild vacuum geometry, and thus resemble strict stellar spacetimes (Fig. 4.3). On the other hand, solutions with $p(0) < 0$ lack such surface and therefore resemble inhomogeneous cosmologies.

2. $-\rho < p(0) < -\rho/3$. In this case the SEC is violated at $l = 0$ while the NEC holds. Solutions with $p(0) \in -(\rho/3, 2\rho/3)$ correspond to the mirror-reflected version of type 1 profiles. Can one construct a regular star whose interior corresponds to this left-hand-side pole of the solution? In these interior solutions pressure decreases inwards from its zero value at the star's surface, becoming all the way negative. This interior geometry can be matched with a patch of the Schwarzschild vacuum spacetime. However, in this case the shape function $r(l)$ is initially increasing (at the surface) towards the interior, so one cannot smoothly connect (without introducing a shell of matter) this interior with a patch of Schwarzschild that extends towards the asymptotically flat region; one could only connect this interior with a Schwarzschild patch covering $r < R$. Therefore, these solutions do not serve to construct regular stars. Decreasing the central pressure below $p(0) < -2\rho/3$ maintains the previous characteristics: pressure increases outwards and crosses zero at a finite radius. The difference with the previous situation is that if one now continued the internal solution beyond the surface of vanishing pressure, one would uncover a curvature singularity at

$$l_{\text{div}} = \frac{\arccos\left(1/B_0\right)}{A}. \tag{4.16}$$

This singularity has an infinite positive pressure. The right-hand part of these geometries (that is, beyond the surface of zero pressure outwards) cannot be used to construct regular hydrostatic equilibrium configurations. As we will see shortly these solutions appear when integrating critical super-Buchdahl stellar configurations from the stellar surface inwards.

3. $p(0) < -\rho$. This guarantees SEC and NEC are violated. Pressure decreases from the radial origin outwards, eventually diverging towards $-\infty$ at (4.16). Later we will briefly comment on these solutions, since they describe the interior patch of the gravastar model [91].

For the sake of completeness, let us comment briefly about the separatrices between families 1-3. The case between the first and second type of solutions corresponds to Einstein's static and homogeneous universe, where pressure is constant [by virtue of (4.20) below and (4.7)] and equal to $-\rho/3$. The instability of this model has a long and interesting story (see for example [205]).

The remaining separatrix solution saturates the null energy condition with constant pressure equal to $-\rho$. Addition of Eqs. (4.5) and (4.6) leads to the relation

$$\frac{r''}{r'} = \phi', \tag{4.17}$$

which results in

$$e^{2\phi} = \left[\cos\left(Al\right)\right]^2, \tag{4.18}$$

presenting a horizon at $l = \pi/2A$. This metric corresponds to de Sitter spacetime in static coordinates

$$ds^2 = -\left[\cos\left(Al\right)\right]^2 dt^2 + dl^2 + \frac{\left[\sin\left(Al\right)\right]^2}{A^2} d\Omega^2, \tag{4.19}$$

revealing the existence of a cosmological horizon at $r(l_{\rm H}) = A^{-1}$.

4.3.2 Critical Buchdahl and super-Buchdahl solutions

Note that taking $B_0 = 1$ in (4.16) makes the pressure diverge at $l = 0$. The redshift function, obtained from integrating Eq. (4.6),

$$e^{2\phi} = e^{2\phi_0}\left[B_0 \cos\left(Al\right) - 1\right]^2, \tag{4.20}$$

vanishes at $l = 0$ for $B_0 = 1$. Here, ϕ_0 is an irrelevant integration constant that amounts to a rescaling of t. For this particular B_0, the pressure (4.15) is found to diverge at the origin as

$$p \simeq \frac{1}{2\pi l^2}. \tag{4.21}$$

Since this solution does not have a regular center, we appeal to integrations from the star surface $l_{\rm S}$ to explore this and other similar cases. For that purpose, one needs to impose the following boundary conditions at the surface of the star:

$$\begin{aligned} &p\left(l_{\rm S}\right) = 0, \quad r\left(l_{\rm S}\right) = R, \\ &\phi\left(l_{\rm S}\right) = \frac{1}{2}\ln\left[1 - C\left(l_{\rm S}\right)\right], \quad r'\left(l_{\rm S}\right) = \sqrt{1 - C\left(l_{\rm S}\right)}, \end{aligned} \tag{4.22}$$

with $C(l_{\rm S}) = 2M_{\rm ADM}/R$. With these boundary conditions, solution (4.21) corresponds to a surface compactness

$$C(l_{\rm S}) = 1 - \left[r'\left(l_{\rm S}\right)\right]^2 = 8/9. \tag{4.23}$$

This result denotes the maximum compactness of regular perfect fluid spheres in hydrostatic equilibrium, or Buchdahl limit [57]. Stellar configurations that have isotropic pressures, have an outwards non-increasing ρ, and whose exterior geometry is the Schwarzschild vacuum geometry are subject to the upper compactness bound (4.23). More compact (super-Buchdahl) stars will have the surface of infinite pressure gradually moved from $r = 0$ towards $r = R$. Beyond this curvature

singularity we can find another geometric patch extending up to $r = 0$, in which p takes values below $-\rho$. Matching these two solutions through a regularizing shell in the limit $C(l_S) \to 1$ displays a gravastar geometry [206].

This ends our discussion concerning classical critical solutions, which will guide us in the classification of their semiclassical counterparts. In the following we turn to the analysis of non-critical configurations, which lack a regular center from the start.

4.3.3 Sub-critical solutions

The analysis of solutions out of criticality is interesting because in the semiclassical case it is not directly clear how to associate a failure in criticality to the value of the mass at the origin. An understanding of the role played by non-criticality at the classical level will therefore allow us to distinguish between critical and non-critical solutions in the semiclassical case.

Let us start by describing what is seen in the inwards integration of a sub-critical star. Reference to these solutions can be found in [56, 207]. An example of a sub-critical sub-Buchdahl star is shown in Fig. 4.4. By imposing $\rho < \rho_{\text{c-clas}}$ the geometry acquires a positive constant mass M_0. The gravitational effect of this mass is perceived by the fluid, which responds to it with an increase in pressure. This increase happens more quickly than in the critical case as to compensate for the extra gravitational pull induced by M_0. As we deepen through the star, compactness passes through a turning point and starts increasing as the radius decreases. Not far below this turning point, the pressure diverges and the geometry has a curvature singularity, as seen in Fig. 4.4.

We obtain the form of this curvature singularity by solving the continuity equation for the perfect fluid of constant density (4.7)

$$p = -\rho + \kappa e^{-\phi(l)}, \tag{4.24}$$

where κ is a constant of integration with dimensions of inverse of length squared. This expression ensures that the pressure is infinite at any surface of zero red-shift function, i.e. when $\phi(l_{\text{div}}) \to -\infty$. Assuming that such surface exists, we approximate the TOV equation at leading order in the pressure as

$$p'(l) = -\frac{4\pi r p^2 + \mathcal{O}(p)}{\sqrt{1 - \dfrac{8\pi r^2 \rho}{3} - \dfrac{M_0}{r}}}. \tag{4.25}$$

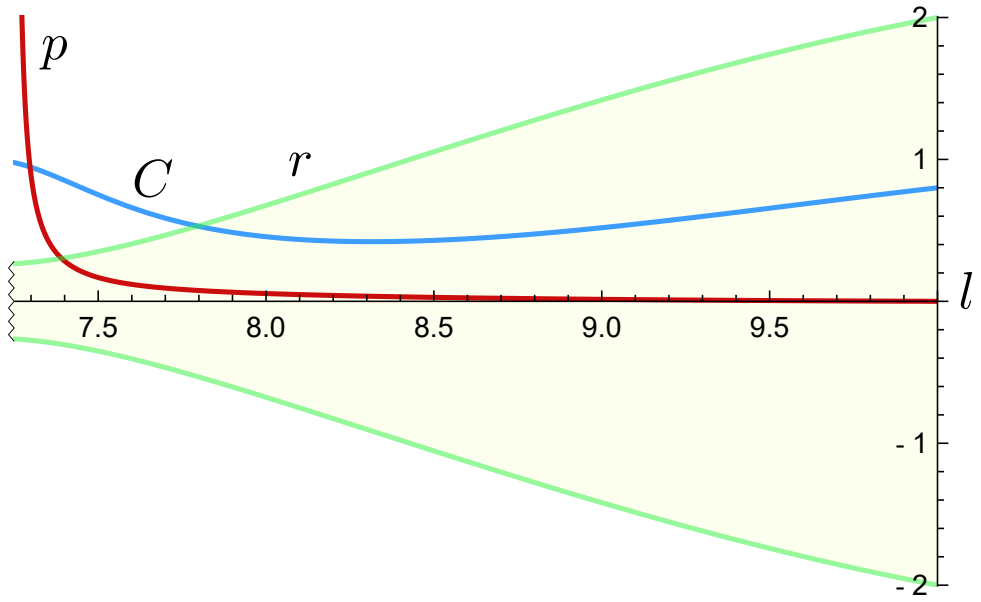

Fig. 4.4.: Plot of a sub-critical, sub-Buchdahl star with $R = 2, C(R) = 0.8$ and $\rho = 0.84\rho_{\text{c-clas}}$. Green lines represent the shape function $r(l)$, while red and blue lines denote the functions $p(l)$ and $C(l)$, respectively. The presence of a positive constant mass $M_0 \simeq 0.07$ generates a (singular) event horizon at $l \simeq 7.25$.

Take into account that the pressure diverges while the denominator in (4.25) is still non-vanishing. In this regime, we can assume the following behavior for the pressure

$$p \simeq \frac{p_+}{(l - l_{\text{div}})^n}, \qquad p_+ > 0, \qquad n > 0. \tag{4.26}$$

Replacing this ansatz in Eq. (4.25) and solving for p_+ and n we find

$$p \simeq (l - l_{\text{div}})^{-1} \frac{\sqrt{1 - 8\pi r_{\text{div}}^2 \rho/3 - M_0/r_{\text{div}}}}{4\pi r_{\text{div}}}, \tag{4.27}$$

where $r_{\text{div}} = r(l_{\text{div}})$. The pressure diverges positively at the surface $l = l_{\text{div}}$, whose location depends on the boundary conditions of the star and, consequently, on M_0. By decreasing ρ (increasing M_0), this divergence approaches the surface of the star. Equivalently, the more super-Buchdahl the star is, the further the pressure divergence moves towards the surface of the star. Recall that, for the super-Buchdahl critical case, we know the position of the infinite pressure divergence in terms of boundary conditions. This explicit expression is lost in the sub-critical situation, since we lack a complete analytic solution.

The resulting geometry resembles a BH surrounded by matter forced to maintain equilibrium, causing a runaway in the pressure of the fluid. This divergence in the

pressure takes place at the same position at which the redshift function, obtained from solving Eq. (4.24) in the $l \to l_{\text{div}}$, vanishes:

$$e^{2\phi} \simeq \left(\frac{l - l_{\text{div}}}{l_{\text{div}}} \right)^2 . \tag{4.28}$$

Since this geometry is not vacuum but filled with a perfect fluid, there is a curvature singularity at the horizon. This is foreseeable by recalling that horizons are incompatible with matter fluids in hydrostatic equilibrium.

4.3.4 Super-critical solutions

Now, we turn to the analysis of super-critical configurations, where we distinguish between sub- and super-Buchdahl stars.

Recall [Subsec. 4.3.3 or Eq. (4.10)] that in the sub-Buchdahl case, the effect of going super-critical (i.e. taking $\rho > \rho_{\text{c-clas}}$) is to add a negative mass M_0 to the spacetime. The repulsive effect that this negative mass exerts on the fluid makes pressure reach a maximum value at some $r > 0$. This can be viewed in the vanishing of the numerator of Eq. (4.9) when r' [as of Eq. (4.10)] becomes large enough as to compensate for the positive $1 + 8\pi r^2 p$ term. In this case, the perfect fluid extends up to $r = 0$, where a naked curvature singularity resides. Figure 4.5 shows examples of pressure profiles for several super-critical configurations. The growth of the pressure is dampened as the solutions are made increasingly super-critical. Integrating (4.10) in the $r \to 0$ limit leads to the relation

$$r \simeq \left[\frac{3\sqrt{|M_0|}}{2} l \right]^{2/3} . \tag{4.29}$$

Therefore, there exists a neighborhood of $r = 0$ in which the geometry is well-approximated by the Schwarzschild vacuum solution with negative ADM mass.

The TOV equation (4.9) can be integrated in terms of analytic functions by making the coordinate change (4.1) and taking the limits $r \to 0$ and $C \to -\infty$, which yields

$$p' \simeq \frac{(\rho + p)}{2r}. \tag{4.30}$$

Integrating and replacing (4.29) we obtain

$$p \simeq -\rho + M_0^{-2} \left(\frac{l}{|M_0|} \right)^{1/3} . \tag{4.31}$$

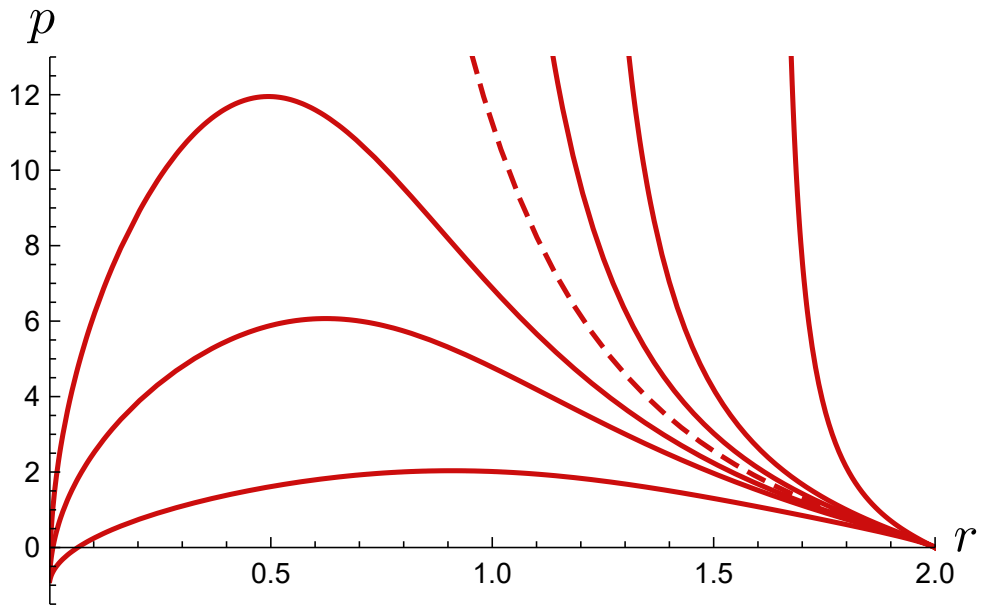

Fig. 4.5.: Plot of the pressure profile for a super-critical, super-Buchdahl star with $C(R) = 0.96$. The curves denote the pressure $p(r)$ (in units of ρ) for the values of the energy density (from right to left) $\rho/\rho_{\text{c-clas}} = 1, 1.8, 2, 2.13, 2.26, 2.4$ and 3. The dashed curve ($\rho/\rho_{\text{c-clas}} \sim 2.13$) corresponds to a separatrix for which pressure diverges at $r = 0$. Note how the divergence in pressure of super-Buchdahl stars moves inwards as the density increases. An increase of the negative mass M_0 finally regularizes the pressure, which tends to the value $p = -\rho$ at the origin.

In the presence of a constant negative mass, the pressure acquires the equation of state of vacuum energy in the limit $r \to 0$. Note that this finite value for the central pressure is reached with infinite derivative, which results in the redshift function being divergent in the $l \to 0$ limit as

$$e^{2\phi} \simeq \left(\frac{|M_0|}{l}\right)^{2/3}. \tag{4.32}$$

In some situations, semiclassical contributions can appear as a cloud of negative mass in the spacetime. The pressure-regularizing effect of this cloud is similar to that of super-criticality. We will revisit this discussion in the analysis of semiclassical solutions. Here, given a super-Buchdahl star, gradually increasing ρ (decreasing M_0) displaces the pressure divergence towards the radial origin, eventually making pressure finite for densities above some $\rho = \rho_{\text{reg-p}}$. These aspects apply to more generic equations of state as well [208–211]. This value of the density constitutes an infinite-pressure separatrix between super-critical solutions singular and regular in pressure (see the dashed line in Fig. 4.5). Hence, solutions with $\rho > \rho_{\text{reg-p}}$ will be regular in the pressure (although the pressure gradient diverges at $l = 0$)

but irregular in the compactness. The value of $\rho_{\text{reg-p}}$ increases with the surface compactness of the star, eventually diverging towards $+\infty$ in the $C(l_{\text{S}}) \to 1$ limit. The particular features of this separatrix solution are analyzed right below.

4.3.5 Classical infinite pressure separatrix

The separatrix solution lies between super-critical configurations irregular and regular in the pressure, although we reserve a separate Subsection for them to highlight their relevance. Consider a super-critical solution extending to $r(0) = 0$. Since $M_0 < 0$, the solution for the shape function $r(l)$ around the origin always obeys Eq. (4.29), and the pressure function can only follow two paths: either it goes to a constant value at $r = 0$, which has to be exactly $-\rho$, in virtue of (4.31), or it diverges necessarily towards positive infinity at $r = 0$. The separatrix solution corresponds to this last possibility.

To derive the precise form of the divergence in pressure, we expand the TOV equation (4.9) in the $l \to 0$ limit under the assumption that $p \gg \rho$, yielding

$$p' \simeq -\frac{4\pi r p^2}{r'}. \tag{4.33}$$

Now, assuming the following ansatz for the pressure

$$p = \frac{p_+}{l^n}, \quad n > 0, \tag{4.34}$$

where p_+ is a positive dimensionless constant, and replacing Eq. (4.29) and this ansatz in Eq. (4.33), we find

$$n = 2, \quad p_+ = 1/3\pi. \tag{4.35}$$

Therefore, the pressure diverges, in the $l \to 0$ limit, with the same power of l as in the separatrix (4.21) between sub-Buchdahl and super-Buchdahl configurations. However, the way the areal radius of spheres $r(l)$ approaches the origin $l = 0$ differs in both cases. In terms of the shape function (4.29), solution (4.35) takes the form

$$p \simeq \frac{3|M_0|}{4\pi r^3}, \tag{4.36}$$

revealing a direct dependence in the constant mass M_0. A pictorial representation of this separatrix is shown in Fig. 4.5. On the other hand, the separatrix described around Eq. (4.21) satisfies

$$p \simeq \frac{1}{2\pi r^2}, \tag{4.37}$$

revealing that the leading behavior in the pressure is independent of M_0 since this separatrix corresponds to a critical configuration.

The separatrix solution (4.36) was analyzed in [56, 204] (see [212] for a compelling physical interpretation) and is particularly interesting because semiclassical corrections deform this solution into a separatrix for the compactness as well (i.e. a critical configuration). The relevance of this separatrix will be clear when analyzing the corresponding semiclassical situation.

4.4 Semiclassical stellar equilibrium

In the following we are going to obtain the semiclassical self-consistent counterparts to the previous classical set of solutions. We introduce, as a source of curvature, the expectation value of the stress-energy tensor of a single massless, minimally coupled scalar field modeled through the CRP-RSET used in previous Chapters. This choice is motivated by the fact that the usual Polyakov approximation is plainly incompatible with regular stellar configurations due to it being singular at $r=0$. In (t,l) coordinates the components of the CRP-RSET [taking (1.14) with the choice of regulator (1.15)] in the Boulware state naturally adapted to stellar spacetimes are

$$\begin{aligned}
\langle\hat{T}_{tt}\rangle^{\text{CRP}} =& \frac{l_{\text{P}}^2}{8\pi\left(r^2+\alpha l_{\text{P}}^2\right)}\left[\left(\phi'\right)^2+2\phi''\right]e^{2\phi},\\
\langle\hat{T}_{ll}\rangle^{\text{CRP}} =& -\frac{l_{\text{P}}^2}{8\pi\left(r^2+\alpha l_{\text{P}}^2\right)}\left(\frac{\phi'}{r'}\right)^2,\\
\langle\hat{T}_{\theta\theta}\rangle^{\text{CRP}} =& \frac{\langle\hat{T}_{\varphi\varphi}\rangle^{\text{CRP}}}{\sin^2\theta} = -\frac{\alpha\left(l_{\text{P}}^2 r\phi'\right)^2}{8\pi\left(r^2+\alpha l_{\text{P}}^2\right)^2}.
\end{aligned} \tag{4.38}$$

Let us now pass to the central part of the Chapter, the analysis of the internal stellar solutions under the hypothesis of having a classical matter component with a constant density ρ in addition to the semiclassical contribution.

4.4.1 Semiclassical equations of stellar interiors

The semiclassical field equations are obtained by plugging the CRP-RSET components in Eq. (4.38) in Eq. (1.6),

$$-2r''r+1-\left(r'\right)^2 = 8\pi r^2\rho+\frac{r^2 l_{\text{P}}^2}{\left(r^2+\alpha l_{\text{P}}^2\right)}\left[\left(\phi'\right)^2+2\phi''\right], \tag{4.39}$$

$$2rr'\phi'-1+\left(r'\right)^2 = 8\pi r^2 p-\frac{r^2 l_{\text{P}}^2}{\left(r^2+\alpha l_{\text{P}}^2\right)}\left(\phi'\right)^2, \tag{4.40}$$

for the tt and ll components, respectively. The CRP-RSET is independently conserved, and so is the classical SET. The system of equations is thus completed by the equation of conservation of the classical matter (4.7) and the equation of state of the uniform density fluid (4.8).

We can construct the semiclassical version of the TOV equation [114] by combining Eqs. (4.40) and (4.7)

$$p' = (\rho + p)\, r' \frac{(r^2 + \alpha l_{\mathrm{P}}^2)}{l_{\mathrm{P}}^2 r} \left(1 \pm \sqrt{1 + \left(\frac{l_{\mathrm{P}}}{r'}\right)^2 \frac{8\pi r^2 p + 1 - (r')^2}{r^2 + \alpha l_{\mathrm{P}}^2}} \right). \tag{4.41}$$

The semiclassical TOV equation is a quadratic polynomial for the gradient of the pressure. Therefore, the two branches of solutions already present in vacuum are retained in situations involving a classical perfect fluid. Hence, observations regarding the nature of these branches made in Chapter 2 also apply to this situation. Note that analytical solutions that describe ultra-compact horizonless stars have been found [114] for the concealed branch by solving Eq. (4.41).

For convenience in the upcoming analysis, field equations (4.39)) and (4.40) can be combined to construct a single differential equation that relates $\phi''(l)$ to the functions $\phi'(l),\ \rho(l),\ p(l)$ and $r(l)$. When expressed in terms of the Schwarzschild coordinates (t, r, θ, ϕ), for which the metric takes the form (1.2), we can use Picard-Lindelöf theorem to constrain the form of the solutions, in a similar spirit to what was done in vacuum and electrovacuum. The change of variable from l to r amounts to the following replacements

$$r'(l) \to \sqrt{1 - C(r)}, \quad \phi'(l) \to \psi(r)\sqrt{1 - C(r)}, \tag{4.42}$$

where $\psi(r) \equiv \phi'(r)$, the prime denoting now the derivative with respect to the coordinate r. The resulting differential equation is written as

$$\psi' = \mathcal{D}\left(\mathcal{A}_0 + \mathcal{A}_1\psi + \mathcal{A}_2\psi^2 + \mathcal{A}_3\psi^3\right), \tag{4.43}$$

where

$$\begin{aligned}
\mathcal{A}_0 =& 4\pi\left(\rho+3p\right),\\
\mathcal{A}_1 =& 4\pi r\left[3\left(\rho+p\right)+\frac{2l_{\rm P}^2}{r^2+\alpha l_{\rm P}^2}p\right]-\frac{2}{r},\\
\mathcal{A}_2 =& 8\pi r^2\left[\rho-p+\frac{l_{\rm P}^2(3p+\rho)}{2(r^2+\alpha l_{\rm P}^2)}+\frac{l_{\rm P}^2 r^2 p}{(r^2+\alpha l_{\rm P}^2)^2}\right]-\frac{2l_{\rm P}^2\left(r^2/2+\alpha l_{\rm P}^2\right)}{\left(r^2+\alpha l_{\rm P}^2\right)^2}-2,\\
\mathcal{A}_3 =& \frac{l_{\rm P}^2 r}{r^2+\alpha l_{\rm P}^2}\left\{4\pi r^2\left[\rho-p+\frac{2l_{\rm P}^2 r^2 p}{(r^2+\alpha l_{\rm P}^2)^2}\right]-\frac{\alpha l_{\rm P}^4}{(r^2+\alpha l_{\rm P}^2)^2}-1\right\},\\
\mathcal{D} =& \frac{r^2+\alpha l_{\rm P}^2}{\left(1+8\pi r^2 p\right)\left[r^2+(\alpha-1)l_{\rm P}^2\right]}.
\end{aligned} \tag{4.44}$$

The right-hand side of (4.43) is a third-order polynomial in ψ. Now, we can formally solve Eq. (4.7) with the equation of state (4.8) to yield Eq. (4.24). In this way, replacing Eq. (4.24) into Eq. (4.43) will result in an integro-differential equation for the variable ψ (although this is not the way we are going to solve the system of equations).

Eq. (4.43) can be expressed in the form

$$\psi' = \mathcal{F}_{\rm Schw} + \mathcal{G}\left(\rho,p,\psi,r\right)\left(\psi-\psi_-\right)\left(\psi-\psi_+\right). \tag{4.45}$$

Here $\mathcal{F}_{\rm Schw}$ is the vacuum-portion of the right-hand side of Eq. (4.43) [i.e. Eq. (2.9)], and

$$\mathcal{G} = \frac{4\pi l_{\rm P}^2 r^2\left[\rho\left(1+r\psi\right)+p\left(3+r+\frac{2l_{\rm P}^2 r}{r^2+\alpha l_{\rm P}^2}\right)\psi\right]}{\left[r^2+(\alpha-1)l_{\rm P}^2\right]\left(1+8\pi r^2 p\right)}. \tag{4.46}$$

Finally, $\psi_\pm$ are the singular exact solutions examined in the vacuum case (2.10). In view of (4.45), matter-dependent contributions vanish for $\psi=\psi_\pm$ in Eq. (4.45), leaving only the vacuum equation, for which they are exact solutions. Finally, it will be useful afterwards to notice that, in the regime $p \gg \rho$, all the p-dependence in Eq. (4.43) disappears, making it a first order differential equation for ψ.

4.4.2 Semiclassical criticality

The classical notion of criticality described in section 4.2.2 is greatly affected by quantum corrections. The vacuum polarization of the scalar field generates a cloud of mass that coats the spacetime, extending to infinity. The semiclassical equivalent to relation (4.11) would now have $M_{\rm cloud}$ defined as

$$M_{\rm cloud} = \int_0^\infty dr\, 4\pi r^2\left[\Theta(R-r)\rho+\rho_{\rm s}\right], \tag{4.47}$$

where Θ is the Heavyside step function and $\rho_{\rm s} = -\langle \hat{T}^t_t \rangle$ denotes the semiclassical energy density. In the vacuum portion of the spacetime, the only contribution to $M_{\rm cloud}$ is semiclassical. It supplies a negative contribution in such a way that the Misner-Sharp mass grows from its asymptotic ADM value as we approach the surface of the object. Once inside the object, we have semiclassical as well as classical contributions to the density. As in the classical case, the Misner-Sharp mass can be ill-defined at the origin (recall that in the classical case this is exclusively related to the possible presence of an M_0 offset). The difference now is that the Misner-Sharp mass can fail to approach zero at the origin by different intertwined reasons. It might be that there is a mismatch between the internal mass and the classical density due to the presence of a nonzero M_0; it might also be that the semiclassical density diverges at the origin; or it might be a combination of both.

As in the semiclassical case the equation for the compactness is intertwined with that of the pressure: given a star radius and compactness, we ignore *a priori* which value of ρ we should use to find a regular compactness at the radial origin (i.e. a zero Misner-Sharp mass at the origin). As we will see, the situation is even more complicated, as in some important cases there does not exist a value of ρ such that the compactness at the origin vanishes. What we do find is that there always exists a value $\rho_{\rm c}$ of ρ separating two rather different qualitative behaviors for the compactness. Therefore, in general terms we will say that a configuration is critical when its density is such that it represents a separatrix between these two regimes.

Having posed these difficulties and a definition of criticality, we now proceed to analyze the semiclassical set of solutions. First, we will study configurations with a regular origin, in the same spirit as we did in the classical analysis of cosmological solutions. Solutions with different sorts of irregularities will be analyzed in detail in the sections that follow.

4.5 Semiclassical stellar-like solutions

The introduction of the RSET as an additional source of curvature makes exploring the space of stellar solutions of the semiclassical equations a more subtle task than in the classical theory. This difficulty can be attributed, in part, to the new length scale $l_{\rm P}$ that makes the physics of solutions sensitive to the overall size of the star. In this Section we address every solutions belonging to the semiclassical sector of Figs. 4.1 and 4.2.

Considering stars whose surface is outside the neck, Figure 4.6 shows a pictorial representation of an $R \gg l_{\rm P}$ slice of the space of solutions. We distinguish four differentiated regions depending on whether the star is sub- or super-critical, and

on whether its compactness surpasses Buchdahl limit or not. The central black dot represents the most compact configuration that is regular in both compactness and pressure. Here, we refer to this compactness bound as the Buchdahl bound for semiclassical stars sourced by the specific regularization of the RP-RSET that we are using. For this particular regularization, stars with large (stellar-like) radius and mass show a Buchdahl limit that corresponds to a perturbative correction over the classical compactness bound of $C(R) = 8/9$. From now on, we distinguish between sub-Buchdahl or super-Buchdahl stars attending to this bound. This will be useful to divide the space of solutions in different regions, as in Fig. 4.6, although this definition has only an operational meaning, and cannot be directly identified as a Buchdahl limit in semiclassical gravity. In particular, defining this limit, which may exist or not, depends on the particular modeling of the semiclassical source. We are interested in probing whether it is possible to obtain regular or quasi-regular configurations largely surpassing the Buchdahl limit. Particularly, we will aim at the rightmost portion of the diagram 4.6, or ultra-compact limit, where semiclassical corrections meet the conditions to become comparable in magnitude to that of the classical SET, thus potentially inducing significant departures from the classical solutions. In what follows we will obtain the specific form of the solutions for all four regions, together with the form of the separatrix solutions $\rho_{\rm c}$.

We now turn to the analysis of integrations from the asymptotically flat region towards the center of the star. This treatment allows to better probe how the RSET acts in response to changes in the surface compactness and the classical density parameter used in the integrations. The boundary conditions required at the surface of the star follow from the classical ones (4.22), with an extra condition for ϕ' (note that we are using l as our radial coordinate for now),

$$\begin{aligned} &p\left(l_{\rm S}\right)=0, \quad r\left(l_{\rm S}\right)=R, \\ &\phi\left(l_{\rm S}\right)=\phi_{\rm S}, \quad r'\left(l_{\rm S}\right)=\mp\sqrt{1-C(R)}. \\ &\phi'\left(l_{\rm S}\right)=\frac{R^2+\alpha l_{\rm P}^2}{R l_{\rm P}^2}\left[\sqrt{1+\frac{R^2}{R^2+\alpha l_{\rm P}^2}\frac{C(R)}{1-C(R)}}\pm 1\right] \\ &\qquad\times\sqrt{1-C(R)}, \end{aligned} \tag{4.48}$$

where $C(R)$ is the value of the compactness at the surface of the star. Here, the $\pm$ signs select the side of the wormhole where the surface of the star is located. We choose the $+$ sign in r' and the $-$ sign in ϕ' for stars whose surface lies outside the neck, and vice versa if the star surface is located inside the neck. Any other sign combination is not compatible with a stellar spacetime.

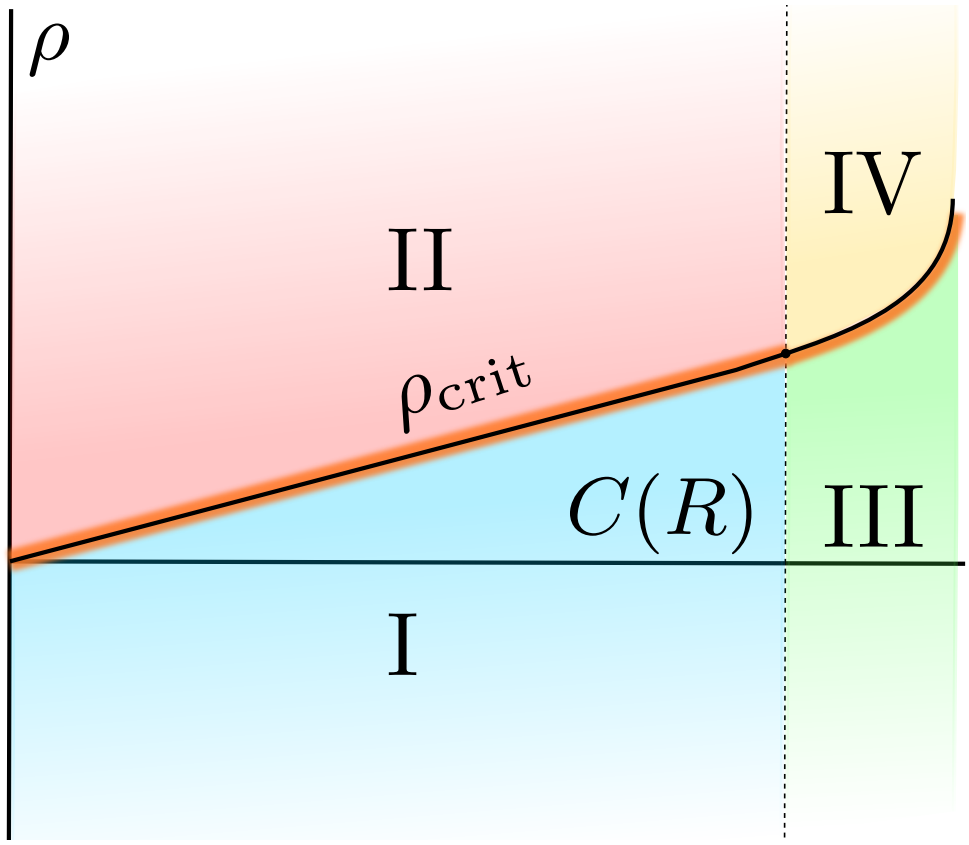

Fig. 4.6.: Pictorial representation of an $R \gg l_{\mathrm{P}}$ slice of the phase space of semi-classical constant-density stars. The vertical and horizontal axes represent the energy density and the surface compactness of stars. The curve ρ_{c} corresponds to a separatrix solution. The vertical dotted line here denotes the Buchdahl limit, in which the central black dot represents the most compact configuration strictly regular in both pressure and compactness, or Buchdahl solution. We distinguish four regions in the resulting figure: region I represents sub-critical sub-Buchdahl stars, region II is for super-critical sub-Buchdahl, region III is for sub-critical super-Buchdahl; and region IV represents super-critical super-Buchdahl stars. In the sub-Buchdahl semiplane (left-hand side of the vertical dotted line), the separatrix ρ_{c} corresponds to strict stellar spacetimes. For super-Buchdahl configurations this separatrix correspond to non-regular solutions, but in its neighbourhood we find quasi-regular configurations (i.e. ϵ-strict stellar configurations). The narrow orange band that surrounds the ρ_{c} line denotes the ϵ-strict regime which spans through regions I, II and III

The above boundary conditions can be inserted in the semiclassical field equations to study how the CRP-RSET behaves at the surface of stars in the $C(R) \to 1$ limit. Computing the RSET over the classical background of the Schwarzschild interior solution causes that both the semiclassical energy density and pressure diverge at the surface of the star R in the limit $C(R) \to 1$. This divergence appears both from the interior region of the star, where ρ is constant and positive, and from the exterior, vacuum portion, where $\rho = 0$. This is so because this limit corresponds to locating the surface on top of the event horizon, where the Boulware state is, by definition, singular.

In a self-consistent approach, on the contrary, the RSET backreacts on the metric and there is no horizon. Instead, we encounter a wormhole neck where the RSET components are finite and have no trace of divergences. Starting from Eqs. (4.39, 4.40), the CRP-RSET components at the surface of a star in the $C(R) \to 1$ limit are

$$\begin{aligned} p_{\rm s}^{\rm r} &= \langle \hat{T}_l^l \rangle^{\rm CRP} = -\frac{1}{8\pi R^2} + \mathcal{O}\Big(\sqrt{1-C}\Big), \\ p_{\rm s}^{\theta} &= \langle \hat{T}_\theta^\theta \rangle^{\rm CRP} = -\frac{\alpha l_{\rm P}^2}{8\pi R^2\,(R^2+\alpha l_{\rm P}^2)} + \mathcal{O}\Big(\sqrt{1-C}\Big), \\ \rho_{\rm s} &= -\langle \hat{T}_t^t \rangle^{\rm CRP} = -\frac{1}{8\pi R^2} + \rho + \mathcal{O}\Big(\sqrt{1-C}\Big). \end{aligned} \tag{4.49}$$

Every component of the CRP-RSET is finite and negative at the surface (this is independent of the regularization scheme for the RP-RSET as long as it reduces to the Polyakov RSET at the surface of the star). In the ultracompact limit, the radial pressure and the energy density are able to compensate their $\mathcal{O}(l_{\rm P}^2)$ suppression, becoming comparable to the classical SET components. The finite jump in ρ at the surface of the fluid sphere contributes positively to the semiclassical energy density. Consequently, the total energy density (the sum of classical and semiclassical contributions) will be positive at the surface given that

$$\rho > \frac{1}{16\pi R^2}. \tag{4.50}$$

This result comes from a local analysis at the surface; the particular form of the RP-RSET at the bulk depends on the specifics of the interior solution. More elaborate approximations to the RSET for massless, minimally coupled fields (like the AHS-RSET) are expected to extend these negative semiclassical contributions to the stellar interior as well. For more realistic equations of state with vanishing energy density at the surface, the complete SET (the sum of the classical and quantum portions) violates all energy conditions at the surface of ultracompact stars.

Now, picture a numerical integration starting at the asymptotically flat region with a positive ADM mass. While in vacuum, compactness increases monotonically until the neck as in Fig. 2.2, and we can decide to locate the surface of the perfect fluid either outside or inside it. At the surface, compactness and radius are fixed, leaving the energy density ρ as the only free parameter. With the aim of constraining the various possibilities embraced by the diagram in Fig. 4.6, we will first describe the behavior of stars situated at regions I and III in the diagram (sub-critical regime) and at regions II, IV (super-critical regime). Since stellar geometries should connect with the vacuum solution in the $\rho \to 0$ limit, we can always devise a star of any compactness that belongs to the sub-critical regime. Similarly, given a star with any $C(R) < 1$, the super-critical regime is explored by increasing ρ beyond the critical density. This classification is valid for stars located either outside or inside the neck, so we proceed by first investigating the former. Our results and acquired intuitions will extend to the study of the latter situation as well.

4.5.1 Solutions with a regular center

From the complete set of solutions, we want to extract first those solutions which are strict stellar configurations, i.e. which have a regular radial center. Recall that these configurations correspond to the critical sub-Buchdahl solutions in Figs. 4.1 and 4.2. We proceed by performing numerical integrations from a regular origin. The following boundary conditions must be imposed at $r = 0$ to integrate Eqs. (4.7), (4.39) and (4.40),

$$\begin{aligned} r(0) = 0, \quad \phi(0) = \phi_{\rm c}, \quad p(0) = p_{\rm c} \\ r'(0) = 1, \quad \phi'(0) = 0. \end{aligned} \tag{4.51}$$

Integrations from a regular origin share many features with their classical counterparts. Given that the choice of $\phi_{\rm c}$ represents just a rescaling of time coordinate, the full space of solutions with regular origin is determined by the two-parameter set $(\rho, p_{\rm c})$.

Depending on the relative values of $p_{\rm c}$ and ρ, three families of solutions are found, the separatrices between them corresponding, as in the classical case, to $p_{\rm c}/\rho = -1/3$ and $p_{\rm c}/\rho = -1$. In this Section we focus on the semiclassical equivalent to the type 1 set of cosmological solutions, for which the null and strong energy conditions hold at $r = 0$. A specific example has been plotted in Fig. 4.7 (see Fig. 4.8 for details on the RSET). Recall from Subsec. 4.3.1 that the positive-pressure portion of type 1 solutions (i.e. those with $p_{\rm c},\ \rho > 0$) corresponds to stellar spacetimes, and so happens in the semiclassical theory. Furthermore, extending the

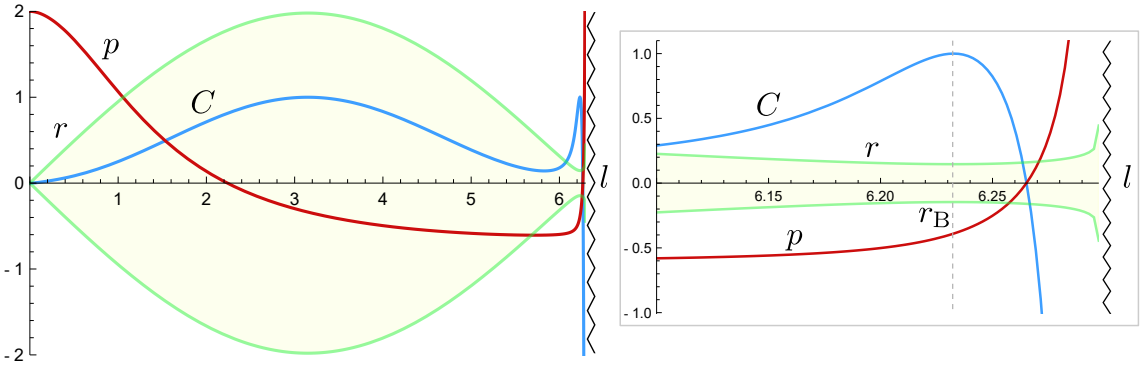

Fig. 4.7.: Plot of the semiclassical counterpart of figure 4.3 with $\rho = 0.03$, $p_c = 2\rho$ and $\alpha - 1 = 10^{-3}$. We have plotted the functions $r(l), C(l)$ and $p(l)$ (in units of ρ) and they appear in green, blue and red, respectively. The right pole of the geometry is shown in detail. Notice how the radial function has a minimal surface (vertical dashed line) at $l \sim 6.23$ and the geometry connects to a singular region (vertical zigzag line) located at $r \to \infty$ but at finite proper distance from $l = 0$.

perfect fluid beyond the surface of zero pressure allows to find the semiclassical counterparts to the classical cosmological solutions. Here, by counterparts, we are referring to the pair of classical and semiclassical solutions with the same ρ and p_c.

Firstly, we are going to describe the characteristics of the solutions that we have been able to find through numerical integrations. Unfortunately, this covers a quite limited range of initial conditions. This is so because of the numerical precision required to handle highly different scales. In the semiclassical approximation, the scale of semiclassical corrections is suppressed by l_P, and has to be resolved with the scale of typical compact objects, of the order of kilometers. Thus, the results described in the remaining of this thesis need to be extrapolated with care to stars of astrophysical size. Still, we do not find a reason to believe that (within the semiclassical equations analyzed here) the physics of solutions with realistic parameter values is going to be radically different from the one detailed in this work. Other authors considered semiclassical corrections to astrophysical-sized stars [213–215] and found quantum corrections to be nearly negligible in most scenarios. These results are consistent with what we find in regimes of low compactness. Let us now describe the characteristics of the numerical solutions and then what appropriate conclusions one can extract from them.

Figure 4.7 depicts the semiclassical counterpart to the classical cosmology from Fig. 4.3, with $\rho = 0.03$ and $p_c = 2\rho$. Restricting ourselves to the positive pressure portion in Fig. 4.7, we observe that the RSET contributes positively to the mass of

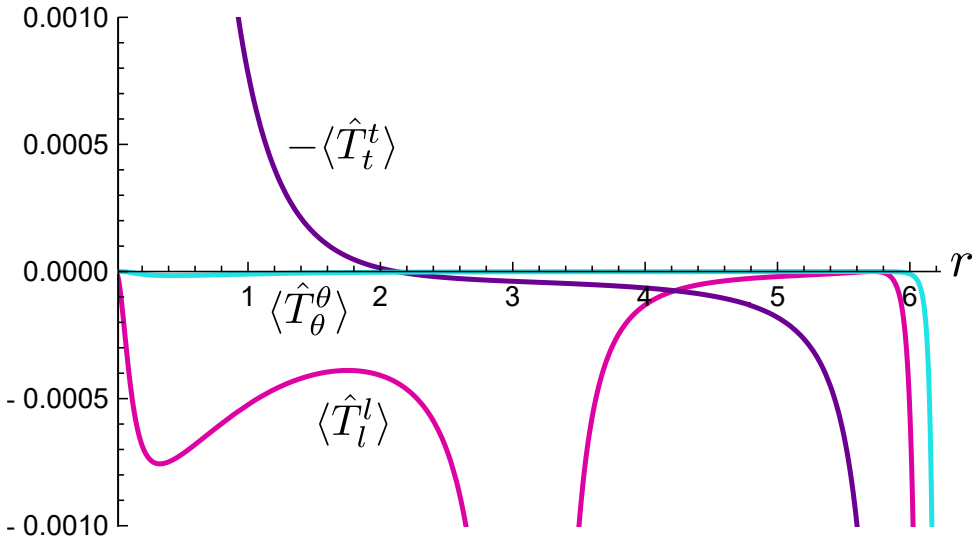

Fig. 4.8.: Plot of the RP-RSET components $-\langle\hat{T}^t_t\rangle$ (dark blue), $\langle\hat{T}^l_l\rangle$ (magenta) and $\langle\hat{T}^\theta_\theta\rangle$ (cyan) for the cosmological solution solution with $p_{\rm c} = 2\rho$, $\rho = 0.03$ and $\alpha - 1 = 10^{-3}$.

the star on average (see the purple curve in Figure 4.8). The spacetime of a regular star that fulfillst the regularity conditions

$$e^{2\phi(l)} = e^{2\phi_{\rm c}} + \phi_1 l^2 + \mathcal{O}\left(l^3\right),\ r(l) = l + r_{\rm c} l^3 + \mathcal{O}\left(l^4\right), \tag{4.52}$$

where ϕ_1 and $r_{\rm c}$ are constants. These conditions follow from the finiteness of the Kretschmann scalar (1.10) at $r = l = 0$. If the star satisfies the SEC and NEC (hence pressure is maximal at $r = 0$), the semiclassical energy density is positive at the center,

$$\rho_{\rm s} = \frac{\phi_1}{4\pi\alpha e^{2\phi_{\rm c}}} > 0, \tag{4.53}$$

its magnitude being inversely proportional to the value of the regulator and to the smallness of the redshift function at the center. Consequently we find that these semiclassical stars —stars very small in astrophysical terms but still with non-Planckian classical densities— are slightly less compact than their classical counterparts, that is, the most compact strictly regular stars always satisfy $C(R) < 8/9$ if their density is not trans-Planckian. This is a consequence of the total energy density (recall, the sum of classical and semiclassical parts) now increasing towards the center, instead of being constant everywhere inside the star.

When these low-density stars are analyzed as integrations from the surface inwards, we find that, for counterparts of the same R and $C(R)$, semiclassical critical stars happen to be less dense than classical critical stars, the remaining mass being supplied by the RSET so that relation (4.11) is fulfilled. This under-density then results in the classical fluid perceiving an amount of mass greater than the

one generated by its own classical energy density and pressures, thus the pressure p needs to be greater at the center than in the classical case to retain equilibrium. Therefore, it becomes clear that the existence of semiclassical stars that surpass the Buchdahl limit requires the appearance of negative interior semiclassical energies.

This result is counter-intuitive with respect to initial expectations that we had regarding semiclassical effects. Initially we expected the total semiclassical energetic contribution to a star to be negative, as indicated by the large negative values of the semiclassical density and pressures (4.49) at the surface of stars in the $C \to 1$ limit. Two observations are pertinent at this point. On the one hand, for sub-Buchdahl stars, the negativity of the semiclassical contribution at the surface is very small, being suppressed by $l_{\rm P}$. On the other hand, the behavior of the CRP-RSET at the origin is predominant and the whole geometry strongly depends on it. In our approach, the regulating scheme for the RP-RSET comes as a cutoff to its total magnitude at the origin. Ideally, one would like to design a regulator bringing the CRP-RSET close to the exact RSET [127] (although it has not been computed in stellar spacetimes at the time of the writing of this thesis). This improved RSET would be sensitive to the local characteristics of the geometry at the origin and so able to properly capture the physics close to $r = 0$. For instance, for regular sub-Buchdahl configurations one expects the RSET to be also small at the origin as neither large curvatures nor horizons are present through the configuration. Notice that from these arguments alone it is not straightforward to say anything about the Buchdahl limit itself.

In any case, the analysis reported here is valuable in clearly illustrating the limitations and strengths of the RP-RSET. It is reasonable to expect that the RP-RSET should be a trustworthy approximation when the physics is driven by non-local effects generated at values of the radius close to where a horizon would have been classically located. On the contrary, it should not provide a reliable approximation when the physics is driven by the values of the RSET at the origin. This motivates our definition of ϵ-strict spacetimes as the solutions of relevance for extracting robust conclusions, since the behavior of any solution close to the origin is necessarily impacted by the choice of regulator. As the regular solutions described in this section are a subset of the ϵ-strict spacetimes, it cannot be assumed that these provide a typical description of the properties of this larger set of solutions. Nevertheless, the existence of a set of non-regular but ϵ-strict solutions provides further motivation to analyze alternative regularizations of the RP-RSET, exploiting the available freedom characteristic of the Polyakov approximation which may be sufficient to regularize these solutions as well. In Chapter 5 we address this problem following a reductionist approach, deforming the regulator only within a sphere around $r = 0$ in ways that guarantee the existence of regular super-Buchdahl stars.

Cosmological solutions

For completeness, as we did in the classical case, let us mention some particularities of the cosmological solutions, independently of whether they can be used as regular stellar interiors or not. Coming back to Fig. 4.7, we observe that the resulting "cosmology" never reaches its would-be right pole. This difference with respect to the classical cosmology from Fig. 4.3 comes from the aforementioned semiclassical contribution to M_{cloud}. In an outwards integration starting at the origin, the semiclassical energy density giving rise to such contribution begins as positive and changes sign eventually. In Fig. 4.8 we observe that the semiclassical energy density grows as the origin $r = 0$ is approached, so that its weight at short distances is very significant. The overall effect of this mass cloud is to prevent the cosmology from being regular at its right pole. As this region is approached, the solution shows a minimal surface or neck that connects to an asymptotic, negative mass singularity, in the same fashion as in the vacuum solution, but now in presence of perfect fluid with divergent pressure. As an additional comment note that, although pressure has a second zero close to the neck, this surface does not connect with the Schwarzschild vacuum geometry in a way that resembles a stellar spacetime.

Now, decreasing p_{c} below zero results in configurations qualitatively similar to Fig. 4.7, but with pressure everywhere negative in between the center and the neck. Taking $p_{\text{c}} = -\rho/3$ results in an Einstein static universe, which receives no semiclassical corrections whatsoever: the RP-RSET is identically zero. Going below this separatrix for p changes the sign of the pressure gradient outside the radial origin, so that p increases outwards. For $-2\rho/3 \lesssim p_{\text{c}} < -\rho/3$ the obtained cosmologies show no neck. Instead, a second $r = 0$ is reached in a singular manner. This is so because the semiclassical contribution to the Misner-Sharp mass is now negative overall. In consequence, the solution tends to the semiclassical counterpart of the Schwarzschild geometry with negative asymptotic mass as the second $r = 0$ surface is approached.

Taking $p_{\text{c}} \lesssim -2\rho/3$ causes the neck to reappear, leading, once again, to an asymptotic singularity at radial infinity. This singularity moves towards smaller l as p_{c} decreases. When the null energy condition is saturated, the divergence has engulfed the radial maximum and the shape function increases monotonically from $r = 0$ outwards. Henceforth, all configurations show a negative-pressure divergence at $r \to +\infty$. Note that, owing to the curvature singularity at infinite r, these profiles cannot resemble the interior portion of gravastar solutions anymore since their shape functions do not match continuously with those of the positive-pressure portion of super-Buchdahl stars.

In summary, the semiclassical counterparts to these cosmological spacetimes have acquired features from configurations with non-regular compactness profiles as far as the behavior of the putative right-hand-side pole is concerned. This is due to the imbalance in mass that originates from quantum corrections as encapsulated in the CRP-RSET. Thus, solutions with non-regular compactness are important in the study of cosmologies with one regular center. In the next sections we derive the properties of solutions with irregular (non-critical) compactness in detail, using the notion of semiclassical criticality to catalog them.

4.5.2 Sub-critical solutions

We begin by considering a star with compactness well below the Buchdahl limit and density well below $\rho_{\rm c}$ (we are referring to the region I from Fig. 4.6). Taking $\rho = 0$ we obtain the semiclassical vacuum solution, which has a wormhole neck at some radius $r_{\rm B} \gtrsim 2M_{\rm ADM}$. By matching the vacuum solution with the surface of a constant-density configuration with small, positive ρ at some $R > r_{\rm B}$, the interior geometry resembles the vacuum solution (in the sense that it develops a wormhole neck in the interior) but with a perfect fluid added to it. As we saw for the cosmology from Fig. 4.7, wormhole necks can appear in the presence of matter. In this section we prove this statement and obtain analytic approximations to this wormhole geometry in certain regimes: around the neck and in the singular asymptotic region deep inside the neck. The procedure followed to derive these expressions closely resembles the one followed in Chapter 2 to derive the semiclassical Schwarzschild counterpart. The effect of increasing ρ is to approach the critical solution $\rho_{\rm c}$ in the space of solutions from Fig. 4.6, pushing the wormhole neck [i.e. a surface where $C(r_{\rm B} = 1)$] to smaller values of r until it disappears for some $\rho_{\rm c}$. Here, all solutions showing a wormhole neck will be called sub-critical. From a critical value of the density upwards (super-critical regime), we find that the geometries do not longer have a neck, having their shape functions extended until $r = 0$. The separatrix solution sits, obviously, between both regimes.

Let us consider in more detail the form of configurations belonging to the sub-critical regime and whose surface is located outside the neck. The first three panels in Fig. 4.10 describe configurations of this kind (see Fig. 4.11 for details on the CRP-RSET components). In virtue of Eq. (4.41), pressure grows monotonically inwards as long as the squared root term is greater than unity. Similarly to the classical sub-critical case, the compactness function C, which decreases as we move away from the surface inwards, encounters a minimum value somewhere in the bulk of the configuration, triggering a runaway in the pressure. Restricting

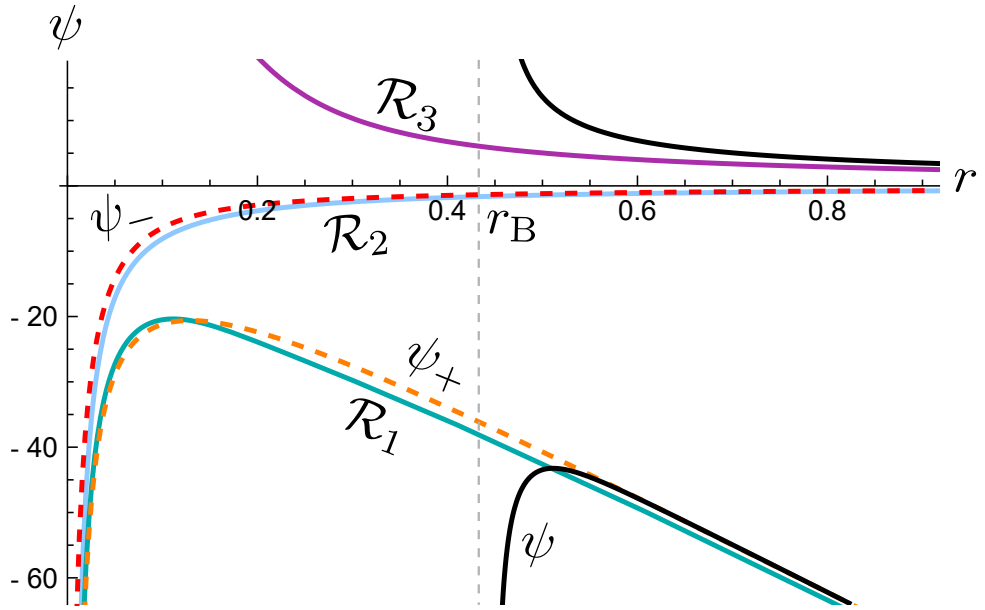

Fig. 4.9.: Numerical plot of the roots $\mathcal{R}_1, \mathcal{R}_2$ and $\mathcal{R}_3$ (cyan, purple and turquoise curves, respectively) together with the exact solutions $\psi_\pm$ (orange and red dashed curves) and an exact numerical solution in black (the neck radius $r_{\rm B}$ is represented by a vertical dashed line). The numerical solution corresponds to a sub-critical super-Buchdahl star with $R = 2, C(R) = 0.95$ and $\rho/\rho_{\text{c-clas}} \simeq 1.67$ with its neck at $l \simeq 0.45$ (vertical dashed line). These values have been chosen to aid visualization. The upper portion of the exact solution lives in the unconcealed branch, whereas the bottom portion lives in the concealed branch. The concealed part of the exact solution gets confined between $\mathcal{R}_3$ and ψ_+, converting towards the vacuum solution asymptotically.

ourselves to the regime where the expression for the pressure in Eq. (4.24) can be well approximated by

$$p \simeq \kappa e^{-\int \psi dr}, \tag{4.54}$$

we find that Eq. (4.43) is approximated by a first-order differential equation of the form

$$\psi' = \mathcal{H}\left(\psi - \mathcal{R}_1\right)\left(\psi - \mathcal{R}_2\right)\left(\psi - \mathcal{R}_3\right), \tag{4.55}$$

where

$$\mathcal{H} = -\frac{l_{\rm P}^2 r}{2\left[r^2 + l_{\rm P}^2\left(\alpha - 1\right)\right]}\left[1 - \frac{2 l_{\rm P}^2 r^2}{\left(r^2 + \alpha l_{\rm P}^2\right)^2}\right] \tag{4.56}$$

and $\{\mathcal{R}_i\}_{i=1}^3$ are three roots with involved and lengthy expressions that depend on r, α and $l_{\rm P}$. Their approximate asymptotic forms for $r \gg \sqrt{\alpha} l_{\rm P}$ are

$$\mathcal{R}_{1,2} \simeq \frac{3 \pm \sqrt{33}}{4r}, \quad \mathcal{R}_3 \simeq -\frac{2r}{l_{\rm P}^2}. \tag{4.57}$$

These roots appear plotted in Fig. 4.9 alongside $\psi_\pm$ as defined in Eq. (2.10), and an exact numerical solution belonging to the sub-critical regime. While $\mathcal{R}_1,\ \mathcal{R}_2$ are monotonic, $\mathcal{R}_3$ reaches a maximum value precisely where the ψ_+ exact solution intersects $\mathcal{R}_3$. This observation will guide us in what follows since, as long as Eq. (4.43) is well-approximated by a first-order differential equation, the shape of the solution ψ is determined by $\psi_\pm$ and $\{\mathcal{R}_i\}_{i=1}^3$.

The approximate expression (4.54) implies that ϕ diverges towards negative values, for which its derivative ψ needs to diverge towards $+\infty$ at some radius $r_{\rm B}$. Therefore, the right-hand side in Eq. (4.55) can be approximated to cubic order in ψ. By solving this approximate equation and expanding the solution in the limit $r \to r_{\rm B}$ we find

$$\psi \simeq \pm\sqrt{\frac{k_0}{4(r-r_{\rm B})}}, \tag{4.58}$$

with

$$k_0 = \frac{2\left[r_{\rm B}^2 + (\alpha-1)l_{\rm P}^2\right]\left(r_{\rm B}^2+\alpha l_{\rm P}^2\right)^2}{r_{\rm B} l_{\rm P}^2\left[(r_{\rm B}^2+\alpha l_{\rm P}^2)^2 - 2r_{\rm B}^2 l_{\rm P}^2\right]} > 0. \tag{4.59}$$

The surface $r = r_{\rm B}$ represents an asymmetric wormhole neck, where the shape function r reaches a minimum value. Integrating Eq. (4.58) and returning to the l coordinate, which is regular through the neck, the approximate behavior of the metric functions obtained is

$$r \simeq \frac{k_1}{4}\left(l-l_{\rm B}\right)^2 + r_{\rm B}, \quad \phi \simeq \frac{\sqrt{k_0 k_1}}{2}\left(l-l_{\rm B}\right) + \phi_{\rm B}, \tag{4.60}$$

where $l_{\rm B}$ and $\phi_{\rm B}$ are the values of the proper coordinate and the exponent of the redshift function at the neck, and

$$k_1 = \frac{4\left(r_{\rm B}^2+\alpha l_{\rm P}^2\right)}{r_{\rm B}^2 l_{\rm P}^2 k_0} > 0. \tag{4.61}$$

Replacing these expressions in Eq. (4.54), we see that the pressure

$$p \simeq p_{\rm B}\left[1 - \frac{\sqrt{k_0 k_1}}{2}\left(l-l_{\rm B}\right)\right] \tag{4.62}$$

is finite and positive through the neck as well. Therefore, locally around the neck, the geometry resembles that of the vacuum solution from Fig. 2.2, but covered by a perfect fluid of constant density with pressures that exceed the value of the density [note that $(p_{\rm B} \gg \rho)$ by consistency with (4.54)].

Inside the neck, the solution jumps from the unconcealed to the concealed branch, where vacuum polarization grows unbounded. The solution ψ takes the $-$ sign

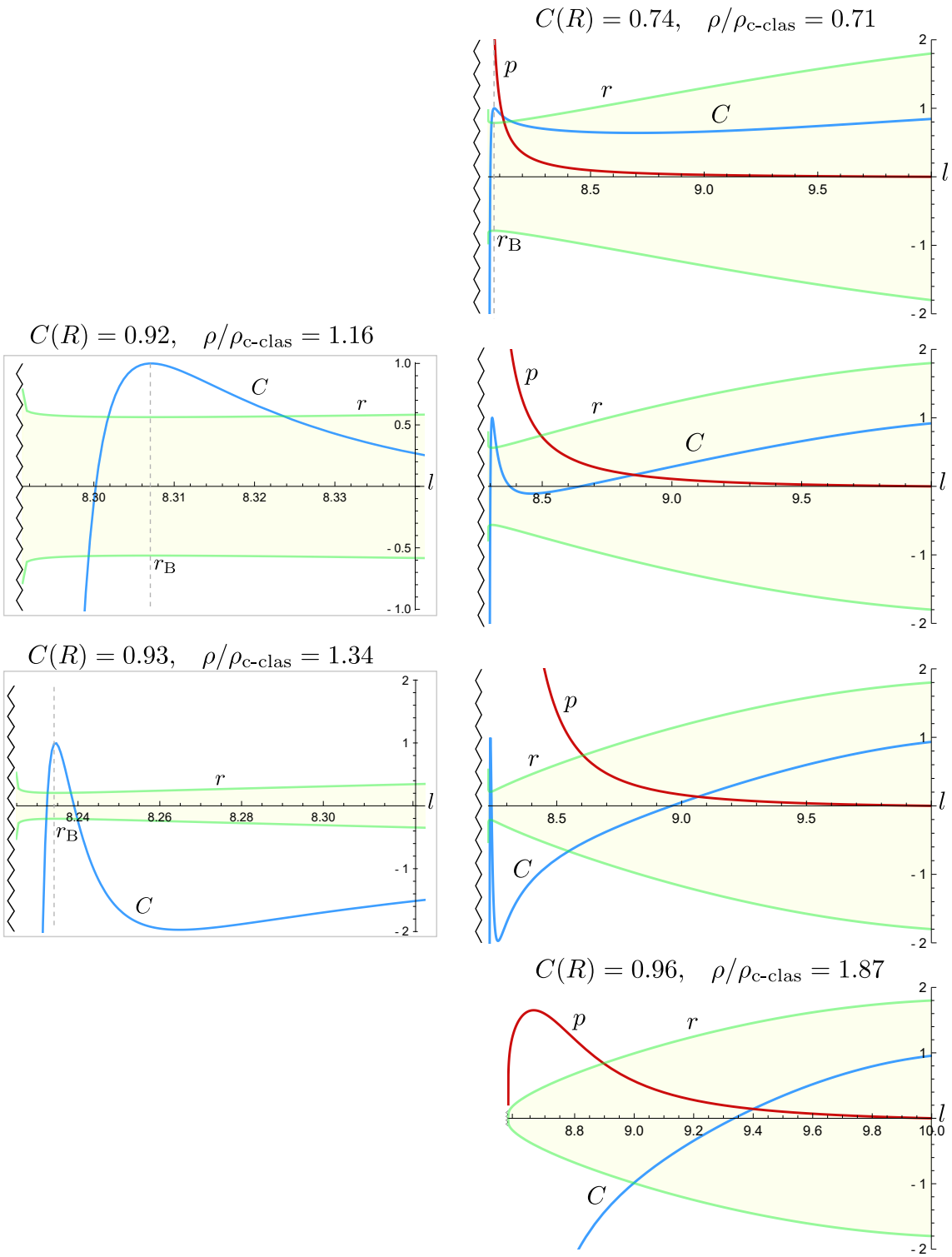

Fig. 4.10.: (Caption next page).

Fig. 4.10.: (Previous page). Semiclassical stars integrated from the surface. The green and blue curves denote $r(l)$ and $C(l)$, and the red curve represents the function $p(l)$. All integrations correspond to stars with $R = 1.8$ and $\alpha - 1 = 10^{-3}$. Their surface compactness and their $\rho/\rho_{\text{c-clas}}$ quotients are, approximately and from top to bottom: $(0.84, 0.71)$, $(0.92, 1.16)$, $(0.93, 1.34)$ and $(0.96, 1.87)$. The second and third panels show a zoomed plot of the near-neck region, highlighting the neck (vertical dashed line) and the singularity (zigzag line). Increasing ρ generates a well of negative mass. This negative mass slows down the increase in pressure, causing a shrinkage of the wormhole neck. Eventually, the neck disappears leaving a naked singularity at $r = 0$. In between sub-critical and super-critical configurations there is an infinite pressure separatrix solution. As the wormhole neck can be as small as desired by adjusting ρ, a mild deformation of the geometry at the core would suffice to make the whole construction regular. See Fig. 4.11 for the RP-RSET components from each solution.

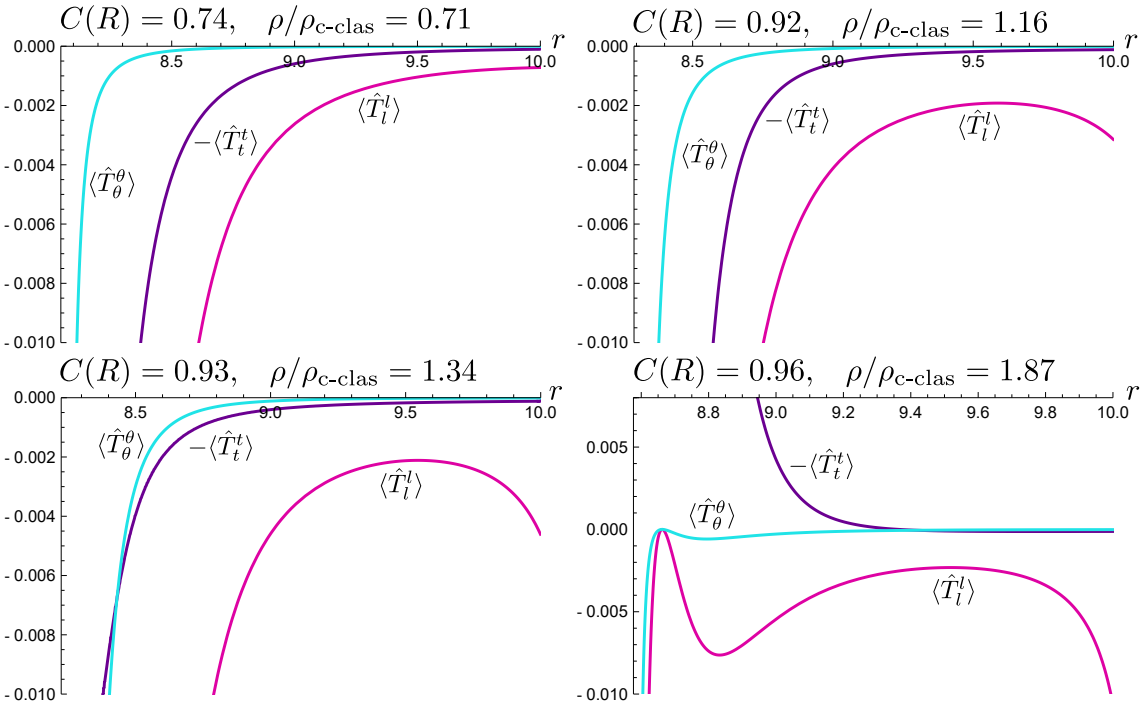

Fig. 4.11.: RSET components $-\langle \hat{T}^t_t \rangle$ (dark blue), $\langle \hat{T}^l_l \rangle$ (magenta) and $\langle \hat{T}^\theta_\theta \rangle$ (cyan) for various stars integrated from the surface. All the integrations correspond to stars with $R = 1.8$ and $\alpha - 1 = 10^{-3}$. They correspond to the solutions appearing in Fig. 4.10, whose surface compactness and $\rho/\rho_{\text{c-clas}}$ quotients are, approximately: $(0.84, 0.71)$ (top left), $(0.92, 1.16)$ (top right), $(0.93, 1.34)$ (bottom left), $(0.96, 1.87)$ (bottom right). Note the abrupt change in the sign of the semiclassical energy density in the transition from the sub-critical to the super-critical regime.

of (4.58) at the interior (concealed) side of the neck, and that $r_{\rm B} > 0$, ψ always takes values below the three roots and the exact solutions that appear represented in Fig. 4.9. By consistency of Eq. (4.55), ψ grows with r until the most negative root, $\mathcal{R}_3$, is crossed. Beyond this point ψ decreases linearly with r, taking values between the exact solution ψ_+ and the root $\mathcal{R}_3$. The former cannot be crossed in virtue of the Picard-Lindelöf theorem, and the latter cannot be encountered for a second time for self-consistency of (4.55). Thus, in the $r \to \infty$ limit, ψ decreases linearly with r (at leading order) and essentially corresponds to the vacuum solution.

To derive the asymptotic form of the metric deep inside the wormhole neck (in radial distance), we assume ψ deviates slightly from the exact solution as $\psi \simeq \psi_+ + \beta(r)$. Replacing this expression in Eq. (4.55) and neglecting terms beyond linear order in β, we obtain

$$\beta' \simeq -\frac{2r}{l_{\rm P}^2}\beta + \mathcal{O}\Big(\beta^2\Big). \tag{4.63}$$

Integrating yields

$$\beta \simeq -e^{-2r^2/l_{\rm P}^2}\beta_0, \tag{4.64}$$

where β_0 is a positive constant of integration of dimensions of inverse of length [the sign in Eq. (4.64) is chosen so that the solution ψ approaches ψ_+ from below]. Now, we further integrate ψ to derive the compactness function and the asymptotic form of the metric

$$\begin{aligned} ds^2 \simeq & e^{-2r^2/l_{\rm P}^2}\left(\frac{r}{l_{\rm P}}\right)^{1-4\alpha}\left\{-a_0\left(1-\frac{l_{\rm P}^2}{8r^2}\right)dt^2\right. \\ & \left. +b_0\left(\frac{r}{l_{\rm P}}\right)^2\left[1-\frac{(9-32\alpha)\,l_{\rm P}^2}{r^2}\right]dr^2\right\} + r^2 d\Omega^2. \end{aligned} \tag{4.65}$$

Here, a_0 and b_0 are dimensionless integration constants. In view of the above expression, the metric has a null singularity at radial infinity, which is located at finite affine distance from the neck for all geodesic paths. In the asymptotic region, the pressure of the fluid diverges exponentially towards positive infinity. The compactness function diverges towards negative infinity exponentially as well, due to the presence of an infinite cloud of negative mass which is being generated by the vacuum energy of the scalar field.

The characteristics of sub-critical solutions are identical to those of the vacuum solution i.e. an asymmetric wormhole with an interior null singularity at infinite r, but filled with an isotropic fluid of constant density and divergent pressures. Despite the classical SET being singular, the dominant contribution to the divergence in curvature invariants comes from semiclassical contributions, and differences

between vacuum and matter geometries appear at subleading order in the approximate metric (4.65). The uppermost panel in Fig. 4.10 contains an example of a sub-Buchdahl, sub-critical star (see top left panel in Fig. 4.11 for details on the RSET).

Semiclassical stellar solutions can be interpreted as a mixture of competing classical and quantum contributions. Taking $\rho = 0$ gives all predominance to the vacuum sector, while increasing ρ endows the geometry with classical-like properties. On the other hand, as the compactness at the surface of the star $C(R)$ is increased (while keeping $\rho < \rho_{\rm c}$ at all times), the wormhole neck follows a trajectory similar to the infinite positive pressure divergence from the classical theory: it moves outwards as $C(R)$ approaches the Buchdahl limit. At this stage, keeping $C(R)$ fixed and giving predominance to the classical fluid (increasing ρ) effectively pushes the wormhole neck towards smaller radii. As a consequence of increasing ρ, a greater amount of the contribution to $M_{\rm cloud}$ in Eq. (4.47) is coming from the classical source rather than the semiclassical vacuum polarization.

The second panel in Fig. 4.10 (top-right panel in Fig. 4.11 for the RSET) exemplifies a super-Buchdahl, sub-critical star where ρ has been chosen so that the neck is pushed inwards appreciably. Given a sub-critical super-Buchdahl configuration and increasing ρ moves the position of the wormhole neck inwards. This is accomplished at the expense of generating a nucleus of negative mass whose repulsive force smears the growth in pressure. The increase in ρ makes the classical fluid contribution prevail, causing compactness to become negative, but not as negative as to compensate the growth in pressure, resulting in a wormhole.

Relevance of ϵ-strict stellar spacetimes and validity of the Polyakov approximation

The third panel in Fig. 4.10 (see bottom left panel in Fig. 4.11 for details on the RSET) shows a geometry with its wormhole neck very close to the radial origin. This neck has a Planckian radius, thus lying in the regime where the physics of the solution is subject to the particular regularization scheme adopted for the RP-RSET. Hence, the regime around where the wormhole neck is reached lies outside the domain of reliability of the Polyakov approximation. Notice that these configurations have the compactness function bouncing from negative numbers to $C(r_{\rm B}) = 1$ at the neck. Hence, by moving the ρ parameter, the compactness of these solutions can be made as small as desired arbitrarily close to $r = 0$. In this precise sense, there is a family among all sub-critical semiclassical solutions that describes ϵ-strict spacetimes, as for these solutions the compactness can be made to obey the bound (4.3) in a sphere of radius r_ϵ by taking a suitable $\rho < \rho_{\rm c}$. Obtaining a

strict stellar spacetime from configurations of this sort would amount to regularize their nucleus. This can be done through appropriate choices of regulator as we will see in Chapter 5. As ϵ-strict spacetimes are absent in the classical space of super-Buchdahl solutions, semiclassical constant-density spheres of high compactness are one step closer to being regular than classical ones, precisely due to the way quantum corrections operate within these structures.

The existence of ϵ-*strict* spacetimes is in a way related to the failure of the Polyakov approximation to properly account for the contributions of vacuum polarization in presence of matter fluid spheres which extend all the way to $r = 0$ [equivalently, to distances where the spacetime metric in Eq. (1.2) cannot be dimensionally reduced to its non-angular sector accurately]. Were the spacetime geometry sourced by an RSET adequate for computing backreaction effects over regular stellar spacetimes, the resulting configurations might have been regular from the start. We are demanding from the RSET more than just yielding finite components at $r = 0$, as we also look for an RSET that captures more accurately the physics at the nucleus of compact relativistic stars (i.e. the expected violation of energy conditions that the CRP-RSET seems unable to reproduce at the core of regular stellar spacetimes that approach the Buchdahl limit (4.53) but more precise, local approximations account for [166] in the case of conformally invariant fields). The redshift function of classical Buchdahl stars vanishes exactly at $r = 0$, as seen in Eq. (4.20). The result by Hiscock [166] indicates that the RSET acquires a negative energy density when nearing a surface of zero redshift. As the CRP-RSET is oblivious to the overall value of the redshift function [only their derivatives enter the field equations (4.39, 4.40)], this characteristic is not being well-captured by this approximation.

The shrinkage of the neck as the density increases goes on until we encounter a separatrix solution with distinct features (see Subsec. 4.5.4 below for details and Fig. 4.10 for a series of configurations that approach this separatrix). For this solution, pressure and compactness diverge towards positive and negative infinity, respectively, at $r = 0$. This is a separatrix solution between two distinct behaviors in the pressure and in the compactness. Hence, attending to our definition of criticality from Subsec. 4.2.2, this solution corresponds to a critical (and singular) configuration. Beyond this critical density $\rho_{\rm c}$, solutions have no neck and their shape function extends to $r = 0$, but in a singular manner. These super-critical configurations are the ones analyzed in the next subsection.

4.5.3 Super-critical solutions

Returning once more to the phase space from Fig. 4.6, sub-critical solutions are situated between the pure vacuum solution, with $\rho = 0$, and solutions which have regular pressure everywhere. Increasing the density allows to observe a transition between the former and the latter, the separatrix between both being $\rho = \rho_{\rm c}$. For stars well below the Buchdahl limit, everything indicates that the lowest value of the density that makes the neck vanish ensures the regularity of the structure. These solutions correspond to the configurations obtained integrating outwards from a regular radial origin (see Subsec. 4.5.1). We find that this critical solution stops being regular beyond certain value of the compactness $C(R)$. This can be deduced from the fact that we have not been able to obtain solutions starting from a regular origin that end up corresponding to super-Buchdahl stars (excluding those with trans-Planckian ρ).

Picture now a super-critical star, for which the spacetime extends up to $r = 0$. An example of this configuration appears in the bottom panel of Fig. 4.10 (see bottom right panel in Fig. 4.11 for the corresponding CRP-RSET components). Sufficiently close to the radial origin, the geometry can be approximated by that of the semiclassical Schwarzschild counterpart with negative mass ADM mass. By evaluating Eq. (4.40) in the $r \to 0$ limit assuming a finite pressure at the origin, we obtain

$$\phi' \simeq \frac{-\alpha + \sqrt{\alpha(\alpha-1)}}{r} r', . \tag{4.66}$$

Notice that, in Schwarzschild coordinates, this corresponds to the exact solution ψ_-, which lives in the unconcealed branch and connects smoothly with the classical solution in the $l_{\rm P} \to 0$ limit. Replacing Eq. (4.66) in Eq. (4.39), we obtain the following relation for the shape function,

$$r' \simeq \left(\frac{|\tilde{M}|}{r}\right)^{(1+\alpha)\left(\sqrt{\frac{\alpha}{\alpha-1}}-1\right)} . \tag{4.67}$$

Here, $\tilde{M}$ is a constant of integration related to the deviations of ρ from $\rho_{\rm c}$. Integrating (4.67) returns the following asymptotic form of the radial function

$$r(l) \simeq \left(|\tilde{M}|^{-1+\sqrt{\frac{\alpha}{\alpha-1}}} l\right)^{\left[\alpha\left(\sqrt{\frac{\alpha}{\alpha-1}}-1\right)+\sqrt{\frac{\alpha}{\alpha-1}}\right]^{-1}} , \tag{4.68}$$

where, in the limit of big α, or when the CRP-RSET is fully suppressed, we recover the classical behavior (4.29). The redshift function indeed diverges towards positive infinity in the limit $l \to 0$,

$$e^{2\phi} \simeq \left(\frac{|\tilde{M}|}{l}\right)^{\frac{2}{1+2\sqrt{\frac{\alpha}{\alpha-1}}}} , \tag{4.69}$$

and the classical fluid acquires the equation of state of vacuum energy at the radial origin

$$p \simeq -\rho + \tilde{M}^{-2}\left(\frac{l}{|\tilde{M}|}\right)^{\frac{1}{1+2\sqrt{\frac{\alpha}{\alpha-1}}}} . \tag{4.70}$$

The finite value of the central pressure is approached with infinite gradient, as in the classical expression (4.31). The divergence of the pressure gradient is stronger than the classical one since the exponent of Eq. (4.70) vanishes in the limit $\alpha \to 1$. Vacuum polarization gets stimulated by the presence of this central negative mass, strengthening the super-critical singularity with respect to the classical situation.

We return now to the bottom picture in Fig. 4.10, which shows an example of a super-Buchdahl, super-critical star. The CRP-RSET (bottom right panel in Fig. 4.11) shows drastic differences with the sub-critical case. Namely, $\rho_{\rm s}$ changes sign with respect to its negative contribution at the surface, diverging towards positive infinity at $r = 0$. The semiclassical pressures diverge towards negative infinity after having encountered a maximum.

4.5.4 Semiclassical infinite pressure separatrix

The semiclassical separatrix between sub-critical and super-critical configurations is reminiscent of the classical separatrix in several aspects that we will detail in what follows. Let us work under the assumption that the separatrix solution has infinite pressure at the radial origin by similarity with the classical case in Subsection 4.3.5. First, we go back to Eq. (4.43), expand the right-hand side in powers of r, and

neglect terms subleading in the pressure, as of (4.54). The coefficients in Eq. (4.43) become

$$\begin{aligned}
A_0 &\simeq 12\pi p,\\
A_1 &\simeq 4\pi r\left(3p+\frac{2p}{\alpha}\right)-\frac{2}{r},\\
A_2 &\simeq -8\pi r^2 p\left[1-\frac{3}{2\alpha}-\mathcal{O}\left(r^2/l_{\rm P}^2\right)\right]-\frac{2}{\alpha}-2,\\
A_3 &\simeq -\frac{r}{\alpha}\left\{4\pi r^2 p\left[1-\mathcal{O}\left(r^2/l_{\rm P}^2\right)\right]+\frac{1}{\alpha}+1\right\},\\
\mathcal{D} &\simeq \frac{\alpha}{(1+8\pi r^2 p)(\alpha-1)}.
\end{aligned} \tag{4.71}$$

We arrange these coefficients in a particularly illustrative form, yielding

$$\begin{aligned}
\psi' \simeq \Bigg\{ & 4\pi p\left[3\alpha+(2+3\alpha)\,r\psi+(3-2\alpha)\,r^2\psi^2-r^3\psi^3\right]\\
& -\frac{2\alpha}{r}\psi-2(1+\alpha)\psi^2-\frac{r(\alpha+1)}{\alpha}\psi^3\Bigg\}\times\frac{1}{(\alpha-1)(1+8\pi r^2 p)}.
\end{aligned} \tag{4.72}$$

This expression is describing a competition between vacuum and matter contributions. By dropping the terms proportional to the pressure in Eq. (4.72) we obtain the solutions to the equation in vacuum

$$\psi=-\frac{\alpha\pm\sqrt{\alpha(\alpha-1)}}{r},\qquad \psi=0, \tag{4.73}$$

where only the $-$ sign returns the Schwarzschild solution in the classical limit (taking $\alpha\to\infty$, an infinitely suppressed CRP-RSET). Note that Eq. (4.73) is equivalent to Eq. (4.66) for the super-critical case, but expressed in Schwarzschild coordinates.

In the regime of approximation described by Eq. (4.54), the pressure is proportional to the integral of ψ. Let us assume the ansatz

$$\psi=\frac{\eta}{r}. \tag{4.74}$$

For this ansatz, the pressure becomes, in virtue of (4.54),

$$p\simeq\kappa\left(\frac{r_0}{r}\right)^{\eta}, \tag{4.75}$$

where r_0 is an integration constant with dimension of length and η needs to take positive values, since $\eta < 0$ is not compatible with the infinite pressure assumption. Inserting Eqs. (4.74) and (4.75) in Eq. (4.72), we obtain

$$\psi' \simeq \left\{ 4\pi\kappa \left(\frac{r_0}{r}\right)^{\eta} \left[3\alpha + (2+3\alpha)\,\eta + (3-2\alpha)\,r^2\eta^2 - \eta^3\right] \right. \\ \left. -\frac{(1+\alpha)\eta}{r^2}\left(2\alpha + 2\eta + \eta^2\right)\right\} \times \frac{1}{(\alpha-1)\left[1 + 8\pi r^2\kappa\left(\frac{r_0}{r}\right)^{\eta}\right]}. \tag{4.76}$$

The value of η determines which source, classical or quantum, provides the dominant contribution to the divergence in ψ'. For $\eta < 2$, the vacuum terms carry the dominant divergence. For $\eta = 2$, the terms in the first and second line all contribute at the same order, whereas for $\eta > 2$, terms proportional to the pressure dominate both the numerator and the denominator in Eq. (4.76). Let us explore these possibilities.

Replacing the derivative of Eq. (4.74) in Eq. (4.76) and taking $\eta = 2$ (which equates vacuum and matter contributions) yields the following relation between integration constants,

$$\kappa = \frac{1+\alpha}{2\pi\alpha r_0^2}. \tag{4.77}$$

Replacing this behavior in the radial Einstein equation (4.40) (in Schwarzschild coordinates) we obtain

$$C \simeq \frac{4(1+\alpha)(-1+r_0^2)}{(4+5\alpha)r_0^2} + \mathcal{O}\left(r^2\right), \tag{4.78}$$

from where only the value $r_0 = 1$ returns a vanishing compactness at the radial origin. The solution

$$p = \frac{1+\alpha}{2\pi\alpha r^2}, \tag{4.79}$$

is reminiscent of the classical separatrix between critical sub- and super-Buchdahl configurations and connects smoothly with the classical Buchdahl solution (4.37) in the $\alpha \to \infty$ limit. The semiclassical counterpart to that separatrix retains its critical character, in the sense that $C(l \to 0) = 0$, while the rate of growth of the pressure increases as α is decreased. Hence, semiclassical corrections contribution towards strengthening the divergence of the pressure in this separatrix.

Once the Buchdahl limit is surpassed the separatrix solution takes a different form. By taking $\eta > 2$ in Eq. (4.76), we are assuming that pressure-dependent

terms carry the leading-order divergences in the expansion. Therefore, Eq. (4.76) can be reduced to

$$-\frac{\eta}{r^2} \simeq \frac{r^{-\eta}\left[3\alpha+(2+3\alpha)\,\eta+(3-2\alpha)\,r^2\eta^2-\eta^3\right]}{2(\alpha-1)r^{2-\eta}}, \tag{4.80}$$

from where the only positive solution is $\eta = 3$. We have a pressure profile of the form

$$p \simeq \frac{\tilde{\kappa}}{r^3}. \tag{4.81}$$

where $\tilde{\kappa}$ is a positive integration constant of dimension length. Replaced in the equation for the compactness we find

$$C \simeq -\frac{8\pi\alpha\tilde{\kappa}}{(9+7\alpha)r}. \tag{4.82}$$

The separatrix between sub-critical and super-critical configurations has an infinite compactness at the origin. This divergence in the compactness is weaker than the curvature singularity from super-critical configurations, which fits right in the separatrix between sub- and super-critical profiles in the super-Buchdahl case. Since the differential equation for the compactness (4.39) is not integrable in terms of analytical functions, we do not know the specific form of the constant $\tilde{\kappa}$. Nevertheless, we expect it should present the correct classical limit.

Separatrices are only perturbatively deformed by semiclassical corrections. Solutions belonging to the sub-critical regime are wormhole geometries, whereas super-critical solutions are naked singularities. The separatrix solutions (4.75) and (4.81) are modified perturbatively by regulator-dependent corrections. This resembles the vacuum situation in a sense, where the separatrix between wormhole geometries and naked singularities at $r = 0$ is precisely Minkowski spacetime, for which vacuum polarization is exactly zero. The infinite pressure separatrices here obtained apparently exhibit a similar stability with respect to quantum corrections.

In the next three Subsections we are going to compute numerically the value of the separatrix density $\rho_{\rm c}$ and how it changes with the surface compactness $C(R)$. Varying the compactness of a family of stars with the same radius R is equivalent to locating the surface at different radii in the vacuum wormhole geometry. We begin by considering the simple case of stars whose surface is outside the neck to later analyze at-the-neck and inside-the-neck stars.

4.5.5 Outside-the-neck stars and pressure regularization

The analyzed behaviors for both sub- and super-critical stars (i.e. top and bottom regions of the phase space in Fig. 4.6) only depend on whether the value of ρ is below or above $\rho_{\rm c}$, and are thus universal for stars either outside or inside the neck. Turning back to the diagram in Fig. 4.6, which qualitatively describes stars with their surfaces outside the neck, we now draw attention to the separatrix solution between regions III and IV (or the super-Buchdahl half-plane). Recall that numerical integrations for these regimes (sub-critical, critical and super-critical) appear represented in the fourth row of Fig. 4.2. Beginning with a sub-critical configuration and integrating from the surface, we can estimate numerically from surface integrations (within some expected numerical uncertainty) the value of the density that sits between the less dense super-critical solution and the most dense sub-critical solution. To the limit of our numerical precision, this density value coincides with $\rho_{\rm c}$. The critical solution acts as a separatrix in the behavior of both pressure and compactness. Notice that, with our definition of criticality, this coincidence does not happen in the classical case: by increasing the parameter ρ we first find $\rho_{\rm c}$, i.e. a change in behavior of C, and later on for $\rho_{\text{reg-p}} > \rho_{\rm c}$ we find the first solution for which pressure becomes finite at the origin. In what follows, we make use of $\rho_{\text{reg-p}}$ to refer to this separatrix in pressure for classical stars and $\rho_{\rm c}$ to denote the critical solution in semiclassical stars.

Let us numerically explore the behavior of the quantity $\rho_{\rm c}$ in different situations. For classical and semiclassical stars with the same radius and compactness (or counterparts), $\rho_{\rm c}$ is appreciably smaller than $\rho_{\text{reg-p}}$. Figure 4.12 shows a comparison between these two densities for stars of various $C(R)$, together with the line $\rho_{\text{c}-\text{clas}}$. Remarkably, we find that $\rho_{\rm c}$ is finite in the limit $C(R) \to 1$. In turn, the negative mass necessary to halt the growth of the pressure is less negative for semiclassical stars with $C(R) \to 1$, when compared to the classical case. See Fig. 4.13 for a detailed plot of the Misner-Sharp mass needed to regularize the pressure in each situation.

The cause of this discrepancy between classical and semiclassical separatrix densities in the $C(R) \to 1$ limit comes from the differences between their respective vacuum solutions. In the case of a classical star the surface where $C(R) = 1$ is the horizon, resulting in infinite surface pressures in the $C(R) \to 1$ limit, which can only be compensated by the introduction of an infinite amount of negative mass. When quantum corrections are incorporated, however, the $C(R) \to 1$ limit corresponds to taking the surface of the star towards the neck of the wormhole, where pressure is indeed finite, in virtue of Eq. (4.62). In consequence, a finite increase in ρ regularizes the pressure profile of the configuration. As observed in

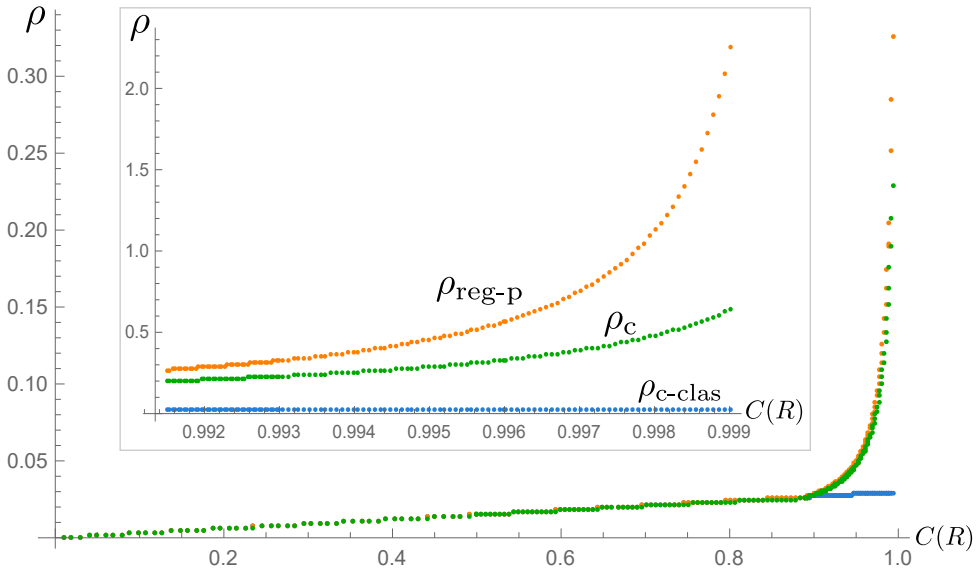

Fig. 4.12.: Plot of $\rho_{\text{reg-p}}$ in terms of the compactness for classical (orange) stars and of ρ_{c} for semiclassical (green) stars with $R = 2$ and $C(R) \in (0, 1)$. The blue line corresponds to the classical critical density (4.13). The orange curve diverges in the $C(R) \to 1$ limit, whereas the green curve reaches a finite value, in this case $\rho_{\text{c}}\,(C(R) \to 1) \simeq 1.366$.

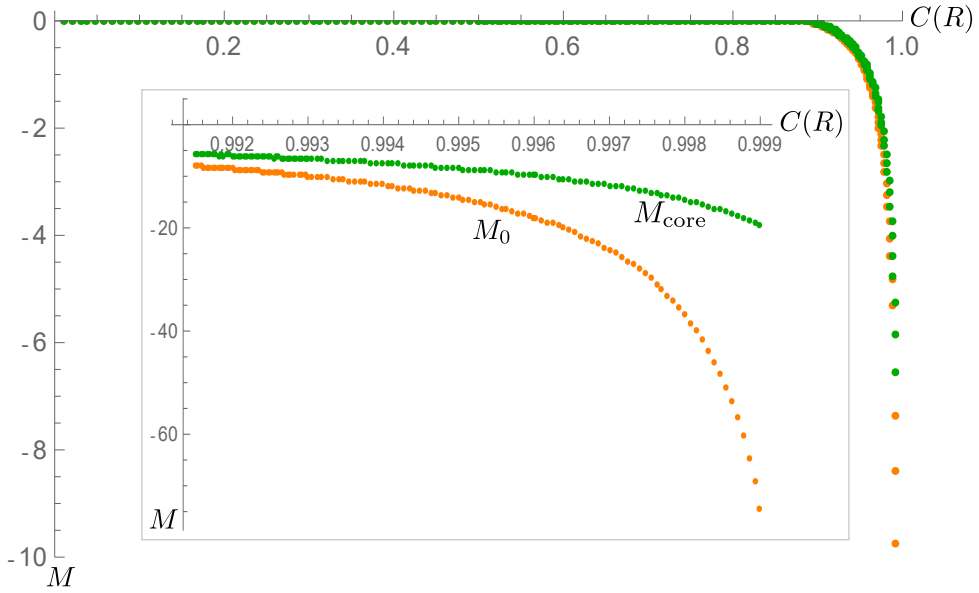

Fig. 4.13.: Plot of the Misner-Sharp mass at a central radius $r_{\text{core}} = \mathcal{O}(l_{\text{P}})$ in terms of the surface compactness for classical (orange) and semiclassical (green) stars with $R = 2$. Notice how the orange curve diverges in the $C(R) \to 1$ limit, as infinite negative masses are required to regularize the pressure in that limit. In the semiclassical case, since the surface of $C(R) = 1$ is a wormhole neck. As pressure at the neck is finite [see Eq. (4.62)] the required negative mass is finite, in this case $M_{\text{core}}\,(C(R) \to 1) \simeq -41.20$.

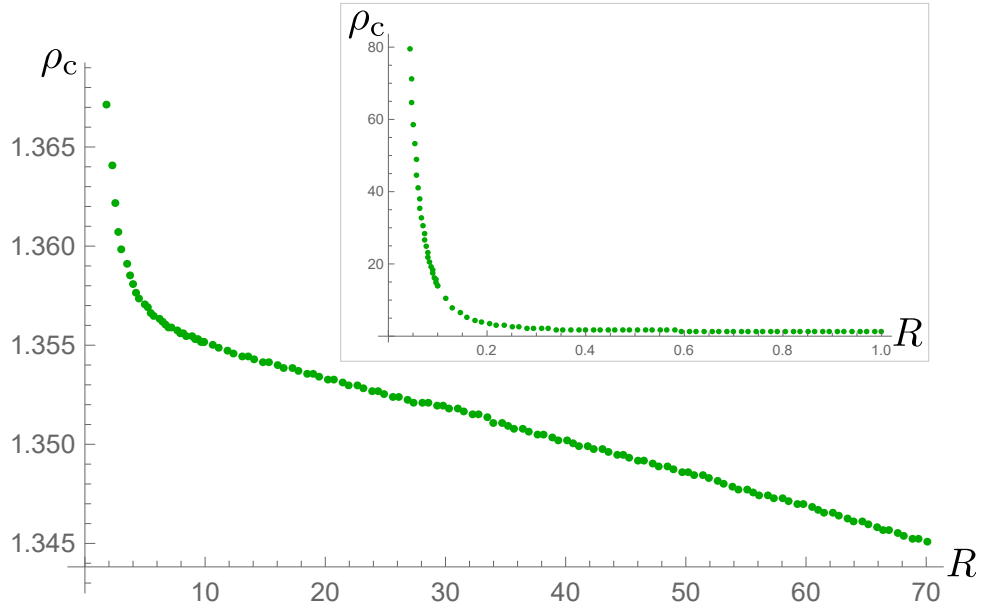

Fig. 4.14.: Plot of ρ_c for semiclassical stars of various radii and compactnes $C(R) = 1 - 10^{-10}$. As R shrinks, the separatrix density diverges, whereas for larger radii (in Planck units) it decreases linearly.

Fig. 4.14, the parameter r_c decreases linearly as the radius of the star is increased while keeping $C(R)$ fixed.

Fig. 4.15 shows that the negative mass core grows much faster with ρ than the rate at which the total mass $M = RC(R)/2$ increases with R while keeping $C(R)$ fixed. This core can be estimated obtaining the value of the Misner-Sharp mass at a security radius where the Misner-Sharp mass has not yet entered into a runaway regime. The values of the density required to strictly regularize the pressure of ultra-compact stars are therefore many orders of magnitude greater than the total Misner-Sharp mass associated with those stars, although they stay finite in the $C(R) \to 1$ limit.

Figures (4.12-4.15) have been obtained by taking $\alpha - 1 = 10^{-6}$. We have observed that increasing the value of α has the effect of making the solutions more alike to their classical counterparts. Consequently, it seems reasonable to assume that ρ_c approaches its classical value $\rho_{\text{reg-p}}$ in the limit $\alpha \to \infty$ as well.

4.5.6 Inside-the-neck stars and pressure regularization

Up to now our analysis has focused on stars located outside the neck of the wormhole. In this Section we turn to locating the surface of the star inside the neck, which in particular implies that these solutions have no well-defined classical limit. In this case, there is again a strong interplay between contributions coming

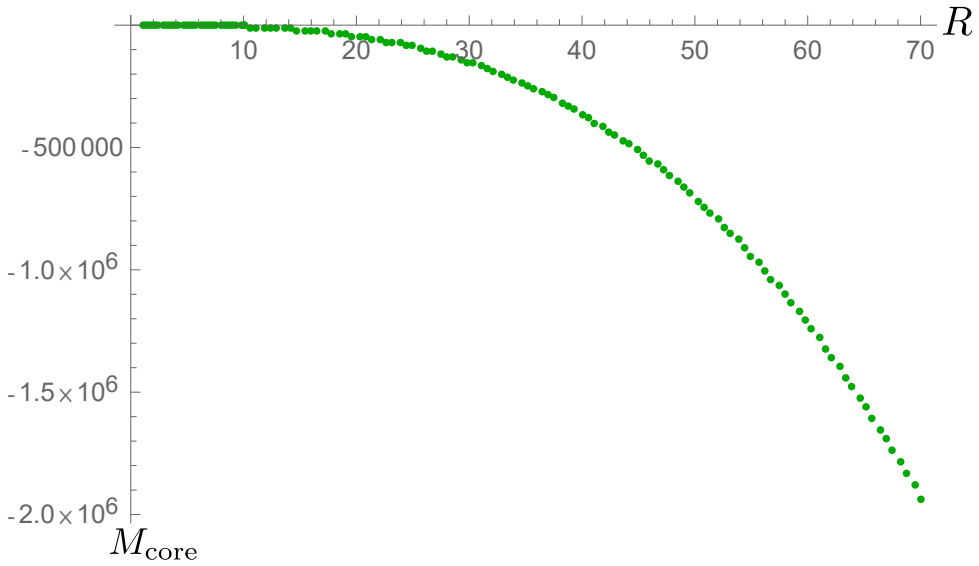

Fig. 4.15.: Plot of the central negative mass M_{core} for semiclassical super-critical stars of various radii and surface compactness $C(R) = 1 - 10^{-10}$. This estimated central mass is obtained by stopping the integration at a security radius far from the region where the Misner-Sharp mass diverges. Notice how the central mass has to be many orders of magnitude higher than the total mass of the star $M \simeq R/2$ for big stars. For small stars have their pressure regularized by negative central masses comparable to their total mass, indicating that the physics of Planckian stars may be different from that of astrophysical bodies.

from the vacuum and classical matter that results in sub-critical, critical and super-critical regimes. There exists also a distinction depending on whether the surface is located close to the neck (super-Buchdahl, $[C(R) \to 1]$), or far from the neck (sub-Buchdahl, $[C(R) \ll 1]$). The last two rows in Fig. 4.2 display numerical plots for all these cases.

In the first of these scenarios the surface of the super-Buchdahl star is located very close to the neck but inside it. If ρ is large enough, a radial maximum takes place just below the surface of the star, inverting the tendency of the radial coordinate to increase as we deepen through the neck. To illustrate this, we work in Schwarzschild coordinates and consider a local analysis of Eq. (4.43) around the surface of a star located inside the neck r_{B} but very close to it, so that the solution admits the approximate form (4.58). This is guaranteed as long as

$$r - r_{\text{B}} \lesssim \frac{l_{\text{P}}^2}{r_{\text{B}}}. \tag{4.83}$$

Now, expanding Eq. (4.43) at leading order in ψ while taking $p = 0$ and ρ positive and constant, the solution is

$$\psi \simeq -\frac{1}{l_{\rm P}}\left\{-\frac{l_{\rm P}^2\alpha\,(r^2-r_{\rm B}^2)}{(r^2+\alpha l_{\rm P}^2)\,(r_{\rm B}^2+\alpha l_{\rm P}^2)}-\alpha\ln\left(\frac{r^2+\alpha l_{\rm P}^2}{r_{\rm B}^2+\alpha l_{\rm P}^2}\right)\right.$$
$$+(1+\alpha)\ln\left[\frac{r^2+l_{\rm P}^2(\alpha-1)}{r_{\rm B}^2+\alpha l_{\rm P}^2(\alpha-1)}\right]-4\pi\rho\left(r^2-R^2\right)$$
$$\left.+4\pi\rho l_{\rm P}^2(\alpha-1)\ln\left[\frac{r^2+l_{\rm P}^2(\alpha-1)}{R^2+l_{\rm P}^2(\alpha-1)}\right]\right\}^{-1/2}. \tag{4.84}$$

For a positive, large enough ρ, the term proportional to $(r^2 - R^2)$ is the dominant contribution to (4.84), which compensates the positive logarithmic terms from vacuum contributions (recall that, initially, r increases as we move away from the surface towards the interior of the star). The interior of the squared root in (4.84) vanishes at some radius $r_{\rm M}$ inside the star, generating a radial maximum and taking the solution back to the concealed branch. Once ρ is large enough as to generate this radial maximum, we encounter again three different scenarios depending on whether ρ is above or below its critical value. If $\rho < \rho_{\rm c}$, a second radial minimum or neck takes place after the first maximum (this is the situation depicted in Figs. 4.16 and 4.17). The metric functions around this second neck have the form (4.60) and connect with a null singularity. Further increments of ρ displace this second neck towards smaller values of r and eventually makes solutions super-critical if $\rho > \rho_{\rm c}$, showing finite pressures everywhere. Examples for each of these cases can be found in the last row from Fig. 4.2.

The second possibility is to consider matter located sufficiently deep inside the neck (in radial distance), the negative mass generated by the scalar field becomes comparable to that of the classical source. The three plots in the sixth line of Fig. 4.2 show the respective sub-critical, critical and super-critical regimes. Here we can observe that, unless the density of the fluid is increased sufficiently, the geometry will adopt the form (4.65) without reaching a radial maximum. Such geometries are completely dominated by vacuum polarization. In this regime, we cannot appeal to the local analysis of (4.84), and we are forced to solve numerically the complete equations. Figure 4.18 shows the value of the energy density $\rho_{\rm c}$ for stars of various surface compactness. These values of the compactness are directly linked to how far inside the neck we are locating the surface of the fluid (see the compactness curve in Fig. 2.2). The energy density $\rho_{\rm c}$ is found to grow linearly as compactness decreases (as we move the surface of the star far from the neck).

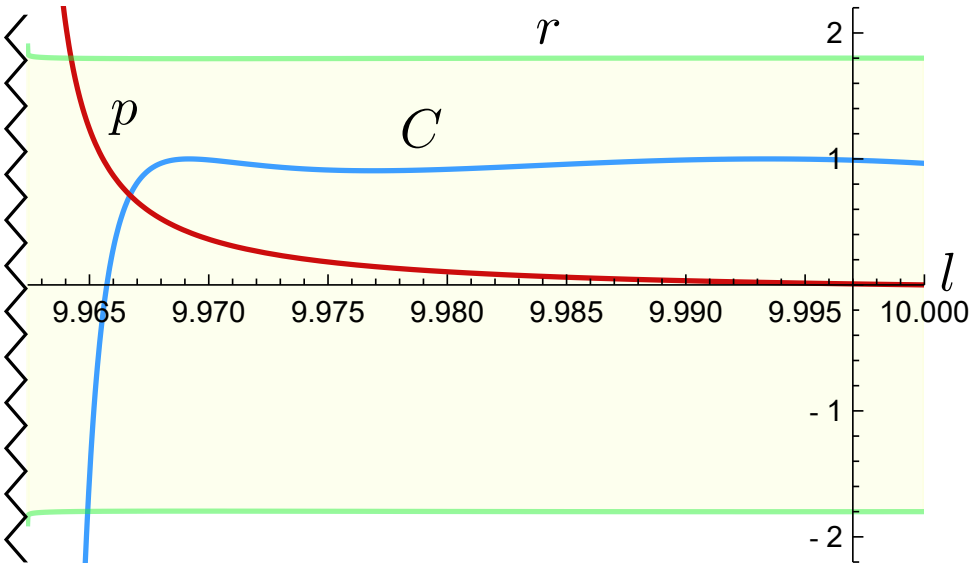

Fig. 4.16.: Plot of a sub-critical star located inside the neck. The blue green and blue curves represent the shape function $r(l)$ and the compactness $C(l)$, respectively. The red curve is the pressure $p(l)$. The dashed and dot-dashed vertical lines represents the radial minimum $r_{\rm B}$ and maximum $r_{\rm M}$, respectively. The singularity is represented by a zigzag line. The parameters chosen are $R = 1.8$, $C(R) = 0.96$, $\rho/\rho_{\text{c-clas}} = 43.4$ and $\alpha - 1 = 10^{-3}$.

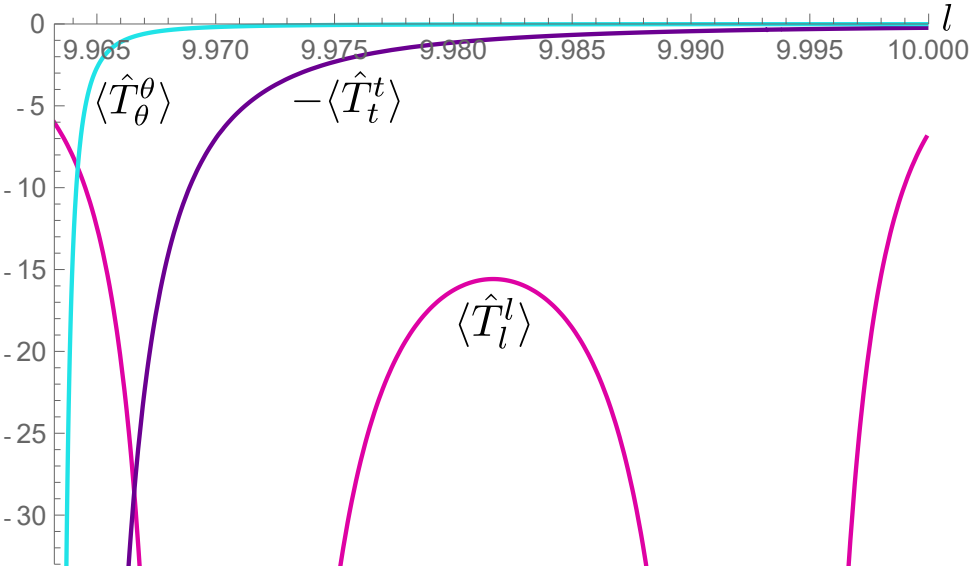

Fig. 4.17.: RSET components $-\langle \hat{T}^t_t \rangle$ (dark blue), $\langle \hat{T}^l_l \rangle$ (magenta) and $\langle \hat{T}^\theta_\theta \rangle$ (cyan) for a sub-critical star located beyond the neck. The parameters of the integration are $R = 1.8$, $C(R) = 0.96$, $\rho/\rho_{\text{c-clas}} = 43.4$ and $\alpha - 1 = 10^{-3}$.

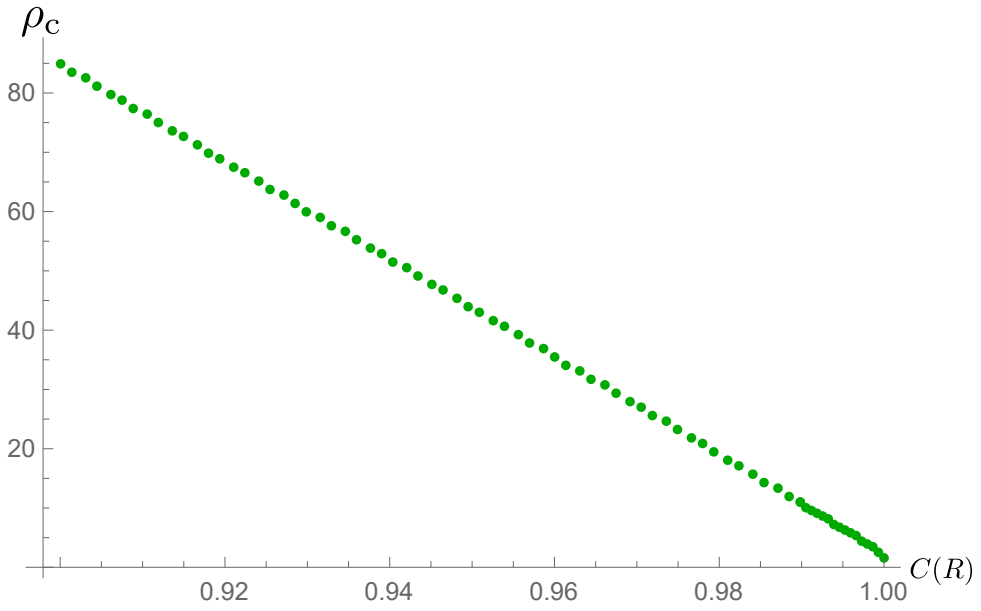

Fig. 4.18.: Plot of $\rho_{\rm c}$ in terms of the compactness for a star located inside the neck. The density required to regularize the structure grows linearly as compactness diminishes, reaching over Planckian densities very quickly.

In conclusion, we have found that all constant-density stars with their surface inside the neck are singular. Infinite pressure separatrices are still expected to be present, but the densities required to reach them are trans-Planckian.

4.5.7 At-the-neck stars and pressure regularization

Finally, we examine the particular case of fluid spheres whose surface is located at the neck of the vacuum wormhole geometry. The fifth line in Fig. 4.2 shows the critical and non-critical regimes for at-the-neck stars. This wormhole neck $r_{\rm B}$ corresponds to $C(r_{\rm B}) = 1$ and a positive redshift function. This scenario has therefore no classical counterpart and the boundary conditions at the surface illustrate an intriguing interplay between quantum and classical contributions.

We combine Eqs. (4.39) and (4.40) to obtain a differential equation of the form

$$r'' = \mathcal{E}\left(r^6\mathcal{B}_0 + l_{\rm P}^2 r^4\mathcal{B}_1 + l_{\rm P}^4 r^2\mathcal{B}_2 + l_{\rm P}^6\mathcal{B}_3\right), \tag{4.85}$$

where

$$\begin{aligned}
\mathcal{B}_0 &= 4\pi l_{\rm P}^2\,(p-\rho) + (r')^2\,,\\
\mathcal{B}_1 &= 1 - \mathcal{H} + 8\pi l_{\rm P}^2\,[\alpha\,(p-\rho) - p] + (3\alpha-2)\,(r')^2\,,\\
\mathcal{B}_2 &= (1-2\alpha)\,\mathcal{H} + 2\alpha l_{\rm P}^2\left[1 + 2\pi\alpha l_{\rm P}^2\,(p-\rho)\right]\\
&\quad + \alpha\,(3\alpha-2)\,(r')^2\,,\\
\mathcal{B}_3 &= \alpha\,(\alpha+1)\left[1 - \mathcal{H} + (\alpha-1)\,(r')^2\right],\\
\mathcal{E} &= \left\{l_{\rm P}^2 r\left[r^2 + (\alpha-1)\,l_{\rm P}^2\right]\left(r^2 + \alpha l_{\rm P}^2\right)\right\}^{-1},
\end{aligned} \tag{4.86}$$

and

$$\mathcal{H} = \left\{1 + 8\pi r^2 p + \left[r^2 + (\alpha-1)\,l_{\rm P}^2\right](r'/l_{\rm P})^2\right\}^{1/2} \times r'\sqrt{r^2 + \alpha l_{\rm P}^2}. \tag{4.87}$$

Let us think of an inwards integration of the semiclassical equations from an asymptotically flat region with positive ADM mass until the neck $r_{\rm B}$, where we decide to locate the surface of radius R of a perfect fluid of constant and positive classical density ρ. Continuity of the metric at the neck demands the shape function and the pressure, which are the only unknown functions appearing in Eq. (4.85), obey expansions of the form

$$\begin{aligned}
r(l) &= R + r_1\,(l-l_{\rm S})^2 + r_2\,(l-l_{\rm S})^3 + \mathcal{O}\,(l-l_{\rm S})^4\,,\\
p(l) &= p_1\,(l-l_{\rm S}) + \mathcal{O}\,(l-l_{\rm S})^2\,,
\end{aligned} \tag{4.88}$$

where $r_1,\ r_2$ and p_1 are arbitrary constants. Replacing expressions (4.88) in Eqs. (4.85) and (4.41), we obtain the following values for the first coefficients in the expansion

$$\begin{aligned}
r_1 &= \frac{(R^2 + \alpha l_{\rm P}^2)\,(1 - 4\pi R^2\rho) + \alpha l_{\rm P}^4}{2R\,(R^2 + \alpha l_{\rm P}^2)\,[R^2 + (\alpha-1)\,l_{\rm P}^2]},\\
p_1 &= -\,\frac{\sqrt{R^2 + \alpha l_{\rm P}^2}}{l_{\rm P} R}\rho,
\end{aligned} \tag{4.89}$$

where $p_1 < 0$ for any positive ρ, indicating that pressure always grows in the interior region of the star. The coefficient r_1, however, vanishes for the density value

$$\rho_{\rm neck} = \frac{1}{4\pi R^2}\left[1 + \frac{\alpha l_{\rm P}^4}{(R^2 + \alpha l_{\rm P}^2)^2}\right], \tag{4.90}$$

hence becoming positive if $\rho > \rho_{\rm neck}$ and negative if $\rho < \rho_{\rm neck}$. The density $\rho_{\rm neck}$ marks the separatrix between two distinct situations: For $\rho < \rho_{\rm neck}$, the geometry

is qualitatively similar to the vacuum solution depicted in Fig. 2.2 (below the surface, $r(l)$ increases as l decreases), whereas for $\rho > \rho_{\text{neck}}$ the geometry is such that, just below the surface, the shape function diminishes with l, resembling the outermost layers of a stellar configuration. Note that, if $\rho < \rho_{\text{c}}$, a neck will nevertheless appear inside the region filled with matter, endowing the solution with a sub-critical character.

The particular case where $\rho = \rho_{\text{neck}}$ is characterized by having $r_1 = 0$. The next-order coefficient in the expansion of the shape function, evaluated for $\rho = \rho_{\text{neck}}$, yields

$$r_2 = -\frac{\left[\left(R^2+\alpha l_{\text{P}}^2\right)^2 - 2R^2 l_{\text{P}}^2\right]\left[\left(R^2+\alpha l_{\text{P}}^2\right)^2 + \alpha l_{\text{P}}^4\right]}{6R^2 l_{\text{P}}\left[R^2+(\alpha-1)\,l_{\text{P}}^2\right]\left(R^2+\alpha l_{\text{P}}^2\right)^{5/2}}, \tag{4.91}$$

which is a negative quantity. Therefore, this solution also has a shape function that decreases just below the surface of the star. It corresponds to a sub-critical configuration since, as long as $R \gg l_{\text{P}}$, it is guaranteed that (4.90) is smaller than ρ_{c} (we infer this by extrapolating the tendency observed in Fig. 4.14 to stars of large radii).

At-the-neck stars clearly show that the predominance of vacuum effects captured through Polyakov's drives the solution towards the formation of a wormhole neck, an "opening" of the spacetime geometry, which eventually leads to an asymptotic singularity. The predominance of classical matter, on the other hand, contributes towards "closing" the geometry and forming a fluid sphere. The interplay between these two effects is what eventually gives rise to ϵ-strict stellar spacetimes. These correspond to nearly "closed" configurations in which vacuum polarization effects end up dominating at the core of the star. In order for the configuration to reach $r = 0$ in a regular manner it must be sourced by an RSET that properly accounts for vacuum polarization at the core of compact stars, so that such "closing" is consistent with the regularity of the entire configuration.

4.6 Conclusions

In this Chapter, we have used the CRP-RSET as a simple model to incorporate semiclassical corrections into the equations of stellar equilibrium. We expect this RSET to qualitatively capture the semiclassical effects caused by a geometry that is near its gravitational radius, that is, describing ultracompact configurations. On the other hand, the ambiguities inherent to the regularization of the Polyakov RSET affects the solutions to the semiclassical equations describing stellar-like objects. We summarize here the main findings that distill from our explorations.

We have found that, for the most part, the set of strict stellar spacetimes for the semiclassical field equations analyzed here is almost coincident with the corresponding classical set. That is, only for sub-Buchdahl stars we find strictly regular semiclassical solutions. However, this should not be understood as showing that semiclassical gravity exhibits a Buchdahl limit essentially equal to that in classical general relativity. This can be illustrated by taking a closer look at the super-Buchdahl non-regular solutions that satisfy our definition of ϵ-strict spacetime. Bare in mind as well that the most compact regular semiclassical star lies below the classical Buchdahl limit $C(R) = 8/9$ due to the positive energies generated by the CRP-RSET in the interior.

When analyzing super-Buchdahl configurations of large size, there is a stark difference between the classical and semiclassical cases. In the classical case, for arbitrarily compact configurations it is not possible to define a small value of the radius r_ϵ so that the compactness remains small enough outside it, and at the same time the pressure is finite up to r_ϵ. For highly compact (very super-Buchdahl) stars, the classical pressures diverge very close to the surface, and the only way to tame such divergences so that they remain finite up to r_ϵ is to become strongly supercritical in the density; this in turn leaves us outside the regime that we have denoted as ϵ-strict. In other words, in classical general relativity there are no ϵ-strict solutions with a compactness that is appreciably greater than the Buchdahl limit. In fact, the compactness of ϵ-strict solutions is bounded by the Buchdahl limit plus small $\mathcal{O}(\epsilon)$ corrections.

For the super-critical solution in the bottom panel of Fig. 4.10, the compactness is within the ϵ-strict bound for $r_\epsilon > 1.8 l_{\rm P}$. Going further into the supercritical regime, the compactness divergence becomes stronger causing the core to grow, thus no longer fitting into the notion of ϵ-strict spacetime, which requires $\epsilon \ll 1$. On the other hand, sub-critical solutions close to the critical one are such that compactness turns from negative to positive values within a narrow region near $r = 0$. Hence, there exist sub-critical solutions with cores in which the compactness remains very close to zero, while the pressure remains bounded. Both below and above criticality we have solutions which are ϵ-strict configurations, for any value of the compactness.

Figure 4.19 shows a comparison between a critical super-Buchdahl star from the classical theory and a series of semiclassical super-Buchdahl stars that approach the critical solution from the sub-critical regime. Close-to-critical semiclassical solutions are far closer to attaining regularity than classical ones, in the sense that the geometric distortions needed to regularize the whole interior do not need to extend all the way to the surface of the star, but can remain confined within a central core of Planckian radius. All in all, the most relevant departure of semiclassical

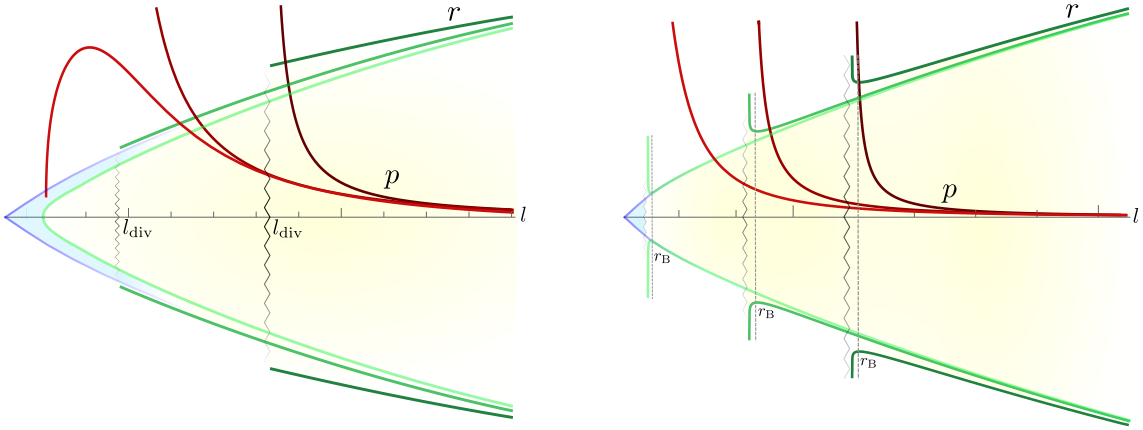

Fig. 4.19.: Left panel: series of classical super-Buchdal stars approaching a finite pressure solution. The green lines represent the shape function r and the red curves denote the pressures p, which diverge at $r(l_{\rm div})$ (zigzag lines). Lighter colors correspond to stars whose density is nearing $\rho_{\text{reg-p}}$ (the critical solution $\rho_{\text{c-clas}}$ has the darkest colors). Any attempt of regularizing the pressure makes the star highly super-critical, causing p' and r' to diverge at $l = 0$. The shape function of a regular star is drawn in blue for comparison. Right panel: series of semiclassical sub-critical super-Buchdahl stars approaching the critical solution. Again, the shape functions r are shown in green, while the pressures p are plotted in red. Lighter colors correspond to stars whose density is nearing $\rho_{\rm c}$. The critical solution is approached together with the regularization in the pressure. The vertical dashed lines represent the necks of the solutions and singularities are represented by vertical zigzag lines. We have drawn in blue the shape function of a hypothetical regular star. Note that regularity requires $r'(0) = 1 + \mathcal{O}(l^2)$. The classical super-critical configuration with finite pressure has $r'(0) \to +\infty$, whereas semiclassical configurations with small wormhole necks are ϵ-strict stellar spacetimes. Regularization of these profiles amounts to selecting a suitable regularization for the RP-RSET.

stars with respect to their classical counterparts is that, in the semiclassical theory, the separatrix solutions in mass and pressure overlap in a narrow region of the parameter space.

The lack of a compactness limit for ϵ-strict spacetimes in semiclassical gravity is the main physical result of this Chapter. Conceptually, this result illustrates that the Polyakov approximation is successful in regularizing the super-Buchdahl classical stellar profiles in the regions of spacetime in which the approximation is expected to be reliable. It is clear that the only missing physical information to complete the picture is the behavior of the semiclassical source around $r = 0$. Among the various ways of regularizing the Polyakov approximation near $r = 0$, in this Chapter we have considered the simplest one on the basis that it proved adequate for the analysis of (electro)-vacuum spacetimes. Our results here indicate that alternative regularizations must be studied in presence of matter, being reasonable to think

that there may exist regularizations in which the ultracompact ϵ-strict spacetimes discussed in this Chapter become regular. The existence of such regularizations, their characteristics, and the physical interpretation of the resulting stars are discussed in the next Chapter.

5 Semiclassical relativistic stars

5.1 Introduction

We arrive at the Chapter containing the central result of this thesis: the derivation of a new model of exotic compact object that results from solving the semiclassical equations in a self-consistent way. Before describing how we derive this result and its principal implications, let us outline the path that lead us to this point.

The outset of this thesis was born from the idea that vacuum polarization effects, captured via approximate RSETs (the one adopted so far being RP-RSET), could generate regular horizonless configurations that share some of the observational properties from ABHs but none of their pathological characteristics. We search for these ultracompact stars under the simplifying assumptions of staticity and spherical symmetry and incorporating the backreaction of the RSET of a massless, minimally coupled scalar field in the Boulware state. Such objects should be identified with the late-time outcome of a modified gravitational collapse process where trapped regions evolve in a non-trivial way that leads to their eventual disappearing.

The semiclassical equations (sourced by the RP-RSET) can be integrated from an asymptotically flat region inwards. Far from the gravitational radius, deviations from the Schwarzschild spacetime amount to perturbatively corrected mass and redshift functions. As the gravitational radius is approached, however, quantum corrections become non-perturbative and destroy the event horizon altogether, producing instead a wormhole neck that connects to a null curvature singularity. In situations where a constant-density classical matter fluid is introduced above this wormhole neck, when the density of this sphere approaches certain critical value $\rho_{\rm c}$ from below, we obtain configurations where the wormhole neck (now appearing in the region filled with matter) becomes progressively smaller. Fig. 4.19 illustrates this effect. The most striking difference between the classical and semiclassical situations is the existence of ϵ-*strict* semiclassical stars beyond the Buchdahl limit.

The fact (see Chapter 1) that the Polyakov approximation must be modified within some central radius (that we denote $r_{\rm core}$ hereafter), together with the appearance of ϵ-*strict* spacetimes just by choosing a cutoff-regulator for the RP-RSET

indicates that more elaborate regulators are potentially capable to generate fully regular stars of arbitrary compactness. We will work with regulator functions $F(r)$ [appearing in the RSET components (1.14)] that differ from the usual Polyakov form $1/r^2$ just for $r < r_{core}$ but which are non-analytical, contrarily to the bare cutoff (1.15). The semiclassical equations that we will solve (leaving F unspecified) take the form

$$C = \frac{-8\pi r^2 p + 2r\psi + F l_{\rm P}^2 r^2 \psi^2}{1 + 2r\psi + F l_{\rm P}^2 r^2 \psi^2}, \tag{5.1}$$

$$C' = \frac{8\pi r^2 \rho - C + F l_{\rm P}^2 r^2 \left(\psi^2 + 2\psi'\right)(1 - C)}{r + F l_{\rm P}^2 r^2 \psi}. \tag{5.2}$$

Our main result is the existence of an entire family of possibilities for F characterized by the requirement of accommodating regular stellar configurations of arbitrary compactness. Among these, there is a particular family of solutions which is found when the compactness of the star is close to the BH limit, that is, amply surpassing the Buchdahl bound. In this limit, their qualitative form is not very much affected by the location of the surface with respect to the putative wormhole neck. These newly found stars display a three-layered structure that appears schematically depicted in Figure 5.1.

The features of all the solutions obtained in this Chapter in the range $r \in (r_{\rm core}, R)$ are universal for all the choices of F considered here. The characteristics of the regular core $r \in [0, r_{\rm core}]$ depend on the particular form of F, which is obtained following a reverse-engineering process: We assume that spacetime is regular inside the core and smoothly connects with the bulk solution at $r_{\rm core}$ (specifically, we assume an analytical pressure profile) and then solve the semiclassical equations inside the core for the regulator, as the usual boundary-value problem. If the regulator F is a regular function everywhere, we have solved the semiclassical equations self-consistently and found a particular F that generates a regular star surpassing the Buchdahl bound. The regulator is not unique. Slight deformations of F translate into slightly deformed stellar cores. For any choice of $r_{\rm core}$ there exist many regulators compatible with ultracompact regular configurations. We will elaborate on these aspects in the upcoming Sections.

This Chapter is organized as follows. In Section 5.2 we summarize the main findings from Chapter 4 regarding semiclassical criticality, ϵ-strict spacetimes, and the most relevant features of classical and semiclassical stellar equilibrium that were already presented there. Section 5.3 details our procedure to construct stars with regular cores and the exploration of their associated space of solutions. Section 5.4 examines the physical properties of semiclassical relativistic stars. In addition, we derive analytical fits to the numerical solutions in terms of five

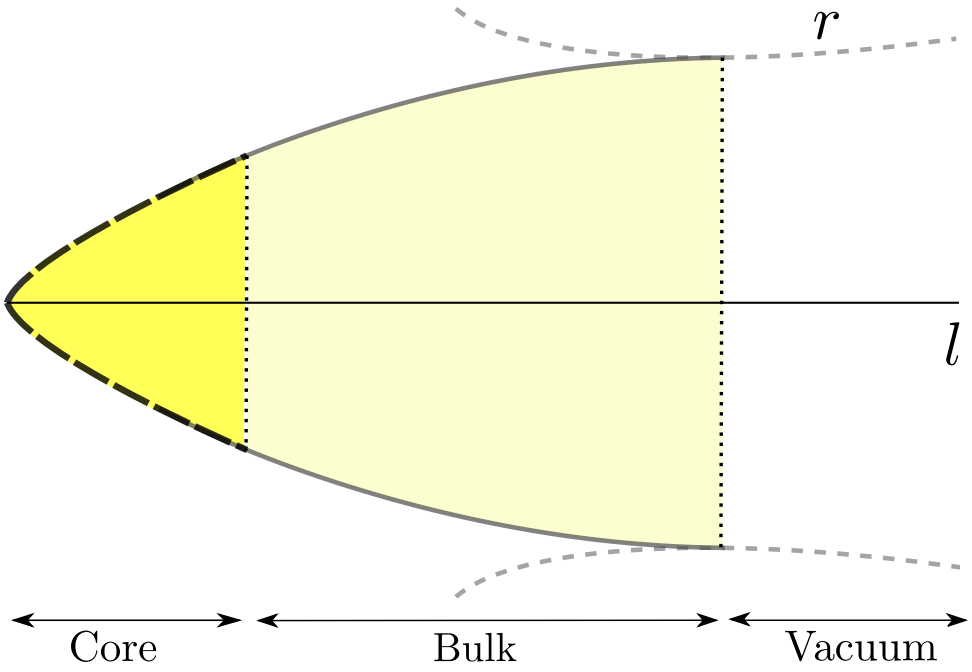

Fig. 5.1.: Pictorial representation of a semiclassical relativistic star. The areal radius r of spheres is shown in terms of a proper coordinate l, defined as $dr/dl = \sqrt{1-C}$. The vacuum region (gray dashed lines) is the semiclassical Schwarzschild solution from Ch. 2 describing an asymmetric wormhole. The bulk (gray continuous lines) is well described by the Polyakov approximation. This approximation breaks down at the core of the star (black dashed lines), but it can be minimally modified to adequately describe this region.

independent parameters. These fits are intended to be used in future studies as the physical properties of the solutions can be modified in a smooth way by varying the parameters. We conclude with some closing remarks in Section 5.5.

5.2 Summary of semiclassical stellar solutions

In the previous Chapter we exhaustively explored the space of semiclassical stellar solutions of constant classical density through the RP-RSET and obtained an entire catalog of regular and irregular solutions. We established a criteria for classifying solutions in terms of a critical (separatrix) behavior in the mass that occurs beyond certain value of the energy density ρ_c. Below we revisit the main differences between the classical and semiclassical space of solutions focusing on the aspects relevant for the current discussion. We provide illustrative diagrams for the classical pressure and Misner-Sharp mass.

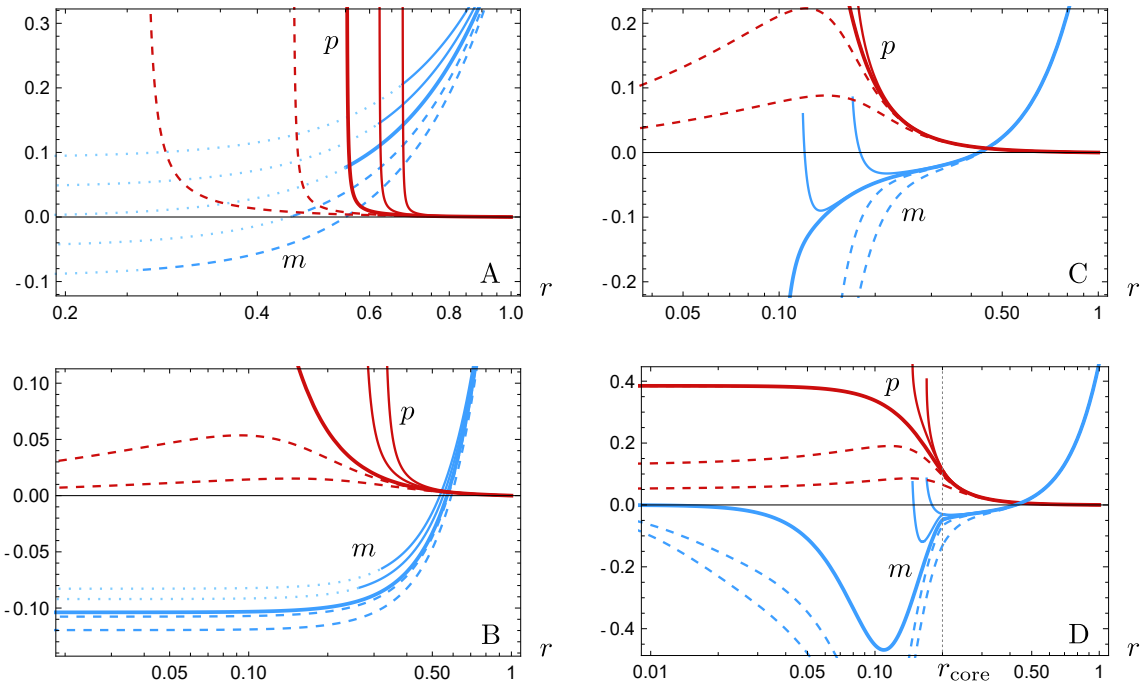

Fig. 5.2.: Plots of the pressure (red) and Misner-Sharp mass (blue) of solutions surrounding: (A) the classical critical solution with $\rho = \rho_{\rm c}$; (B) the classical separatrix in pressure; (C) the semiclassical critical solution with $F(r) = 1/(r^2 + \alpha l_{\rm p}^2)\,,\ \alpha = 1.01$; and (D) a semiclassical ultracompact stellar solution with a regular core of size $r_{\rm core} \simeq 0.2$. For every integration, we have chosen the values $R = 1$ and $C_R = 0.92$ for visualization purposes. The values of ρ increase from right to left in the pressure profiles (e.g. thin dashed lines correspond to greater ρ than thin continuous lines).

5.2.1 Criticality and classical stellar solutions

Returning to Fig. 5.1 and having integrated the exterior portion of the spacetime from the asymptotically flat region inwards with the RP-RSET, we start our bulk integration, which takes as parameter the density ρ (4.8). In principle, given the initial conditions $\{R, C_R\}$, there is a *critical* value $\rho_{\rm c}$ for which the configuration is regular all the way down to the center $r = 0$. When this does not occur (as for stars with C_R sufficiently close to 1), we consider $\rho_{\rm c}$ as the value of the density corresponding to a qualitative change in the behavior of the compactness (or the Misner-Sharp mass, equivalently) at the origin (see Sec. 4.4.2 for a thorough discussion of this point).

The various regimes in our numerical integrations for a star that surpasses the Buchdahl bound $C_R = 8/9$ are represented in Figure 5.2. For strictly classical stars $\langle \hat{T}^{\mu}_{\nu} \rangle = 0$ and the critical solution with $\rho = \rho_{\rm c-clas}$ (thick line in Fig. 5.2A) has vanishing Misner-Sharp mass at $r = 0$, separating solutions with positive and negative mass at $r = 0$. However, solutions with densities around $\rho_{\rm c-clas}$ exhibit

pressures that diverge at some radius far away from $r = 0$ (thin dashed lines in Fig. 5.2A). Stars with $\rho \gg \rho_{\mathrm{c-clas}}$ have this infinite pressure surface pushed inwards until, eventually, a solution where pressure diverges exactly at $r = 0$ is reached (thick line in Fig. 5.2B). Pressure profiles surrounding this separatrix display a large negative mass at $r = 0$. By increasing the value of ρ, pressure is made finite everywhere at the cost of making the compactness function singular at $r = 0$.

The semiclassical situation shown in Fig. 5.2C under the simple regulator choice (1.15) is radically different from the classical scenario and reveals appealing properties. The first one is that the critical solution for $\rho = \rho_{\mathrm{c}}$ represents two separatrices that appear *together* in mass and pressure (the separatrix corresponds again to the thick lines in Fig. 5.2C). The second compelling property is manifested for solutions where $\rho \lesssim \rho_{\mathrm{c}}$. For these sub-critical stars close to criticality (thin continuous lines in Fig. 5.2C), $m(r)$ acquires negative values followed by a bounce back to positive values, eventually reaching a surface where a wormhole neck is finally formed; the pressure reaches the neck with finite values (we have stopped these integrations at the neck since it is a singular surface for the r coordinate). There are sub-critical solutions with arbitrarily small necks.

Both aforementioned characteristics, i.e. a simultaneous separatrix behaviour in mass and pressure and a vanishing central mass, must be fulfilled by any star that is regular. Therefore, we vindicate that the Polyakov approximation manages to generate ϵ-*strict* ultracompact stars, in the following sense. For the geometry to be regular at the center of spherical symmetry, the mass function must vanish there while having finite pressure. Hence, if we consider a small core around the center, regular configurations will have small masses (due to continuity) and finite pressures. This is not the case in the classical theory (Figs. 5.2A and 5.2B), where finite pressures for configurations beyond the Buchdahl limit require large negative values of the mass. Crucially, semiclassical physics is able to produce ultracompact configurations compatible with this vanishing of the mass and a finite pressure at a central core. Remarkably, the core can be Planck-sized for an ultracompact stellar object of say radius $R \sim 3$ km. Strict regularity is not fulfilled because of the singularity at $r = 0$ of the Polyakov approximation (1.13). The CRP-RSET (1.15) also fails to provide a strictly regular geometry (Fig. 5.2C), as a singularity beyond a wormhole neck is produced inside the core.

5.3 Core regularization

The Polyakov approximation fails to capture the correct physics close to the radial origin. We stress, as detailed in Subsec. 1.2.2, that deforming the Polyakov ap-

proximation is not a choice, but a necessity to avoid its singular nature at $r = 0$. We consider the minimal extensions to achieve this goal that go beyond the CRP-RSET (1.15). We show in this Section that these minimal deformations of the Polyakov approximation suffice to produce regular configurations in a generic way, i.e., there exists a whole family of regulators F leading to regular configurations.

We follow a reverse-engineering logic which consists in making an ansatz for a regular geometry in the range $r \in (0, r_{\text{core}})$ and then obtaining the regulator F that sources the geometry via the RP-RSET, in case it exists. We derive an expression for C from the rr component of the semiclassical equations (5.1) and replace it in the tt component (5.2). Furthermore, through conservation of the classical SET (4.7), we find the relation

$$p'' = \mathcal{D}\left[\mathcal{A}_0 + \mathcal{A}_1\,(p') + \mathcal{A}_2\,(p')^2 + \mathcal{A}_3\,(p')^3\right], \tag{5.3}$$

where

$$\begin{aligned}
\mathcal{A}_0 =& -8\pi r\,(\rho+p)^3\,(\rho+3p)\,,\\
\mathcal{A}_1 =& \,4\,(\rho+3p)^2\left[6\pi r^2\,(\rho+p) + 4\pi F l_{\text{P}}^2 r^2 p - 1\right],\\
\mathcal{A}_2 =& -r\,(\rho+p)\left[16\pi r^2\,(\rho-2p) - l_{\text{P}}^2\,(2F + rF')\right.\\
&\left.+8\pi F l_{\text{P}}^2 r^2\,(\rho+5p) - 8\pi F' l_{\text{P}}^2 r^3 p - 6\right],\\
\mathcal{A}_3 =& \,F l_{\text{P}}^2 r^2\left[8\pi r^2\,(\rho-p) - l_{\text{P}}^2\,(2F - rF')\right.\\
&\left.-8\pi F' l_{\text{P}}^2 r^3 p - 2\right],\\
\mathcal{D} =& \,2r\left(1 - l_{\text{P}}^2 F\right)(\rho+p)^2\left(1 + 8\pi r^2 p\right).
\end{aligned} \tag{5.4}$$

By imposing an ansatz for the pressure and its derivatives in the region $r \in [0, r_{\text{core}}]$, Eq. (5.3) becomes a first-order differential equation for the regulator F which, upon solving, determines the entire core geometry. Naturally, if the resulting F is everywhere regular inside the core, compactness is regular from (5.1) and consequently the spacetime metric.

We consider a pressure profile for the core [whose classical energy density is constant, recall Eq. (4.8)] that is everywhere finite and has a global maximum at $r = 0$ (conditions necessary for regularity). At r_{core}, continuity of the metric enforces pressure to be continuous up to its second derivative. The simplest analytic function that satisfies these conditions is the fifth-order polynomial

$$p = p_0 + p_0'' r^2/2 + c_0 r^3 + c_1 r^4 + c_2 r^5, \tag{5.5}$$

where the pressure at the origin p_0 and its second derivative p_0'' are positive and negative constants, respectively. Determining the coefficients $\{c_i\}_{i=0}^2$ is straightforward given the aforementioned conditions. Now we take a fixed numerical solution for the bulk region $r \in (r_{\text{core}}, R)$. This amounts to choosing a particular pressure profile that results from integrating the semiclassical equations with the Polyakov or CRP-RSET (this makes no difference as long as $r_{\text{core}} \gg \sqrt{\alpha} l_{\text{P}}$). Typically, we consider the bulk pressure profile that corresponds to the critical solution ρ_{c} or a nearby solution in the space of parameters. Given a core size r_{core}, the pressure function inside the core is determined upon fixing the two remaining free parameters $\{p_0, p_0''\}$ by hand.

We performed a numerical exploration of wide range of values of the parameters $\{p_0, p_0''\}$ given a set of fixed solutions for $r > r_{\text{core}}$. The results are represented in Fig. 5.3, where whole parametric regions of regular solutions are shown. These regions exist for central cores of any size, although the central values of the curvature increase with decreasing r_{core}. We can impose the reasonable condition $\mathcal{K} < 1/l_{\text{P}}^4$ on the Kretschmann scalar (1.10). Consequently, we encounter that the value of r_{core} has a lower bound, as the RSET magnitudes required to regularize an ϵ-*strict* configuration when r_{core} is extremely small become increasingly high. If, on the contrary, we make the core bigger in size, the value of the Kretschmann scalar at the center will diminish, as the RSET contributions can be distributed along a bigger portion of the star instead of concentrated in a Planckian central core.

The existence of regular super-Buchdahl stars in semiclassical gravity is a remarkably non-trivial result. Of course, the Einstein equations guarantee that any given spacetime geometry (take, for example, a regular super-Buchdahl star) is generated by some stress-energy tensor that will certainly violate energy conditions. This should not be mistaken with our approach here, as we are imposing that the pressure inside the core obeys a polynomial form and asking whether this is compatible with a stress-energy tensor that can be divided in two parts: a classical, uniform density perfect fluid and the Polyakov RSET multiplied by some radial function. As it is not guaranteed that a prescribed geometry will be compatible with the Polyakov RSET multiplied by a function, it might have happened that no F existed for any regular ansatz. Hence, that this compatibility is realized for the simple polynomial example in Eq. (5.5) is a strong indication that the Polyakov approximation is able to capture an important fraction of the relevant physics.

The strictly regular solutions we have obtained have a clear interpretation in terms of the regulating functions F. By modifying the regulator inside the core we are distorting the space of solutions (Fig. 5.2D) so that the new critical solution corresponds to a regular configuration. The regular separatrix solution exhibits an interior region of negative mass (encompassing the core and part of the bulk) that exerts the gravitational repulsion necessary to sustain the whole structure for

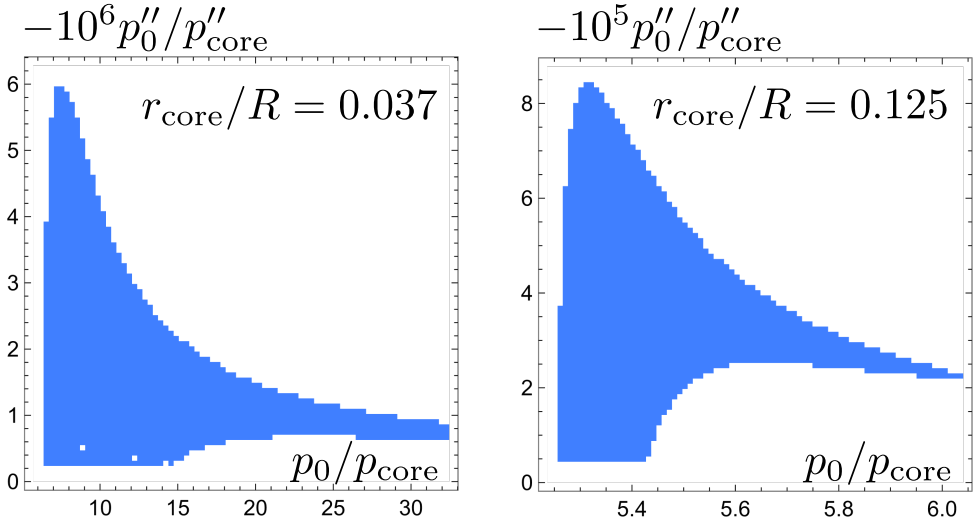

Fig. 5.3.: The left and right panels denote the parameter space for the analytical-pressure core of stars with $R \simeq 163,\ C_R = 1-10^{-4}$. We have chosen $r_{\rm core}/R = 0.037$ and $r_{\rm core}/R = 0.125$ for the core radius, respectively. The colored region denotes entirely regular solutions. The horizontal axis is the quotient between the central and the core-boundary pressures p_0, $p_{\rm core}$. The vertical axis is the quotient between the second derivatives of the pressure at the origin, p_0'', and at the core boundary, $p_{\rm core}''$. We have not constrained the central curvature of these solutions to be non-Planckian.

values of C_R for which a sphere composed of a classical fluid alone would inevitably collapse under its own gravity.

As the bulk geometry of the star is unaffected by the characteristics of the regular core, the surface compactness C_R and radius R are fixed constants in our integrations. Therefore, the mass-radius diagram for semiclassical relativistic stars shown in Fig. 1.1 is independent of $r_{\rm core}$. The most remarkable feature that we can extract from this diagram is that semiclassical relativistic stars can be arbitrarily close to the BH limit. In fact, there is no further upper bound to the compactness of these objects. Their surface can lie at the wormhole neck ($C_R = 1$), being as compact as BHs in terms of their mass distribution, but with a positive redshift function everywhere (thus horizonless).

5.4 Physical properties and analytic fits

Let us discuss now the most remarkable physical characteristics of semiclassical relativistic stars. Figure 5.4 contains a pictorial representation (analogous to Fig. 5.1) but now with the metric functions overlaid. This Figure shows both the pure vacuum solution (short-dashed lines), an example of a sub-critical super-

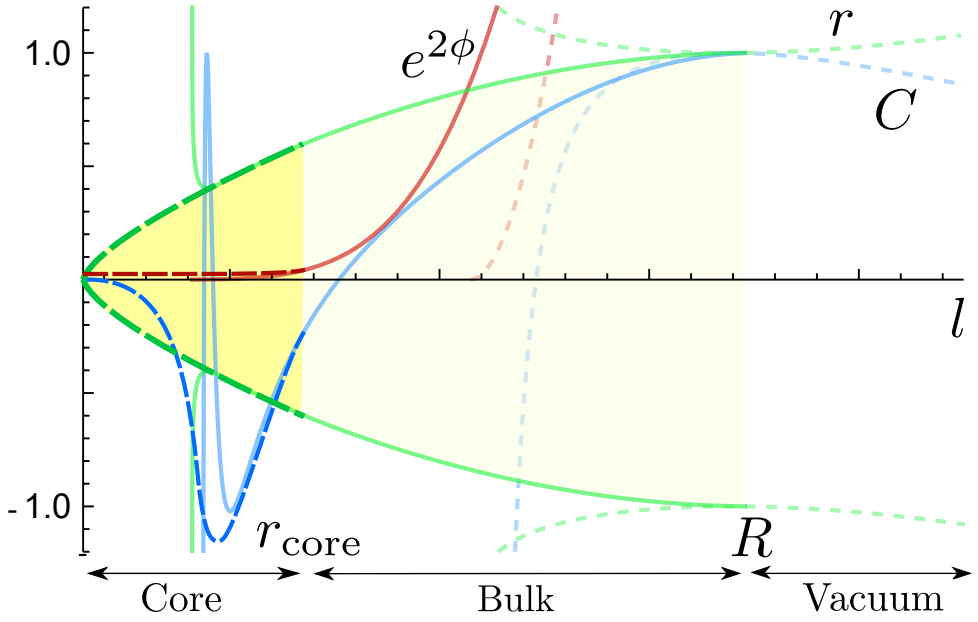

Fig. 5.4.: Example of a semiclassical ultracompact star. The color code is the following: in terms of a proper coordinate l we have drawn in green, red and blue the dimensionless radial coordinate $r(l)/R$, the compactness $C(l)$ and the redshift function $e^{2\phi(l)}/e^{2\phi(R)}$. The exterior spacetime (dashed, light-colored lines) is the semiclassical Schwarzschild solution from Ch. 2 describing an asymmetric wormhole. The interior spacetime (continuous lines) is an exact solution of the semiclassical equations with the RP-RSET. At the core of the star this solution develops a wormhole neck as well. The RP-RSET can be modified in the outskirts of this interior neck to obtain a regular core (dashed, dark-colored lines). This Figure is a version of Fig. 5.1 showing the metric functions.

Buchdahl star of the kind reviewed in Subsec. 4.5.4 from Chapter 4 (in continuous lines), and a semiclassical relativistic star with a regular core (in long-dashed lines). For the vacuum and bulk regions, $F = 1/r^2$, while the core region has the regulator F distorted in a way compatible with regularity.

Semiclassical stars have a compactness (or, equivalently, a Misner-Sharp mass) that becomes negative in their interiors, vanishing at $r = 0$ from negative values. This kind of regularized negative mass interiors require negative total energy densities to exist, so the semiclassical density is growing negative enough to compensate for the positive classical density. Such negative mass cores obey, at $r = 0$, the expansions

$$\begin{aligned} C &= -C_0 r^2 + \mathcal{O}\left(r^3\right), \qquad p = p_0 + p_1 r^2 + \mathcal{O}\left(r^3\right), \\ \psi &= \psi_0 r + \mathcal{O}\left(r^3\right), \qquad F = F_0 + \mathcal{O}(r), \end{aligned} \tag{5.6}$$

where $C_0,\ p_0$ and ψ_0 are positive constants and F_0 is constant with (yet) unknown sign. Replacing these expansions in (5.2) and taking the $r \to 0$ limit we obtain, at leading order

$$-3C_0 r = 8\pi r\rho + 2F_0 l_{\rm P}^2 r\psi_0 + \mathcal{O}(r^2). \tag{5.7}$$

Evidently, having a central core of this kind requires a sufficiently negative central semiclassical density, for which $F_0 \equiv F(0) < 0$. The particular form adopted by the regulator inside the core is tied to our analytical choice of pressure profile. We can take other (non-analytical) pressure profiles that look very similar to the polynomial fits (5.5) and the non-linearity of the semiclassical equations will return a considerably different F, but always fulfilling $F_0 < 0$. The polynomial pressure core must not be taken as a reliable descriptor of the physics at the center of semiclassical stars. Rather, it should be understood as a proof of the existence of such configurations under minimal assumptions. Nevertheless, it is always the case that a star with maximal pressure and whose mass vanishes from negative numbers at $r = 0$ must have negative densities at the center. These negative densities can be provided by a modified Polyakov approximation that reproduces four-dimensional RSET approximations that are accurate near $r = 0$, such as the AHS-RSET [127].

Figures 5.5 and 5.6 show the Misner-Sharp mass and classical pressure profiles for semiclassical relativistic stars with different core sizes. Given some $r_{\rm core}$, the mass profile inside the core is determined by our choice of the parameters p_0 and p_0''. Larger cores have less negative Misner-Sharp mass, although these values are distributed throughout a larger portion of the stellar interior. Larger cores also allow for smaller values of p_0.

Parametrized shapes

To end this Section we provide a family of analytical geometries that shows the main characteristics of semiclassical relativistic stars. They exhibit a negative mass region in the interior of the structure together with a redshift that decreases inwards. This family accommodates qualitatively to foreseeable solutions found using different approximation schemes to the RSET. Alternatively, it can be taken as a parametrized phenomenological approach to this type of ultracompact objects. They also reproduce the effect of varying the size of the core.

Defining $\hat{r} = r/R$, the five-parameter family of metrics is:

$$ds^2 = -e^{2\phi(\hat{r})}dt^2 + R^2\left[1 - C(\hat{r})\right]^{-1} d\hat{r}^2 + R^2\hat{r}^2 d\Omega_2^2, \tag{5.8}$$

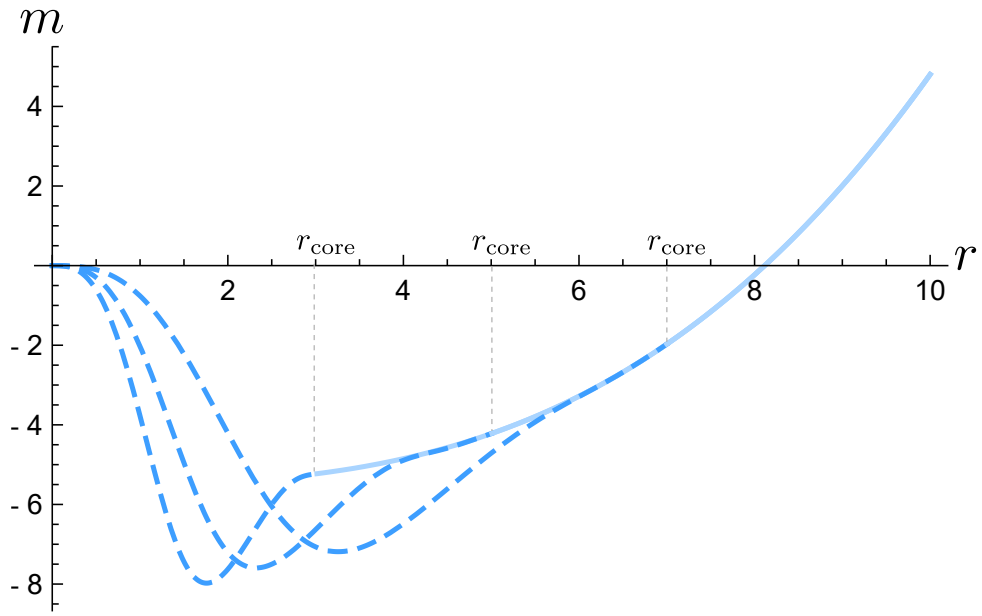

Fig. 5.5.: Misner-Sharp mass for semiclassical relativistic stars stars with $C_R = 0.96,\ R = 10$ and $r_{\text{core}} = 0.3R,\ 0.5R\ , 0.7R$, respectively. As the regular core is made smaller, the RP-RSET needs to attain larger magnitudes inside it. Consequently, the Misner-Sharp mass reaches more negative values to compensate for the gravitational pull of the outer layers of the star.

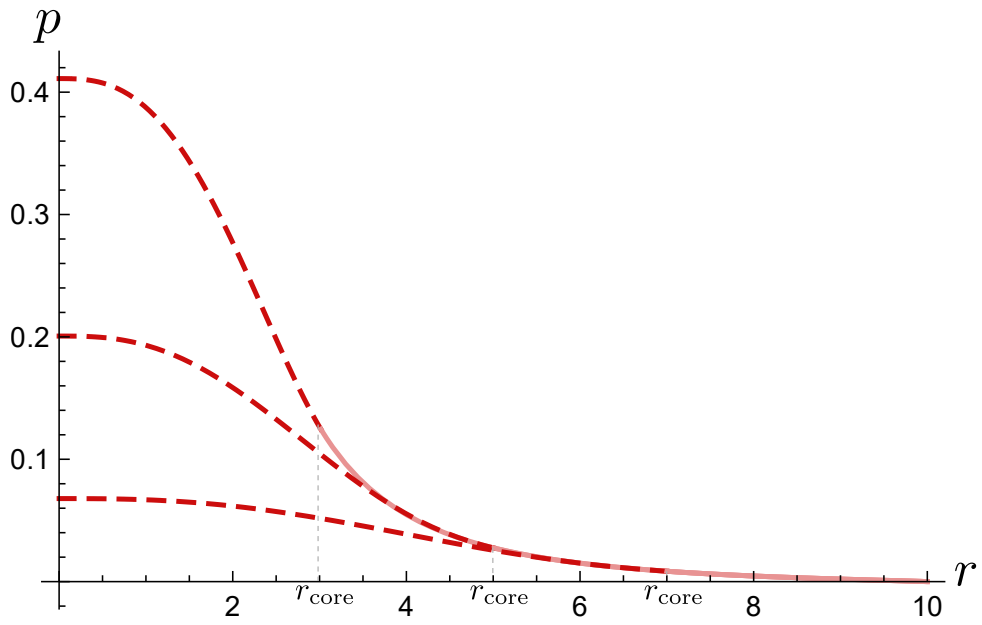

Fig. 5.6.: Classical pressure for semiclassical relativistic stars stars with $C_R = 0.96,\ R = 10$ and $r_{\text{core}} = 0.3R,\ 0.5R\ , 0.7R$, respectively. As the regular core is made larger, smaller central classical pressures are sufficient to maintain the whole star in equilibrium.

with

$$e^{2\phi(\hat{r})} = \begin{cases} 1 - C_R/(\hat{r}+\beta_0), & 1 \leq \hat{r} < \infty \\ \beta_1 a_0^{\beta_2 \hat{r}^2} + a_1 \hat{r}^6 e^{a_2(\hat{r}-1)}, & 0 \leq \hat{r} < 1 \end{cases}$$
$$C(\hat{r}) = \begin{cases} C_R/\hat{r}, & 1 \leq \hat{r} < \infty \\ \beta_3 \left[\cos\left(\beta_4 \hat{r}\right) - 1\right] e^{-\beta_4 \hat{r}} + a_3 \hat{r}^2, & 0 \leq \hat{r} < 1 \end{cases} \tag{5.9}$$

The constants $\{a_i\}_{i=0}^3$ depend on the 5 independent parameters $\{\beta_i\}_{i=0}^4$:

$$\begin{aligned} a_0 =& \frac{1 - C_R + \beta_0}{\beta_1 \left(1+\beta_0\right)}, \quad a_1 = 1 - \frac{C_R}{1+\beta_0} - \beta_1 a_0^{\beta_2}, \\ a_2 =& \left\{ 2\beta_1 a_0^{\beta_2} \left[3 - 2\beta_2 \log a_0\right] + \frac{C_R\left(7+6\beta_0\right)}{\left(1+\beta_0\right)^2} - 6 \right\} a_1^{-1}, \\ a_3 =& \beta_3 e^{-\beta_4} \left(1 - \cos\beta_4\right) + C_R. \end{aligned} \tag{5.10}$$

Thus, the family of metrics (5.9) is characterized by five form parameters $\{\beta_i\}_{i=0}^4$ with a clear physical interpretation. β_0 introduces an offset in the redshift $e^{2\phi(r)}$ associated with the fact that the external semiclassical metrics we have found are almost Schwarzschild up to very close to the gravitational radius. $\beta_1 \in (0, e^{2\phi(R)})$ represents the redshift at the origin. $\beta_2 \in [0,1)$ controls the flatness of the redshift profile in the interior region. Finally $\beta_3, \beta_4 > 0$ determine the width and depth of the negative energy internal region. Figure 5.7 shows a comparison between a numerical solution and the corresponding analytical fit.

5.5 Closing remarks

Neutron stars are the most compact relativistic stars known to exist. We have shown that semiclassical gravity, the most straightforward and conservative extension of GR, can accommodate more compact stellar configurations supported by quantum vacuum polarization. This result has been obtained using a well-motivated semiclassical source given by a minimal deformation of the Polyakov approximation. Our scheme is approximate and, despite its limitations, i.e. ambiguities in specifying the RP-RSET, the signature properties of semiclassical stars (namely, a negative-mass interior surrounded by a positive-mass crust and classical pressures that increase monotonically towards the center) hold for all the solutions explored here. A semiclassical star surpassing Buchdahl's limit with maximal pressure at $r = 0$ always displays a negative-mass interior [see Eq. (5.7)]. Thus, given the ambiguities of our construction (and which are inherent to semiclassical theories)

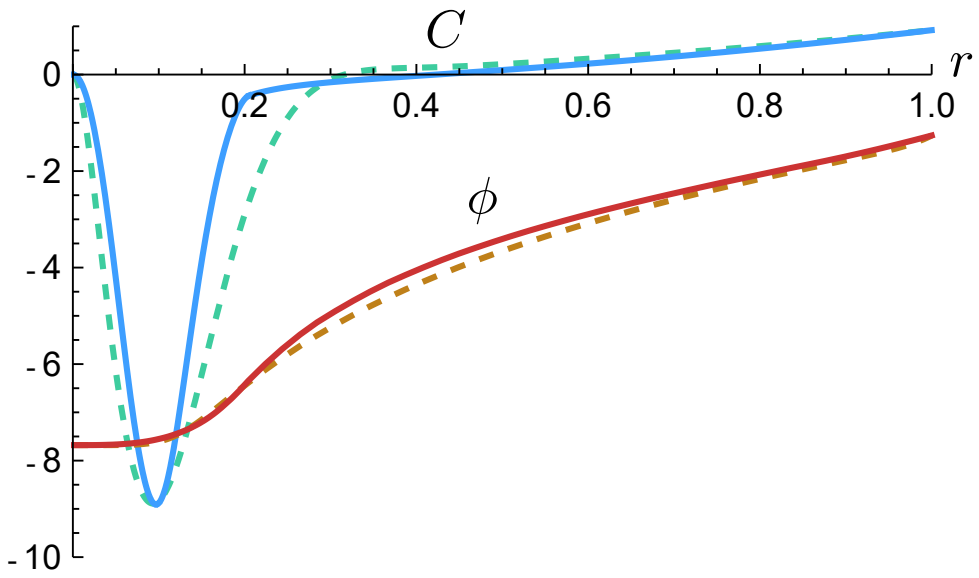

Fig. 5.7.: Comparison between a numerical solution describing a semiclassical ultracompact object (continuous lines, compactness $C(r)$ in blue and redshift $\phi(r)$ in red) and a particular solution of the parametrized family of geometries (5.9) (dashed lines). The numerical solution is the separatrix from Figure 5.2D. The parameters of the analytical fit are $\beta_0 = 10^{-4},\ \beta_1 = 2.14 \times 10^{-7},\ \beta_2 = 0.905,\ \beta_3 = 42.8$ and $\beta_4 = 16.8$.

we should understand semiclassical relativistic stars not as a definite model whose characteristics are tightly constrained, but as a novel type of exotic compact object whose specific properties will depend on the modeling of the RSET, but for which semiclassical effects are definitely responsible.

Semiclassical contributions are suppressed by $l_{\rm P}$, so significant quantum contributions need of some other scale that compensates for this suppression. As seen in Section 4.5 [Eq. (4.49), specifically], this suppression is eliminated in the $C(R) \to 1$ limit, for which the RSET becomes an $\mathcal{O}(1)$ contribution. Based on this argument, stars whose surface is extremely close to its gravitational radius receive notable semiclassical corrections. However, there is another scale that produces significant semiclassical contributions: the proximity to the Buchdahl limit. As the surface compactness of a constant density sphere approaches $8/9$, spacetime curvature grows unboundedly at $r = 0$, triggering a divergence in the RSET components [167]. The backreaction of the RSET can then add an extra repulsion that prevents pressure from diverging and allows to surpass the Buchdahl limit. This transition can be observed in the mass-radius diagram from Fig. 1.1. We find whole families of semiclassical stars whose surface compactness ranges from the Buchdahl limit to the BH limit itself. The phenomenological implications of this result are promising, as they allow to probe the observational properties of exotic compact objects at nearly unexplored compactness values [216].

Following this line of thought, semiclassical relativistic stars are the result of a balance between classical and quantum effects. In fact, these stars have classical energy densities much larger than the typical volumetric density associated with fluid spheres of mass M and radius R (compare ρ_{c} and $\rho_{\text{c-clas}}$ in Fig. 4.12). These large classical densities are however compensated by correspondingly large negative semiclassical densities, so that the total positive mass M is given by the offset between the two. This might imply that semiclassical relativistic stars cannot be obtained from the adiabatic collapse of a less compact uniform density fluid sphere and that some alternative process must be involved in their formation. The role of semiclassical physics in changing the outcome of gravitational collapse is a vivid subject of debate [217], specially in what refers to the evolution of inner horizons [116]. Another crucial aspect is the stability of the static stars found here against various perturbations. An important obstruction to address this problem is the absence of well-defined dynamic semiclassical equations on which we can analyze the growth or decay over time of perturbations. For this purpose, an RSET that is dynamical and regular at $r = 0$ should be first found.

Lastly, we want to highlight the close resemblance between semiclassical stars and gravastars [91]. Gravastars have positive interior densities and are supported by negative pressures, resembling a de-Sitter interior, whereas semiclassical stars have positive pressures but negative energy densities. The SET of a gravastar violates the strong energy condition but satisfies the null one, and the converse occurs for the total SET of semiclassical stars. Even within semiclassical gravity evidence for configurations resembling gravastars has been found [114]. Semiclassical stars, contrarily to gravastars, do not need any matter shell with anisotropic pressures at their surface [162].

A clear extension of this work is to analyze whether similar solutions exist when using the AHS-RSET, which is $(3+1)$-dimensional [127]. This RSET is a perfectly well-defined source in stellar spacetimes, with the shortcoming that it exhibits high-order terms in the derivatives of the metric. To conclude this thesis, we present, in the next Chapter, a method of reduction of order that transforms the high-derivative terms in the AHS-RSET into low-derivative ones, yielding a novel RSET approximation that is amenable to backreaction studies in vacuum spacetimes and relativistic stars. Using this approximation, we have found preliminary evidence for the existence of stellar spacetimes with akin characteristics (i.e. surpassing the Buchdahl limit by means of a negative mass interior). While we finish polishing all the aspects of this work, we include in this thesis some preliminary results supporting this statement and an exhaustive analysis of the corresponding vacuum solutions. These investigations suggest the existence of new stages of stellar

equilibrium beyond relativistic stars without the need for new physics beyond the effects of quantum vacuum polarization.

6

Beyond the Polyakov approximation: order-reduced semiclassical gravity

6.1 Introduction

In this Chapter we will explore a different analytical approximation to the RSET based on applying a perturbative order-reduction procedure to the analytical AHS-RSET [127]. We will work out this procedure in detail and use it to find vacuum and stellar semiclassical solutions. Apart from developing this alternative approximation scheme, one of the central interests of these explorations is to extract robust physical conclusions that are preserved when changing the approximation scheme. An example of such robust conclusions could be that in static situations event horizons disappear and are replaced by pathological singularities, as shown in Chapter 2 and previous works [112, 218]. We present some early work showing that semiclassical stars are realized under an order-reduced version of the AHS-RSET, and that their characteristics are very similar to the solutions presented in Chapter 5.

6.1.1 The AHS-RSET: strengths and shortcomings

In [127], Anderson, Hiscock and Samuel derived the RSET of a scalar field of arbitrary mass and coupling in static and spherically symmetric spacetimes, i.e. a field obeying the equation of motion

$$\Box\phi - \left(m^2 + \xi\mathcal{R}\right)\phi = 0, \tag{6.1}$$

where $\Box$ is the d'Alembertian operator, m is the field mass, and ξ the coupling to the Ricci scalar $\mathcal{R}$. As already discussed in the Introduction, this exact RSET can

be decomposed into two independently conserved parts, one of which is entirely analytical and the other requires numerical calculation,

$$\langle \hat{T}^{\mu}_{\nu} \rangle_{\text{ren}} = \langle \hat{T}^{\mu}_{\nu} \rangle_{\text{AHS}} + \langle \hat{T}^{\mu}_{\nu} \rangle_{\text{num}}. \tag{6.2}$$

The analytical portion $\langle \hat{T}_{\mu\nu} \rangle_{\text{AHS}}$ already captures the defining features of the standard vacuum states at horizons, yields the correct trace anomaly in the conformally invariant case ($m = 0,\ \xi = 1/6$), and is well defined at the center of stellar spacetimes (with a caveat shown in Appendix C.2, where the explicit form is provided). This last characteristic is absent in the Polyakov approximation. Nonetheless, as a drawback, the analytical part, or AHS-RSET, exhibits terms that have up to fourth order derivatives of the metric functions (these expressions were also derived by Popov for the Boulware state [219]). Their presence is a consequence of the quasi-local nature of the regularization procedure and they bring an enlargement of the space of solutions of semiclassical gravity with respect to standard GR (a straightforward demonstration of which is the enlargement of the initial conditions necessary to have a well-posed initial value problem).

However, as it is clearly exposed in [140, 141, 144], many of these solutions cannot be regarded as physical. On the one hand, these higher-derivative equations exhibit non-physical solutions in a manner analogous to the Dirac-Abraham-Lorentz equation of classical electrodynamics [148] (e.g. runaway solutions, pre-acceleration effects). Bear in mind that, while such pathologies are linked to the presence of higher-order temporal derivatives [220], higher-order spatial derivatives can also entail the presence of non-physical solutions, see e.g. [221].

On the other hand, there is the argument made by Simon [222] that such solutions are non-perturbative in $\hbar$, and therefore inconsistent with the idea that the semiclassical equations (1.6) are derived upon truncating the effective action of the theory at linear order in $\hbar$ [141, 223]. This process should eliminate all non-perturbative behavior in $\hbar$ from the start. In addition to these problems, it is the case that finding the self-consistent solutions to the higher-derivative semiclassical equations by brute force, despite being doable in some situations (see [221]), requires exploring an enormous space of parameters and defining a trustworthy criterion for selecting which solutions are physical. Henceforth, it is reasonable to subject the AHS-RSET to a procedure of order reduction so that we are left with a second-order system of differential equations.

We will work out in detail the method of reduction of order in the next Section but, before that, let us advance a few observations. As we will see, the procedure of the order reduction naturally leads to a new analytical approximation for the RSET which satisfies all the desirable properties that an RSET should have (as

captured by Wald's axioms [224], which exact RSETs obtained through covariant regularization procedures satisfy). We then apply our method towards obtaining geometries incorporating semiclassical backreaction in the absence of classical matter. In cosmological scenarios, the order-reduced equations admit analytical solutions [144, 154, 155]. On the contrary, the geometries here obtained are found through numerical integration, but analytic arguments allow to constraint the form of the various solutions that appear.

Before ending this Introduction, it is worth highlighting the advantages and limitations of the analytical approximation to the RSET obtained in [127]. To which extent the very AHS-RSET is a good approximation to the total RSET depends on the background geometry on which it is evaluated and on the mass of the scalar field. Dependence on the background requires computing $\langle\hat{T}^{\mu}_{\nu}\rangle_{\rm num}$ in each scenario and check whether the correction it entails can be safely neglected compared to $\langle\hat{T}^{\mu}_{\nu}\rangle_{\rm AHS}$. For conformally invariant fields in the Schwarzschild BH spacetime, $\langle\hat{T}^{\mu}_{\nu}\rangle_{\rm AHS}$ reduces to the Page-Brown-Ottewill RSET [225], which has been shown to be an extremely good approximation [134]. In Reissner-Nordström spacetimes, however, the AHS-RSET becomes a progressively worse approximation as the charge-to-mass ratio is increased [127]. Whether something similar occurs in other spacetimes (like regular stellar geometries) is yet to be known.

As for the effect of the field mass, in flat spacetime the components of the AHS-RSET reduce to

$$\begin{aligned}\langle\hat{T}^{r}_{r}\rangle_{\rm AHS} =& \frac{\kappa^4}{1440\pi^2} - \frac{\kappa^2 m^2}{96\pi^2} + \frac{m^4}{128\pi^2}\left(4\log\nu - 3\right),\\ \langle\hat{T}^{t}_{t}\rangle_{\rm AHS} =& -\frac{\kappa^4}{480\pi^2} + \frac{\kappa^2 m^2}{96\pi^2} + \frac{m^4}{128\pi^2}\left(4\log\nu + 1\right),\end{aligned} \tag{6.3}$$

with $\langle\hat{T}^{\theta}_{\theta}\rangle_{\rm AHS} = \langle\hat{T}^{\varphi}_{\varphi}\rangle_{\rm AHS} = \langle\hat{T}^{r}_{r}\rangle_{\rm AHS}$. The first term on the right-hand side of (6.3) is the thermal bath seen by a static observer for which the field is in a state with nonzero temperature $\kappa/2\pi$. For massive fields, ν can either equal $me^{\gamma}/2\kappa$ or $m/2\lambda$ depending on whether the field is in a thermal or zero-temperature state, respectively (λ is a positive parameter related to an infrared cutoff in the otherwise divergent frequency integrals in [127] and γ is Euler's constant). For massless fields, ν is an arbitrary parameter. Ambiguities present in RSET definitions have to be ultimately fixed via experiments. A suitable RSET is unique up to the addition of a local, conserved quantity, thus the local physics described by it is ambiguous (we had to deal with a similar form of ambiguity already within the framework of the Polyakov approximation). One crucial aspect of backreaction analyses is whether robust physical conclusions can be extracted despite this ambiguity in the local terms. One such conclusion would be the non-existence of event horizons for fields

in the Boulware state, as the divergence of a vacuum state is not a local property, but a signature of the global field modes becoming singular at some region of spacetime.

Recall that suitable RSETs must reproduce standard results in Minkowski spacetime, where the RSET can be renormalized to zero via normal ordering [34]. In the zero-temperature massive case, the AHS-RSET (6.3) has mass-dependent anomalous contributions in flat spacetime that cannot be canceled in all components by a particular choice of ν. These contributions also arise in the context of the cosmological constant problem [226], where massive scalar fields in Minkowski generate non-vanishing quantum pressures and densities. As the involved integrals over the frequency are divergent, some regularization method must be applied. Those which violate Lorentz invariance (like a bare cutoff in the frequency) yield an effective quantum fluid that does not satisfy the equation of state of vacuum energy. The infrared cutoff λ plays a similar role here, as the components (6.3) describe a cosmological constant only in the $\nu \to 0$ and $\nu \to \infty$ limits, the latter corresponding to the absence of any infrared cutoff λ in the renormalization procedure. In that case, the RSET components (6.3) diverge, although in a way that satisfies the equation of state of vacuum energy. As this discussion extends beyond the scope of this thesis, we adopt the view that the analytical approximation alone cannot be trusted if the field is massive since, in BH spacetimes, their components will be non-vanishing in the asymptotically flat region for the Boulware state. Consequently, we set $m = 0$ for the remaining of this work.

The Chapter is organized as follows. Section 6.2 describes the order-reduction procedure and the derivation of the order-reduced RSET approximation in the Boulware vacuum state. Then, in Section 6.3 we solve the semiclassical equations in vacuum self-consistently using this new RSET approximation and analyze the characteristics of the solutions. Section 6.4 discusses the accuracy of the order-reduced RSET (OR-RSET) by addressing how it differs from the AHS-RSET for particular solutions. Additionally, we compare these results with our analysis from Chapter 2 using the CRP-RSET in Subsec. 6.4.1. In particular, we discuss which elements are specific of the approximation and which ones are more generic. We have included some preliminary application of the method of reduction of order to constant-density stars in Section 6.5. We conclude in Section 6.6 with a summary of our results.

6.2 Reducing the order of the AHS-RSET in vacuum

The order reduction procedure did not originate in semiclassical analyses, but is much older and emerged in the context of the electromagnetic radiation reaction equation [149]. The method applies to any theory where higher-order contributions in a set of ordinary differential equations are multiplied by some small parameter [150, 152] in terms of which the solutions can be expanded.

In the context of semiclassical gravity, order reduction was first applied to prove the stability of flat space [222] and the absence of a Starobinski inflationary phase driven by semiclassical backreaction [155]. Then, it has been applied as well for obtaining the dynamics of Friedmann-Lemaître-Robertson-Walker and Kasner cosmologies [144, 154, 227] and the study of averaged energy conditions [140]. Here we present the first application of this method to static and spherically symmetric spacetimes. We slightly change the notation with respect to previous Chapters and write the line element as

$$ds^2 = -f(r)dt^2 + h(r)dr^2 + r^2 d\Omega^2, \tag{6.4}$$

where $d\Omega^2$ is the line element of the unit 2-sphere.

The tt and rr components of the vacuum semiclassical equations 1.6 now take the form

$$\begin{aligned} \frac{h(1-h) - rh'}{h^2 r^2} &= 8\pi\hbar \langle \hat{T}^t_t \rangle_{\text{AHS}}, \\ \frac{rf'f - fh}{fhr^2} &= 8\pi\hbar \langle \hat{T}^r_r \rangle_{\text{AHS}}, \end{aligned} \tag{6.5}$$

where the right-hand side contains higher-derivative terms. The concrete and lengthy form of the AHS-RSET, which is not very illustrative, can be seen in [127]; we recall it here in Appendix C for completeness. Neglecting terms $\mathcal{O}(\hbar)$ in (6.5) leads to

$$\begin{aligned} \frac{h(1-h) - rh'}{h^2 r^2} &= \mathcal{O}(\hbar), \\ \frac{rf' + f - fh}{fhr^2} &= \mathcal{O}(\hbar). \end{aligned} \tag{6.6}$$

These expressions can be differentiated consecutively to derive recursion relations between $f,\ h$, and their higher-order derivatives $\{f^{(n)}\}_{n=1}^{\infty}$ and $\{h^{(n)}\}_{n=1}^{\infty}$. For h,

said relations are obtained by solving the tt equation directly, which can then be used to derive the f relations from the rr equation. The result is

$$\begin{aligned} h^{(n)} &= (-1)^n \frac{n!\, h^n}{r^n} (h-1) + \mathcal{O}(\hbar), \\ f^{(n)} &= (-1)^{n+1} \frac{n!\, f}{r^n} (h-1) + \mathcal{O}(\hbar). \end{aligned} \tag{6.7}$$

Relations (6.7) are now inserted in the AHS-RSET components $\langle \hat{T}^t_t \rangle_{\text{AHS}}$ and $\langle \hat{T}^r_r \rangle_{\text{AHS}}$ (Sec. C.1 in App. C) until they only depend on f and h. After a lengthy but straightforward calculation using symbolic computation software, the resulting expressions are

$$\begin{aligned} 16\pi^2 \langle \hat{T}^t_t \rangle_{\text{OR}} =& -\frac{\kappa^4}{30 f^2} + \kappa^2 \left(\xi - \frac{1}{6}\right) \frac{3\,(h-1)^2}{6 f h r^2} + \frac{(h-1)^2\,(h^2+6h+33)}{480 h^2 r^4} \\ & - \left(\xi - \frac{1}{6}\right) \frac{(h-1)^2\,(h^2+2h+5)}{8 h^2 r^4}, \\ 16\pi^2 \langle \hat{T}^r_r \rangle_{\text{OR}} =& \frac{\kappa^4}{90 f^2} - \kappa^2 \left(\xi - \frac{1}{6}\right) \frac{(h-1)\,(h+3)}{6 f h r^2} - \frac{(h-1)^2\,(h^2+6h-15)}{1440 h^2 r^4} \\ & + \left(\xi - \frac{1}{6}\right) \frac{(h-1)^2\,(h+3)^2}{24 h^2 r^4}, \end{aligned} \tag{6.8}$$

where the suffix OR stands for Order-Reduced. Taking $\kappa = 0$ selects the Boulware vacuum state. On the other hand, by taking κ equal to the surface gravity of the Schwarzschild BH we ensure the finiteness of the RSET components at the horizon, thus selecting the Hartle-Hawking vacuum state.

So far, we have applied the method of order reduction to the tt and rr components of the AHS-RSET. If we continue and apply the same method to the angular components of the AHS-RSET, it turns out that the set of order-reduced field equations do not satisfy the Bianchi identities [152]. In other words, we find that the order-reduced RSET is not covariantly conserved, but satisfies

$$\nabla_\mu \langle \hat{T}^\mu_\nu \rangle_{\text{OR}} = \mathcal{O}(\hbar). \tag{6.9}$$

However, as it is discussed just below, we propose a different algorithm for order reduction that leads to a covariantly conserved RSET. This will be used in our analysis of solutions.

6.2.1 The covariantly conserved OR-RSET and its properties

The method followed to obtain a covariantly conserved RSET is already familiar to us: we just need to add the angular components needed to obtain conservation. This is identical to what we did to obtain the RP-RSET (1.14). The only non-trivial component of the divergence of the OR-RSET (6.9) is

$$\nabla_\mu \langle \hat{T}^\mu_r \rangle_{\rm OR} = \partial_r \langle \hat{T}^r_r \rangle_{\rm OR} + \frac{2}{r}\left(\langle \hat{T}^r_r \rangle_{\rm OR} - \langle \hat{T}^\theta_\theta \rangle_{\rm OR} \right) + \frac{f'}{2f}\left(\langle \hat{T}^r_r \rangle_{\rm OR} - \langle \hat{T}^t_t \rangle_{\rm OR} \right). \tag{6.10}$$

Using the expressions for $\langle \hat{T}^t_t \rangle_{\rm OR}$ and $\langle \hat{T}^r_r \rangle_{\rm OR}$ in Eq. (6.8) we can deduce the angular components necessary to force this divergence to vanish. Specifically, we find

$$\begin{aligned} 16\pi^2 \langle \hat{T}^\theta_\theta \rangle_{\rm OR} = 16\pi^2 \langle \hat{T}^\varphi_\varphi \rangle_{\rm OR} = & \frac{\kappa^4}{90 f^2} - \kappa^2 \left(\xi - \frac{1}{6} \right) \frac{f\left(h^2+3\right) + f'\left(h-1\right)\left(h-3\right)}{12 f^2 h r} \\ & - \frac{h-1}{1440 f h^2 r^4} \Big\{ f \left[h^3 (r-1) + h^2 (3r-5) + 3h(r+7) - 15(r+1) \right] \\ & + f'(h-1)\left(h^2+6h+21\right) \Big\} \\ & + \left(\xi - \frac{1}{6} \right) \frac{h-1}{24 f h^2 r^4} \Big\{ f(h+3) \left[h^2(r-1) - 2h + 3(r+1) \right] \\ & + r f'(h-1)\left(h^2+3h+6\right) \Big\}. \end{aligned} \tag{6.11}$$

We have thus constructed a new approximation to the RSET valid for beackreaction studies in vacuum spacetimes. The OR-RSET approximation is divergenceless, yields the correct values at the event horizon, and vanishes in flat spacetime in the Boulware state. It therefore satisfies all Wald's axioms [224]. In addition, it is not a higher-derivative quantity, which makes it an excellent RSET candidate to address the semiclassical backreaction problem.

Before turning to analyze the set of self-consistent solutions of these semiclassical equations, let us make a few further observations. On the one hand, the reduction of order in the vacuum case gets rid of the ν parameter. This allows us to give unique and unambiguous results for the corresponding solutions, and simplifies the analysis significantly.

On the other hand, when the OR-RSET is evaluated on the Schwarzschild spacetime, $f(r) = h(r)^{-1} = 1 - 2M/r$, we realize that it gives the exact result

$$\langle \hat{T}^\mu_\nu \rangle^{\rm (Schw)}_{\rm OR} = \langle \hat{T}^\mu_\nu \rangle^{\rm (Schw)}_{\rm AHS}. \tag{6.12}$$

This is not surprising upon realizing that the Schwarzschild metric is an exact solution to Eq. (6.6), thus the $\mathcal{O}\left(\hbar^2\right)$ terms neglected in our expansion vanish identically. Therefore, for the Schwarzschild metric only, the reduction of order is an exact procedure, i.e. the OR-RSET coincides with the AHS-RSET. Furthermore, considering arbitrary spherically symmetric spacetimes and restricting ourselves to the $m = 0,\ \xi = 1/6$ case, the trace of the OR-RSET is state-independent.

6.3 Classification of vacuum solutions

Equipped with the OR-RSET from Eqs. (6.8) and (6.11), we are now ready to address the backreaction problem. In principle, the domain of consistency of the order reduction *à la* Simon [222] is limited to solving the order-reduced equations (expressions displayed below) perturbatively [140]. This requires assuming from the onset that the Einstein tensor and the OR-RSET admit perturbative expansions in $\hbar$ and then solve the expanded equations order by order. Whereas entirely consistent, this logic eliminates the possibility of any non-perturbative backreaction effect associated with the Boulware state, which any proper RSET should capture as well, and which is responsible for the interesting physics that we have discussed in an important part of this thesis. We stick to our modified gravity perspective and solve the semiclassical equations in a self-consistent fashion. We will review the logic behind this approach and on the comparison between results derived with the CRP-RSET in Subsec. 6.4.1. For the moment, its just necessary to keep in mind that, regardless of its origin, the OR-RSET satisfies all the requirements for a legitimate semiclassical source, and in the following we are treating it as such.

In this Section, we will classify the self-consistent semiclassical solutions in vacuum for arbitrary coupling ξ and ADM mass M (note that in this Chapter we use the symbol M instead of M_{ADM} as in Chapters 4 and 5). The geometries here depicted also describe, for $M > 0$, the spacetime exterior to any static stellar configuration in this approximation.

The tt and rr components of the semiclassical equations with the OR-RSET in Eq. (6.8) can be cast in the form of a dynamical system

$$h' = -\frac{(h-1)\,h}{r} + \frac{l_{\text{P}}^2}{r^3}(h-1)^2\left[(\xi-\xi_{\text{c}})\,h^2 + 2\left(\xi-\xi_{\text{c}}+\frac{1}{30}\right)h + 5\left(\xi-\frac{83}{300}\right)\right], \tag{6.13}$$

$$\frac{f'}{f} = \frac{(h-1)}{r} + \frac{l_{\text{P}}^2}{3hr^3}(h-1)^2\left[(\xi-\xi_{\text{c}})\,h^2 + 6\,(\xi-\xi_{\text{c}})\,h + 9\left(\xi-\frac{25}{3}\right)\right], \tag{6.14}$$

where $l_{\rm P}^2 = \hbar/16\pi$ (notice the redefinition of this symbol with respect to previous Chapters) and $\xi_{\rm c} = 11/60$. We have solved this system of equations numerically by imposing asymptotically flat boundary conditions at some distant radius, namely requiring that

$$f\left(r\right) = h\left(r\right)^{-1} = 1 - \frac{2M}{r}, \tag{6.15}$$

in the limit $r \to \infty$ (in practice, we are considering $r \gg M$). Depending on the sign of the ADM mass M (again, notice the slight notation change with respect to Chapters 4 and 5), we find two distinct types of solutions. The regime of interest for us is $M > 0$, as it describes the Schwarzschild counterpart and the exterior geometry of relativistic stars in order-reduced semiclassical gravity. Furthermore, for $M > 0$, there is a critical value of the coupling

$$\xi_{\rm c} = 11/60, \tag{6.16}$$

that denotes a separatrix between two regimes of solutions. The special value $\xi_{\rm c}$ appears as a correction (originated by the trace anomaly) to the conformal coupling $\xi = 1/6$ for which Eq. (6.1) becomes invariant under conformal transformations.

In what follows, we turn to describe the main features of the numerical solutions we have obtained, while also providing analytic arguments to constrain the form of the solutions whenever possible.

6.3.1 Positive asymptotic mass ($M > 0$)

Coupling $\xi < \xi_{\rm c}$

Starting from the asymptotic expressions (6.15), it is possible to constrain the form of the solutions to Eqs. (6.13, 6.14) for the case $\xi < \xi_{\rm c}$ through simple analytic arguments. First, we turn our attention to Eq. (6.13). It is straightforward to check that its right-hand side is always negative. Conditions (6.15) guarantee that $h > 1$ asymptotically, so h increases inwards with no turning points. In principle, the function h could adopt one of the following behaviors: i) reaching a finite value at $r = 0$, ii) diverging at $r = 0$, or iii) diverging at $r > 0$. As for possibility i), the semiclassical equations enforce the conditions $h(0) = 1$ and $h'(0) = 0$. Let us prove this statement by assuming that the following expansions hold for the metric functions around $r = 0$:

$$h = \sum_{n=0}^{\infty} h_n r^n, \quad f = \sum_{n=0}^{\infty} f_n r^n. \tag{6.17}$$

By replacing them in Eqs. (6.13, 6.14), we obtain the following values for the lowest order expansion parameters

$$\begin{aligned} h_0 =& 1, \quad h_1 = f_1 = h_3 = f_3 = 0, \\ h_2 =& \frac{3}{2l_{\rm P}^2\,(4\xi - 1)}, \quad f_2 = \frac{(90\xi - 17)}{15\,(4\xi - 1)} f_0, \end{aligned} \tag{6.18}$$

with $f_0 > 0$ a constant denoting the value of the redshift at the origin. Under these conditions, $r = 0$ is a regular point of the solution. Now, since we have $h > 1$ asymptotically and h cannot have turning points, possibility i) is discarded, as a finite value of h at $r = 0$ must be a maximum (or minimum). Regarding the behavior ii), an infinite $h(0)$ is inconsistent with Eq. (6.13) which, at leading order, would take the form

$$h' \propto \frac{h^4}{r^3}. \tag{6.19}$$

Solutions are inconsistent with assuming a divergent h at $r = 0$. Thus, we must discard possibility ii) as well. In conclusion, iii) holds and h must diverge at some radius $r = r_{\rm D} > 0$.

Let us highlight that the OR-RSET is finite for spherically symmetric spacetimes which are regular at $r = 0$. This is so even under the fact that the OR-RSET is derived assuming the absence of any classical matter, for which the resulting classical solutions are all singular (excluding flat spacetime, for which the RSET vanishes in the Boulware state). This characteristic is appealing because it suggests that our method is well defined for stellar spacetimes, a characteristic absent from the Polyakov [156] and s-wave approximations [101] (if unregularized). See Sec. C.2 in App. C for a discussion on the regularity of the AHS-RSET.

We now turn our attention to the differential equation for f, Eq. (6.14). In virtue of (6.15) we have, asymptotically, $f > 0$ and $f' > 0$. Again, the term between brackets on the right-hand side of the equation is negative. Thus, if h increases monotonically as r decreases, these negative terms will eventually compensate the positive contribution from the first term on the right-hand side, generating a turning point in the f function.

We analyze now the divergent behavior of h at some radius $r = r_{\rm D} > 0$. Close to $r_{\rm D}$, Eqs. (6.13, 6.14) are approximated by

$$\begin{aligned} h' \simeq& \frac{l_{\rm P}^2}{r_{\rm D}^3}\,(\xi - \xi_{\rm c})\,h^4, \\ \frac{f'}{f} \simeq& \frac{l_{\rm P}^2}{3r_{\rm D}^3}\,(\xi - \xi_{\rm c})\,h^3. \end{aligned} \tag{6.20}$$

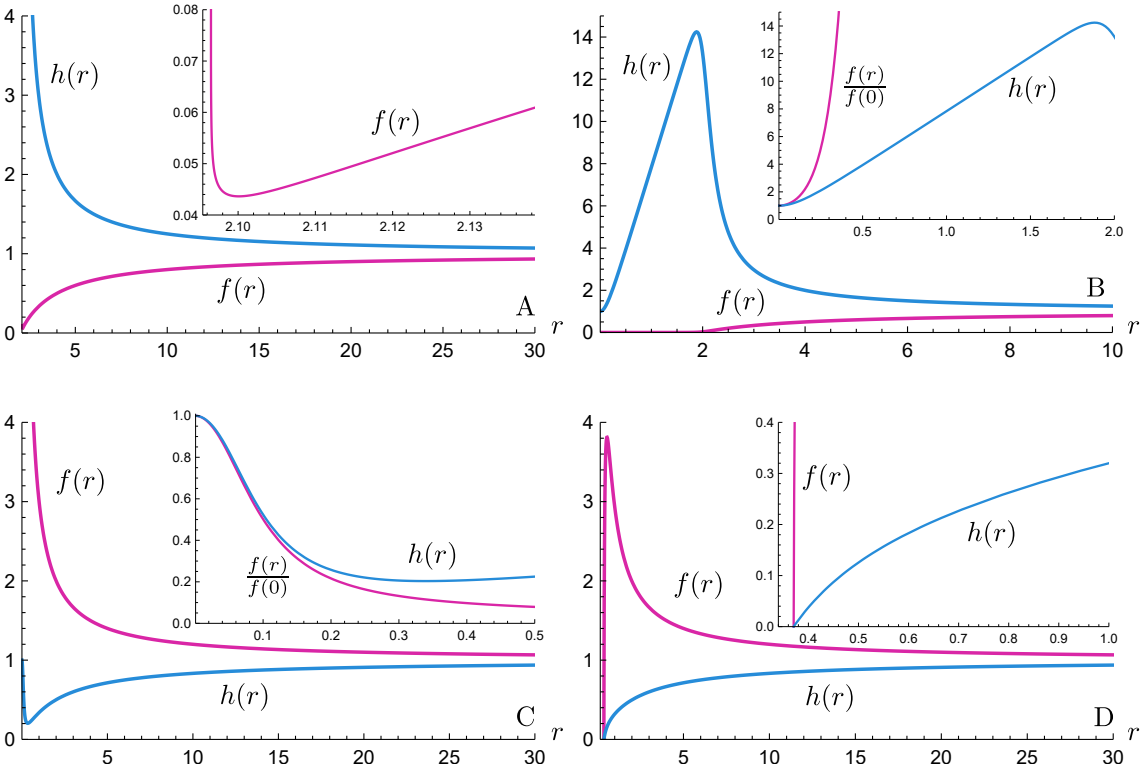

Fig. 6.1.: Panels A and B: self-consistent semiclassical solutions with $M = 1$ for fields of coupling $\xi = 0$ and $\xi = 1$, respectively (the values have been chosen for illustrative purposes). The geometry with $\xi \leq \xi_c$ (in particular, $\xi = 0$) is a timelike naked singularity whereas for $\xi > \xi_c$ (in particular, $\xi = 1$) we have a regular geometry with Planckian curvatures. Panels C and D: self-consistent semiclassical solutions with $M = -1$ for fields of coupling $\xi = 0$ and $\xi = 1$, respectively. For $\xi < 83/300$ (in particular, $\xi = 0$), the geometry describes a core of negative Misner-Sharp mass $m(r)$, at whose center the redshift can be maximal (if $\xi \leq \xi_c$) or minimal (if $\xi_c < \xi \leq 83/300$). For $\xi > 83/300$ (in particular, $\xi = 1$) the geometry has a null singularity at the surface where h and f vanish.

The differential equation for h can be integrated directly, yielding

$$h \simeq r_{\rm D} \left[3 l_{\rm p}^2 \left(\xi_{\rm c} - \xi\right) x\right]^{-1/3}, \tag{6.21}$$

where $x = r - r_{\rm D}$. Replacing this expression in the equation for f returns

$$f \simeq \frac{f_{\rm D}}{x^{1/9}}, \tag{6.22}$$

where $f_{\rm D}$ is a positive integration constant bearing a relation with the ADM mass M, not relevant here.

The curvature scalar adopts the expression

$$R=\frac{2}{r^2}\left(1-\frac{1}{h}\right)+\frac{2}{hr}\left(\frac{h'}{h}-\frac{f'}{f}+\frac{rf'h'}{4fh}\right)+\frac{1}{2h}\left[\left(\frac{f'}{f}\right)^2-\frac{2f''}{f}\right]. \tag{6.23}$$

Near $r=r_{\rm D}$, where the approximate solutions (6.21) and (6.22) hold, the curvature scalar (6.23) becomes

$$R\simeq-\chi_0 x^{-5/3}, \tag{6.24}$$

with

$$\chi_0=\frac{8}{9r_{\rm D}}\left[\frac{l_{\rm P}^2\left(\xi_{\rm c}-\xi\right)}{9}\right]^{1/3}. \tag{6.25}$$

In view of Eq. (6.24), the metric has a curvature singularity at $r=r_{\rm D}$. This is a consequence of allowing the Boulware state to backreact onto the background geometry in a self-consistent (and non-perturbative) way.

The reader can consult panel A in Fig. 6.1 for plots of the metric functions in terms of r. As numerical integrations of Eqs. (6.13, 6.14) reveal, $r_{\rm D}$ is a surface located slightly above the classical Schwarzschild radius $2M$. The radial distance $\Delta_{\rm D}=r_{\rm D}-2M$ depends on the ADM mass of the geometry for every fixed value of the coupling ξ. Fig. 6.2 contains some example cases for various ξ. As M increases, $\Delta_{\rm D}$ tends to the ξ-dependent constant Δ_∞. Figure 6.3 shows that Δ_∞ decreases as ξ increases, vanishing in the $\xi\to\xi_{\rm c}$ limit, i.e. the configuration with the highest ξ belonging to this family.

Coupling $\xi=\xi_{\rm c}$

Now we turn to analyze the particular case where $\xi=\xi_{\rm c}$. In this situation, similar analytic arguments as the ones exhibited above apply to Eq. (6.13), that is, h grows monotonically inwards until it diverges at some finite radius $r_{\rm D}$ as above. The f function, however, does not reach a turning point, since the $\mathcal{O}(h^2)$ and $\mathcal{O}(h)$ terms between brackets at the right-hand side in (6.14) vanish and the $\mathcal{O}(h^0)$ terms are suppressed by $l_{\rm P}^2$ with respect to the $\mathcal{O}(l_{\rm P}^0)$ terms. Close to $r_{\rm D}$, the field equations admit the expansions

$$\begin{aligned} h'&\simeq-\frac{l_{\rm P}^2}{15r_{\rm D}^3}h^3,\\ \frac{f'}{f}&\simeq\frac{(15r_{\rm D}^2+2l_{\rm P}^2)}{15r_{\rm D}^3}h. \end{aligned} \tag{6.26}$$

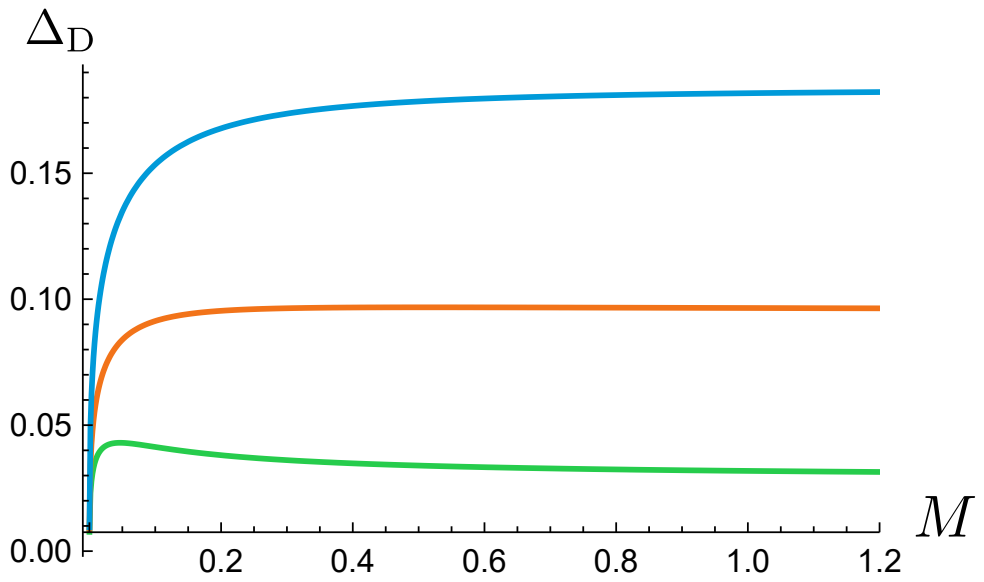

Fig. 6.2.: Radial distance $\Delta_{\rm D} = r_{\rm D} - 2M$ as a function of the ADM mass M for different values of the coupling ξ. The green, orange and blue curves correspond to $\xi = \{1/6, 0, -1/2\}$, respectively. The distance $\Delta_{\rm D}$ vanishes in the $M \to 0$ limit and quickly reaches a constant value as M increases.

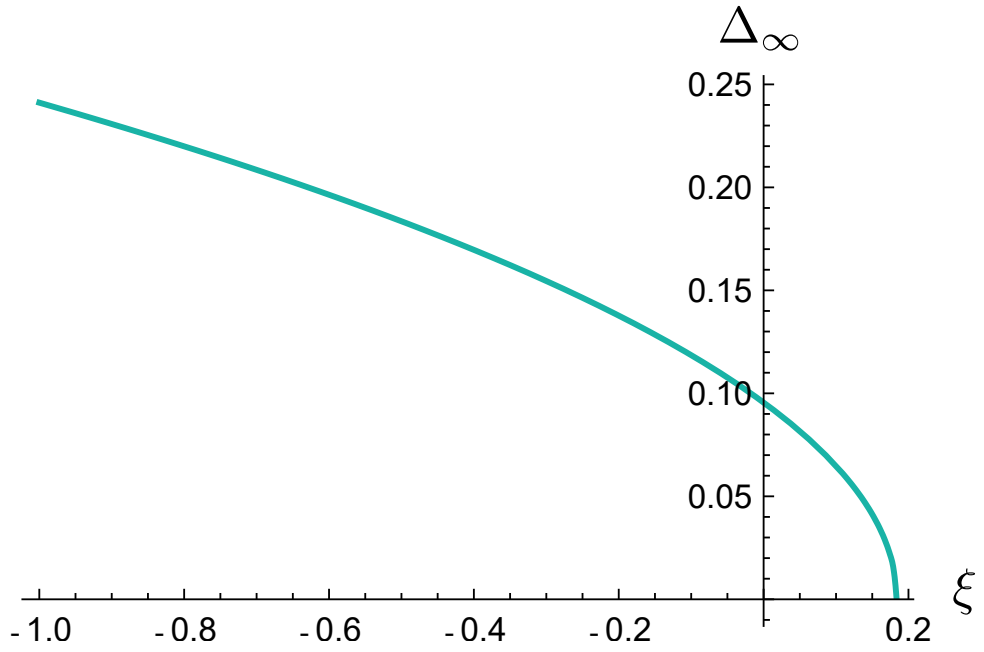

Fig. 6.3.: Asymptotic value of the radial distance Δ_∞ obtained as M is increased. This quantity diverges as $\xi \to -\infty$ and decreases with increasing ξ, vanishing in the $\xi \to \xi_{\rm c}$ limit.

Integrating them and expanding the solution for f in powers of $x = r - r_{\rm D}$ we have

$$h \simeq \sqrt{\frac{15 r_{\rm D}^3}{2 l_{\rm P}^2}} x^{-1/2},$$
$$f \simeq f_{\rm c} \left[1 + \frac{60 r_{\rm D}^2 + 8 l_{\rm P}^2}{\sqrt{2 r_{\rm D}^3} l_{\rm P}} x^{1/2} \right], \tag{6.27}$$

with $f_{\rm c} > 0$. The critical solution $\xi = \xi_{\rm c}$ has divergent h but vanishing redshift function f at $r_{\rm D}$. This results again in a curvature singularity at $r = r_{\rm D}$ such that the curvature scalar

$$R \simeq -\frac{15 r_{\rm D}^2 + 2 l_{\rm P}^2}{60 r_{\rm D}} x^{-1}, \tag{6.28}$$

diverges slower than in Eq. (6.24).

Coupling $\xi > \xi_{\rm c}$

Increasing the coupling beyond its critical value $\xi_{\rm c}$ results in geometries of a drastically different nature.

We draw our attention to Eq. (6.13) first. At large r there is an initial tendency of h to increase inwards which will eventually be reverted by the (now positive) contribution coming from the $\mathcal{O}(h^4)$ term in the right-hand side of (6.13). Hence, h cannot diverge towards positive infinity at finite radius. Similarly, h cannot vanish at some positive r since that would necessarily imply $h = 1$ there. Because of (6.13), h is bounded from below by the value $h = 1$, which corresponds to a minimum for h. The only remaining possibility is that h goes to a constant value at $r = 0$. Recall that the only value of $h(0)$ consistent with Eq. (6.13) is $h(0) = 1$ —see Eqs. (6.17, 6.18)— which corresponds to a finite Ricci scalar at $r = 0$. On the other hand, the f function decreases monotonically from the asymptotic region inwards, reaching a finite value at $r = 0$, as the term within brackets in Eq. (6.14) is everywhere positive for $\xi > \xi_{\rm c}$.

The metric functions obtained from numerical integration of the Eqs. (6.13, 6.14) are displayed in Fig. 6.1B. Despite being regular, these spacetimes are not well defined from a semiclassically-consistent perspective, as their curvature scalars have Planckian magnitudes. Indeed, inserting Eqs. (6.17) and (6.18) into Eq. (6.23), we obtain

$$R = \frac{45\,(\xi - 16/75)}{8 l_{\rm P}^2 (\xi - 1/4)^2} + \mathcal{O}\big(r^2\big), \tag{6.29}$$

close to the origin.

The metrics from Figs. 6.1A and 6.1B are similar for $r \gg 2M$, i.e. the region where semiclassical corrections are perturbative. Thus, within their regimes of

validity, these geometries approximate well the exterior spacetime of any semiclassical stellar object for any field coupling ξ to the curvature . We will define a criteria to estimate the closeness between solutions to the order-reduced and higher-order systems in the next section.

So far we have classified the space of vacuum solutions with positive ADM mass. For couplings $\xi \leq \xi_{\rm c}$ we find geometries where the event horizon gets replaced by a naked curvature singularity. For couplings $\xi > \xi_{\rm c}$ we obtain regular spacetimes with curvatures that become Planckian below the region where the event horizon would have appeared. This drastic change of behavior can be traced back to which pointwise energy conditions [108] the OR-RSET violates depending on the coupling near the would-be event horizon: for $\xi \leq \xi_{\rm c}$ the null energy condition is violated and the strong energy condition holds, whereas for $\xi > \xi_{\rm c}$ both the null and strong energy conditions are violated.

6.3.2 Negative asymptotic mass ($M < 0$)

For the sake of completeness, we provide here detailed descriptions of the geometries obtained when Eqs. (6.13, 6.14) are integrated for negative ADM mass. In the classical theory, $M < 0$ corresponds to a naked singularity. In some situations, the semiclassical backreaction can even regularize these singularities. This characteristic is of interest to the study of stellar spacetimes for reasons that will become clear in what follows.

We first address the case $\xi \leq \xi_{\rm c}$. For $M < 0$ we have in virtue of Eq. (6.15) that $h < 1$, $h' > 0$, $f > 1$, and $f' < 0$ asymptotically. By inspection of Eq. (6.13) we observe the RSET contribution (i.e. the terms within brackets) is everywhere negative for $\xi \leq \xi_{\rm c}$. As the equations are integrated inwards, these contributions will decrease, cancelling the $\mathcal{O}(l_{\rm p}^0)$ term, until h reaches a minimum. Afterwards, consistency of Eq. (6.13) indicates that h can only grow inwards until reaching $h = 1$ at $r = 0$, where the resulting solution is described by the expansions (6.18) derived previously (which hold for $M < 0$ as well). On the other hand, f must increase monotonically inwards (since the right hand side of (6.14) is always negative) and it can only reach a finite value at $r = 0$ [again obeying Eq. (6.18)], while h lies always below $h = 1$ for $r > 0$, which would correspond to a maximum.

Near $r = 0$, the expansion of the metric functions (6.18) now enforces $h_2 < 0$ and $f_2 > 0$. Numerical integration of the semiclassical equations is displayed in Fig. 6.1C. This solution has a clear interpretation in terms of the Misner-Sharp mass $m(r) = r\left(1 - h^{-1}\right)/2$ [41, 228], which is negative everywhere. In the classical solution, this mass would be $m(r) = -M$ and would inevitably generate a curvature singularity at $r = 0$. Here, the zero-point energies from the scalar field provide a

(positive) contribution to this negative mass that balances it exactly at $r = 0$. The Ricci scalar is negative and Planckian at $r = 0$.

The semiclassical equations in an order-reduced version accommodate solutions that display whole regions of negative mass that get regularized at $r = 0$ by semiclassical effects. This is a characteristic that semiclassical relativistic stars in a Regularized Polyakov RSET clearly display. These results look appealing in the sense that, if the innermost layers of a semiclassical star with a negative mass interior generate relevant RSETs, these tensors can contribute towards the regularization of such negative mass core thus making the interior geometry entirely regular. Turns out this is precisely what happens in order-reduced semiclassical gravity, and we give a brief glimpse on some preliminary results showing this in Sec. 6.5.

Moving on to the regime where $\xi_{\mathrm{c}} < \xi < 83/300$, we obtain solutions with a similar behavior to that where $\xi \leq \xi_{\mathrm{c}}$ for the h function as in Fig. 6.1C, but the redshift f now has a maximum at some $r > 0$ and reaches a minimum at $r = 0$. This is because the contributions within brackets in (6.14) change sign for $\xi > \xi_{\mathrm{c}}$.

For $\xi > 83/300$ we have a change in the behavior of h. In this case, Eq. (6.13) now ensures that there will be no turning points in h for any r. The function f encounters again a turning point as the term within brackets in Eq. (6.13) is positive. Assuming h vanishes at some radius r_0 as

$$h = h_1(r - r_0) + \mathcal{O}(r - r_0)^2, \tag{6.30}$$

and replacing this equation in Eq. (6.13) yields

$$h_1 = \frac{5l_{\mathrm{P}}^2}{r_0^3}\left(\xi - \frac{83}{300}\right). \tag{6.31}$$

With the expansion (6.31), Eq. (6.14) can be approximated by

$$f' \simeq \chi_1 f\,(r - r_0)^{-1}, \tag{6.32}$$

with

$$\chi_1 = \frac{3\,(\xi - 5/36)}{5\,(\xi - 83/300)}. \tag{6.33}$$

Solving Eq. (6.32) yields

$$f \simeq (r - r_0)^{\chi_1}. \tag{6.34}$$

Finally, the curvature scalar (6.23) diverges at r_0 as

$$R \simeq \frac{(3 - \chi_1)\,\chi_1}{2h_1\,(r - r_0)^3}. \tag{6.35}$$

Figure 6.1D shows a particular example of a solution belonging to this branch. For $\xi > 83/300$, the resulting geometries display a null singularity. Since the ADM mass of the spacetime is negative, this singularity does not have the same physical relevance as the one that appeared in the positive ADM mass case from Fig. 6.1A.

6.4 Accuracy of the OR-RSET

An important aspect at this stage of the analysis is to what extent the solutions to the order-reduced system are good approximations. This question lacks sense in the framework of the RP-RSET as it follows from a dimensional reduction, not a perturbative reduction of order, thus the accuracy of such reduction is not something that we can quantify. However, the order-reduced system under consideration here does proceed from a more close-to-exactness system of semiclassical equations, so we can analyze how well do the order-reduced solutions resemble those from this high-derivative system. We undertake this analysis in what follows.

First, we need to establish criteria that define the "proximity" between solutions to the order-reduced system

$$G^{\mu}_{\nu} = 8\pi\hbar\langle\hat{T}^{\mu}_{\nu}\rangle_{\text{OR}} \tag{6.36}$$

and solutions to the higher-derivative system (1.6). We do so by defining

$$\mathcal{H}^{\mu}_{\nu} = G^{\mu}_{\nu} - 8\pi\hbar\langle\hat{T}^{\mu}_{\nu}\rangle_{\text{AHS}}, \tag{6.37}$$

where G^{μ}_{ν} and $\langle\hat{T}^{\mu}_{\nu}\rangle_{\text{AHS}}$ are calculated replacing the solutions f, h from (6.36), and measuring the size of $\mathcal{H}^{\mu}_{\nu}$. As long as $\mathcal{H}^{\mu}_{\nu} = \mathcal{O}\left(\hbar^2\right)$, the terms $\mathcal{O}\left(\hbar^2\right)$ neglected in the expansions (6.6) will correspond to subdominant contributions. Therefore, the solutions to Eq. (6.36) will amount to perturbative corrections of the solutions to Eq. (6.37), the discrepancy being given by the magnitude of the truncated terms.

We have examined the validity of solutions belonging to the regimes described in Section 6.3 by plotting, in Fig. 6.4, the relative magnitude $\log|\mathcal{H}^{r}_{r}/\langle\hat{T}^{r}_{r}\rangle_{\text{OR}}|$. The choice of the rr component mitigates the error in numerically differentiating the solutions f and h, since the highest-order terms in this quantity are proportional to $f^{(3)}$. Results show that the relative difference between the order-reduced solutions and the higher-order ones approaches a constant value at large distances, indicating that $\mathcal{H}^{r}_{r}$ decreases at the same rate as the component $\langle\hat{T}^{r}_{r}\rangle_{\text{OR}}$, with a relative proportionality constant. The value of this constant is independent of the arbitrary renormalization scale ν appearing in the expressions from Appendix C, Sec. C.1, but the quotient initially increases inwards for $\nu < 1$ and decreases inwards for $\nu > 1$.

This is related to the change in sign of the $\log \nu$ terms appearing in the AHS-RSET. The quotient diverges at spacetime singularities or $r = 0$, and independently of whether the spacetime is singular or regular. In the case of positive ADM mass geometries with $\xi \leq \xi_{\rm c}$, the quotient approaches a divergence at $r_{\rm D}$, precisely where the OR-RSET has dominant non-perturbative contributions. This is consistent with what we would expect from an order-reduced prescription.

6.4.1 Comparison between approximations

As a proxy to the study of more complicated field contents in semiclassical theories, it is customary to consider the propagation of a single massless and minimally coupled scalar field. We have seen that, throughout the years, different approaches to modeling the RSET of minimal scalar fields have been developed [101, 127, 156]. In this thesis we have put special emphasis in the RP-RSET as it is fully analytical and preserves second-order equations of motion. However, this framework has its limitations exploring more elaborate schemes becomes an eventual necessity. Given the difficulties in handling a potentially exact RSET (see Subsec. 1.2.1), most of the approaches involve making approximations. All standard approximations properly capture effects associated with vacuum states (e.g. correct asymptotic values at event horizons and infinity). Preference of one over another depends on the specifics of the problem under consideration.

However, despite their resemblance in what refers to non-local contributions, these approximations differ in their way of estimating purely local, curvature-dependent contributions. The Polyakov approximation lacks information about the behavior of field modes at $r = 0$, which has to be provided by hand (see Subsec. 1.2.2). The AHS-RSET and the OR-RSET, on the other hand, are regular at $r = 0$ (in the first case, under certain parity conditions for the metric, see Appendix C.2), and from this viewpoint can be considered an improvement with respect to Polyakov's approximation. However, the AHS-RSET exhibits the free parameter ν (which accompanies purely local contributions) that affects the sign and magnitude of the RSET components.

Another discrepancy between the Polyakov and OR RSETs is the amount of branches of solutions that they give place to. The introduction of these additional branches is rooted to the differential structure of the RSET. In the Regularized Polyakov approximation we had two branches (2.11), concealed and unconcealed, that are not disconnected from each other as jumps between them take place in the self-consistent vacuum solutions explored in Chapters 2 and 3. In the more elaborate s-wave approximation that incorporates backscattering effects, the solution is also an asymmetric wormhole but the singularity is now timelike [112]

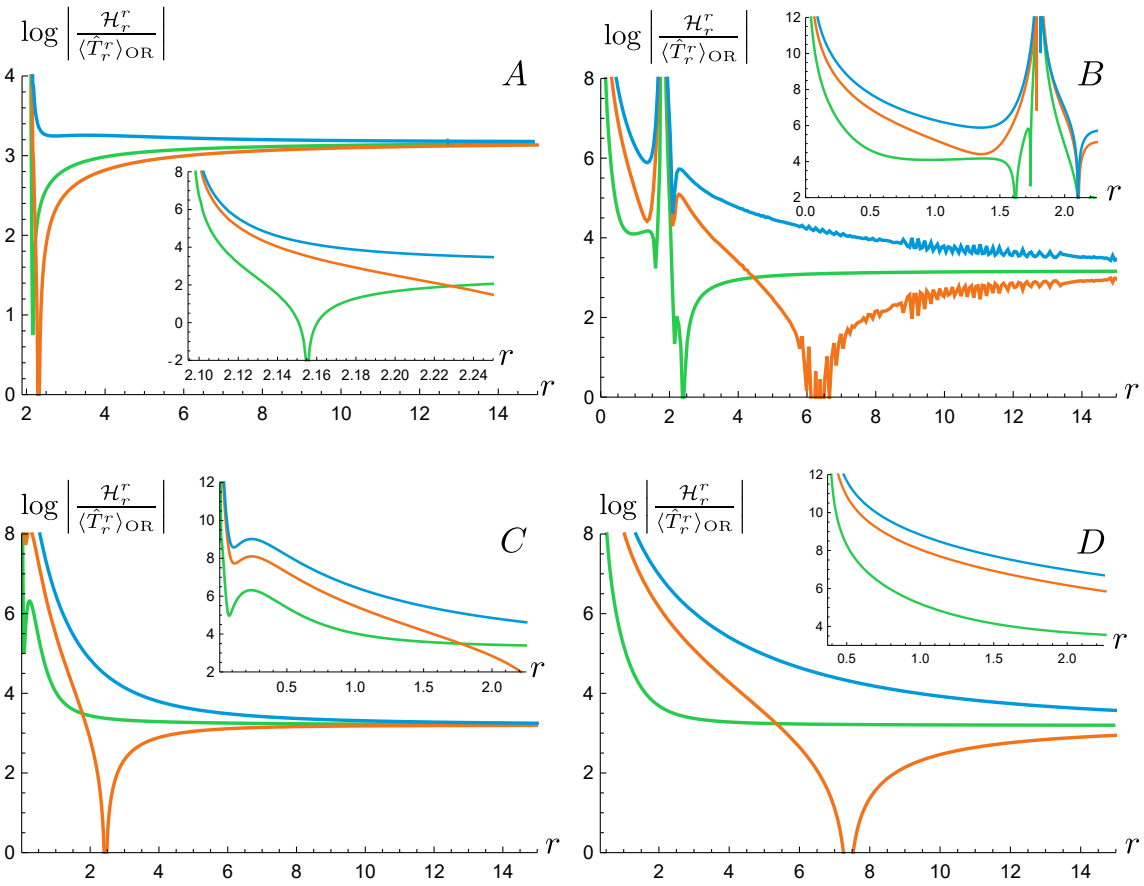

Fig. 6.4.: Plots of $\log|\mathcal{H}^r_r/\langle\hat{T}^r_r\rangle_{\rm OR}|$, a quantity measuring the deviation of the reduced order solutions with respect to the exact solutions to the higher-order semiclassical equations. Panels *A* and *B* correspond to solutions with $M = 1$ and $\xi = \{0, 1\}$, respectively, whereas panels *C* and *D* correspond to solutions with $M = -1$ and $\xi = \{0, 1\}$, respectively. As the AHS-RSET displays a free parameter ν, we set $\nu = \{1, 10^{-5}, 10^{10}\}$ for the green, orange and blue curves (the small oscillatory behavior in panel *B* corresponds to numerical noise). We see that the validity of the solutions is not drastically affected by the value of ν. The validity of these solutions becomes progressively worse as r diminishes, but the mismatch between solutions tends to the constant value $c \simeq 3.17$ in the region of perturbative semiclassical corrections.

(although appears to be at infinite radial distance as well [170]), which enhances the pathological nature of eternal vacuum solutions in semiclassical gravity.

The AHS-RSET also contains numerous branches associated to non-perturbative solutions. The only example we know of a non-perturbative solution to the semiclassical equations sourced by the AHS-RSET is [221], where symmetric wormholes are obtained. These wormholes are not asymptotically flat, hence they cannot be compared with the asymptotically flat spacetimes that we obtained with the Polyakov approximation. On the contrary, the OR-RSET (6.8) cannot introduce non-perturbative branches of solutions as they have been eliminated in the order reduction.

For instance, in the situation in this Chapter, we did not find wormhole solutions of any kind in the $\xi = 0$ case. The geometry instead reaches a timelike (naked) singularity just above where the Schwarzschild radius would have been located (see Figs 6.1A and 6.2). The same can be shown to happen by applying an order reduction to the Polyakov approximation: The resulting vacuum solution would result in a naked curvature singularity without the appearance of a wormhole neck. What these analyses reveal is that the characteristics of self-consistent solutions in regions where non-perturbative effects kick in depends strongly on the physical content of the RSET approximation under consideration and its derivative order. Nonetheless, different approximations to the RSET all lead to static vacuum solutions with positive ADM mass in which the event horizon has been substituted by a singularity of one type or another. See Fig. 2.3 for a comparative between the Penrose diagrams associated to each situation.

Interestingly, the results presented in this thesis suggest that the situation is different when considering the more physical non-vacuum solutions. In Chapter 5 we found semiclassical stellar configurations surpassing the Buchdahl compactness limit [57]. These solutions are all found using just the perturbative (or unconcealed) branch. Next Section contains some preliminary analyses showing that similar solutions are found using an order-reduced version of the AHS-RSET in stellar situations. We take this as an indication that branches of solutions that are not analytic in the $\hbar \to 0$ limit may not be a requisite to access interesting new situations. This idea reinforces the robustness of said solutions, as seemingly unrelated approaches (leading to drastically different RSETs) give rise to similar geometries.

Our philosophy in this thesis is not to argue for a particular approximation scheme as the best one; it is more to put all the possibilities on the table to see what they can offer. By adopting the view that the only trustworthy semiclassical self-consistent solutions are those perturbatively connected to a classical solution, the resulting solutions could turn out not to be very interesting, as these could not

display any new qualitative behaviors. Instead, in this thesis our point of view is more heuristic and closer to the phenomenological philosophy underneath modified theories of gravity: motivating a possible form for some modifications of GR and then analyzing the new equations without caring how these equations might show up hierarchically from an even deeper description of spacetime.

6.5 Stellar equilibrium in order-reduced semiclassical gravity

Let us advance here some results involving classical matter, where the order-reduction method shows some differences. In particular, the analogue of Eqs. (6.7) acquire extra contributions proportional to the classical stress-energy tensor $T^{\rm C}_{\mu\nu}$. At the end of the process we obtain an order-reduced RSET that can be decomposed as

$$\langle\hat{T}^{\mu}_{\nu}\rangle_{\rm MOR} = \langle\hat{T}^{\mu}_{\nu}\rangle_{\rm OR} + \langle\hat{\mathcal{F}}^{\mu}_{\nu}\rangle + \hat{\mathcal{G}}^{\mu}_{\nu}\log\nu, \tag{6.38}$$

where MOR stands for Matter-Order-Reduced. Here, $\langle\hat{\mathcal{F}}^{\mu}_{\nu}\rangle$ (brackets indicate that this term is κ-dependent) and $\hat{\mathcal{G}}^{\mu}_{\nu}$ are functions of the classical SET and vanish together with it. As $\langle\hat{T}^{\mu}_{\nu}\rangle_{\rm OR}$ is covariantly conserved and $\langle\hat{T}^{\mu}_{\nu}\rangle_{\rm MOR}$ is conserved for all ν, we conclude that both $\langle\hat{\mathcal{F}}^{\mu}_{\nu}\rangle$ and $\hat{\mathcal{G}}^{\mu}_{\nu}$ are independently conserved quantities. In particular, $\hat{\mathcal{G}}^{\mu}_{\nu}$ is local and can thus be identified with the ambiguity present in the definition of any proper RSET (which should be unique up to the addition of a local, conserved quantity). The order reduction can be interpreted as a way of partially fixing this ambiguity by selecting one functional form for the quantities $\langle\hat{\mathcal{F}}^{\mu}_{\nu}\rangle$ and $\hat{\mathcal{G}}^{\mu}_{\nu}$ for each classical SET under consideration. There still remains the freedom in the arbitrary parameter ν (absent in the vacuum case) that corresponds to different choices of renormalization length scale. Finally, if the classical SET in (1.6) is regular at $r = 0$, then the corresponding $\langle\hat{T}^{\mu}_{\nu}\rangle_{\rm MOR}$ will be regular as well. This puts the MOR-RSET on equal footing with regularized versions of the Polyakov approximation.

6.5.1 Reducing the order of the AHS-RSET in stars

When a classical SET is present, the reduction of order is slightly more involved than in vacuum, although the logic behind the procedure is the same. We start from

the $\mathcal{O}(\hbar)$ equations equivalent to (6.6), but including a constant-density perfect fluid (4.4), such that

$$\begin{aligned}\frac{h(1-h)-rh'}{h^2r^2} =&-8\pi\rho+\ \mathcal{O}(\hbar),\\ \frac{rf'+f-fh}{fhr^2} =&8\pi p+\ \mathcal{O}(\hbar).\end{aligned} \tag{6.39}$$

Consecutively differentiating the equation for f' will introduce derivatives of p, which can be converted into terms proportional to ρ and p via the conservation relation (4.7). The following relations are obtained

$$\begin{aligned}rh' =&h\left[1+(\Omega-1)\,h\right],\\ r^2h'' =&2h^2\left[2\Omega-1+(\Omega-1)^2\,h\right],\\ r^3h^{(3)} =&2h^2\left[4\Omega+3\,(\Omega-1)\,(3\Omega-1)\,h+3\,(\Omega-1)^3\,h^2\right],\\ r^4h^{(4)} =&8h^2\left[\Omega+\Omega\,(11\Omega-8)\,h+3\,(\Omega-1)^2\,(4\Omega-1)\,h^2+3\,(\Omega-1)^4\,h^3\right],\end{aligned} \tag{6.40}$$

and

$$\begin{aligned}rf' =&-f\left[1-(P+1)\,h\right],\\ 2r^2f'' =&f\left[4+(\Omega+P-4)\,h+(\Omega+P)\,(P+1)\,h^2\right],\\ 4r^3f^{(3)} =&-f\left[24-(\Omega+9P+24)\,h-3\,(\Omega+P)\,(\Omega+3P-2)\,h^2\right.\\ &\left.-3\,(\Omega+P)\,(\Omega-1)\,(P+1)\,h^3\right],\\ 8r^4f^{(4)} =&f\left[192+(7\Omega-57P-192)\,h+(\Omega+P)\,(26\Omega+63P+33)\,h^2\right.\\ &+3\,(\Omega+P)\,(\Omega-1)\,(5\Omega+22P-3)\,h^3\\ &\left.+15\,(\Omega+P)\,(\Omega-1)^2\,(P+1)\,h^4\right],\end{aligned} \tag{6.41}$$

where $P=8\pi r^2p$ and $\Omega=8\pi r^2\rho$.

We can replace relations (6.40) and (6.41) in the AHS-RSET and impose covariant conservation, as we did in Section 6.2, to obtain the MOR-RSET. For simplicity (and to establish a faithful comparative with the RP-RSET), we only include here the expressions of the MOR-RSET in the Boulware vacuum state ($\kappa=0$) and in the minimally coupled case ($\xi=0$). The impact of varying the coupling will be explored elsewhere. The components of the MOR-RSET are

$$23040\pi^2r^4h^2\langle\hat{T}^a_a\rangle_{\text{MOR}}=\mathcal{S}^a_a+\mathcal{T}^a_a\left(\log f+2\log\nu\right) \tag{6.42}$$

with $a=\{t,r,\theta,\varphi\}$ and

$$
\begin{aligned}
\mathcal{S}_t^t =& 249-4\left(17\Omega+63P+105\right)h\\
&+2\left[\Omega\left(117\Omega+188\right)+6P\left(105\Omega+148P+53\right)\right]h^2\\
&-4\left(P+1\right)^2\left(77\Omega+135P-3\right)h^3+33\left(P+1\right)^4h^4,\\
\mathcal{T}_t^t =& \left(\Omega+P\right)\left[60h-30\left(\Omega+13P+4\right)h^2+60\left(P+1\right)^2h^3\right],\\
\mathcal{S}_r^r =& -75-\left(54\Omega+382P-84\right)h\\
&-\left[6\Omega\left(5\Omega+6\right)+4P\left(30\Omega-93P-100\right)-46\right]h^2\\
&+2\left(P+1\right)^2\left(45\Omega+57P-22\right)h^3-11\left(P+1\right)^4h^4,\\
\mathcal{T}_r^r =& \left(\Omega+P\right)\left[66h-6\left(3\Omega+5P+6\right)h^2-30\left(P+1\right)^2h^3\right],\\
\mathcal{S}_\theta^\theta =& 75rfh'-\left\{81rf'-\left[r\left(27\Omega+191P-42\right)h'+75\right]f\right\}h\\
&+\left[6r(22\Omega+16P+21)f'-84f\right]h^2\\
&-\Big\{r\left[\Omega(45\Omega+221)+3P(175\Omega+184P+59)+20\right]f'\\
&-\Big[r(45\Omega+57P-22)(P+1)^2h'-2\left(15\Omega^2+60\Omega P-186P^2+23\right)\Big]f\Big\}h^3,\\
&-\left(P+1\right)\Big\{r\left[45\Omega^2-78\Omega+P\left(46\Omega-63P-128\right)+14\right]f'\\
&+\Big[11r\left(P+1\right)^3h'-4P\left(45\Omega+57P-11\right)-44\Big]f\Big\}h^4\\
&+11\left(P+1\right)^3\left[r\left(\Omega-1\right)f'-\left(3P-1\right)f\right]h^5,\\
\mathcal{T}_\theta^\theta =& \left(\Omega+P\right)\Big(-33rfhh'-15rh^2f'\\
&+3\Big\{5r\left(\Omega+7P+2\right)f'-\Big[5r\left(P+1\right)^2h'+6\Omega+10P\Big]f\Big\}h^3\\
&+15\left(P+1\right)\left[r\left(\Omega-1\right)f'-4Pf\right]h^4\Big).
\end{aligned}
\tag{6.43}
$$

The MOR-RSET is perfectly regular at the center of stellar spacetimes and reduces to the OR-RSET in vacuum ($\Omega=P=0$). Note that this RSET now depends on the arbitrary parameter ν. Although, generally, its value is unconstrained, for constant-density stars there is a way to fix it in terms of the other integration parameters, as we now show. Upon matching the exterior vacuum geometry with the surface of a constant density fluid sphere we need to impose the continuity of the redshift function at the surface (this being a necessary condition for the absence of distributional components in the stress-energy tensor). For constant-density stars, the jump in Ω from $\Omega=0$ to $\Omega=8\pi R^2\rho$ at $r=R$ translates into a discontinuity in $\langle\hat{T}_r^r\rangle_{\text{MOR}}$ at the surface. In turn, Eq. (6.14) causes f' to be discontinuous at $r=R$. In order to have a smooth matching between interior and exterior geometries, this

jump needs to be compensated by a particular choice of renormalization constant ν, which has to obey

$$\log \nu = -\log f(R) + \frac{h(R)\left(15h(R) - 5\Omega(R) - 6\right) - 9}{2\left[h(R)\left(5h(R) + 3\Omega(R) + 6\right) - 11\right]}. \tag{6.44}$$

Notice that this fixing of ν is a consequence of the choice of equation of state for the classical sector. Imposing another equation of state that satisfies $\Omega(R) = P(R) = 0$ would leave ν unconstrained.

6.5.2 Stellar solutions

Having derived an analytical RSET which fulfills all the properties to be used in stellar spacetimes, we proceed to integrate the order-reduced semiclassical equations searching for regular stars that surpass the Buchdahl limit. Note that, since we are assuming minimal coupling and absence of matter shells at the surface fixes the value of ν (6.44), the MOR-RSET is uniquely determined and is less ambiguous than the RP-RSET, which was unique up to an arbitrary radial function.

We numerically integrate the vacuum equations with $\xi = 0$ from an asymptotically flat region inwards for some positive ADM mass, obtaining the spacetime depicted in Fig. 6.1A. At some radius $R > r_{\rm D}$ we locate the surface of a fluid sphere with surface compactness $C_{\rm R}$ and fix ν via relation (6.44). The only free parameter left is the dimensionless energy density $\Omega(R)$, which we vary through several orders of magnitude seeking for solutions that are regular up to the center of the star (in practice, we consider that the integration reaches a regular center when r becomes five orders of magnitude smaller than R).

We present here a few integrations of the semiclassical equations and summarize the general properties of the corresponding solutions to establish a connection with the results from Chapter 5. Figures 6.5 and 6.6 show the Misner-Sharp mass and classical pressures of stars that approach and surpass the Buchdahl limit. These stars are perfectly regular and are characterized by a large interior region where the Misner-Sharp mass is negative and by classical pressures that grow inwards. As we increase the surface compactness, their negative mass interior grows in size (and mass becomes more negative), counterbalancing the gravitational pull of the object. Contrarily to the situation with the RP-RSET, for each R and $C_{\rm R}$ there is a broad range of densities $\Omega(R)$ that return critical, strictly regular solutions. By increasing $\Omega(R)$, we obtain stars where pressure has a local minimum at $r = 0$ after reaching a global maximum at some radius $r > 0$. The components of the MOR-RSET are shown in Figs. 6.7, 6.8 and 6.9. The semiclassical energy density

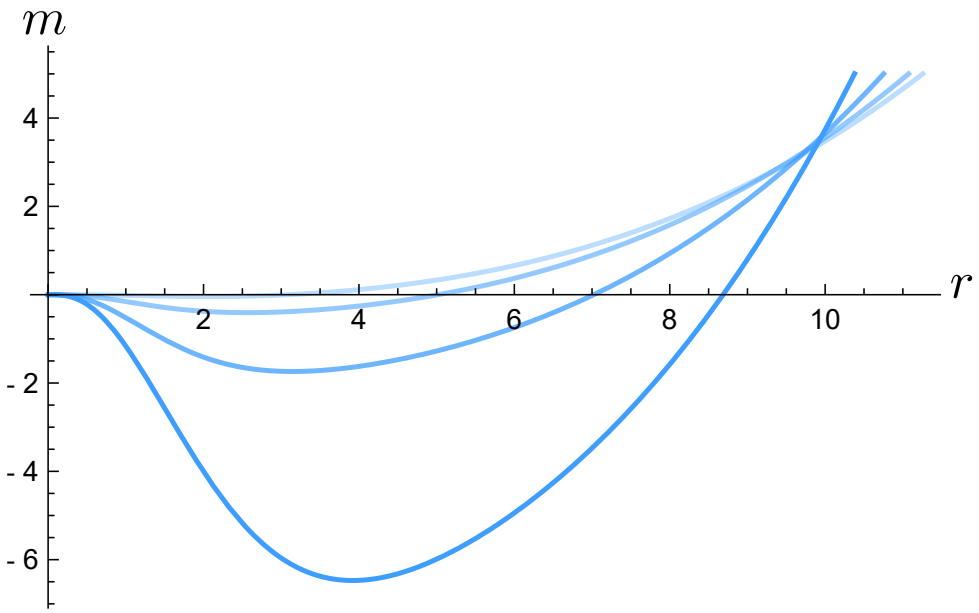

Fig. 6.5.: Plots of the Misner-Sharp mass of semiclassical stars sourced by the MOR-RSET with $M_{\rm R} = 5$ and, from lighter to darker, $C_{\rm R} \simeq \{0.89, 0.9, 0.93, 0.96\}$ and $\Omega(R) = \{0.24, 0.27, 0.36, 0.67\}$. The mass becomes more negative in the interior as $C_{\rm R}$ is increased.

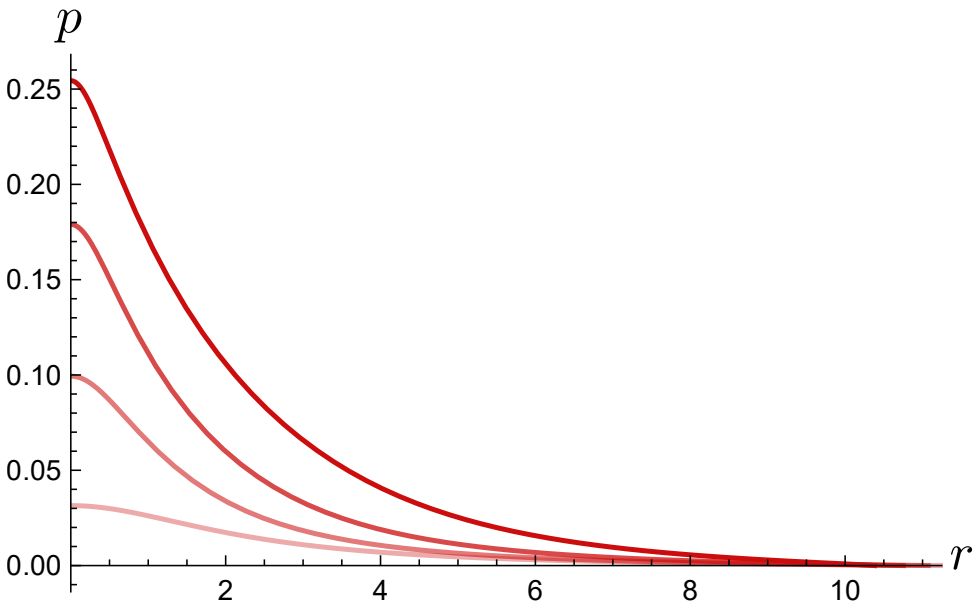

Fig. 6.6.: Plots of the classical pressure of semiclassical stars sourced by the MOR-RSET with $M_{\rm R} = 5$ and, from lighter to darker shades, $C_{\rm R} \simeq \{0.89, 0.9, 0.93, 0.96\}$ and $\Omega(R) = \{0.24, 0.27, 0.36, 0.67\}$. Central pressures increase with $C_{\rm R}$.

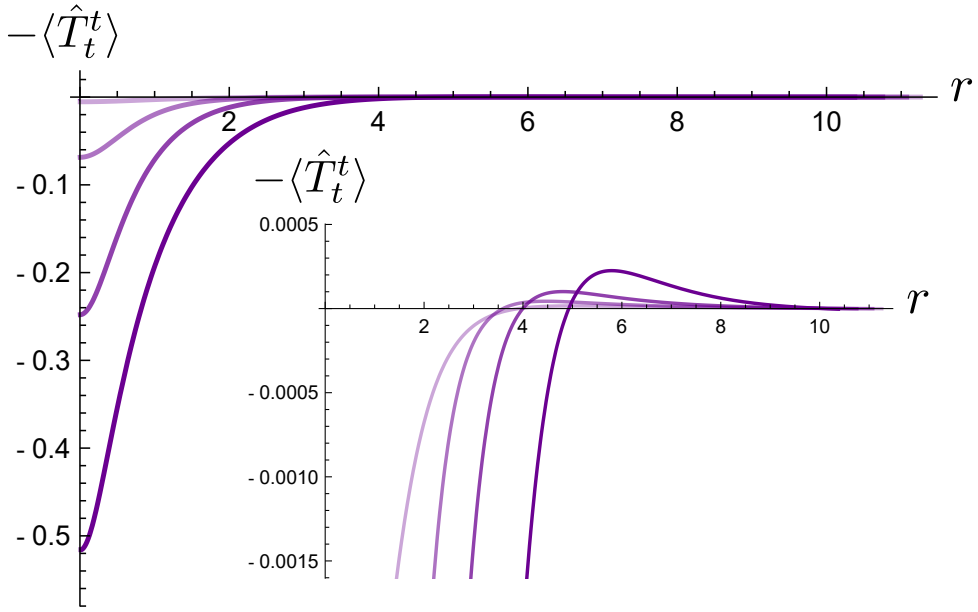

Fig. 6.7.: Semiclassical energy density of stars with $M_{\rm R} = 5$ and, from lighter to darker shades, $C_{\rm R} \simeq \{0.89, 0.9, 0.93, 0.96\}$ and $\Omega(R) = \{0.24, 0.27, 0.36, 0.67\}$. The energy density at the center is negative and one order of magnitude larger than the radial and angular pressures. In the central regions of the star, the total energy density decreases inwards, allowing to surpass the Buchdahl limit.

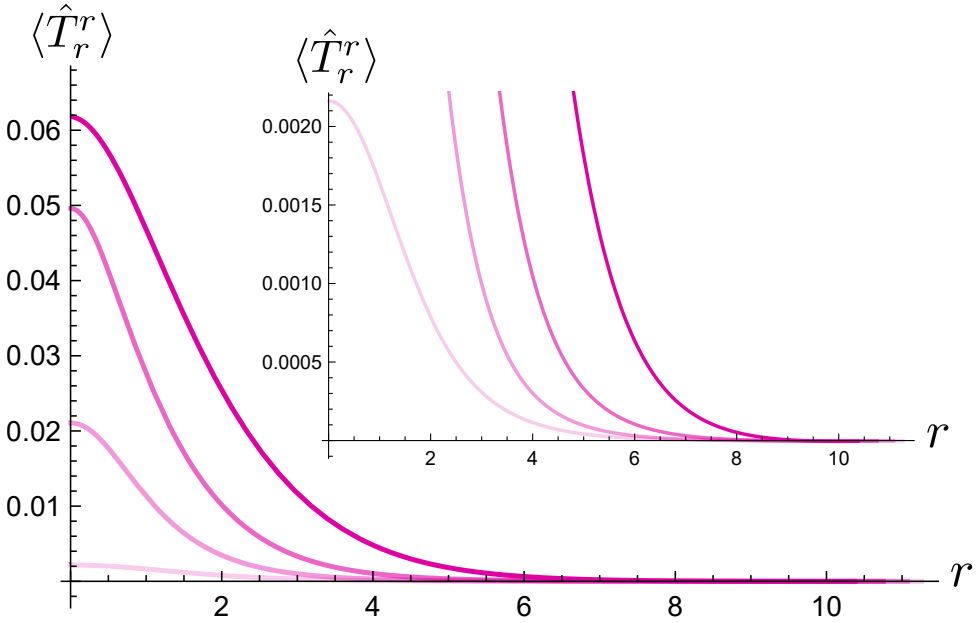

Fig. 6.8.: Semiclassical radial pressure of stars with $M_{\rm R} = 5$ and, from lighter to darker shades, $C_{\rm R} \simeq \{0.89, 0.9, 0.93, 0.96\}$ and $\Omega(R) = \{0.24, 0.27, 0.36, 0.67\}$. The semiclassical radial pressure behaves similarly to the classical one, increasing with the compactness.

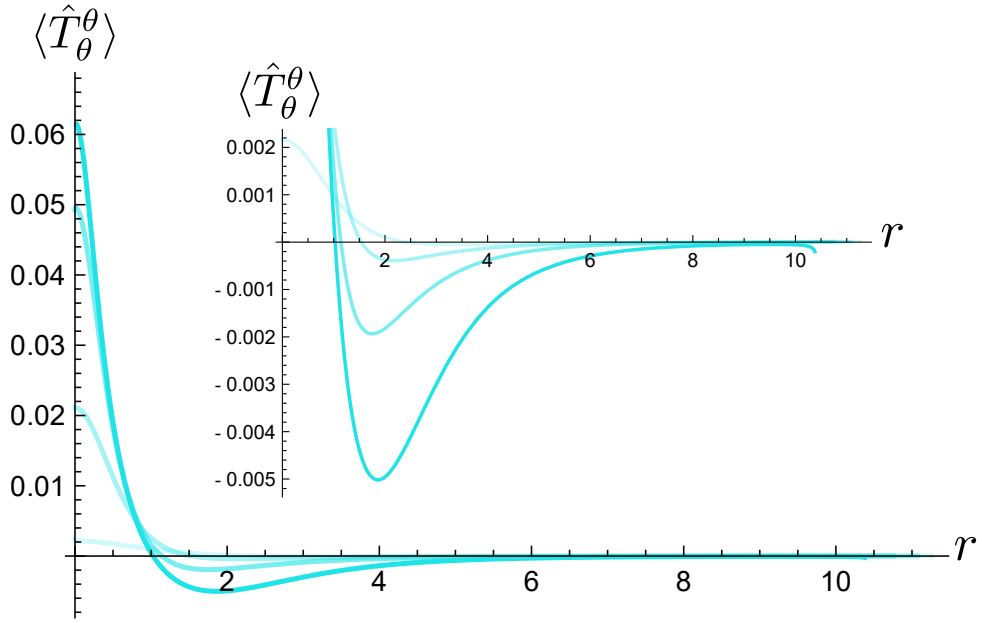

Fig. 6.9.: Semiclassical angular pressure of stars with $M_{\rm R} = 5$ and, from lighter to darker shades, $C_{\rm R} \simeq \{0.89, 0.9, 0.93, 0.96\}$ and $\Omega(R) = \{0.24, 0.27, 0.36, 0.67\}$. While classical pressure is isotropic, semiclassical angular pressure is negative in a large portion of the bulk of the star but becomes positive as the center, where it needs to match the radial pressure for regularity.

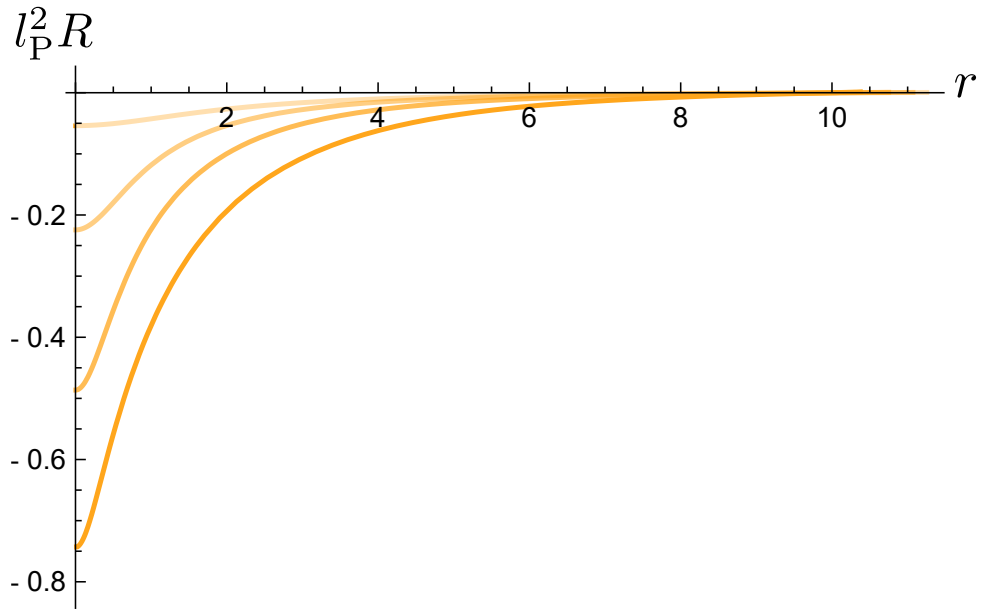

Fig. 6.10.: Ricci scalar of semiclassical stars sourced by the MOR-RSET with $M_{\rm R} = 5$ and, from lighter to darker shades, $C_{\rm R} \simeq \{0.89, 0.9, 0.93, 0.96\}$ and $\Omega(R) = \{0.24, 0.27, 0.36, 0.67\}$. The magnitude of the Ricci scalar at $r = 0$ increases with $C_{\rm R}$.

has a similar behavior to that of the RP-RSET in semiclassical stars: positive in the bulk of the star and negative and large at the center, changing sign in between. Finally, Figure 6.10 shows the Ricci scalar at the interior, which approaches but does not surpass Planckian values.

Perturbative reduction of order eliminates non-perturbative branches of solutions, which the RP-RSET, on the contrary, introduces. We find remarkable that semiclassical stars exist regardless of the presence of these branches. This suggests the existence of universal features that are captured by all analytical RSET approximations. Results presented in this thesis only apply to massless, minimally coupled fields, but we will explore more general properties of semiclassical stars and the effect that varying the coupling ξ have on them in the future.

6.6 Conclusions

In this Chapter we have addressed the problem of semiclassical backreaction by reducing the order of the semiclassical equations in spherically symmetric vacuum and stellar situations. If said equations were tackled in full glory (with the AHS-RSET as source), solving them self-consistently would prove to be an extremely time consuming task due to their large space of solutions. In addition, there is no definite method for disregarding solutions based solely on their physical consistency.

Inspired by previous works in the literature [144], we have developed a procedure for obtaining regular, order-reduced RSET approximations that satisfy all the properties expected from a suitable RSET. We used this procedure to find the solutions to the semiclassical equations in vacuum. The results here obtained are consistent with our analyses from Chapter 2 that made use of the CRP-RSET in the region where semiclassical corrections are perturbative and the case $\xi = 0$. In the region in which the semiclassical corrections are non-perturbative these approaches agree in the fact that the event horizon is replaced by a curvature singularity.

For completion, we have analyzed what happens for other couplings in vacuum. When the coupling is increased beyond its separatrix value $\xi_c = 11/60$ the spacetime becomes regular and horizonless. However, curvature invariants become Planckian inside the region where the classical event horizon would have been located. For negative values of the ADM mass, there are both regular and irregular spacetimes depending on ξ. The regular ones could resemble the innermost regions of semiclassical relativistic stars that display negative-mass interiors generated by the effects of quantum vacuum polarization.

Following the procedure outlined in Sec. 6.2, it is possible to obtain order-reduced RSETs in various situations. The most straightforward extensions of this

method would imply adding a classical electromagnetic field and/or a cosmological constant. In doing so, the validity of the very same AHS-RSET (from which the OR-RSET is constructed) requires careful evaluation [127]. Ideally, any application of the AHS-RSET (or its order-reduced counterpart) should come along with a detailed analysis of the complete RSET incorporating the numerical part $\langle \hat{T}^{\mu}_{\nu} \rangle_{\text{num}}$, but this is technically challenging and escapes the scope of this thesis.

The reduction of order that we have followed here is maximal in the sense that it eliminates all additional branches of solutions. However, a window remains open for the construction of partially order-reduced RSETs that, while yielding second-order equations of motion, still retain terms proportional to f', h', f'' and h'', in a similar fashion to the RP-RSET (1.14). Is it possible to find a way to reduce the order of the AHS-RSET while retaining "physically meaningful" branches of solutions? If so, how would this affect singularities? While the non-perturbative characteristics revealed in vacuum solutions would be modified significantly, solutions that involve regular fluid spheres are more robust as the additional branches are not explored.

Before turning to the Conclusions of this thesis, we have provided details about the forthcoming analysis of semiclassical solutions incorporating a classical perfect fluid. We have derived an order-reduced RSET approximation valid for constant-density stars and analyzed its backreaction in the case $\xi = 0$. The result is a whole family of semiclassical stellar configurations that surpass the Buchdahl limit and which resemble qualitatively the ones found in Chapter 5 through the RP-RSET. While more general characteristics of these fluid spheres are distilled, we presented some preliminary results to exemplify this point. The fact that different modelings of the semiclassical equations end up describing similar physical scenarios provides considerable robustness to semiclassical analyses.

7

Conclusion

> *How could the invisible return to being visible?*
>
> — **Roberto Calasso**
> The celestial hunter

We are entering a revolutionary era for gravitational physics thanks to gravitational-wave astronomy and observations with the Event Horizon Telescope. In this exciting context, we expect future observations to allow to test general relativity with unprecedented precision. This will open a window towards exploring the structure of ABHs at scales gradually closer to their supposed event horizons [25]. Thus, if an astrophysically explorable surface is present instead of the event horizon, it might leave some observational imprint noticeable in future gravitational-wave [28, 229] (even electromagnetic [30]) observations.

Efforts to confront the GR BH paradigm are becoming increasingly common, mainly because the pathological features of the BH paradigm beg exploring alternative routes. The absence of long-lived event horizons would entail that BHs exist in our universe only as ephemeral objects, fated to disappear as matter relaxes towards a horizonless object [230]. While we await progress in this direction, a complementary approach is to search for equilibrium configurations that can describe such horizonless end-states. We have found, to the date of the writing of this thesis, the strongest theoretical evidence yet for the existence of ultracompact stars that can serve as alternatives to GR BHs without the need for new physics beyond the effects of quantum vacuum polarization.

Advances of this thesis

In classical GR, the Schwarzschild BH is identified as the late-time outcome of spherically symmetric gravitational collapse, long after all matter has disappeared behind the event horizon and the BH has radiated away all its multipole moments. Being the most conservative theory that incorporates quantum effects, the self-consistent counterparts to GR vacuum solutions from semiclassical gravity should admit a similar interpretation. In this thesis we have obtained geometries incorporating the

backreaction of the zero-point energies of a quantum scalar field, also known as vacuum polarization effects. These contributions are captured by the RSET, which we have modeled in two separate ways: via a dimensional reduction (RP-RSET), and through a perturbative reduction of order (OR/MOR-RSETs). Both methods return RSETs that are analytical, regular, and of second order in the derivatives of the metric. Under the assumptions of staticity and asymptotic flatness, the natural vacuum state for the quantum field is the Boulware vacuum. This state is manifestly singular at event horizons, this singularity translating into a divergent RSET. In vacuum, its corresponding backreaction over the background spacetime causes the event horizon to disappear, being replaced by a wormhole neck connecting to a null curvature singularity in the RP-RSET approximation (see Chapters 2 and 3), and by a naked curvature singularity in the OR-RSET approximation (Chapter 6). The case for extremal BHs is even subtler, as their extremal horizon is transformed into a curvature singularity itself (Sec. 3.5). The absence of static event horizons in semiclassical gravity has been confirmed via other RSET approximations as well [112, 168, 170, 192, 218], showing that it is a generic feature of semiclassical gravity. From our investigations we conclude, on the one hand, that the only horizons consistent with semiclassical physics are evaporative and dynamic. On the other hand, we evidence that the static vacuum counterparts are inadequate to faithfully describe the end-states of gravitational collapse due to their singularities. In consequence, we turned to explore the viability of spherical distributions of matter in equilibrium supported by quantum vacuum polarization.

Vacuum polarization provides the repulsive effects necessary to preserve hydrostatic equilibrium in situations where classical matter alone is fated to collapse under its own gravity. These effects translate into potential violations of one or several of the assumptions behind the Buchdahl theorem [57]. These are: The assumption of a Schwarzschild exterior, the presence of large anisotropies in the pressure, and a total energy density that decreases towards the innermost layers of the star (see Sec. 1.3). These conditions are saturated by a perfect fluid obeying the constant-density equation of state. Under this simple choice for the classical matter sector, we explored, in Chapter 4, the complete space of semiclassical stellar solutions (see Fig. 4.6) modeling the semiclassical sector via the CRP-RSET. By comparing with its classical counterpart, we found striking differences in the semiclassical space of solutions, namely in the so-called ϵ-*strict* stellar spacetimes. These are stars whose compactness can be arbitrarily large while having arbitrarily-small mass within a central sphere of Planckian radius. These configurations are possible thank to the backreaction of the CRP-RSET which, despite unable to generate regular stars surpassing the Buchdahl limit, misses the shot only slightly. These findings motivated exploring alternative regularizations of the RP-RSET in Chapter 5 and

led to the central result of this thesis: We discovered whole families of RP-RSETs that allow for the existence of regular stars that surpass the Buchdahl limit.

These so-called semiclassical relativistic stars exhibit generic properties that are independent from the specific regularization of the RP-RSET, and are also reproduced via the MOR-RSET from Ch. 6. They are composed by a combination of classical and quantum matter and exhibit negative mass interiors with redshift functions that become minimum at the center. Our semiclassical relativistic stars are the first exact model of exotic compact object in a semiclassical theory of gravity. Remarkably, their surface compactness can take any value between 0 and 1 (see the family of solutions depicted in Fig. 1.1). Upon surpassing the Buchdahl limit, a drastic change of regime occurs in the RSET (confirmed to exist also for conformally invariant fields [167]). The specific formation mechanism responsible for these objects remains an open subject, but the fact that they are not isolated in the space of solutions is an appealing characteristic that differentiates semiclassical relativistic stars from other BH mimickers in the literature [91–93, 231–234].

Future topics

The analyses presented in this thesis delve into previously unexplored terrain and are unveiling a surprisingly rich field of study: stellar equilibrium in semiclassical gravity. Our investigations can serve as the bedrock for future studies, some of which we briefly summarize here.

One possibility is generalizing the semiclassical star proposal to situations where the classical and semiclassical matter are modeled in different ways [86, 213, 214]. Regarding the RSET, the approach of reducing the order of the AHS-RSET seems the way to go for future studies as it is regular at $r = 0$ by construction and allows to explore the effect of non-minimally coupled fields. There is an analogous analytical approximation for spin $1/2$ fields that could be subjected to a similar procedure [235]. Constructing analytical RSETs from the trace anomaly [168] appears a promising alternative as well. Regarding the classical SET, the constant-density equation of state is a convenient toy model due to its simplicity, but it amounts to an idealized description of the behavior of ordinary matter at high densities. Exploring other equations of state and obtaining their associated MOR-RSETs that they generate would allow to probe how generic are the results presented in this thesis, in particular regarding the absence of upper compactness bounds [164] in semiclassical gravity.

At the time of the writing of this thesis there exist no results for the exact RSET of non-conformally-invariant scalar fields in the interior of relativistic stars [166]. Therefore, we have no way of estimating the accuracy of the RP- and MOR-RSETs

with respect to their exact counterparts. Recently developed regularization and efficient numerical methods to compute the RSET [236, 237] can be applied to simple stellar models, not only to evaluate the accuracy of analytical RSET approximations, but to know the precise way quantum corrections diverge at the Buchdahl limit (without requiring additional simplifications), in the aim of analyzing their implications on stellar equilibrium.

The various stellar models we have derived in this thesis (the exact solutions and analytical fits from Chapter 5 and the exact solutions to the order-reduced semiclassical equations from Chapter 6) can be subjected to phenomenological studies, such as analyzing the propagation of classical fields over their spacetimes. As shown in the diagram 1.1, semiclassical stars can display an outer light ring. Hence, propagating fields will bounce at the stellar center [70] and at the photon sphere, producing echoing patterns in the amplitude of fields. The form and periodicity of these echoes relate to the time a signal needs to escape the object and to the particular scaling of the associated time scale with the compactness. On a related front, analyzing the stability of semiclassical stars under (spherical) adiabatic perturbations [238] requires time-dependent equations of motion. The RP-RSET could provide such framework, but the regularization procedure followed in this thesis cannot be generalized to non-static situations [145] in a covariant way. The AHS-RSET is valid in static spacetimes only, so addressing this point goes beyond our current capabilities.

Another crucial aspect for future consideration is the formation mechanisms behind semiclassical stars. If we acknowledge that, at the early stages of gravitational collapse, matter crosses its own gravitational radius following nearly a free-falling trajectory, then in which ways can the trapped region evolve to allow the formation of a horizonless object? The most likely scenario is that the collapsing star overcomes some bouncing process that expels it outwards. These bounces can be modeled in GR and modified theories of gravity [217, 239–241], but they also are predicted in the framework of effective quantum-gravitational theories [242, 243] and within semiclassical gravity itself [115, 116], where the backreaction of the Polyakov RSET around inner horizons can drive them into an expansive phase. This initially expanding tendency, if extrapolated, would imply the inner horizon meets the outer one in a timescale of the order of the BH mass. Even in the plausible case that semiclassical gravity was unable, in the end, of providing a fully self-consistent description of a regular collapse towards a horizonless object, it strongly suggests that trapped regions may evaporate faster than the timescales associated to Hawking evaporation. Semiclassical stars may lie at the very end of this chain of events.

Finally, the generalization of these results to stationary and axisymmetric configurations should be eventually considered. In absence of an axisymmetric version of Birkhoff's theorem, spinning stars can show significant deviations from the Kerr spacetime [244], although quality factors based on curvature invariants allow to parametrize them [245]. As for QFTCS, the main obstruction is to derive the RSET in spinning spacetimes, with the notable exceptions of the BTZ BH [246], the RSET of massless, minimally coupled scalars in the Unruh state in Kerr BHs [247] and its flux components at inner horizons [139]. Generic results via subtraction of unrenormalized expectation values have been derived [248–250]. There are exciting new discoveries ahead for quantum field theory in BHs.

Concluding remarks

Due to its nonlinear character, the theory of general relativity conceals a distinctive complexity even within its simplest solutions. According to general relativity, black holes are essentially vacuum objects whose extreme degeneracy makes them describable in terms only of their mass, charge, and angular momentum. Their event horizons make black holes the ultimate black box: The knowledge we acquire through their gravitational interaction with their environments reveals no information about their internal structure, which remains hidden to us.

It is precisely behind these dark curtains, in their innermost regions, where quantum gravitational effects come at play. Current endeavors to derive a satisfactory and consistent theory of quantum gravity depict black holes as purely gravitational objects, in which quantum fields (other than the gravitational field itself) play no significant role aside from being responsible for Hawking radiation. We believe, on the contrary, that the material content of spacetime is indeed relevant for describing both astrophysical black holes and the formation mechanisms leading to them. Within the framework of semiclassical gravity, we showed that quantum vacuum polarization gives rise to horizonless semiclassical stars that are drastically distinct from the standard evaporating BHs, opening a slit for probing their interiors through gravitational waves and other astrophysical probes.

Semiclassical stars have much more complex structures than the vacuum, bald black holes from Einstein's general relativity. This complexity is what gives a physical origin to their observed mass, which results from the balanced combination of classical and quantum contributions. In view of this, the troublesome information paradox would cease to exist as their regular interiors are in causal contact with the outside universe. The implications that might follow from these explorations in semiclassical physics are difficult to foresee but appear to us as an unmissable thread.

A

Renormalized stress-energy tensor in four dimensions

In this Appendix we outline the main characteristics of the Hadamard regularization method [126] to derive the RSET of a scalar field with arbitrary mass and Ricci coupling in static, spherically symmetric spacetimes. The technicalities of the method applied to a variety of black-hole spacetimes are detailed in the literature (see [130, 131, 251] and references therein) and we avoid them here.

The unrenormalized stress-energy tensor

The action for a scalar field Φ on $3+1$ dimensions is

$$S = -\frac{\sqrt{-g}}{2}\int d^4x \left[g^{\mu\nu}\Phi_{,\mu}\Phi_{,\nu} + \left(m^2 + \xi R\right)\Phi^2\right], \tag{A.1}$$

where g denotes the determinant of $g_{\mu\nu}$ and the coma denotes a partial derivative. Constants m and ξ are the mass and coupling of the field, respectively. Variation of the action with respect to the scalar field Φ yields the equation of motion

$$\frac{\delta S}{\delta \Phi} = \left(\Box - m^2 - \xi R\right)\Phi = 0, \tag{A.2}$$

where $\Box = g^{\mu\nu}\nabla_\mu\nabla_\nu$. The stress-energy tensor is defined by the relation

$$\begin{aligned} T^{\mu\nu} = \; 2\frac{\delta S}{\delta g_{\mu\nu}} &= (1-2\xi)\,\Phi^{;\mu}\Phi^{;\nu} + \left(2\xi - \frac{1}{2}\right) g^{\mu\nu}\Phi_{;\alpha}\Phi^{;\alpha} - 2\xi\Phi\Phi^{;\mu\nu} \\ &\quad + 2\xi g^{\mu\nu}\Phi\Box\Phi + \xi\left(R^{\mu\nu} - \frac{1}{2}Rg^{\mu\nu}\right)\Phi^2 - \frac{m^2}{2}g^{\mu\nu}\Phi^2, \end{aligned} \tag{A.3}$$

where the semicolons denote covariant derivatives. This object becomes ill-defined after the scalar field Φ is canonically quantized (see [33, 34] for details on this procedure). In physical terms, this singularity is caused by the ultraviolet modes of the field that give an infinite contribution to the "unregularized" SET, as SETs are purely local quantities that must be evaluated at a single spacetime point.

In static spherically symmetric spacetimes described by the line element (6.4) we can derive the renormalized expression for (A.3) in a closed form. This derivation was first carried out by Anderson, Hiscock and Samuel [127] relying on the metric (6.4) being Wick-rotated to its Euclidean form

$$ds^2 = f(r)d\tau + h(r)dr^2 + r^2 d\Omega^2 \tag{A.4}$$

where $\tau = it$. The Fourier-transformed version of (A.2) in the Euclidean space satisfies

$$\left(\Box - m^2 - \xi R\right) G_{\rm E}(x, x') = -\frac{\delta^4(x, x')}{\sqrt{g}} \tag{A.5}$$

with $x = (\tau, r, \theta, \phi)$. In the Euclidean metric, $\Box$ is now an elliptic operator and it has a well defined inverse. $G_{\rm E}(x.x')$ is the Euclidean propagator.

The singular structure of the unrenormalized SET comes clear from the fact that (A.3) can be written as the coincidence limit of the action of a differential operator acting upon the Euclidean propagator [126],

$$\langle \hat{T}^{\mu\nu} \rangle_{\rm ren} = {\rm Re}\left[\lim_{x \to x'} \mathcal{D}^{\mu\nu} G_{\rm E}\left(x, x'\right)\right], \tag{A.6}$$

where Re denotes the real part and the differential operator

$$\begin{aligned} \mathcal{D}^{\mu\nu} = &\left(1 - 2\xi\right) g^{\nu}_{\nu'} \nabla^{\mu} \nabla^{\nu'} + \left(2\xi - \frac{1}{2}\right) g^{\mu\nu} g^{\alpha}_{\alpha'} \nabla^{\alpha'} \nabla_{\alpha} - 2\xi \nabla^{\mu} \nabla^{\nu} \\ &+ 2\xi g^{\mu\nu} \nabla_{\alpha} \nabla^{\alpha} + \xi \left(R^{\mu\nu} - \frac{1}{2} R g^{\mu\nu}\right) - \frac{1}{2} m^2 g^{\mu\nu} \end{aligned} \tag{A.7}$$

acting on $G_{\rm E}$ reduces to Eq. (A.3) in the coincidence limit $x \to x'$. Here, $g^{\nu'}_{\nu}$ denote the bivectors of geodesic parallel transport which parallel transport along a geodesic the objects upon which they act.

The Hadamard parametrix

Whereas $G_{\rm E}(x, x')$ only makes sense as a bivalued distribution, that is, acting upon points x and x' separated in spacetime, we need to evaluate this object and its derivatives in the coincidence limit in order to construct a SET operator. Operators constructed naively this way diverge in the coincidence limit, and this divergence is inherited from the singular structure that characterizes the Euclidean propagator. Fortunately, the local singular structure of all the divergences appearing in the Euclidean propagator has been well-known for a long time [252, 253]. In

four dimension the Euclidean Green's function possesses the following singularity structure,

$$G_{\text{Esing}}(x,x') = \frac{1}{8\pi^2}\left[\frac{\Delta^{1/2}(x,x')}{\sigma(x,x')} + V(x,x')\log\sigma(x,x') + W(x,x')\right]. \qquad \text{(A.8)}$$

In this expression, $2\sigma(x,x')$ denotes the square of the geodesic distance between x and x' [254], the term $\Delta^{1/2}(x,x')$ is the biscalar form of the VanVleck-Morette determinant [128], $V(x,x')$ is the tail term of the Hadamard parametrix [255] and $W(x,x')$ a biscalar that encodes all the information about the state. These scalars admit covariant Taylor expansions in powers of σ (the reader can find the pertinent expressions in [126, 128]).

The logic behind the stress-tensor regularization via the Hadamard form is similar to the point-splitting regularization method developed by Christensen [123]. This regularization consists in expressing the singular part of the propagator and/or SET in a form suitable for direct subtraction from the corresponding unrenormalized expressions. Whereas the covariant Taylor expansion of the Hadamard form (A.8) is done in every spacetime direction, subtractions are performed in the partial coincidence limit where the separation is only in the t coordinate. This separation is naturally adapted to the staticity of the spacetime, but in general it is not obvious which is the separation that most simplifies subtracting divergences. For example, the Hadamard renormalization of the RSET at horizons requires taking a partial coincidence limit that leaves a separation in the r direction [130, 251].

Euclidean propagator

Before the subtraction of counterterms can be attempted, we first need to rearrange the Euclidean propagator and all the terms involving parallel transport bivectors and covariant derivatives of G_{E} as sums over the wave modes of the homogeneous radial equation that follows from (A.2) after decomposing the scalar field in spherical harmonics [see Eq. (B.1)]. After some algebra, it is possible to express the propagator as

$$G_{\text{E}}(x,x') = \int d\tilde{\mu}\cos\left[\omega\left(\tau-\tau'\right)\right]\sum_{l=0}^{\infty}\left(2l+1\right)P_l\left(\cos\gamma\right)C_{\omega l}p_{\omega l}(r_<)q_{\omega l}(r_>), \qquad \text{(A.9)}$$

where, depending on the temperature T of the state we have

$$\begin{aligned}\int d\hat{\mu}F(\omega) &\equiv \frac{1}{4\pi^2}\int_0^\infty d\omega F(\omega), \quad T=0 \\ &\equiv \frac{\kappa}{4\pi^2}\sum_{n=1}^{\infty}F(\omega)+\frac{\kappa}{8\pi^2}F(0), \quad T>0,\end{aligned} \tag{A.10}$$

where $\kappa = 2\pi T$. In Eq. (A.9), P_l is a Legendre Polynomial and

$$\cos\gamma \equiv \cos\theta\cos\theta' + \sin\theta\sin\theta'\cos(\phi-\phi'). \tag{A.11}$$

The modes $p_{\omega l}$ and $q_{\omega l}$ are the linearly-independent solutions ($p_{\omega l}$ and $p_{\omega l}$ being regular at the lower and upper limits of the integration region, respectively) to the homogeneous radial equation

$$\frac{1}{h}\frac{d^2S}{dr^2}+\left[\frac{2}{rh}+\frac{1}{2fh}\frac{df}{dr}-\frac{1}{2h^2}\frac{dh}{dr}\right]\frac{dS}{dr}-\left[\frac{n^2\kappa^2}{f}+\frac{l(l+1)}{r^2}+m^2+\xi R\right]S=0. \tag{A.12}$$

The constant $C_{\omega l}$ obeys the Wronskian condition

$$C_{nl}\left[p_{nl}\frac{dq_{nl}}{dr}-q_{nl}\frac{dp_{nl}}{dr}\right]=-\frac{1}{r^2}\left(\frac{h}{f}\right)^{1/2}. \tag{A.13}$$

In selecting the states upon which the RSET is evaluated, we consider only those whose singularity structure is of the Hadamard form. This is the Hadamard condition [256] that makes possible to covariantly subtract divergences to bivalued tensors that are ill-defined in the coincidence limit.

Hadamard regularization

The RSET can be expressed in terms of the Euclidean propagator and its derivatives [131]

$$\begin{aligned}\langle\hat{T}^{\mu}_{\nu}\rangle_{\text{ren}} =& 2\left(\frac{1}{2}-\xi\right)\left[g^{\mu\nu'}G_{\text{E}}(x,x')_{;\nu\nu'}\right]_{\text{ren}}+\left(2\xi-\frac{1}{2}\right)\left[g^{\alpha\beta'}G_{\text{E}}(x,x')_{;\alpha\beta'}\right]_{\text{ren}} \\ &-2\xi\left[g^{\mu\nu}G_{\text{E}}(x,x')_{;\mu\nu}\right]_{\text{ren}}+2\xi\left[g^{\alpha\beta}G_{\text{E}}(x,x')_{;\alpha\beta}\right]_{\text{ren}} \\ &+\xi\left(R^{\mu}_{\nu}-\frac{1}{2}R\right)\left[G_{\text{E}}(x,x')\right]_{\text{ren}}-\frac{m^2}{2}\left[G_{\text{E}}(x,x')\right]_{\text{ren}}+\frac{2v_1}{8\pi^2}+\mathcal{M}^{\mu}_{\nu},\end{aligned} \tag{A.14}$$

with

$$\mathcal{M}^{\mu}_{\nu}=\frac{m^2}{16\pi^2}\left\{\left(\xi-\frac{1}{6}\right)\left(R^{\mu}_{\nu}-\frac{1}{2}R\right)-\frac{3}{8}m^2\right\} \tag{A.15}$$

and

$$v_1 = \frac{1}{720}\left(R_{\mu\nu\rho\sigma}R^{\mu\nu\rho\sigma}\right) - \frac{1}{24}\left(\xi - \frac{1}{5}\right)\Box R + \frac{1}{8}\left(\xi - \frac{1}{6}\right)^2 R^2 + \frac{1}{4}m^2\left(\xi - \frac{1}{6}\right)R + \frac{m^4}{8}. \tag{A.16}$$

Here, the singular terms appearing in the Hadamard parametrix (A.8) after covariantly-Taylor-expanding it can be cast into mode sums using known relations [257]. Finally, the total coincidence limit $\epsilon = \tau - \tau' = 0$ is taken and the terms within brackets are split in a sum between a numerical component and an analytical part, such as

$$\begin{aligned}\left[g^{\mu\nu'}G_{\rm E}(x,x')_{;\mu\nu'}\right]_{\rm ren} &= \lim_{\epsilon\to 0}\left[g^{\mu\nu'}G_{\rm E}(x,x')_{;\mu\nu'} - g^{\mu\nu'}G_{\rm Esing}(x,x')_{;\mu\nu'}\right] \\ &= \left[g^{\mu\nu'}G_{\rm E}(x,x')_{;\mu\nu'}\right]_{\rm num} + \left[g^{\mu\nu'}G_{\rm E}(x,x')_{;\mu\nu'}\right]_{\rm an}. \end{aligned} \tag{A.17}$$

This decomposition applies to the RSET as well [see Eq. (1.4) and App. C for the pertinent expressions], as detailed in Sections 1.2 and 6.1. An equivalent splitting was also found in cosmological scenarios [132], where it is argued that each part carries distinct physical information. The Hadamard method outlined here makes use of the Euclidean modes and naturally incorporates the temperature of the state into the definition of the RSET. The Boulware state is recovered by taking all the temperature-dependent terms to zero. As the numerical and analytical portions of the RSET are independently conserved, in Chapter 6 we take the analytical part as an approximation to the exact RSET.

The infinite sum modes present in $\langle\hat{T}^\mu_\nu\rangle_{\rm num}$ converge slowly (strict convergence of the sums over l is guaranteed by adding the corresponding counterterms that compensate a surface divergence present when the coincidence limit is taken for the propagator, see [127]) and would require summation over a vast quantity of modes. To bypass this problem Howard and Candelas [134, 135] developed a method that consisted in splitting the sums in two parts by adding and subtracting a sufficiently high-order WKB expansion, as in

$$\begin{aligned}\langle\hat{T}^\mu_\nu\rangle_{\rm num} = \lim_{\epsilon\to 0}\Big[&\left(\langle\hat{T}^\mu_\nu\rangle_{\rm unren} - \langle\hat{T}^\mu_\nu\rangle_{\rm WKB}\right) \\ &+ \left(\langle\hat{T}^\mu_\nu\rangle_{\rm WKB} - \langle\hat{T}^\mu_\nu\rangle_{\rm WKBdiv}\right)\Big] \\ = \langle\hat{T}^\mu_\nu\rangle_{\rm modes} &+ \langle\hat{T}^\mu_\nu\rangle_{\rm WKBfin}. \end{aligned} \tag{A.18}$$

This method was applied to compute the vacuum polarization and RSET of a conformally invariant field $(m = 0, \xi = 1/6)$ in a thermal state in the Schwarzschild spacetime. Anderson, Hiscock and Samuel [127] later improved the ratio of convergence of the sums by including higher orders in the WKB expansions and found the analytic portion exhibits a spurious logarithmic divergence at the outer

event horizon of the Reissner-Nordström BH. This divergence is associated to the failure of the WKB approximation at the horizon [258].

B

Renormalized stress-energy tensor in two dimensions

Dimensional reduction and near-horizon approximation

In the near-horizon approximation [101], the dynamics of a minimally coupled scalar field reduces to that of a conformally coupled scalar that propagates over a $1+1$ spacetime. To illustrate the emergence of conformal invariance in the wave equation we analyze the propagation of a classical massless and minimally coupled scalar field on the Schwarzschild spacetime. The wave equation (A.2) can be reduced to a partial differential equation for the (t, r_*) variables via the method of separation of variables. We assume the field obeys a decomposition of the form

$$\Phi(t, r, \phi, \varphi) = \sum_{l,m} \frac{F_l(t, r)}{r} Y_{lm}(\theta, \varphi), \tag{B.1}$$

where $Y_{lm}(\theta, \phi)$ are the spherical harmonics. This way, the four-dimensional equation of motion for the field reduces to a $(1+1)$-dimensional wave equation that, in the massless and minimally coupled case $(m = \xi = 0)$, becomes

$$\left[-\frac{\partial^2}{\partial t^2} + \frac{\partial^2}{\partial r_*^2} - V_l(r)\right] F_l(t, r) = 0, \tag{B.2}$$

where r_* is defined as the tortoise coordinate

$$\frac{dr_*}{dr} = \sqrt{\frac{f}{h}}, \tag{B.3}$$

and $V_l(r)$ is the potential term

$$V_l(r) = \frac{f\,l\,(l+1)}{r^2} + \frac{f'h - fh'}{2h^2 r}. \tag{B.4}$$

For the Schwarzschild spacetime (1.3), the potential results

$$V_l(r) = \left(1 - \frac{2M}{r}\right)\left[\frac{l(l+1)}{r^2} + \frac{2M}{r^3}\right], \tag{B.5}$$

acting as an effective barrier against which the field modes backscatter.

In the near-horizon limit $r \to 2M$, the potential (B.5) vanishes and the wave equation (B.2) reduces to

$$\partial_u \partial_v F_l(u,v) = 0, \tag{B.6}$$

where the coordinates u, v are the retarded and advanced null coordinates

$$u = t - r_*, \quad v = t + r_*. \tag{B.7}$$

Eq. (B.2) describing the propagation of a minimal field becomes conformally invariant in the near-horizon limit. Precisely, Eq.(B.6) is the form the wave equation adopts for a conformally invariant field propagating over a dimensionally-reduced metric corresponding to the (t, r) sector of the higher-dimensional spacetime (6.4),

$$ds^2_{(2)} = -f(r)dt^2 + h(r)dr^2. \tag{B.8}$$

In two spacetime dimensions every metric is conformally flat and can be reduced to the double-null form

$$ds^2_{(2)} = \mathcal{C}(u,v)dudv, \tag{B.9}$$

where the conformal factor $\mathcal{C}$ contains all the geometric information of the spacetime.

Eq. (B.6) has another nice property, being that it admits analytical solutions in the form of positive-frequency plane waves which, in absence of reflective boundaries and appropriately normalized obey

$$p^{\mathrm{B}}_u = (4\pi\omega)^{-1/2} e^{-i\omega u}, \quad p^{\mathrm{B}}_v = (4\pi\omega)^{-1/2} e^{-i\omega v}. \tag{B.10}$$

The existence of a complete basis of analytical positive-frequency modes simplifies the RSET derivation drastically as its dependence on the modes (B.10) is through a pair of integrals over ω that can be analytically performed. This, together with the fact that point-splitting regularization becomes simpler the less directions are available to split the points along, enables to obtain entirely analytical expressions for the $(1+1)$-dimensional RSET of the massless minimally coupled field.

Covariant point-splitting renormalization

We outline now how the RSET is obtained through the covariant point-splitting regularization procedure, and refer the reader to [119] for the technical details. The SET for the massless, minimally coupled scalar field in $1+1$ dimensions adopts the form

$$T_{\mu\nu} = \nabla_\mu \Phi \nabla_\nu \Phi - \frac{1}{2} g_{\mu\nu} \nabla^\sigma \Phi \nabla_\sigma \Phi. \tag{B.11}$$

The point-split version of this operator, assuming a generic separation ϵ between the points alongisde some geodesic, is

$$\begin{aligned} T_{\mu\mu}\left(x;\epsilon,t^\rho\right) = &\left[e^\alpha_{(\mu}(\epsilon) e^\beta_{\nu)}(-\epsilon) - \frac{1}{2} g_{\mu\nu} e^\alpha_\sigma(\epsilon) e^{\sigma\beta}(-\epsilon)\right] \\ &\times \frac{1}{2}\left\{\nabla_\alpha \Phi(x'), \nabla_\beta \Phi(-x')\right\}. \end{aligned} \tag{B.12}$$

In this expression, the curvy brackets and parentheses represent the symmetrizations

$$\{A,B\} = AB + BA, \quad A_{(\mu\nu)} = \frac{1}{2}\left(A_{\mu\nu} + A_{\nu\mu}\right). \tag{B.13}$$

The quantity $e^\alpha_\mu(\epsilon)$ is equivalent to the parallel transport bivector $g^{\alpha'}_\mu(x,x')$, although we have replaced x' by x_ϵ and denoted the proper distance between the points x_ϵ and x as $|\epsilon|$. Parallel transport bivectors obey

$$de^\alpha_\mu/d\epsilon + \Gamma^\alpha_{\nu\rho} e^\nu_\mu t^\rho = 0, \;\; \text{with } e^\alpha(0)_\mu = \delta^\alpha_\mu. \tag{B.14}$$

Finally, t^ρ is the vector tangent to the geodesic at x, namely

$$dx^\rho_\epsilon/d\epsilon = t^\rho(\epsilon), \quad t_\rho t^\rho = \Sigma = \pm 1, \tag{B.15}$$

and $\Sigma < 0$ denotes a timelike character of the geodesic.

Now, the parallel transport equations (B.14) can be solved for a vector $a^\mu(\epsilon) = e^\mu_\rho(\epsilon) a^\rho_1$ in power series of ϵ. Assuming both $a^\mu(\epsilon)$ and $t^\mu(\epsilon)$ can be Taylor-expanded as

$$\begin{aligned} a^\mu(\epsilon) &= a^\mu_1 + \epsilon a^\mu_2 + \frac{1}{2}\epsilon^2 a^\mu_3 + \mathcal{O}\left(\epsilon^3\right), \\ t^\mu(\epsilon) &= t^\mu_1 + \epsilon t^\mu_2 + \frac{1}{2}\epsilon^2 t^\mu_3 + \mathcal{O}\left(\epsilon^3\right). \end{aligned} \tag{B.16}$$

Replacing these expressions into the parallel transport equation for a general vector a^μ,

$$da^\mu(\epsilon)/d\epsilon + \Gamma^\mu_{\nu\rho}(x_\epsilon) a^\nu(\epsilon) t^\rho(\epsilon) = 0, \tag{B.17}$$

and expanding the Christoffel symbols in power series of ϵ, we obtain a series of expressions relating the a_n^μ coefficients with a_1^μ and t_1^μ. Replacing the resulting expansions in (B.12) and using the fact that parallel transport bivectors e_μ^α are diagonal matrices in double null coordinates, the expectation values of the SET components (maintaining the separation between points) reduce to the simple form

$$\begin{aligned}
\langle \hat{T}_{uv} \rangle_\epsilon &= 0, \\
\langle \hat{T}_{uu} \rangle_\epsilon &= (4\pi)^{-1} U_{-\epsilon} U_\epsilon \int_0^\infty d\omega \omega e^{i\omega \Delta u}, \\
\langle \hat{T}_{vv} \rangle_\epsilon &= (4\pi)^{-1} V_{-\epsilon} V_\epsilon \int_0^\infty d\omega \omega e^{i\omega \Delta v},
\end{aligned} \tag{B.18}$$

with

$$\begin{aligned}
U_\epsilon &= e_u^u(\epsilon) = t^u(\epsilon)/t_1^u \\
&= 1 - \mathcal{C}^{-1}\mathcal{C}_u t_1^u \epsilon + \frac{1}{2}\mathcal{C}\left[\mathcal{C}^{-3}\left(3\mathcal{C}_u^2 - \mathcal{C}\mathcal{C}_{uu}\right) t_1^u - \frac{1}{4} R t_1^v\right] t_1^u \epsilon^2 + \mathcal{O}\left(\epsilon^3\right), \\
V_\epsilon &= 1 - \mathcal{C}^{-1}\mathcal{C}_v t_1^v \epsilon + \frac{1}{2}\mathcal{C}\left[\mathcal{C}^{-3}\left(2\mathcal{C}_v^2 - \mathcal{C}\mathcal{C}_{vv}\right) t_1^v - \frac{1}{4} R t_1^u\right] t_1^v \epsilon^2 + \mathcal{O}\left(\epsilon^3\right),
\end{aligned} \tag{B.19}$$

and

$$\Delta u = u_\epsilon - u_{-\epsilon}, \quad \Delta v = v_\epsilon - v_{-\epsilon}, \tag{B.20}$$

where

$$u_\epsilon \equiv x_\epsilon^u = u_0 + t_1^u \epsilon - \frac{1}{2}\mathcal{C}^{-1}\mathcal{C}_u \left(t_1^u\right)^2 \epsilon^2 + \mathcal{O}\left(\epsilon^3\right), \tag{B.21}$$

and similarly for v_ϵ. Notice how these expansions only involve up to second derivatives of the metric functions, contrarily to the expansions involved in computing the $3+1$ RSET that include up to fourth derivatives of the metric [128]. The absence of high-derivative terms, together with the analyticity of the wave modes are the principal advantages of dimensional reduction.

The integrals in (B.18) can be done analytically [119]. Then, expansions (B.19) and (B.21) are inserted in the RSET components and the latter is expanded in powers of ϵ up to terms that vanish in the $\epsilon \to 0$ limit,

$$\langle \hat{T}_{\mu\nu}\left(x; \epsilon, t^\rho\right) \rangle = (8\pi)^{-1} \left[\left(\Sigma\epsilon^2\right)^{-1} - \frac{1}{6} R\right] \left(g_{\mu\nu} - 2\Sigma^{-1} t_\mu t_\nu\right) + \theta_{\mu\nu}, \tag{B.22}$$

from where we simply subtract all the terms that diverge with $\epsilon \to 0$ and those which depend on the tangent vector t^μ, i.e. the direction in which the points are taken together. The final expressions are

$$\begin{aligned}\langle \hat{T}_{\mu\nu}(x) \rangle &= \theta_{\mu\nu} - (48\pi)^{-1} R g_{\mu\nu} \\ \theta_{uu} &= -(12\pi)^{-1} \mathcal{C}^{\frac{1}{2}} \partial_u^2 \left(\mathcal{C}^{-\frac{1}{2}} \right), \\ \theta_{vv} &= -(12\pi)^{-1} \mathcal{C}^{\frac{1}{2}} \partial_v^2 \left(\mathcal{C}^{-\frac{1}{2}} \right), \\ \theta_{uv} &= \theta_{vu} = 0. \end{aligned} \tag{B.23}$$

This method is completely analogous to the Hadamard subtraction method (indeed, the subtracted terms correspond to the covariant Taylor expansion of the Hadamard parametrix in $1+1$ dimensions).

The RSET (B.23) yields the correct trace anomaly in two dimensions

$$\langle \hat{T}^\mu_\mu \rangle = \frac{R}{24\pi}, \tag{B.24}$$

given by the breaking of conformal invariance by the quantization procedure. Moreover, this RSET is conserved in two dimensions by construction

$$\nabla^\nu \langle \hat{T}_{\mu\nu} \rangle = 0. \tag{B.25}$$

Vacuum state definitions

The relation between the RSET components in different vacua is given by the Schwarzian derivative between the pair of null coordinates in terms of which the field modes behave as plane waves. We remind the reader that a choice of positive frequency wave modes determines a set of creation and annihilation operators in terms of which both the notion of vacuum state and of particle is defined [33, 101].

For example, the set of plane-wave modes (B.10) corresponds to the Boulware vacuum state, as they behave as plane waves in the null infinity regions of spacetime, $(u \to -\infty,\ v = v_0)$ and $(u \to u_0,\ v = +\infty)$ for past and future null infinities, respectively. A static observer at the asymptotic regions of the spacetime perceives this vacuum state as empty (it tends to Minkowski vacuum asymptotically). However, the Boulware modes oscillate infinitely as the past and future event horizons are approached, $(u \to +\infty,\ v = v_{\rm H})$ and $(u = u_{\rm H}, v \to -\infty)$, respectively. This characteristic propagates to the RSET in the form of a divergence at the event horizon.

We can consider an entirely different set of modes defined with respect to the Kruskal coordinates (U, V),

$$p_U^{\mathrm{H}} = (4\pi\omega)^{-1/2} e^{-i\omega U}, \quad p_V^{\mathrm{H}} = (4\pi\omega)^{-1/2} e^{-i\omega V} \tag{B.26}$$

that are regular at the event horizon, with the Kruskal coordinates defined as

$$U = -\kappa^{-1} e^{-\kappa u}, \quad V = \kappa^{-1} e^{\kappa v}, \tag{B.27}$$

with $\kappa = 1/4M$ the surface gravity of the Schwarzschild BH. The state resulting from this election is the Hartle-Hawking state, that compensates the Boulware divergence by adding thermal fluxes to the RSET equally divergent at the horizon but with opposite signs. Static observers at future and past null inifinities perceive a thermal bath of radiation at the temperature of the BH horizon. The Hartle-Hawking state describes a BH in (unstable) equilibrium with the very same radiation it emits. The consistency of such a configuration requires adding an artificial outer boundary to the spacetime, so that the entirety of the radiation remains confined within a finite region. The characteristics and backreaction effects of this configuration have been extensively analyzed in the literature [259, 260].

The RSETs constructed from two different bases of plane-wave modes (in this case, those associated to the Hartle-Hawking and Boulware vacuums, respectively) are related by the Schwarzian derivative [261]

$$\begin{aligned} \langle \mathrm{H}|\hat{T}_{uu}|\mathrm{H}\rangle - \langle \mathrm{B}|\hat{T}_{uu}|\mathrm{B}\rangle &= -(24\pi)^{-1}\{U, u\}, \\ \langle \mathrm{H}|\hat{T}_{vv}|\mathrm{H}\rangle - \langle \mathrm{B}|\hat{T}_{vv}|\mathrm{B}\rangle &= -(24\pi)^{-1}\{V, v\} \end{aligned} \tag{B.28}$$

defined as

$$\{U, u\} = \frac{d^3U}{du^3}\Big/\frac{dU}{du} - \frac{3}{2}\left(\frac{d^2U}{du^2}\Big/\frac{dU}{du}\right)^2. \tag{B.29}$$

For the Schwarzschild spacetime, these terms equal

$$\{U, u\} = \{V, v\} = -\frac{\kappa^2}{2}, \tag{B.30}$$

These terms compensate the divergence of the Boulware state at the horizon, yielding a finite RSET there. Finally, the Unruh state is defined with respect to the modes

$$p_U^{\mathrm{U}} = (4\pi\omega)^{-1/2} e^{-i\omega U}, \quad p_v^{\mathrm{U}} = (4\pi\omega)^{-1/2} e^{-i\omega v}, \tag{B.31}$$

and corresponds to a state regular at the future event horizon but singular at the past event horizon. The $|\mathrm{in}\rangle$ vacuum state associated to a collapsing BH long after

the trapped region has formed approaches the Unruh vacuum state. The state-dependent terms (B.30) are constant at radial infinity (in two dimensions). The vacuum state compatible with the asymptotic flatness and staticity is the Boulware vacuum, for which the RSET decays sufficiently quick with r. The emergence of conformal symmetry near the event horizon is the underlying reason for this $1+1$ RSET to be able to capture properly relevant fraction of the physics of $3+1$ RSETs.

C

The Anderson-Hiscock-Samuel RSET

C.1 Components of the AHS-RSET

Below we show the components of the AHS-RSET for a massless field with arbitrary coupling ξ (keeping temperature-dependent terms). Comparing these expressions with those of the OR-RSET [Eqs. (6.8, 6.11)], we observe that the simplification is dramatic.

$$1440\pi^2\langle\hat{T}_t^t\rangle_{\text{AHS}} = -\frac{3\kappa^4}{f^2} + \left(\frac{75\left(f'\right)^2}{f^3h} + \frac{30h'f'}{f^2h^2} - \frac{120f'}{f^2hr} + \frac{30h'}{fh^2r} - \frac{60f''}{f^2h} + \frac{30}{fr^2} - \frac{30}{fhr^2}\right)\left(\xi\right.$$

$$\left. - \frac{1}{6}\right)\kappa^2 + \frac{7\left(f'\right)^4}{32f^4h^2} + \frac{7\left(h'\right)^3}{h^5r} + \frac{3\left(f'\right)^2}{4f^2h^2r^2} + \frac{5f'h'}{2fh^3r^2} + \frac{\left(f'\right)^2f''}{8f^3h^2}$$

$$+ \frac{19\left(h'\right)^2f''}{8fh^4} + \frac{9f'h'f''}{8f^2h^3} + \frac{\left(f'\right)^2h''}{4f^2h^3} + \frac{f'h''}{2fh^3r} + \frac{13f'h'h''}{8fh^4} + \frac{h''}{h^3r^2}$$

$$+ \frac{2f^{(3)}}{fh^2r} + \frac{h^{(3)}}{h^3r} + \frac{f^{(4)}}{2fh^2} - \frac{f'f^{(3)}}{2f^2h^2} - \frac{3\left(f''\right)^2}{8f^2h^2} - \frac{f''h''}{fh^3} - \frac{3h'f^{(3)}}{2fh^3} - \frac{f'h^{(3)}}{4fh^3}$$

$$- \frac{\left(f'\right)^3h'}{16f^3h^3} - \frac{19\left(f'\right)^2\left(h'\right)^2}{32f^2h^4} - \frac{7f'\left(h'\right)^3}{4fh^5} - \frac{3\left(f'\right)^3}{4f^3h^2r} - \frac{2h'f''}{fh^3r} - \frac{5\left(f'\right)^2h'}{4f^2h^3r}$$

$$- \frac{13h'h''}{2h^4r} - \frac{3f'\left(h'\right)^2}{2fh^4r} - \frac{7\left(h'\right)^2}{4h^4r^2} - \frac{2h'}{h^3r^3} + \frac{1}{r^4} - \frac{1}{h^2r^4} + \left(-\frac{49\left(f'\right)^4}{32f^4h^2}\right.$$

$$- \frac{29h'\left(f'\right)^3}{16f^3h^3} + \frac{11\left(f'\right)^3}{8f^3h^2r} + \frac{3h'\left(f'\right)^2}{2f^2h^3r} + \frac{29f''\left(f'\right)^2}{8f^3h^2} + \frac{3h''\left(f'\right)^2}{4f^2h^3}$$

$$- \frac{57\left(h'\right)^2\left(f'\right)^2}{32f^2h^4} + \frac{5\left(f'\right)^2}{8f^2h^2r^2} + \frac{13\left(h'\right)^2f'}{8fh^4r} + \frac{5h'f'}{4fh^3r^2} + \frac{27h'f''f'}{8f^2h^3}$$

$$+ \frac{13h'h''f'}{8fh^4} - \frac{3f^{(3)}f'}{2f^2h^2} - \frac{h^{(3)}f'}{4fh^3} - \frac{7\left(h'\right)^3f'}{4fh^5} - \frac{13f''f'}{4f^2h^2r} - \frac{3h''f'}{4fh^3r} + \frac{7\left(h'\right)^3}{2h^5r}$$

$$+ \frac{19\left(h'\right)^2f''}{8fh^4} + \frac{h''}{2h^3r^2} + \frac{2f^{(3)}}{fh^2r} + \frac{h^{(3)}}{2h^3r} + \frac{f^{(4)}}{2fh^2} - \frac{9\left(f''\right)^2}{8f^2h^2} - \frac{f''h''}{fh^3}$$

$$\left. - \frac{3h'f^{(3)}}{2fh^3} - \frac{13h'f''}{4fh^3r} - \frac{13h'h''}{4h^4r} - \frac{7\left(h'\right)^2}{8h^4r^2} - \frac{h'}{h^3r^3} + \frac{1}{2r^4} - \frac{1}{2h^2r^4}\right)\log f$$

$$+\left(-\frac{49\left(f'\right)^4}{16f^4h^2}-\frac{29h'\left(f'\right)^3}{8f^3h^3}+\frac{11\left(f'\right)^3}{4f^3h^2r}+\frac{3h'\left(f'\right)^2}{f^2h^3r}+\frac{29f''\left(f'\right)^2}{4f^3h^2}\right.$$

$$+\frac{3h''\left(f'\right)^2}{2f^2h^3}-\frac{57\left(h'\right)^2\left(f'\right)^2}{16f^2h^4}+\frac{5\left(f'\right)^2}{4f^2h^2r^2}+\frac{13\left(h'\right)^2f'}{4fh^4r}+\frac{5h'f'}{2fh^3r^2}$$

$$+\frac{27h'f''f'}{4f^2h^3}+\frac{13h'h''f'}{4fh^4}-\frac{3f^{(3)}f'}{f^2h^2}-\frac{h^{(3)}f'}{2fh^3}-\frac{7\left(h'\right)^3f'}{2fh^5}-\frac{13f''f'}{2f^2h^2r}$$

$$-\frac{3h''f'}{2fh^3r}+\frac{7\left(h'\right)^3}{h^5r}+\frac{19\left(h'\right)^2f''}{4fh^4}+\frac{h''}{h^3r^2}+\frac{4f^{(3)}}{fh^2r}+\frac{h^{(3)}}{h^3r}+\frac{f^{(4)}}{fh^2}$$

$$-\frac{9\left(f''\right)^2}{4f^2h^2}-\frac{2f''h''}{fh^3}-\frac{3h'f^{(3)}}{fh^3}-\frac{13h'f''}{2fh^3r}-\frac{13h'h''}{2h^4r}-\frac{7\left(h'\right)^2}{4h^4r^2}-\frac{2h'}{h^3r^3}$$

$$\left.+\frac{1}{r^4}-\frac{1}{h^2r^4}\right)\log\nu+\left(-\frac{945\left(f'\right)^4}{8f^4h^2}-\frac{495h'\left(f'\right)^3}{4f^3h^3}+\frac{165\left(f'\right)^3}{f^3h^2r}\right.$$

$$+\frac{405h'\left(f'\right)^2}{2f^2h^3r}+\frac{495f''\left(f'\right)^2}{2f^3h^2}+\frac{45h''\left(f'\right)^2}{f^2h^3}-\frac{855\left(h'\right)^2\left(f'\right)^2}{8f^2h^4}+\frac{45\left(f'\right)^2}{2f^2hr^2}$$

$$-\frac{45\left(f'\right)^2}{2f^2h^2r^2}+\frac{285\left(h'\right)^2f'}{fh^4r}+\frac{15h'f'}{fh^2r^2}+\frac{405h'f''f'}{2f^2h^3}+\frac{195h'h''f'}{2fh^4}$$

$$-\frac{90f^{(3)}f'}{f^2h^2}-\frac{15h^{(3)}f'}{fh^3}-\frac{105\left(h'\right)^3f'}{fh^5}-\frac{270f''f'}{f^2h^2r}-\frac{120h''f'}{fh^3r}-\frac{45h'f'}{fh^3r^2}$$

$$+\frac{60\left(h'\right)^2}{h^4r^2}+\frac{90h'}{h^3r^3}+\frac{285\left(h'\right)^2f''}{2fh^4}+\frac{30f''}{fh^2r^2}+\frac{195h'h''}{h^4r}+\frac{120f^{(3)}}{fh^2r}$$

$$+\frac{30f^{(4)}}{fh^2}-\frac{135\left(f''\right)^2}{2f^2h^2}-\frac{60f''h''}{fh^3}-\frac{90h'f^{(3)}}{fh^3}-\frac{30h^{(3)}}{h^3r}-\frac{270h'f''}{fh^3r}$$

$$\left.-\frac{210\left(h'\right)^3}{h^5r}-\frac{30f''}{fhr^2}-\frac{30h''}{h^3r^2}-\frac{30h'}{h^2r^3}-\frac{60}{hr^4}+\frac{60}{h^2r^4}\right)\left(\xi-\frac{1}{6}\right)$$

$$+\left[\frac{945\left(f'\right)^4}{4f^4h^2}+\frac{270h'\left(f'\right)^3}{f^3h^3}-\frac{720\left(f'\right)^3}{f^3h^2r}+\frac{855\left(h'\right)^2\left(f'\right)^2}{4f^2h^4}-\frac{540f''\left(f'\right)^2}{f^3h^2}\right.$$

$$-\frac{90h''\left(f'\right)^2}{f^2h^3}-\frac{360h'\left(f'\right)^2}{f^2h^3r}+\frac{270\left(f'\right)^2}{f^2hr^2}-\frac{90\left(f'\right)^2}{f^2h^2r^2}+\frac{900\left(h'\right)^2f'}{fh^4r}+\frac{180h'f'}{fh^2r^2}$$

$$+\frac{900f''f'}{f^2h^2r}+\frac{180f^{(3)}f'}{f^2h^2}-\frac{405h'f''f'}{f^2h^3}-\frac{360h''f'}{fh^3r}-\frac{900h'f'}{fh^3r^2}+\frac{180\left(h'\right)^2}{h^4r^2}$$

$$+\frac{135\left(f''\right)^2}{f^2h^2}+\frac{360h'}{h^2r^3}+\frac{360f''}{fh^2r^2}-\frac{360h'f''}{fh^3r}-\frac{360f''}{fhr^2}-\frac{360h'}{h^3r^3}+\frac{180}{r^4}-\frac{360}{hr^4}$$

$$+\frac{180}{h^2r^4}+\left(-\frac{2205\left(f'\right)^4}{8f^4h^2}-\frac{1305h'\left(f'\right)^3}{4f^3h^3}+\frac{585\left(f'\right)^3}{f^3h^2r}+\frac{675h'\left(f'\right)^2}{f^2h^3r}+\frac{1305f''\left(f'\right)^2}{2f^3h^2}\right.$$

$$+\frac{135h''\left(f'\right)^2}{f^2h^3}-\frac{2565\left(h'\right)^2\left(f'\right)^2}{8f^2h^4}-\frac{90\left(f'\right)^2}{f^2h^2r^2}+\frac{630\left(h'\right)^2f'}{fh^4r}+\frac{90h'f'}{fh^3r^2}+\frac{1215h'f''f'}{2f^2h^3}$$

$$+\frac{585h'h''f'}{2fh^4}-\frac{270f^{(3)}f'}{f^2h^2}-\frac{45h^{(3)}f'}{fh^3}-\frac{315\left(h'\right)^3f'}{fh^5}-\frac{990f''f'}{f^2h^2r}-\frac{270h''f'}{fh^3r}+\frac{450\left(h'\right)^2}{h^4r^2}$$

$$+\frac{360h'}{h^3r^3}+\frac{855\left(h'\right)^2f''}{2fh^4}+\frac{1170h'h''}{h^4r}+\frac{360f^{(3)}}{fh^2r}+\frac{90f^{(4)}}{fh^2}-\frac{405\left(f''\right)^2}{2f^2h^2}-\frac{180f''h''}{fh^3}$$

$$\left.-\frac{270h'f^{(3)}}{fh^3}-\frac{180h^{(3)}}{h^3r}-\frac{720h'f''}{fh^3r}-\frac{1260\left(h'\right)^3}{h^5r}-\frac{180h''}{h^3r^2}+\frac{90}{r^4}-\frac{540}{hr^4}+\frac{450}{h^2r^4}\right)\log f$$

$$+\left(-\frac{2205\left(f'\right)^4}{4f^4h^2}-\frac{1305h'\left(f'\right)^3}{2f^3h^3}+\frac{1170\left(f'\right)^3}{f^3h^2r}+\frac{1350h'\left(f'\right)^2}{f^2h^3r}+\frac{1305f''\left(f'\right)^2}{f^3h^2}+\frac{270h''\left(f'\right)^2}{f^2h^3}\right.$$

$$-\frac{2565\left(h'\right)^2\left(f'\right)^2}{4f^2h^4}-\frac{180\left(f'\right)^2}{f^2h^2r^2}+\frac{1260\left(h'\right)^2f'}{fh^4r}+\frac{180h'f'}{fh^3r^2}+\frac{1215h'f''f'}{f^2h^3}+\frac{585h'h''f'}{fh^4}$$

$$-\frac{540f^{(3)}f'}{f^2h^2}-\frac{90h^{(3)}f'}{fh^3}-\frac{630\left(h'\right)^3f'}{fh^5}-\frac{1980f''f'}{f^2h^2r}-\frac{540h''f'}{fh^3r}+\frac{900\left(h'\right)^2}{h^4r^2}+\frac{720h'}{h^3r^3}$$

$$+\frac{855\left(h'\right)^2f''}{fh^4}+\frac{2340h'h''}{h^4r}+\frac{720f^{(3)}}{fh^2r}+\frac{180f^{(4)}}{fh^2}-\frac{405\left(f''\right)^2}{f^2h^2}-\frac{360f''h''}{fh^3}-\frac{540h'f^{(3)}}{fh^3}$$

$$\left.\left.-\frac{360h^{(3)}}{h^3r}-\frac{1440h'f''}{fh^3r}-\frac{2520\left(h'\right)^3}{h^5r}-\frac{360h''}{h^3r^2}+\frac{180}{r^4}-\frac{1080}{hr^4}+\frac{900}{h^2r^4}\right)\log\nu\right]\left(\xi-\frac{1}{6}\right)^2,$$

(C.1)

$$
\begin{aligned}
1440\pi^2\langle\hat{T}_r^r\rangle_{\text{AHS}} = {} & \frac{\kappa^4}{f^2} + \left(-\frac{15\,(f')^2}{f^3h} - \frac{30f'}{f^2hr} - \frac{30}{fr^2} + \frac{30}{fhr^2}\right)\left(\xi - \frac{1}{6}\right)\kappa^2 + \frac{(f')^4}{32f^4h^2} \\
& + \frac{7\,(f')^2\,(h')^2}{32f^2h^4} + \frac{2f'}{fh^2r^3} + \frac{(f')^3\,h'}{16f^3h^3} + \frac{f'h'}{2fh^3r^2} + \frac{2f'f''}{f^2h^2r} + \frac{h'f''}{fh^3r} + \frac{f'h''}{fh^3r} \\
& + \frac{f'f^{(3)}}{4f^2h^2} - \frac{(f'')^2}{8f^2h^2} - \frac{(f')^2\,f''}{8f^3h^2} - \frac{f'h'f''}{4f^2h^3} - \frac{(f')^2\,h''}{8f^2h^3} - \frac{f^{(3)}}{fh^2r} - \frac{(f')^3}{2f^3h^2r} \\
& - \frac{(f')^2\,h'}{4f^2h^3r} - \frac{7f'\,(h')^2}{4fh^4r} - \frac{2f''}{fh^2r^2} + \left(\frac{7\,(f')^4}{32f^4h^2} + \frac{3h'\,(f')^3}{16f^3h^3} - \frac{5\,(f')^3}{8f^3h^2r}\right. \\
& + \frac{7\,(h')^2\,(f')^2}{32f^2h^4} - \frac{3f''\,(f')^2}{8f^3h^2} - \frac{h''\,(f')^2}{8f^2h^3} - \frac{h'\,(f')^2}{2f^2h^3r} - \frac{(f')^2}{8f^2h^2r^2} + \frac{h'f'}{4fh^3r^2} \\
& + \frac{3f''f'}{2f^2h^2r} + \frac{h''f'}{2fh^3r} + \frac{f^{(3)}f'}{4f^2h^2} - \frac{h'f''f'}{4f^2h^3} - \frac{7\,(h')^2\,f'}{8fh^4r} + \frac{f'}{fh^2r^3} + \frac{7\,(h')^2}{8h^4r^2} \\
& \left. + \frac{h'f''}{2fh^3r} - \frac{(f'')^2}{8f^2h^2} - \frac{f^{(3)}}{2fh^2r} - \frac{f''}{fh^2r^2} - \frac{h''}{2h^3r^2} + \frac{1}{2r^4} - \frac{1}{2h^2r^4}\right)\log f \\
& + \left(\frac{7\,(f')^4}{16f^4h^2} + \frac{3h'\,(f')^3}{8f^3h^3} - \frac{5\,(f')^3}{4f^3h^2r} + \frac{7\,(h')^2\,(f')^2}{16f^2h^4} - \frac{3f''\,(f')^2}{4f^3h^2} - \frac{h''\,(f')^2}{4f^2h^3}\right. \\
& - \frac{h'\,(f')^2}{f^2h^3r} - \frac{(f')^2}{4f^2h^2r^2} + \frac{h'f'}{2fh^3r^2} + \frac{3f''f'}{f^2h^2r} + \frac{h''f'}{fh^3r} + \frac{f^{(3)}f'}{2f^2h^2} - \frac{h'f''f'}{2f^2h^3} \\
& - \frac{7\,(h')^2\,f'}{4fh^4r} + \frac{2f'}{fh^2r^3} + \frac{7\,(h')^2}{4h^4r^2} + \frac{h'f''}{fh^3r} - \frac{(f'')^2}{4f^2h^2} - \frac{f^{(3)}}{fh^2r} - \frac{2f''}{fh^2r^2} \\
& \left. - \frac{h''}{h^3r^2} + \frac{1}{r^4} - \frac{1}{h^2r^4}\right)\log\nu + \left(\frac{135\,(f')^4}{8f^4h^2} + \frac{45h'\,(f')^3}{4f^3h^3} + \frac{45\,(f')^3}{f^3h^2r}\right. \\
& + \frac{105\,(h')^2\,(f')^2}{8f^2h^4} - \frac{45f''\,(f')^2}{2f^3h^2} - \frac{15h''\,(f')^2}{2f^2h^3} - \frac{15\,(f')^2}{2f^2hr^2} - \frac{165\,(f')^2}{2f^2h^2r^2} \\
& + \frac{105\,(h')^2\,f'}{2fh^4r} + \frac{15f^{(3)}f'}{f^2h^2} - \frac{15h'f''f'}{f^2h^3} - \frac{75f''f'}{f^2h^2r} - \frac{30h''f'}{fh^3r} - \frac{30h'f'}{fh^3r^2} \\
& \left. + \frac{30f'}{fhr^3} - \frac{90f'}{fh^2r^3} + \frac{60f''}{fh^2r^2} + \frac{30f^{(3)}}{fh^2r} - \frac{15\,(f'')^2}{2f^2h^2} - \frac{30h'f''}{fh^3r}\right)\left(\xi - \frac{1}{6}\right)
\end{aligned}
$$

$$
\begin{aligned}
&+\Bigg[-\frac{45\left(f'\right)^4}{2f^4h^2}-\frac{45h'\left(f'\right)^3}{2f^3h^3}+\frac{45f''\left(f'\right)^2}{f^3h^2}-\frac{180h'\left(f'\right)^2}{f^2h^3r}\\
&-\frac{90\left(f'\right)^2}{f^2hr^2}+\frac{450\left(f'\right)^2}{f^2h^2r^2}+\frac{180f''f'}{f^2h^2r}-\frac{360h'f'}{fh^3r^2}-\frac{360f'}{fhr^3}+\frac{360f'}{fh^2r^3}\\
&+\Bigg(\frac{315\left(f'\right)^4}{8f^4h^2}+\frac{135h'\left(f'\right)^3}{4f^3h^3}+\frac{90\left(f'\right)^3}{f^3h^2r}+\frac{315\left(h'\right)^2\left(f'\right)^2}{8f^2h^4}\\
&+\frac{45h'\left(f'\right)^2}{f^2h^3r}-\frac{135f''\left(f'\right)^2}{2f^3h^2}-\frac{45h''\left(f'\right)^2}{2f^2h^3}-\frac{360\left(f'\right)^2}{f^2h^2r^2}\\
&+\frac{315\left(h'\right)^2f'}{fh^4r}+\frac{45f^{(3)}f'}{f^2h^2}-\frac{45h'f''f'}{f^2h^3}-\frac{270f''f'}{f^2h^2r}-\frac{180h''f'}{fh^3r}\\
&-\frac{360h'f'}{fh^3r^2}-\frac{360f'}{fh^2r^3}+\frac{630\left(h'\right)^2}{h^4r^2}+\frac{360f''}{fh^2r^2}+\frac{180f^{(3)}}{fh^2r}\\
&-\frac{45\left(f''\right)^2}{2f^2h^2}-\frac{180h'f''}{fh^3r}-\frac{360h''}{h^3r^2}+\frac{90}{r^4}+\frac{540}{hr^4}-\frac{630}{h^2r^4}\Bigg)\log f\\
&+\Bigg(\frac{315\left(f'\right)^4}{4f^4h^2}+\frac{135h'\left(f'\right)^3}{2f^3h^3}+\frac{180\left(f'\right)^3}{f^3h^2r}+\frac{315\left(h'\right)^2\left(f'\right)^2}{4f^2h^4}\\
&+\frac{90h'\left(f'\right)^2}{f^2h^3r}-\frac{135f''\left(f'\right)^2}{f^3h^2}-\frac{45h''\left(f'\right)^2}{f^2h^3}-\frac{720\left(f'\right)^2}{f^2h^2r^2}\\
&+\frac{630\left(h'\right)^2f'}{fh^4r}+\frac{90f^{(3)}f'}{f^2h^2}-\frac{90h'f''f'}{f^2h^3}-\frac{540f''f'}{f^2h^2r}\\
&-\frac{360h''f'}{fh^3r}-\frac{720h'f'}{fh^3r^2}-\frac{720f'}{fh^2r^3}+\frac{1260\left(h'\right)^2}{h^4r^2}\\
&+\frac{720f''}{fh^2r^2}+\frac{360f^{(3)}}{fh^2r}-\frac{45\left(f''\right)^2}{f^2h^2}-\frac{360h'f''}{fh^3r}\\
&-\frac{720h''}{h^3r^2}+\frac{180}{r^4}+\frac{1080}{hr^4}-\frac{1260}{h^2r^4}\Bigg)\log\nu\Bigg]\left(\xi-\frac{1}{6}\right)^2,
\end{aligned}
\tag{C.2}
$$

$$1440\pi^2\langle\hat{T}^{\theta}_{\theta}\rangle_{\mathrm{AHS}}$$

$$= \frac{\kappa^4}{f^2} + \left(\frac{75\left(f'\right)^2}{2f^3h} + \frac{15h'f'}{2f^2h^2} - \frac{15f'}{f^2hr} - \frac{15f''}{f^2h} - \frac{15h'}{fh^2r}\right)\left(\xi - \frac{1}{6}\right)\kappa^2 + \frac{17\left(f'\right)^4}{32f^4h^2}$$

$$+ \frac{7f'\left(h'\right)^3}{4fh^5} + \frac{31\left(f'\right)^2\left(h'\right)^2}{32f^2h^4} + \frac{7\left(f''\right)^2}{8f^2h^2} + \frac{13\left(f'\right)^3h'}{16f^3h^3} + \frac{f'f''}{f^2h^2r} + \frac{11h'f''}{4fh^3r} + \frac{f''}{fh^2r^2}$$

$$+ \frac{f'h''}{4fh^3r} + \frac{f''h''}{fh^3} + \frac{3f'f^{(3)}}{4f^2h^2} + \frac{3h'f^{(3)}}{2fh^3} + \frac{f'h^{(3)}}{4fh^3} - \frac{f^{(4)}}{2fh^2} - \frac{13\left(f'\right)^2f''}{8f^3h^2} - \frac{2f'h'f''}{f^2h^3}$$

$$- \frac{3\left(f'\right)^2h''}{8f^2h^3} - \frac{19\left(h'\right)^2f''}{8fh^4} - \frac{13f'h'h''}{8fh^4} - \frac{3f^{(3)}}{2fh^2r} - \frac{\left(f'\right)^3}{2f^3h^2r} - \frac{3\left(f'\right)^2h'}{4f^2h^3r} - \frac{3f'\left(h'\right)^2}{4fh^4r}$$

$$- \frac{3f'h'}{2fh^3r^2} - \frac{f'}{fh^2r^3} + \left(\frac{21\left(f'\right)^4}{32f^4h^2} + \frac{13h'\left(f'\right)^3}{16f^3h^3} - \frac{3\left(f'\right)^3}{8f^3h^2r} + \frac{25\left(h'\right)^2\left(f'\right)^2}{32f^2h^4}\right.$$

$$- \frac{13f''\left(f'\right)^2}{8f^3h^2} - \frac{5h''\left(f'\right)^2}{16f^2h^3} - \frac{h'\left(f'\right)^2}{2f^2h^3r} - \frac{\left(f'\right)^2}{4f^2h^2r^2} + \frac{7\left(h'\right)^3f'}{8fh^5} + \frac{7f''f'}{8f^2h^2r} + \frac{h''f'}{8fh^3r}$$

$$+ \frac{5f^{(3)}f'}{8f^2h^2} + \frac{h^{(3)}f'}{8fh^3} - \frac{25h'f''f'}{16f^2h^3} - \frac{13h'h''f'}{16fh^4} - \frac{3\left(h'\right)^2f'}{8fh^4r} - \frac{3h'f'}{4fh^3r^2} - \frac{f'}{2fh^2r^3}$$

$$+ \frac{5\left(f''\right)^2}{8f^2h^2} + \frac{h'}{2h^3r^3} + \frac{11h'f''}{8fh^3r} + \frac{f''}{2fh^2r^2} + \frac{13h'h''}{8h^4r} + \frac{f''h''}{2fh^3} + \frac{3h'f^{(3)}}{4fh^3} - \frac{f^{(4)}}{4fh^2}$$

$$\left. - \frac{19\left(h'\right)^2f''}{16fh^4} - \frac{3f^{(3)}}{4fh^2r} - \frac{h^{(3)}}{4h^3r} - \frac{7\left(h'\right)^3}{4h^5r} - \frac{1}{2r^4} + \frac{1}{2h^2r^4}\right)\log f$$

$$+\left(\frac{21\left(f'\right)^4}{16f^4h^2}+\frac{13h'\left(f'\right)^3}{8f^3h^3}-\frac{3\left(f'\right)^3}{4f^3h^2r}+\frac{25\left(h'\right)^2\left(f'\right)^2}{16f^2h^4}-\frac{13f''\left(f'\right)^2}{4f^3h^2}\right.$$

$$-\frac{5h''\left(f'\right)^2}{8f^2h^3}-\frac{h'\left(f'\right)^2}{f^2h^3r}-\frac{\left(f'\right)^2}{2f^2h^2r^2}+\frac{7\left(h'\right)^3f'}{4fh^5}+\frac{7f''f'}{4f^2h^2r}+\frac{h''f'}{4fh^3r}$$

$$+\frac{5f^{(3)}f'}{4f^2h^2}+\frac{h^{(3)}f'}{4fh^3}-\frac{25h'f''f'}{8f^2h^3}-\frac{13h'h''f'}{8fh^4}-\frac{3\left(h'\right)^2f'}{4fh^4r}-\frac{3h'f'}{2fh^3r^2}$$

$$-\frac{f'}{fh^2r^3}+\frac{5\left(f''\right)^2}{4f^2h^2}+\frac{h'}{h^3r^3}+\frac{11h'f''}{4fh^3r}+\frac{f''}{fh^2r^2}+\frac{13h'h''}{4h^4r}+\frac{f''h''}{fh^3}+\frac{3h'f^{(3)}}{2fh^3}$$

$$\left.-\frac{f^{(4)}}{2fh^2}-\frac{19\left(h'\right)^2f''}{8fh^4}-\frac{3f^{(3)}}{2fh^2r}-\frac{h^{(3)}}{2h^3r}-\frac{7\left(h'\right)^3}{2h^5r}-\frac{1}{r^4}+\frac{1}{h^2r^4}\right)\log\nu$$

$$+\left(-\frac{645\left(f'\right)^4}{8f^4h^2}-\frac{675h'\left(f'\right)^3}{8f^3h^3}+\frac{90\left(f'\right)^3}{f^3h^2r}+\frac{405h'\left(f'\right)^2}{4f^2h^3r}+\frac{675f''\left(f'\right)^2}{4f^3h^2}\right.$$

$$+\frac{30h''\left(f'\right)^2}{f^2h^3}-\frac{285\left(h'\right)^2\left(f'\right)^2}{4f^2h^4}-\frac{15\left(f'\right)^2}{2f^2hr^2}+\frac{45\left(f'\right)^2}{2f^2h^2r^2}+\frac{225\left(h'\right)^2f'}{4fh^4r}$$

$$+\frac{135h'f'}{2fh^3r^2}+\frac{135h'f''f'}{f^2h^3}+\frac{195h'h''f'}{4fh^4}-\frac{60f^{(3)}f'}{f^2h^2}-\frac{15h^{(3)}f'}{2fh^3}-\frac{105\left(h'\right)^3f'}{2fh^5}$$

$$-\frac{285f''f'}{2f^2h^2r}-\frac{45h''f'}{2fh^3r}-\frac{15h'f'}{2fh^2r^2}+\frac{30f'}{fh^2r^3}+\frac{285\left(h'\right)^2f''}{4fh^4}+\frac{15f''}{fhr^2}+\frac{45f^{(3)}}{fh^2r}$$

$$\left.+\frac{15f^{(4)}}{fh^2}-\frac{45\left(f''\right)^2}{f^2h^2}-\frac{30f''h''}{fh^3}-\frac{45h'f^{(3)}}{fh^3}-\frac{90h'f''}{fh^3r}-\frac{45f''}{fh^2r^2}\right)\left(\xi-\frac{1}{6}\right)$$

$$
+\left[\frac{405\left(f'\right)^4}{2f^4h^2}+\frac{225h'\left(f'\right)^3}{f^3h^3}-\frac{495\left(f'\right)^3}{f^3h^2r}+\frac{405\left(h'\right)^2\left(f'\right)^2}{2f^2h^4}-\frac{450f''\left(f'\right)^2}{f^3h^2}\right.
$$

$$
-\frac{90h''\left(f'\right)^2}{f^2h^3}-\frac{405h'\left(f'\right)^2}{f^2h^3r}+\frac{90\left(f'\right)^2}{f^2hr^2}-\frac{270\left(f'\right)^2}{f^2h^2r^2}+\frac{810\left(h'\right)^2f'}{fh^4r}
$$

$$
+\frac{90h'f'}{fh^2r^2}+\frac{630f''f'}{f^2h^2r}+\frac{180f^{(3)}f'}{f^2h^2}-\frac{360h'f''f'}{f^2h^3}-\frac{360h''f'}{fh^3r}-\frac{270h'f'}{fh^3r^2}
$$

$$
+\frac{540f'}{fhr^3}-\frac{540f'}{fh^2r^3}+\frac{90\left(f''\right)^2}{f^2h^2}+\frac{180f''}{fh^2r^2}-\frac{180h'f''}{fh^3r}-\frac{180f''}{fhr^2}
$$

$$
+\left(-\frac{1755\left(f'\right)^4}{8f^4h^2}-\frac{1035h'\left(f'\right)^3}{4f^3h^3}+\frac{675\left(f'\right)^3}{2f^3h^2r}+\frac{450h'\left(f'\right)^2}{f^2h^3r}+\frac{1035f''\left(f'\right)^2}{2f^3h^2}+\frac{225h''\left(f'\right)^2}{2f^2h^3}\right.
$$

$$
-\frac{2115\left(h'\right)^2\left(f'\right)^2}{8f^2h^4}+\frac{90\left(f'\right)^2}{f^2h^2r^2}+\frac{1485\left(h'\right)^2f'}{2fh^4r}+\frac{270h'f'}{fh^3r^2}+\frac{495h'f''f'}{f^2h^3}+\frac{585h'h''f'}{2fh^4}
$$

$$
-\frac{225f^{(3)}f'}{f^2h^2}-\frac{45h^{(3)}f'}{fh^3}-\frac{315\left(h'\right)^3f'}{fh^5}-\frac{585f''f'}{f^2h^2r}-\frac{315h''f'}{fh^3r}+\frac{270f'}{fhr^3}-\frac{90f'}{fh^2r^3}+\frac{630h'}{h^3r^3}
$$

$$
+\frac{855\left(h'\right)^2f''}{2fh^4}+\frac{1170h'h''}{h^4r}+\frac{270f^{(3)}}{fh^2r}+\frac{90f^{(4)}}{fh^2}-\frac{315\left(f''\right)^2}{2f^2h^2}-\frac{180f''h''}{fh^3}-\frac{270h'f^{(3)}}{fh^3}
$$

$$
\left.-\frac{180h^{(3)}}{h^3r}-\frac{630h'f''}{fh^3r}-\frac{1260\left(h'\right)^3}{h^5r}-\frac{180f''}{fh^2r^2}-\frac{270h'}{h^2r^3}-\frac{90}{r^4}-\frac{540}{hr^4}+\frac{630}{h^2r^4}\right)\log f
$$

$$
+\left(-\frac{1755\left(f'\right)^4}{4f^4h^2}-\frac{1035h'\left(f'\right)^3}{2f^3h^3}+\frac{675\left(f'\right)^3}{f^3h^2r}+\frac{900h'\left(f'\right)^2}{f^2h^3r}+\frac{1035f''\left(f'\right)^2}{f^3h^2}+\frac{225h''\left(f'\right)^2}{f^2h^3}\right.
$$

$$
-\frac{2115\left(h'\right)^2\left(f'\right)^2}{4f^2h^4}+\frac{180\left(f'\right)^2}{f^2h^2r^2}+\frac{1485\left(h'\right)^2f'}{fh^4r}+\frac{540h'f'}{fh^3r^2}+\frac{990h'f''f'}{f^2h^3}+\frac{585h'h''f'}{fh^4}
$$

$$
-\frac{450f^{(3)}f'}{f^2h^2}-\frac{90h^{(3)}f'}{fh^3}-\frac{630\left(h'\right)^3f'}{fh^5}-\frac{1170f''f'}{f^2h^2r}-\frac{630h''f'}{fh^3r}+\frac{540f'}{fhr^3}-\frac{180f'}{fh^2r^3}+\frac{1260h'}{h^3r^3}
$$

$$
+\frac{855\left(h'\right)^2f''}{fh^4}+\frac{2340h'h''}{h^4r}+\frac{540f^{(3)}}{fh^2r}+\frac{180f^{(4)}}{fh^2}-\frac{315\left(f''\right)^2}{f^2h^2}-\frac{360f''h''}{fh^3}-\frac{540h'f^{(3)}}{fh^3}
$$

$$
\left.\left.-\frac{360h^{(3)}}{h^3r}-\frac{1260h'f''}{fh^3r}-\frac{2520\left(h'\right)^3}{h^5r}-\frac{360f''}{fh^2r^2}-\frac{540h'}{h^2r^3}-\frac{180}{r^4}-\frac{1080}{hr^4}+\frac{1260}{h^2r^4}\right)\log\nu\right]\left(\xi\right.
$$

$$
\left.-\frac{1}{6}\right)^2,
$$

(C.3)

and

$$\langle \hat{T}^{\varphi}_{\varphi} \rangle_{\text{AHS}} = \langle \hat{T}^{\theta}_{\theta} \rangle_{\text{AHS}}. \tag{C.4}$$

C.2 Regularity of the AHS-RSET

The expressions (C.1-C.3) give rise to a covariantly conserved RSET obtained directly by taking the analytical byproduct of following the point-splitting renormalization procedure (as in [127]) or the Hadamard renormalization prescription (see App. A). The higher-derivative terms naturally arise upon isolating and subtracting all the ultraviolet divergent terms that appear in the field propagator from which the RSET is constructed. Thus, these expressions are purely geometrical and invoke no additional assumptions about the spacetime over which they are obtained, resulting in an RSET that is regular at the center of spherical symmetry, with one caveat that we detail in the following. It is straightforward to check that regularity of the Kretschmann invariant

$$\mathcal{K} = R^{\mu\nu\rho\sigma} R_{\mu\nu\rho\sigma} \tag{C.5}$$

of the metric (6.4) at $r = 0$ enforces the metric functions to obey the expansions

$$\begin{aligned} f(r) =& a_0 + a_2 r^2 + a_3 r^3 + a_4 r^4 + \mathcal{O}\left(r^5\right), \\ h(r) =& 1 + b_2 r^2 + b_3 r^3 + b_4 r^4 + \mathcal{O}\left(r^5\right), \end{aligned} \tag{C.6}$$

These conditions ensure the finiteness at $r = 0$ of all other invariants constructed from contractions of the Ricci and Riemann tensors and the Ricci scalar [13]. Notice how the Kretschmann invariant constraints the value of the coefficients in (C.6) up to second-order terms in r because it only involves up to second-order derivatives of the metric functions (notice the absence of linear terms in r in the expansion). However, in replacing the expansions (C.6) in the AHS-RSET we obtain, for the $\langle \hat{T}^{t}_{t} \rangle^{\text{AHS}}$ component

$$\begin{aligned} 1440\pi^2 \langle \hat{T}^{t}_{t} \rangle^{\text{AHS}} =& \frac{12 a_3}{a_0 r} \left[1 + \log\left(a_0 \nu^2\right) + 60 \left(\xi - \frac{1}{6}\right) \right. \\ & \left. + 180 \log\left(a_0 \nu^2\right) \left(\xi - \frac{1}{6}\right)^2 \right] \\ & + \frac{4 b_3}{r} \left[2 + \log\left(a_0 \nu^2\right) + 60 \left(\xi - \frac{1}{6}\right) \right. \\ & \left. - 360 \log\left(a_0 \nu^2\right) \left(\xi - \frac{1}{6}\right)^2 \right] + \mathcal{O}\left(r^0\right). \end{aligned} \tag{C.7}$$

Notice the divergence at $r = 0$ when the terms a_3 and b_3 are nonzero. Here we omit the remaining RSET components as they show similar divergences.

The presence of higher-derivative terms of the metric in the RSET imposes more restrictive conditions for regularity than those given by the finiteness of curvature invariants themselves. This adds an extra degree of non-physicality to RSET approximations that exhibit higher-derivative terms due to these terms becoming singular at $r = 0$ on geometries that are entirely regular in classical general relativity. The OR-RSET is $\langle \hat{T}^{\mu}_{\nu} \rangle_{\text{OR}} = \mathcal{O}(r^0)$ over any metric whose curvature invariants are finite, while also diverging at the regions where the state in which it is evaluated becomes singular, so here we advocate its use over the AHS-RSET in scenarios where the point $r = 0$ belongs to the spacetime.

D

Lists of publications and abbreviations

List of publications

The articles to which the author contributed during the realization of this thesis are listed below (in reverse chronological order).

1. J. Arrechea, C. Barceló, R. Carballo-Rubio, Luis J. Garay.
   Semiclassical relativistic stars
   Sci. Rep. **12**, 15958 (2022)
   DOI: 10.1038/s41598-022-19836-8

2. J. Arrechea, C. Barceló, R. Carballo-Rubio, Luis J. Garay.
   Semiclassical constant-density spheres in a regularized Polyakov approximation
   Phys. Rev. D **104**, 084071 (2021)
   DOI: 10.1103/PhysRevD.104.084071

3. J. Arrechea, C. Barceló, Luis J. Garay, G. García-Moreno.
   Inversion of statistics and thermalization in the Unruh effect
   Phys. Rev. D **104**, 065004 (2021)
   DOI: 10.1103/PhysRevD.104.065004

4. J. Arrechea, C. Barceló, V. Boyanov, R. Carballo-Rubio, Luis J. Garay.
   Vacuum semiclassical gravity does not leave space for safe singularities
   Universe **7**, 281 (2021)
   DOI: 10.3390/universe7080281

5. J. Arrechea, C. Barceló, R. Carballo-Rubio, Luis J. Garay.
   Reissner-Nordström geometry counterpart in semiclassical gravity
   Class. Quant. Grav. **38**, 115014 (2021)
   DOI: 10.1088/1361-6382/abf628

6. J. Arrechea, A. Delhom, A. Jiménez-Cano
Inconsistencies in four dimensional Einstein-Gauss-Bonnet gravity
Chin. Phys. C **45**, 013107 (2020)
DOI: 10.1088/1674-1137/abc1d4

7. J. Arrechea, A. Delhom, A. Jiménez-Cano
Comment on "Einstein-Gauss-Bonnet Gravity in Four-Dimensional Spacetime"
Phys. Rev. Lett. **125**, 149002 (2020)
DOI: 10.1103/PhysRevLett.125.149002

8. J. Arrechea, C. Barceló, R. Carballo-Rubio, Luis J. Garay.
Schwarzschild geometry counterpart in semiclassical gravity
Phys. Rev. D **101**, 064059 (2020)
DOI: 10.1103/PhysRevD.101.064059

List of abbreviations

Below you can find a list of all the abbreviations used in this thesis:

BH(s)	Black Hole(s)
ABH(s)	Astrophysical Black Hole(s)
GR	General Relativity
ADM	Arnowitt-Deser-Misner
TOV	Tolman-Oppenheimer-Volkoff
SET(s)	Stress-Energy Tensor(s)
RSET(s)	Renormalized Stress-Energy Tensor(s)
DP-RSET)	Distorted Polyakov RSET
RP-RSET	Regularized Polyakov RSET
CRP-RSET	Cutoff-Regularized Polyakov RSET
AHS-RSET	Anderson-Hiscock-Samuel RSET
OR-RSET	Order-Reduced RSET
MOR-RSET	Matter-Order-Reduced RSET
NEC	Null Energy Condition
SEC	Strong Energy Condition

Bibliography

[1] Julio Arrechea, Carlos Barceló, Raúl Carballo-Rubio, and Luis J. Garay. "Schwarzschild geometry counterpart in semiclassical gravity". In: *Phys. Rev. D* 101 (6 2020), p. 064059 (cit. on pp. v, x).

[2] Julio Arrechea, Carlos Barceló, Valentin Boyanov, and Luis J. Garay. "Vacuum Semiclassical Gravity Does Not Leave Space for Safe Singularities". In: *Universe* 7.8 (2021), p. 281. arXiv: 2010.09048 [gr-qc] (cit. on pp. v, x).

[3] Julio Arrechea, Carlos Barceló, Raúl Carballo-Rubio, and Luis J. Garay. "Reissner–Nordström geometry counterpart in semiclassical gravity". In: *Class. Quant. Grav.* 38.11 (2021), p. 115014. arXiv: 2102.03544 [gr-qc] (cit. on pp. v, x).

[4] Julio Arrechea, Carlos Barceló, Raúl Carballo-Rubio, and Luis J. Garay. "Semiclassical constant-density spheres in a regularized Polyakov approximation". In: *Phys. Rev. D* 104.8 (2021), p. 084071. arXiv: 2105.11261 [gr-qc] (cit. on pp. v, x).

[5] Julio Arrechea, Carlos Barceló, Raúl Carballo-Rubio, and Luis J. Garay. "Breaking Buchdahl: Ultracompact stars in semiclassical gravity". In: *16th Marcel Grossmann Meeting on Recent Developments in Theoretical and Experimental General Relativity, Astrophysics and Relativistic Field Theories*. Oct. 2021. arXiv: 2110.15680 [gr-qc] (cit. on pp. v, x).

[6] Julio Arrechea, Carlos Barceló, Raúl Carballo-Rubio, and Luis J. Garay. "Semiclassical relativistic stars". In: *Sci. Rep.* 12.1 (2022), p. 15958. arXiv: 2110.15808 [gr-qc] (cit. on pp. v, x, 2).

[7] Julio Arrechea, Carlos Barceló, Raúl Carballo-Rubio, and Luis J. Garay. "Asymptotically flat vacuum solutions in order-reduced semiclassical gravity". In: (Dec. 2022). arXiv: 2212.09375 [gr-qc] (cit. on pp. v, x).

[8] W. Rindler. "Visual horizons in world-models". In: *Mon. Not. Roy. Astron. Soc.* 116 (1956), pp. 662–677 (cit. on p. 1).

[9] David Finkelstein. "Past-Future Asymmetry of the Gravitational Field of a Point Particle". In: *Phys. Rev.* 110 (4 May 1958), pp. 965–967 (cit. on p. 1).

[10] Robert Geroch. “What is a singularity in general relativity?” In: *Annals of Physics* 48.3 (July 1968), pp. 526–540 (cit. on p. 1).

[11] S.W. Hawking and G.F.R. Ellis. *The Large Scale Structure of Space-Time*. Cambridge Monographs on Mathematical Physics. Cambridge University Press, 1973 (cit. on pp. 1, 3, 6).

[12] Erik Curiel. “Singularities and Black Holes”. In: *The Stanford Encyclopedia of Philosophy*. Ed. by Edward N. Zalta. Fall 2021. Metaphysics Research Lab, Stanford University, 2021 (cit. on p. 1).

[13] Raúl Carballo-Rubio, Francesco Di Filippo, Stefano Liberati, and Matt Visser. “Geodesically complete black holes”. In: *Phys. Rev. D* 101 (2020), p. 084047. arXiv: 1911.11200 [gr-qc] (cit. on pp. 1, 15, 204).

[14] Roger Penrose. “Gravitational collapse and space-time singularities”. In: *Phys. Rev. Lett.* 14 (1965), pp. 57–59 (cit. on p. 1).

[15] R. Penrose. “Gravitational collapse: The role of general relativity”. In: *Riv. Nuovo Cim.* 1 (1969), pp. 252–276 (cit. on p. 1).

[16] R. Penrose. “SINGULARITIES AND TIME ASYMMETRY”. In: *General Relativity: An Einstein Centenary Survey*. 1980, pp. 581–638 (cit. on p. 1).

[17] Roger Penrose. “Singularities in Cosmology”. In: *Confrontation of Cosmological Theories with Observational Data*. Ed. by M. S. Longair. Dordrecht: Springer Netherlands, 1974, pp. 263–272 (cit. on p. 1).

[18] B. P. Abbott et al. “Observation of Gravitational Waves from a Binary Black Hole Merger”. In: *Phys. Rev. Lett.* 116.6 (2016), p. 061102. arXiv: 1602.03837 [gr-qc] (cit. on pp. 1, 4).

[19] B. P. Abbott et al. “GW170817: Observation of Gravitational Waves from a Binary Neutron Star Inspiral”. In: *Phys. Rev. Lett.* 119.16 (2017), p. 161101. arXiv: 1710.05832 [gr-qc] (cit. on p. 1).

[20] Kazunori Akiyama et al. “First M87 Event Horizon Telescope Results. I. The Shadow of the Supermassive Black Hole”. In: *Astrophys. J. Lett.* 875 (2019), p. L1. arXiv: 1906.11238 [astro-ph.GA] (cit. on pp. 1, 4).

[21] Kazunori Akiyama et al. “First Sagittarius A* Event Horizon Telescope Results. I. The Shadow of the Supermassive Black Hole in the Center of the Milky Way”. In: *Astrophys. J. Lett.* 930.2 (2022), p. L12 (cit. on pp. 1, 4).

[22] Marek A. Abramowicz, Wlodek Kluzniak, and Jean-Pierre Lasota. “No observational proof of the black hole event-horizon”. In: *Astron. Astrophys.* 396 (2002), pp. L31–L34. arXiv: astro-ph/0207270 (cit. on pp. 1, 4).

[23] Matt Visser. “Physical observability of horizons”. In: *Phys. Rev. D* 90.12 (2014), p. 127502. arXiv: 1407.7295 [gr-qc] (cit. on pp. 1, 4).

[24] Jahed Abedi, Hannah Dykaar, and Niayesh Afshordi. “Echoes from the Abyss: Tentative evidence for Planck-scale structure at black hole horizons”. In: *Phys. Rev. D* 96.8 (2017), p. 082004. arXiv: 1612.00266 [gr-qc] (cit. on p. 1).

[25] Raúl Carballo-Rubio, Francesco Di Filippo, Stefano Liberati, and Matt Visser. “Phenomenological aspects of black holes beyond general relativity”. In: *Phys. Rev.* D98.12 (2018), p. 124009. arXiv: 1809.08238 [gr-qc] (cit. on pp. 1, 175).

[26] Vitor Cardoso and Paolo Pani. “Testing the nature of dark compact objects: a status report”. In: *Living Rev. Rel.* 22.1 (2019), p. 4. arXiv: 1904.05363 [gr-qc] (cit. on pp. 1, 4, 5, 21).

[27] Bob Holdom. “Not quite black holes at LIGO”. In: *Phys. Rev. D* 101 (6 Mar. 2020), p. 064063 (cit. on p. 1).

[28] Jahed Abedi, Niayesh Afshordi, Naritaka Oshita, and Qingwen Wang. “Quantum Black Holes in the Sky”. In: *Universe* 6.3 (2020), p. 43. arXiv: 2001.09553 [gr-qc] (cit. on pp. 1, 175).

[29] Sebastian Murk. “Nomen non est omen: why it is too soon to identify ultra-compact objects as black holes”. In: (Oct. 2022). arXiv: 2210.03750 [gr-qc] (cit. on pp. 1, 4).

[30] Raúl Carballo-Rubio, Vitor Cardoso, and Ziri Younsi. “Toward very large baseline interferometry observations of black hole structure”. In: *Phys. Rev. D* 106.8 (2022), p. 084038. arXiv: 2208.00704 [gr-qc] (cit. on pp. 1, 5, 175).

[31] Werner Israel. “Event horizons in static electrovac space-times”. In: *Commun. Math. Phys.* 8 (1968), pp. 245–260 (cit. on p. 1).

[32] B. Carter. “Axisymmetric Black Hole Has Only Two Degrees of Freedom”. In: *Phys. Rev. Lett.* 26 (6 Feb. 1971), pp. 331–333 (cit. on p. 1).

[33] N. D. Birrell and P. C. W. Davies. *Quantum Fields in Curved Space*. Cambridge Monographs on Mathematical Physics. Cambridge, UK: Cambridge Univ. Press, 1984 (cit. on pp. 1, 6, 8, 181, 191).

[34] R.M. Wald. *Quantum Field Theory in Curved Spacetime and Black Hole Thermodynamics*. Chicago Lectures in Physics. University of Chicago Press, 1994 (cit. on pp. 1, 148, 181).

[35] L. Parker and D. Toms. *Quantum Field Theory in Curved Spacetime: Quantized Fields and Gravity*. Cambridge Monographs on Mathematical Physics. Cambridge University Press, 2009 (cit. on p. 1).

[36] Bei-Lok B. Hu and Enric Verdaguer. *Semiclassical and Stochastic Gravity: Quantum Field Effects on Curved Spacetime*. Cambridge Monographs on Mathematical Physics. Cambridge University Press, 2020 (cit. on pp. 1, 6, 10).

[37] Colin Montgomery, Wayne Orchiston, and Ian Whittingham. "Michell, Laplace and the origin of the black hole concept". In: *Journal of Astronomical History and Heritage* 12.2 (July 2009), pp. 90–96 (cit. on p. 2).

[38] John Michell. "On the Means of Discovering the Distance, Magnitude, &c. of the Fixed Stars, in Consequence of the Diminution of the Velocity of Their Light, in Case Such a Diminution Should be Found to Take Place in any of Them, and Such Other Data Should be Procured from Observations, as Would be Farther Necessary for That Purpose." In: *Phil. Trans. Roy. Soc. Lond.* 74 (1784), pp. 35–57 (cit. on p. 2).

[39] Pierre-Simon Laplace. *Exposition du systéme du monde*. 2nd ed. Cambridge Library Collection - Mathematics. Cambridge University Press, 2009 (cit. on p. 2).

[40] Karl Schwarzschild. "On the gravitational field of a mass point according to Einstein's theory". In: *Sitzungsber. Preuss. Akad. Wiss. Berlin (Math. Phys.)* 1916 (1916), pp. 189–196. arXiv: `physics/9905030` (cit. on p. 2).

[41] Charles W. Misner and David H. Sharp. "Relativistic equations for adiabatic, spherically symmetric gravitational collapse". In: *Phys. Rev.* 136 (1964), B571–B576 (cit. on pp. 2, 72, 159).

[42] Walter C. Hernandez and Charles W. Misner. "Observer Time as a Coordinate in Relativistic Spherical Hydrodynamics". In: *Astrophys. J.* 143 (1966), p. 452 (cit. on pp. 2, 72).

[43] Sean A. Hayward. "Gravitational energy in spherical symmetry". In: *Phys. Rev.* D53 (1996), pp. 1938–1949. arXiv: `gr-qc/9408002 [gr-qc]` (cit. on pp. 2, 72).

[44] R. Arnowitt, S. Deser, and C. W. Misner. "Energy and the Criteria for Radiation in General Relativity". In: *Phys. Rev.* 118 (4 May 1960), pp. 1100–1104 (cit. on p. 2).

[45] J. T. Jebsen. “On the general spherically symmetric solutions of Einstein’s gravitational equations in vacuo”. In: *General Relativity and Gravitation* 37.12 (Dec. 2005), pp. 2253–2259 (cit. on p. 2).

[46] G.D. Birkhoff and R.E. Langer. *Relativity and Modern Physics*. Harvard University Press, 1923 (cit. on p. 2).

[47] Abbé Georges Lemaître. “The Expanding Universe”. In: *General Relativity and Gravitation* 29.5 (May 1997), pp. 641–680 (cit. on pp. 3, 72, 83).

[48] G. Szekeres. “On the singularities of a Riemannian manifold”. In: *Publ. Math. Debrecen* 7 (1960), pp. 285–301 (cit. on p. 3).

[49] M. D. Kruskal. “Maximal Extension of Schwarzschild Metric”. In: *Phys. Rev.* 119 (5 Sept. 1960), pp. 1743–1745 (cit. on p. 3).

[50] J. R. Oppenheimer and H. Snyder. “On Continued Gravitational Contraction”. In: *Phys. Rev.* 56 (5 Sept. 1939), pp. 455–459 (cit. on p. 3).

[51] Roger Penrose. “Gravitational Collapse and Space-Time Singularities”. In: *Phys. Rev. Lett.* 14 (3 Jan. 1965), pp. 57–59 (cit. on p. 3).

[52] S. W. Hawking and R. Penrose. “The Singularities of gravitational collapse and cosmology”. In: *Proc. Roy. Soc. Lond. A* 314 (1970), pp. 529–548 (cit. on p. 3).

[53] C.W. Misner, K.S. Thorne, J.A. Wheeler, and D.I. Kaiser. *Gravitation*. Princeton University Press, 2017 (cit. on pp. 3, 6, 74).

[54] Karl Schwarzschild. “On the gravitational field of a sphere of incompressible fluid according to Einstein’s theory”. In: *Sitzungsber. Preuss. Akad. Wiss. Berlin (Math. Phys.)* 1916 (1916), pp. 424–434. arXiv: `physics/9912033 [physics.hist-ph]` (cit. on p. 3).

[55] Richard C. Tolman. “Static Solutions of Einstein’s Field Equations for Spheres of Fluid”. In: *Phys. Rev.* 55 (4 Feb. 1939), pp. 364–373 (cit. on pp. 3, 75, 83).

[56] G. M. Volkoff. “On the Equilibrium of Massive Spheres”. In: *Phys. Rev.* 55 (4 Feb. 1939), pp. 413–413 (cit. on pp. 3, 75, 76, 87, 92).

[57] H. A. Buchdahl. “General Relativistic Fluid Spheres”. In: *Phys. Rev.* 116 (4 1959), pp. 1027–1034 (cit. on pp. 3, 18, 74, 86, 164, 176).

[58] J. R. Oppenheimer and G. M. Volkoff. “On Massive Neutron Cores”. In: *Phys. Rev.* 55 (4 Feb. 1939), pp. 374–381 (cit. on pp. 3, 76).

[59] Clifford E. Rhoades and Remo Ruffini. “Maximum Mass of a Neutron Star”. In: *Phys. Rev. Lett.* 32 (6 Feb. 1974), pp. 324–327 (cit. on p. 3).

[60] John L. Friedman and James R. Ipser. “On the Maximum Mass of a Uniformly Rotating Neutron Star”. In: 314 (Mar. 1987), p. 594 (cit. on p. 3).

[61] B. K. Harrison, K. S. Thorne, M. Wakano, and J. A. Wheeler. *Gravitation Theory and Gravitational Collapse*. 1965 (cit. on p. 3).

[62] D. Lynden-Bell and M. J. Rees. “On Quasars, Dust and the Galactic Centre”. In: *Monthly Notices of the Royal Astronomical Society* 152.4 (July 1971), pp. 461–475. eprint: https://academic.oup.com/mnras/article-pdf/152/4/461/9402718/mnras152-0461.pdf (cit. on p. 4).

[63] M. Schmidt. “3C 273 : A Star-Like Object with Large Red-Shift”. In: 197.4872 (Mar. 1963), p. 1040 (cit. on p. 4).

[64] C. T. Bolton. “Identification of Cygnus X-1 with HDE 226868”. In: 235.5336 (Feb. 1972), pp. 271–273 (cit. on p. 4).

[65] A. M. Ghez, S. Salim, Seth D. Hornstein, et al. “Stellar orbits around the galactic center black hole”. In: *Astrophys. J.* 620 (2005), pp. 744–757. arXiv: astro-ph/0306130 (cit. on p. 4).

[66] Roy P. Kerr. “Gravitational field of a spinning mass as an example of algebraically special metrics”. In: *Phys. Rev. Lett.* 11 (1963), pp. 237–238 (cit. on p. 4).

[67] Werner Collmar, Norbert Straumann, Sandip K. Chakrabarti, et al. “Panel Discussion: The Definitive Proofs of the Existence of Black Holes”. In: *Black Holes: Theory and Observation*. Ed. by Friedrich W. Hehl, Claus Kiefer, and Ralph J.K. Metzler. Berlin, Heidelberg: Springer Berlin Heidelberg, 1998, pp. 481–489 (cit. on p. 4).

[68] Vitor Cardoso and Paolo Pani. “Tests for the existence of black holes through gravitational wave echoes”. In: *Nat. Astron.* 1.1 (2017), pp. 586–591. arXiv: 1707.03021 [gr-qc] (cit. on p. 4).

[69] Zachary Mark, Aaron Zimmerman, Song Ming Du, and Yanbei Chen. “A recipe for echoes from exotic compact objects”. In: *Phys. Rev. D* 96.8 (2017), p. 084002. arXiv: 1706.06155 [gr-qc] (cit. on p. 4).

[70] Alfredo Urbano and Hardi Veermäe. “On gravitational echoes from ultracompact exotic stars”. In: *JCAP* 04 (2019), p. 011. arXiv: 1810.07137 [gr-qc] (cit. on pp. 4, 5, 18, 74, 178).

[71] Taishi Ikeda, Massimo Bianchi, Dario Consoli, et al. “Black-hole microstate spectroscopy: Ringdown, quasinormal modes, and echoes”. In: *Phys. Rev. D* 104 (6 2021), p. 066021 (cit. on pp. 4, 5).

[72] Alexandre Toubiana, Stanislav Babak, Enrico Barausse, and Luis Lehner. "Modeling gravitational waves from exotic compact objects". In: *Phys. Rev. D* 103.6 (2021), p. 064042. arXiv: 2011.12122 [gr-qc] (cit. on p. 4).

[73] Sean A. Hayward. "Marginal surfaces and apparent horizons". In: (1993). arXiv: gr-qc/9303006 (cit. on p. 4).

[74] Abhay Ashtekar and Badri Krishnan. "Dynamical horizons and their properties". In: *Phys. Rev. D* 68 (2003), p. 104030. arXiv: gr-qc/0308033 (cit. on p. 4).

[75] Abhay Ashtekar and Badri Krishnan. "Isolated and dynamical horizons and their applications". In: *Living Rev. Rel.* 7 (2004), p. 10. arXiv: gr-qc/0407042 (cit. on p. 4).

[76] Tommaso De Lorenzo, Costantino Pacilio, Carlo Rovelli, and Simone Speziale. "On the Effective Metric of a Planck Star". In: *Gen. Rel. Grav.* 47.4 (2015), p. 41. arXiv: 1412.6015 [gr-qc] (cit. on p. 4).

[77] Sean A. Hayward. "Formation and Evaporation of Nonsingular Black Holes". In: *Phys. Rev. Lett.* 96 (3 Jan. 2006), p. 031103 (cit. on p. 5).

[78] Frank Saueressig, Natalia Alkofer, Giulio D'Odorico, and Francesca Vidotto. "Black holes in Asymptotically Safe Gravity". In: *PoS* FFP14 (2016), p. 174. arXiv: 1503.06472 [hep-th] (cit. on p. 5).

[79] Jahed Abedi and Hessamaddin Arfaei. "Obstruction of black hole singularity by quantum field theory effects". In: *JHEP* 03 (2016), p. 135. arXiv: 1506.05844 [gr-qc] (cit. on p. 5).

[80] Abhay Ashtekar, Javier Olmedo, and Parampreet Singh. "Regular black holes from Loop Quantum Gravity". In: (Jan. 2023). arXiv: 2301.01309 [gr-qc] (cit. on p. 5).

[81] Francesco Di Filippo, Raúl Carballo-Rubio, Stefano Liberati, Costantino Pacilio, and Matt Visser. "On the Inner Horizon Instability of Non-Singular Black Holes". In: *Universe* 8.4 (2022), p. 204. arXiv: 2203.14516 [gr-qc] (cit. on p. 5).

[82] Alfio Bonanno, Amir-Pouyan Khosravi, and Frank Saueressig. "Regular black holes with stable cores". In: *Phys. Rev. D* 103.12 (2021), p. 124027. arXiv: 2010.04226 [gr-qc] (cit. on p. 5).

[83] Raúl Carballo-Rubio, Francesco Di Filippo, Stefano Liberati, Costantino Pacilio, and Matt Visser. "Comment on "Stability properties of Regular Black Holes"". In: (Dec. 2022). arXiv: 2212.07458 [gr-qc] (cit. on p. 5).

[84] Steven L. Liebling and Carlos Palenzuela. “Dynamical Boson Stars”. In: *Living Rev. Rel.* 15 (2012), p. 6. arXiv: 1202.5809 [gr-qc] (cit. on p. 5).

[85] Richard Brito, Vitor Cardoso, Carlos A. R. Herdeiro, and Eugen Radu. “Proca stars: Gravitating Bose–Einstein condensates of massive spin 1 particles”. In: *Phys. Lett. B* 752 (2016), pp. 291–295. arXiv: 1508.05395 [gr-qc] (cit. on p. 5).

[86] Miguel Alcubierre, Juan Barranco, Argelia Bernal, et al. “Boson stars and their relatives in semiclassical gravity”. In: (Dec. 2022). arXiv: 2212.02530 [gr-qc] (cit. on pp. 5, 177).

[87] Guilherme Raposo, Paolo Pani, Miguel Bezares, Carlos Palenzuela, and Vitor Cardoso. “Anisotropic stars as ultracompact objects in General Relativity”. In: *Phys. Rev.* D99.10 (2019), p. 104072. arXiv: 1811.07917 [gr-qc] (cit. on p. 5).

[88] Gianmassimo Tasinato. “Ultracompact vector stars”. In: *Phys. Rev. D* 106 (4 Aug. 2022), p. 044022 (cit. on p. 5).

[89] L. Del Grosso, G. Franciolini, P. Pani, and A. Urbano. “Fermion soliton stars”. In: (Jan. 2023). arXiv: 2301.08709 [gr-qc] (cit. on p. 5).

[90] Gonzalo J. Olmo, Diego Rubiera-Garcia, and Aneta Wojnar. “Stellar structure models in modified theories of gravity: Lessons and challenges”. In: *Phys. Rept.* 876 (2020), pp. 1–75. arXiv: 1912.05202 [gr-qc] (cit. on p. 5).

[91] Pawel O. Mazur and Emil Mottola. “Gravitational vacuum condensate stars”. In: *Proc. Nat. Acad. Sci.* 101 (2004), pp. 9545–9550. arXiv: gr-qc/0407075 (cit. on pp. 5, 85, 142, 177).

[92] Bob Holdom and Jing Ren. “Not quite a black hole”. In: *Phys. Rev. D* 95 (8 2017), p. 084034 (cit. on pp. 5, 177).

[93] Samir D. Mathur. “The Fuzzball proposal for black holes: An Elementary review”. In: *Fortsch. Phys.* 53 (2005), pp. 793–827. arXiv: hep-th/0502050 [hep-th] (cit. on pp. 5, 177).

[94] Paolo Pani, Emanuele Berti, Vitor Cardoso, Yanbei Chen, and Richard Norte. “Gravitational wave signatures of the absence of an event horizon. I. Nonradial oscillations of a thin-shell gravastar”. In: *Phys. Rev. D* 80 (2009), p. 124047. arXiv: 0909.0287 [gr-qc] (cit. on p. 5).

[95] John F. Donoghue. “General relativity as an effective field theory: The leading quantum corrections”. In: *Phys. Rev. D* 50 (1994), pp. 3874–3888. arXiv: gr-qc/9405057 (cit. on p. 5).

[96] Carlo Rovelli. “Notes for a brief history of quantum gravity”. In: *9th Marcel Grossmann Meeting on Recent Developments in Theoretical and Experimental General Relativity, Gravitation and Relativistic Field Theories (MG 9)*. June 2000, pp. 742–768. arXiv: gr-qc/0006061 (cit. on p. 6).

[97] Steven Carlip. “Is Quantum Gravity Necessary?” In: *Class. Quant. Grav.* 25 (2008). Ed. by Daniel Arteaga and Enric Verdaguer, p. 154010. arXiv: 0803.3456 [gr-qc] (cit. on p. 6).

[98] S. W. Hawking. “Black hole explosions?” In: 248.5443 (Mar. 1974), pp. 30–31 (cit. on p. 6).

[99] S. W. Hawking. “Particle Creation by Black Holes”. In: *Commun. Math. Phys.* 43 (1975). Ed. by G. W. Gibbons and S. W. Hawking. [Erratum: Commun.Math.Phys. 46, 206 (1976)], pp. 199–220 (cit. on p. 6).

[100] Bryce S. DeWitt. “Quantum Field Theory in Curved Space-Time”. In: *Phys. Rept.* 19 (1975), pp. 295–357 (cit. on p. 6).

[101] A. Fabbri and J. Navarro-Salas. *Modeling Black Hole Evaporation*. Imperial College Press, 2005 (cit. on pp. 6, 24, 38, 39, 154, 162, 187, 191).

[102] Don N. Page. “Particle Emission Rates from a Black Hole: Massless Particles from an Uncharged, Nonrotating Hole”. In: *Phys. Rev. D* 13 (1976), pp. 198–206 (cit. on p. 6).

[103] Norma G. Sanchez. “Absorption and Emission Spectra of a Schwarzschild Black Hole”. In: *Phys. Rev. D* 18 (1978), p. 1030 (cit. on p. 6).

[104] L. Susskind. *The Black Hole War: My Battle with Stephen Hawking to Make the World Safe for Quantum Mechanics*. Little, Brown, 2008 (cit. on p. 6).

[105] William G. Unruh and Robert M. Wald. “Information Loss”. In: *Rept. Prog. Phys.* 80.9 (2017), p. 092002. arXiv: 1703.02140 [hep-th] (cit. on p. 6).

[106] S. A. Fulling. “"Radiation" and "vacuum polarization" near a black hole”. In: *Phys. Rev. D* 15 (8 Apr. 1977), pp. 2411–2414 (cit. on p. 6).

[107] Carlos Barceló, Stefano Liberati, Sebastiano Sonego, and Matt Visser. “Black Stars, Not Holes”. In: *Scientific American* 301 (2009), pp. 38–45 (cit. on pp. 6, 71).

[108] Matt Visser. “Gravitational vacuum polarization. II. Energy conditions in the Boulware vacuum”. In: *Physical Review D* 54.8 (1996), pp. 5116–5122 (cit. on pp. 7, 19, 159).

[109] Tomohiro Harada, Vitor Cardoso, and Daiki Miyata. “Particle creation in gravitational collapse to a horizonless compact object”. In: *Phys. Rev. D* 99.4 (2019), p. 044039. arXiv: 1811.05179 [gr-qc] (cit. on p. 7).

[110] Carlos Barceló, Valentin Boyanov, Raúl Carballo-Rubio, and Luis J. Garay. "Semiclassical gravity effects near horizon formation". In: *Class. Quant. Grav.* 36.16 (2019), p. 165004. arXiv: 1904.06558 [gr-qc] (cit. on p. 7).

[111] R. Brout, S. Massar, R. Parentani, and Ph. Spindel. "A Primer for black hole quantum physics". In: *Phys. Rept.* 260 (1995), pp. 329–454. arXiv: 0710.4345 [gr-qc] (cit. on p. 7).

[112] A. Fabbri, S. Farese, J. Navarro-Salas, G. J. Olmo, and H. Sanchis-Alepuz. "Semiclassical zero-temperature corrections to Schwarzschild spacetime and holography". In: *Physical Review D* 73.10 (2006) (cit. on pp. 7, 10, 13, 23, 24, 26, 38, 145, 162, 176).

[113] Sumanta Chakraborty, Suprit Singh, and T. Padmanabhan. "A quantum peek inside the black hole event horizon". In: *JHEP* 06 (2015), p. 192. arXiv: 1503.01774 [gr-qc] (cit. on p. 7).

[114] Raúl Carballo-Rubio. "Stellar Equilibrium in Semiclassical Gravity". In: *Physical Review Letters* 120.6 (Feb. 2018) (cit. on pp. 7, 93, 142).

[115] Carlos Barceló, Valentin Boyanov, Raúl Carballo-Rubio, and Luis J. Garay. "Black hole inner horizon evaporation in semiclassical gravity". In: *Class. Quant. Grav.* 38.12 (2021), p. 125003. arXiv: 2011.07331 [gr-qc] (cit. on pp. 7, 178).

[116] Carlos Barceló, Valentin Boyanov, Raúl Carballo-Rubio, and Luis J. Garay. "Classical mass inflation versus semiclassical inner horizon inflation". In: *Phys. Rev. D* 106.12 (2022), p. 124006. arXiv: 2203.13539 [gr-qc] (cit. on pp. 7, 142, 178).

[117] L. Parker. "Particle creation in expanding universes". In: *Phys. Rev. Lett.* 21 (1968), pp. 562–564 (cit. on p. 7).

[118] S. W. Hawking. "Breakdown of predictability in gravitational collapse". In: *Phys. Rev. D* 14 (10 1976), pp. 2460–2473 (cit. on pp. 7, 71).

[119] P. C. W. Davies and S. A. Fulling. "Quantum Vacuum Energy in Two Dimensional Space-Times". In: *Proceedings of the Royal Society of London. Series A, Mathematical and Physical Sciences* 354.1676 (1977), pp. 59–77 (cit. on pp. 7, 8, 189, 190).

[120] Julian S. Schwinger. "On gauge invariance and vacuum polarization". In: *Phys. Rev.* 82 (1951). Ed. by K. A. Milton, pp. 664–679 (cit. on p. 7).

[121] W. G. Unruh. "Notes on black hole evaporation". In: *Phys. Rev. D* 14 (1976), p. 870 (cit. on p. 7).

[122] Julio Arrechea, Carlos Barceló, Luis J. Garay, and Gerardo Garcıa-Moreno. "Inversion of statistics and thermalization in the Unruh effect". In: *Phys. Rev. D* 104 (6 Sept. 2021), p. 065004 (cit. on p. 7).

[123] S. M. Christensen. "Vacuum expectation value of the stress tensor in an arbitrary curved background: The covariant point-separation method". In: *Phys. Rev. D* 14 (10 1976), pp. 2490–2501 (cit. on pp. 8, 183).

[124] Leonard Parker and S. A. Fulling. "Adiabatic regularization of the energy momentum tensor of a quantized field in homogeneous spaces". In: *Phys. Rev. D* 9 (1974), pp. 341–354 (cit. on p. 8).

[125] Robert M. Wald. "Axiomatic Renormalization of the Stress Tensor of a Conformally Invariant Field in Conformally Flat Space-Times". In: *Annals Phys.* 110 (1978), pp. 472–486 (cit. on p. 8).

[126] M. R. Brown and A. C. Ottewill. "Photon propagators and the definition and approximation of renormalized stress tensors in curved space-time". In: *Phys. Rev. D* 34 (6 Sept. 1986), pp. 1776–1786 (cit. on pp. 8, 181–183).

[127] Paul R. Anderson, William A. Hiscock, and David A. Samuel. "Stress-energy tensor of quantized scalar fields in static spherically symmetric spacetimes". In: *Phys. Rev. D* 51 (8 1995), pp. 4337–4358 (cit. on pp. 8, 9, 40, 102, 138, 142, 145, 147, 149, 162, 173, 182, 185, 204).

[128] Yves Decanini and Antoine Folacci. "Hadamard renormalization of the stress-energy tensor for a quantized scalar field in a general spacetime of arbitrary dimension". In: *Phys. Rev. D* 78 (2008), p. 044025. arXiv: gr-qc/0512118 (cit. on pp. 8, 183, 190).

[129] Peter Taylor, Cormac Breen, and Adrian Ottewill. "Mode-sum prescription for the renormalized stress energy tensor on black hole spacetimes". In: *Phys. Rev. D* 106.6 (2022), p. 065023. arXiv: 2201.05174 [gr-qc] (cit. on pp. 8, 11).

[130] Adrian C. Ottewill and Peter Taylor. "Renormalized Vacuum Polarization and Stress Tensor on the Horizon of a Schwarzschild Black Hole Threaded by a Cosmic String". In: *Class. Quant. Grav.* 28 (2011), p. 015007. arXiv: 1010.3943 [gr-qc] (cit. on pp. 8, 181, 183).

[131] Cormac Breen and Adrian C. Ottewill. "Hadamard renormalization of the stress energy tensor in a spherically symmetric black hole space-time with an application to lukewarm black holes". In: *Phys. Rev. D* 85 (8 2012), p. 084029 (cit. on pp. 8, 181, 184).

[132] Paul R. Anderson and Wayne Eaker. “Analytic approximation and an improved method for computing the stress-energy of quantized scalar fields in Robertson-Walker spacetimes”. In: *Phys. Rev. D* 61 (2 Dec. 1999), p. 024003 (cit. on pp. 9, 185).

[133] Eric D. Carlson, William H. Hirsch, Benedikt Obermayer, Paul R. Anderson, and Peter B. Groves. “Stress energy tensor for the massless spin 1/2 field in static black hole space-times”. In: *Phys. Rev. Lett.* 91 (2003), p. 051301. arXiv: gr-qc/0305045 (cit. on p. 9).

[134] K. W. Howard. “VACUUM $<$ T (MU) (NU) $>$ IN SCHWARZSCHILD SPACE-TIME”. In: *Phys. Rev. D* 30 (1984), pp. 2532–2547 (cit. on pp. 9, 147, 185).

[135] K. W. Howard and P. Candelas. “Quantum Stress Tensor in Schwarzschild Space-Time”. In: *Phys. Rev. Lett.* 53 (5 July 1984), pp. 403–406 (cit. on pp. 9, 185).

[136] Paul R. Anderson. “A method to compute φ^2 in asymptotically flat, static, spherically symmetric spacetimes”. In: *Phys. Rev. D* 41 (4 Feb. 1990), pp. 1152–1162 (cit. on p. 9).

[137] Adam Levi, Ehud Eilon, Amos Ori, and Maarten van de Meent. “Renormalized stress-energy tensor of an evaporating spinning black hole”. In: *Phys. Rev. Lett.* 118.14 (2017), p. 141102. arXiv: 1610.04848 [gr-qc] (cit. on p. 9).

[138] N. D. Birrell and P. C. W. Davies. “On falling through a black hole into another universe”. In: *Nature* 272 (1978), p. 35 (cit. on pp. 9, 44).

[139] Noa Zilberman, Marc Casals, Amos Ori, and Adrian C. Ottewill. “Quantum Fluxes at the Inner Horizon of a Spinning Black Hole”. In: *Phys. Rev. Lett.* 129.26 (2022), p. 261102. arXiv: 2203.08502 [gr-qc] (cit. on pp. 9, 44, 179).

[140] Eanna E. Flanagan and Robert M. Wald. “Does back reaction enforce the averaged null energy condition in semiclassical gravity?” In: *Phys. Rev. D* 54 (1996), pp. 6233–6283. arXiv: gr-qc/9602052 (cit. on pp. 10, 146, 149, 152).

[141] Jonathan Z. Simon. “The Stability of flat space, semiclassical gravity, and higher derivatives”. In: *Phys. Rev. D* 43 (1991), pp. 3308–3316 (cit. on pp. 10, 12, 146).

[142] C. Barcelo, R. Carballo, and L. J. Garay. "Two formalisms, one renormalized stress-energy tensor". In: *Phys. Rev. D* 85 (2012), p. 084001. arXiv: 1112.0489 [gr-qc] (cit. on p. 10).

[143] Alexei A. Starobinsky. "A New Type of Isotropic Cosmological Models Without Singularity". In: *Phys. Lett. B* 91 (1980). Ed. by I. M. Khalatnikov and V. P. Mineev, pp. 99–102 (cit. on p. 10).

[144] Leonard Parker and Jonathan Z. Simon. "Einstein equation with quantum corrections reduced to second order". In: *Physical Review D* 47.4 (1993), pp. 1339–1355 (cit. on pp. 10, 12, 146, 147, 149, 172).

[145] Renaud Parentani and Tsvi Piran. "The Internal geometry of an evaporating black hole". In: *Phys. Rev. Lett.* 73 (1994), pp. 2805–2808. arXiv: hep-th/9405007 [hep-th] (cit. on pp. 10, 13, 16, 23, 71, 178).

[146] Paul R. Anderson, William A. Hiscock, and Daniel J. Loranz. "Semiclassical stability of the extreme Reissner-Nordstrom black hole". In: *Phys. Rev. Lett.* 74 (1995), pp. 4365–4368. arXiv: gr-qc/9504019 (cit. on pp. 11, 67).

[147] William A. Hiscock, Shane L. Larson, and Paul R. Anderson. "Semiclassical effects in black hole interiors". In: *Phys. Rev. D* 56 (1997), pp. 3571–3581. arXiv: gr-qc/9701004 (cit. on p. 11).

[148] F. Rohrlich. "The self-force and radiation reaction". In: *American Journal of Physics* 68.12 (2000), pp. 1109–1112. eprint: https://doi.org/10.1119/1.1286430 (cit. on pp. 11, 146).

[149] L.D. Landau and E.M. Lifshitz. *The Classical Theory of Fields: Volume 2*. Course of theoretical physics. Elsevier Science, 1975 (cit. on pp. 12, 149).

[150] LLuis Bel, T. Damour, N. Deruelle, J. Ibanez, and J. Martin. "Poincaré-invariant gravitational field and equations of motion of two pointlike objects: The postlinear approximation of general relativity". In: *Gen. Rel. Grav.* 13 (1981), pp. 963–1004 (cit. on pp. 12, 149).

[151] Paul R. Anderson, Carmen Molina-Parıs, and Emil Mottola. "Linear response, validity of semiclassical gravity, and the stability of flat space". In: *Phys. Rev. D* 67 (2 Jan. 2003), p. 024026 (cit. on p. 12).

[152] L. Bel and H. Sirousse Zia. "Regular reduction of relativistic theories of gravitation with a quadratic Lagrangian". In: *Phys. Rev. D* 32 (12 Dec. 1985), pp. 3128–3135 (cit. on pp. 12, 149, 150).

[153] Ramiro Cayuso and Luis Lehner. "Nonlinear, noniterative treatment of EFT-motivated gravity". In: *Phys. Rev. D* 102.8 (2020), p. 084008. arXiv: 2005.13720 [gr-qc] (cit. on p. 12).

[154] Paul Halpern. “Semiclassical corrections to Kasner cosmologies”. In: *Gen. Rel. Grav.* 26 (1994), pp. 781–796 (cit. on pp. 12, 147, 149).

[155] Jonathan Z. Simon. “No Starobinsky inflation from self-consistent semiclassical gravity”. In: *Phys. Rev. D* 45 (6 Mar. 1992), pp. 1953–1960 (cit. on pp. 12, 147, 149).

[156] Alexander M. Polyakov. “Quantum Geometry of Bosonic Strings”. In: *Phys. Lett.* B103 (1981), pp. 207–210 (cit. on pp. 13, 154, 162).

[157] Curtis G. Callan Jr., Steven B. Giddings, Jeffrey A. Harvey, and Andrew Strominger. “Evanescent black holes”. In: *Phys. Rev. D* 45.4 (1992), R1005. arXiv: hep-th/9111056 (cit. on p. 13).

[158] O. B. Zaslavskii. “Boulware state in exactly solvable models of 2D dilaton gravity”. In: *Mod. Phys. Lett. A* 21 (2006), pp. 2283–2290. arXiv: hep-th/0608183 (cit. on pp. 13, 38).

[159] Alex Simpson and Matt Visser. “Black-bounce to traversable wormhole”. In: *JCAP* 02 (2019), p. 042. arXiv: 1812.07114 [gr-qc] (cit. on p. 15).

[160] G. F. R. Ellis and B. G. Schmidt. “Singular space-times”. In: *Gen. Rel. Grav.* 8 (1977), pp. 915–953 (cit. on pp. 15, 44, 64, 69).

[161] Shai Ayal and Tsvi Piran. “Spherical collapse of a massless scalar field with semiclassical corrections”. In: *Phys. Rev. D* 56 (1997), pp. 4768–4774. arXiv: gr-qc/9704027 (cit. on p. 16).

[162] Celine Cattoen, Tristan Faber, and Matt Visser. “Gravastars must have anisotropic pressures”. In: *Classical and Quantum Gravity* 22.20 (Sept. 2005), pp. 4189–4202 (cit. on pp. 18, 142).

[163] Paschalis Karageorgis and John G. Stalker. “Sharp bounds on 2m/r for static spherical objects”. In: *Class. Quant. Grav.* 25 (2008), p. 195021. arXiv: 0707.3632 [gr-qc] (cit. on p. 18).

[164] Artur Alho, José Natário, Paolo Pani, and Guilherme Raposo. “Compactness bounds in general relativity”. In: *Phys. Rev. D* 106.4 (2022), p. L041502. arXiv: 2202.00043 [gr-qc] (cit. on pp. 18, 177).

[165] Christopher J. Fewster. “Lectures on quantum energy inequalities”. In: (2012). arXiv: 1208.5399 [gr-qc] (cit. on p. 19).

[166] William A. Hiscock. “Gravitational vacuum polarization around static spherical stars”. In: *Phys. Rev. D* 37 (8 1988), pp. 2142–2150 (cit. on pp. 19, 71, 111, 177).

[167] Ignacio A. Reyes and Giovanni Maria Tomaselli. “Compact stars in Quantum Field Theory”. In: (Jan. 2023). arXiv: 2301.00826 [gr-qc] (cit. on pp. 19, 71, 141, 177).

[168] Pau Beltrán-Palau, Adrián del Rıo, and José Navarro-Salas. “Quantum corrections to the Schwarzschild metric from vacuum polarization”. In: (Dec. 2022). arXiv: 2212.08089 [gr-qc] (cit. on pp. 19, 38, 176, 177).

[169] David G. Boulware. “Quantum field theory in Schwarzschild and Rindler spaces”. In: *Phys. Rev. D* 11 (6 Mar. 1975), pp. 1404–1423 (cit. on p. 23).

[170] Pei-Ming Ho and Yoshinori Matsuo. “Static Black Holes With Back Reaction From Vacuum Energy”. In: *Class. Quant. Grav.* 35.6 (2018), p. 065012. arXiv: 1703.08662 [hep-th] (cit. on pp. 23, 26, 34, 164, 176).

[171] Myungseok Eune, Yongwan Gim, and Wontae Kim. “Something special at the event horizon”. In: *Mod. Phys. Lett. A* 29.40 (2014), p. 1450215. arXiv: 1401.3501 [hep-th] (cit. on pp. 24, 45).

[172] Daniel J. Loranz, William A. Hiscock, and Paul R. Anderson. “Thermal divergences on the event horizons of two-dimensional black holes”. In: *Phys. Rev. D* 52 (8 Oct. 1995), pp. 4554–4558 (cit. on pp. 24, 45, 67).

[173] John Archibald Wheeler. “Geons”. In: *Phys. Rev.* 97 (2 Jan. 1955), pp. 511–536 (cit. on pp. 25, 37).

[174] Ernst Leonard Lindelöf. “Sur l’application de la méthode des approximations successives aux équations différentielles ordinaires du premier ordre”. In: *Comptes rendus hebdomadaires des séances de l’Académie des sciences*. Comptes rendus de l’Académie des sciences (1894), pp. 454–457 (cit. on p. 27).

[175] Luis C. Barbado, Carlos Barcelo, and Luis J. Garay. “Hawking radiation as perceived by different observers”. In: *Class. Quant. Grav.* 28 (2011), p. 125021. arXiv: 1101.4382 [gr-qc] (cit. on p. 29).

[176] Pei-Ming Ho and Yoshinori Matsuo. “Static black hole and vacuum energy: thin shell and incompressible fluid”. In: *Journal of High Energy Physics* 2018.3 (Mar. 2018) (cit. on pp. 33, 83).

[177] O. B. Zaslavskii. “Boulware state and semiclassical thermodynamics of black holes in a cavity”. In: *Phys. Rev. D* 68 (12 Dec. 2003), p. 127502 (cit. on p. 38).

[178] Yohan Potaux, Debajyoti Sarkar, and Sergey N. Solodukhin. “Quantum states and their back-reacted geometries in 2D dilaton gravity”. In: *Phys. Rev. D* 105 (2 Jan. 2022), p. 025015 (cit. on p. 38).

[179] A. Bonanno, S. Silveravalle, and A. Zuccotti. “Nonsymmetric wormholes and localized big rip singularities in Einstein-Weyl gravity”. In: *Phys. Rev. D* 105 (12 June 2022), p. 124059 (cit. on p. 38).

[180] H. Reissner. *Über die Eigengravitation des elektrischen Feldes nach der Einsteinschen Theorie*. Jan. 1916 (cit. on p. 43).

[181] Hermann Weyl. *Zur Gravitationstheorie*. Jan. 1917 (cit. on p. 43).

[182] G. Nordström. “On the Energy of the Gravitation field in Einstein’s Theory”. In: *Koninklijke Nederlandse Akademie van Wetenschappen Proceedings Series B Physical Sciences* 20 (Jan. 1918), pp. 1238–1245 (cit. on p. 43).

[183] G. B. Jeffery. “The Field of an Electron on Einstein’s Theory of Gravitation”. In: *Proceedings of the Royal Society of London. Series A, Containing Papers of a Mathematical and Physical Character* 99.697 (1921), pp. 123–134 (cit. on p. 43).

[184] Amos Ori. “Inner structure of a charged black hole: An exact mass-inflation solution”. In: *Phys. Rev. Lett.* 67 (7 Aug. 1991), pp. 789–792 (cit. on p. 44).

[185] Roberto Balbinot and Eric Poisson. “Mass inflation: The semiclassical regime”. In: *Phys. Rev. Lett.* 70 (1 Jan. 1993), pp. 13–16 (cit. on p. 44).

[186] William A. Hiscock. “Stress-energy tensor near a charged, rotating, evaporating black hole”. In: *Phys. Rev. D* 15 (10 1977), pp. 3054–3057 (cit. on p. 44).

[187] Maja Buric and Voja Radovanovic. “Quantum corrections for the Reisner-Nordstrom black hole”. In: *Class. Quant. Grav.* 16 (1999), pp. 3937–3951. arXiv: gr-qc/9907036 (cit. on p. 45).

[188] O. B. Zaslavskii. “Near extremal and extremal quantum corrected two-dimensional charged black holes”. In: *Class. Quant. Grav.* 21 (2004), pp. 2687–2701. arXiv: gr-qc/0404009 (cit. on p. 45).

[189] Bobo Wang and Chao-guang Huang. “Back reaction on a Reissner-Nordstrom black hole”. In: *Phys. Rev. D* 63 (2001), p. 124014 (cit. on p. 45).

[190] J. Matyjasek and O. B. Zaslavsky. “Quantum back reaction of massive fields and selfconsistent semiclassical extreme black holes and acceleration horizons”. In: *Phys. Rev. D* 64 (2001), p. 104018. arXiv: gr-qc/0102109 (cit. on p. 45).

[191] Brett E. Taylor, William A. Hiscock, and Paul R. Anderson. “Semiclassical charged black holes with a quantized massive scalar field”. In: *Phys. Rev. D* 61 (2000), p. 084021. arXiv: gr-qc/9911119 (cit. on p. 45).

[192] Sandip P. Trivedi. “Semiclassical extremal black holes”. In: *Phys. Rev. D* 47 (10 May 1993), pp. 4233–4238 (cit. on pp. 45, 64, 67, 176).

[193] C. Barbachoux and A. Fabbri. “Semiclassical zero temperature black holes in spherically reduced theories”. In: *Phys. Rev. D* 66 (2002), p. 024012. arXiv: hep-th/0201133 (cit. on pp. 45, 64, 67).

[194] Paul R. Anderson, William A. Hiscock, and Brett E. Taylor. “Do Semiclassical Zero Temperature Black Holes Exist?” In: *Phys. Rev. Lett.* 85 (12 Sept. 2000), pp. 2438–2441 (cit. on p. 67).

[195] David A. Lowe. “Comment on “Do Semiclassical Zero Temperature Black Holes Exist”””. In: *Phys. Rev. Lett.* 87 (2 June 2001), p. 029001 (cit. on p. 67).

[196] Paul R. Anderson, William A. Hiscock, and Brett E. Taylor. “Anderson, Hiscock, and Taylor Reply:” in: *Phys. Rev. Lett.* 87 (2 June 2001), p. 029002 (cit. on p. 67).

[197] Roberto Balbinot, Serena Fagnocchi, Alessandro Fabbri, Sara Farese, and Jose Navarro-Salas. “On the quantum stress tensor for extreme 2-D Reissner-Nordstrom black holes”. In: *Phys. Rev. D* 70 (2004), p. 064031. arXiv: hep-th/0405263 (cit. on p. 67).

[198] R. Balbinot, A. Fabbri, S. Farese, and R. Parentani. “Hawking radiation from extremal and nonextremal black holes”. In: *Phys. Rev. D* 76 (12 Dec. 2007), p. 124010 (cit. on p. 67).

[199] Dean Morgan, Stuart Thom, Elizabeth Winstanley, and Phil M. Young. “Some general properties of the renormalized stress-energy tensor for static quantum states on (n+1)-dimensional spherically symmetric black holes”. In: *Gen. Rel. Grav.* 39 (2007), pp. 1719–1734. arXiv: 0705.1131 [gr-qc] (cit. on p. 67).

[200] Valeri P. Frolov, P. Sutton, and A. Zelnikov. “The Dimensional reduction anomaly”. In: *Phys. Rev. D* 61 (2000), p. 024021. arXiv: hep-th/9909086 (cit. on p. 68).

[201] P. Sutton. “The Dimensional reduction anomaly in spherically symmetric space-times”. In: *Phys. Rev. D* 62 (2000), p. 044033. arXiv: hep-th/0003290 (cit. on p. 68).

[202] Robert P. Geroch. “Topology in general relativity”. In: *J. Math. Phys.* 8 (1967), pp. 782–786 (cit. on p. 71).

[203] A. Krasinski. “Editor’s Note: The Expanding Universe, by the Abbé Georges Lemaître”. In: *Gen. Rel. and Grav.* 29 (1997), pp. 637–640 (cit. on p. 72).

[204] Max Wyman. “Radially Symmetric Distributions of Matter”. In: *Phys. Rev.* 75 (12 June 1949), pp. 1930–1936 (cit. on pp. 75, 76, 92).

[205] Carlos Barcelo and Grigory Volovik. “A Stable Einstein universe”. In: *JETP Lett.* 80 (2004), pp. 209–213. arXiv: gr-qc/0405105 (cit. on p. 85).

[206] Pawel O. Mazur and Emil Mottola. “Surface tension and negative pressure interior of a non-singular ‘black hole’”. In: *Class. Quant. Grav.* 32.21 (2015), p. 215024. arXiv: 1501.03806 [gr-qc] (cit. on p. 87).

[207] R.C. Tolman. *Relativity, Thermodynamics, and Cosmology*. Dover Books on Physics. Dover Publications, 1987 (cit. on p. 87).

[208] J. Smoller and B. Temple. “Solutions of the Oppenheimer–Volkoff Equations Inside $9/8^{ths}$ of the Schwarzschild Radius”. In: (Mar. 1997) (cit. on p. 90).

[209] Andrzej Woszczyna, Marek Kutschera, Sebastian Kubis, et al. “Nakedly singular non-vacuum gravitating equilibrium states”. In: *Gen. Rel. Grav.* 48.1 (2016), p. 5 (cit. on p. 90).

[210] Łukasz Bratek, Joanna Jałocha, and Andrzej Woszczyna. “Nakedly singular counterpart of Schwarzschild’s incompressible star. A barotropic continuity condition in the center”. In: *Gen. Rel. Grav.* 51.11 (2019), p. 142. arXiv: 1906.09140 [gr-qc] (cit. on p. 90).

[211] Charis Anastopoulos and Ntina Savvidou. “Classification theorem and properties of singular solutions to the Tolman-Oppenheimer-Volkoff equation”. In: (Oct. 2020). arXiv: 2010.02279 [gr-qc] (cit. on p. 90).

[212] Amal Kumar Raychaudhuri. “Volkoff’s Massive Spheres”. In: *Phys. Rev.* 84 (1 Oct. 1951), pp. 166–166 (cit. on p. 92).

[213] Guilherme L. Volkmer, Dimiter Hadjimichef, Moises Razeira, Benno Bodmann, and César A. Zen Vasconcellos. “Ultra-compact objects in semiclassical gravity”. In: *Astron. Nachr.* 340.9-10 (2019). Ed. by C. A. Zen Vasconcellos, A. Pérez Martınez, H. Pérez Rojas, et al., pp. 914–919 (cit. on pp. 100, 177).

[214] Guilherme Lorenzatto Volkmer and Dimiter Hadjimichef. “Semiclassical Effects in Color Flavor Locked Strange Stars”. In: *Braz. J. Phys.* 52.5 (2022), p. 179. arXiv: 2107.06052 [hep-ph] (cit. on pp. 100, 177).

[215] Guilherme Lorenzatto Volkmer. “On the possibility of ultracompact stars in semiclassical gravity”. PhD thesis. Rio Grande do Sul U., 2022 (cit. on p. 100).

[216] Roman A. Konoplya, C. Posada, Z. Stuchlık, and A. Zhidenko. “Stable Schwarzschild stars as black-hole mimickers”. In: *Phys. Rev. D* 100.4 (2019), p. 044027. arXiv: 1905.08097 [gr-qc] (cit. on p. 141).

[217] Daniele Malafarina. “Classical collapse to black holes and quantum bounces: A review”. In: *Universe* 3.2 (2017), p. 48. arXiv: 1703.04138 [gr-qc] (cit. on pp. 142, 178).

[218] Clément Berthiere, Debajyoti Sarkar, and Sergey N. Solodukhin. “The fate of black hole horizons in semiclassical gravity”. In: *Phys. Lett.* B786 (2018), pp. 21–27. arXiv: 1712.09914 [hep-th] (cit. on pp. 145, 176).

[219] Arkady A. Popov. “Analytical approximation of the stress energy tensor of a quantized scalar field in static spherically symmetric space-times”. In: *Phys. Rev. D* 67 (2003), p. 044021. arXiv: hep-th/0302039 (cit. on p. 146).

[220] Dražen Glavan. “Perturbative reduction of derivative order in EFT”. In: *JHEP* 02 (2018), p. 136. arXiv: 1710.01562 [hep-th] (cit. on p. 146).

[221] David Hochberg, Arkadiy Popov, and Sergey V. Sushkov. “Self-Consistent Wormhole Solutions of Semiclassical Gravity”. In: *Physical Review Letters* 78.11 (Mar. 1997), pp. 2050–2053 (cit. on pp. 146, 164).

[222] Jonathan Z. Simon. “The Stability of flat space, semiclassical gravity, and higher derivatives”. In: *Phys. Rev. D* 43 (1991), pp. 3308–3316 (cit. on pp. 146, 149, 152).

[223] Gary T. Horowitz. “Semiclassical relativity: The weak-field limit”. In: *Phys. Rev. D* 21 (6 Mar. 1980), pp. 1445–1461 (cit. on p. 146).

[224] Robert M. Wald. “The Back Reaction Effect in Particle Creation in Curved Space-Time”. In: *Commun. Math. Phys.* 54 (1977), pp. 1–19 (cit. on pp. 147, 151).

[225] M. R. Brown, A. C. Ottewill, and Don N. Page. “Conformally invariant quantum field theory in static Einstein space-times”. In: *Phys. Rev. D* 33 (10 May 1986), pp. 2840–2850 (cit. on p. 147).

[226] Jerome Martin. “Everything You Always Wanted To Know About The Cosmological Constant Problem (But Were Afraid To Ask)”. In: *Comptes Rendus Physique* 13 (2012), pp. 566–665. arXiv: 1205.3365 [astro-ph.CO] (cit. on p. 148).

[227] Grazyna Siemieniec-Ozieblo and Andrzej Woszczyna. “Order reduction in semiclassical cosmology”. In: *Phys. Rev. D* 59 (1999), p. 083504. arXiv: astro-ph/9901416 (cit. on p. 149).

[228] Jr. Hernandez Walter C. and Charles W. Misner. “Observer Time as a Coordinate in Relativistic Spherical Hydrodynamics”. In: 143 (1966), p. 452 (cit. on p. 159).

[229] Jahed Abedi, Hannah Dykaar, and Niayesh Afshordi. “Echoes from the Abyss: Tentative evidence for Planck-scale structure at black hole horizons”. In: *Phys. Rev. D* 96.8 (2017), p. 082004. arXiv: 1612.00266 [gr-qc] (cit. on p. 175).

[230] Carlos Barceló, Stefano Liberati, Sebastiano Sonego, and Matt Visser. “Fate of gravitational collapse in semiclassical gravity”. In: *Physical Review D* 77.4 (2008) (cit. on p. 175).

[231] Jose P. S. Lemos and Oleg B. Zaslavskii. “Quasi black holes: Definition and general properties”. In: *Phys. Rev. D* 76 (2007), p. 084030. arXiv: 0707.1094 [gr-qc] (cit. on p. 177).

[232] Ram Brustein and A. J. M. Medved. “Black holes as collapsed polymers”. In: *Fortsch. Phys.* 65.1 (2017), p. 1600114. arXiv: 1602.07706 [hep-th] (cit. on p. 177).

[233] Saibal Ray, Rikpratik Sengupta, and Himanshu Nimesh. “Gravastar: An alternative to black hole”. In: *Int. J. Mod. Phys. D* 29.05 (2020), p. 2030004 (cit. on p. 177).

[234] Ram Brustein, A. J. M. Medved, and Tamar Simhon. “Black holes as frozen stars”. In: *Phys. Rev. D* 105 (2 Jan. 2022), p. 024019 (cit. on p. 177).

[235] Peter B. Groves, Paul R. Anderson, and Eric D. Carlson. “Method to compute the stress energy tensor for the massless spin 1/2 field in a general static spherically symmetric space-time”. In: *Phys. Rev. D* 66 (2002), p. 124017. arXiv: gr-qc/0207066 (cit. on p. 177).

[236] Adam Levi and Amos Ori. “Versatile Method for Renormalized Stress-Energy Computation in Black-Hole Spacetimes”. In: *Phys. Rev. Lett.* 117 (23 Nov. 2016), p. 231101 (cit. on p. 178).

[237] Peter Taylor and Cormac Breen. “A mode-sum prescription for the regularized stress energy tensor on black hole spacetimes”. In: (Jan. 2022). arXiv: 2201.05174 [gr-qc] (cit. on p. 178).

[238] J.L. Friedman and N. Stergioulas. *Rotating Relativistic Stars*. Cambridge Monographs on Mathematical Physics. Cambridge University Press, 2013 (cit. on p. 178).

[239] Suddhasattwa Brahma and Dong-han Yeom. “Effective black-to-white hole bounces: The cost of surgery”. In: *Class. Quant. Grav.* 35.20 (2018), p. 205007. arXiv: 1804.02821 [gr-qc] (cit. on p. 178).

[240] J. Ben Achour, S. Brahma, S. Mukohyama, and J. -P. Uzan. “Towards consistent black-to-white hole bounces from matter collapse”. In: *JCAP* 09 (2020), p. 020. arXiv: 2004.12977 [gr-qc] (cit. on p. 178).

[241] Tim Schmitz. “Exteriors to bouncing collapse models”. In: *Phys. Rev. D* 103.6 (2021), p. 064074. arXiv: 2012.04383 [gr-qc] (cit. on p. 178).

[242] Viqar Husain, Jarod George Kelly, Robert Santacruz, and Edward Wilson-Ewing. “Quantum Gravity of Dust Collapse: Shock Waves from Black Holes”. In: *Phys. Rev. Lett.* 128.12 (2022), p. 121301. arXiv: 2109.08667 [gr-qc] (cit. on p. 178).

[243] Muxin Han, Carlo Rovelli, and Farshid Soltani. “On the geometry of the black-to-white hole transition within a single asymptotic region”. In: (Feb. 2023). arXiv: 2302.03872 [gr-qc] (cit. on p. 178).

[244] Jacopo Mazza, Edgardo Franzin, and Stefano Liberati. “A novel family of rotating black hole mimickers”. In: *JCAP* 04 (2021), p. 082. arXiv: 2102.01105 [gr-qc] (cit. on p. 179).

[245] Alfonso Garcia-Parrado Gomez-Lobo and Jose M. M. Senovilla. “A set of invariant quality factors measuring the deviation from the Kerr metric”. In: *Gen. Rel. Grav.* 45 (2013). [Erratum: Gen.Rel.Grav. 45, 1129 (2013)], pp. 1095–1127. arXiv: 1211.6884 [gr-qc] (cit. on p. 179).

[246] Marc Casals, Alessandro Fabbri, Cristián Martınez, and Jorge Zanelli. “Quantum Backreaction on Three-Dimensional Black Holes and Naked Singularities”. In: *Phys. Rev. Lett.* 118.13 (2017), p. 131102. arXiv: 1608.05366 [gr-qc] (cit. on p. 179).

[247] Adam Levi, Ehud Eilon, Amos Ori, and Maarten van de Meent. “Renormalized Stress-Energy Tensor of an Evaporating Spinning Black Hole”. In: *Phys. Rev. Lett.* 118 (14 Apr. 2017), p. 141102 (cit. on p. 179).

[248] Bruce Jensen, John McLaughlin, and Adrian Ottewill. “Renormalized Electromagnetic Energy Density on the Horizon of a Kerr Black Hole”. In: *Class. Quant. Grav.* 5 (1988), p. L187 (cit. on p. 179).

[249] Adrian C. Ottewill and Elizabeth Winstanley. “The Renormalized stress tensor in Kerr space-time: general results”. In: *Phys. Rev. D* 62 (2000), p. 084018. arXiv: gr-qc/0004022 (cit. on p. 179).

[250] Marc Casals, Sam R. Dolan, Brien C. Nolan, Adrian C. Ottewill, and Elizabeth Winstanley. "Quantization of fermions on Kerr space-time". In: *Phys. Rev. D* 87.6 (2013), p. 064027. arXiv: 1207.7089 [gr-qc] (cit. on p. 179).

[251] Peter Taylor. "Regular Quantum States on the Cauchy Horizon of a Charged Black Hole". In: *Class. Quant. Grav.* 37.4 (2020), p. 045004. arXiv: 1904.05941 [gr-qc] (cit. on pp. 181, 183).

[252] J. Hadamard. *Lectures on Cauchy's Problem in Linear Partial Differential Equations*. Dover phoenix editions. Dover Publications, 2003 (cit. on p. 182).

[253] Bryce S DeWitt and Robert W Brehme. "Radiation damping in a gravitational field". In: *Annals of Physics* 9.2 (1960), pp. 220–259 (cit. on p. 182).

[254] J.L. Synge. *Relativity: The General Theory*. North-Holland series in physics v. 1. North-Holland Publishing Company, 1960 (cit. on p. 183).

[255] Adrian C. Ottewill and Barry Wardell. "Quasilocal contribution to the scalar self-force: Geodesic motion". In: *Phys. Rev. D* 77 (2008), p. 104002. arXiv: 0711.2469 [gr-qc] (cit. on p. 183).

[256] Christopher J Fewster and Rainer Verch. "The necessity of the Hadamard condition". In: *Classical and Quantum Gravity* 30.23 (Nov. 2013), p. 235027 (cit. on p. 184).

[257] I.S. Gradshteyn and I.M. Ryzhik. *Table of Integrals, Series, and Products*. Elsevier Science, 2014 (cit. on p. 185).

[258] R. Balbinot, A. Fabbri, Valeri P. Frolov, et al. "Vacuum polarization in the Schwarzschild space-time and dimensional reduction". In: *Phys. Rev. D* 63 (2001), p. 084029. arXiv: hep-th/0012048 (cit. on p. 186).

[259] James W. York. "Black hole in thermal equilibrium with a scalar field: The back-reaction". In: *Phys. Rev. D* 31 (4 Feb. 1985), pp. 775–784 (cit. on p. 192).

[260] Paul R. Anderson, William A. Hiscock, Janet Whitesell, and James W. York. "Semiclassical black hole in thermal equilibrium with a nonconformal scalar field". In: *Phys. Rev. D* 50 (10 Nov. 1994), pp. 6427–6434 (cit. on p. 192).

[261] A. Fabbri, S. Farese, and J. Navarro-Salas. "Generalized Virasoro anomaly and stress tensor for dilaton coupled theories". In: *Phys. Lett. B* 574 (2003), pp. 309–318. arXiv: hep-th/0309160 (cit. on p. 192).